2018

Studies of the Activation of Carbon-Gold and Carbon-Hydrogen Bonds by the Pentaruthenium Carbonyl Cluster Ru5(μ5-C)(CO)15

Jonathan Darrell Tedder
University of South Carolina

Studies of the Activation of Carbon-Gold and Carbon-Hydrogen Bonds by the Pentaruthenium Carbonyl Cluster $Ru_5(\mu_5\text{-}C)(CO)_{15}$

by

Jonathan Darrell Tedder

Bachelor of Science
University of South Carolina, 2013

Submitted in Partial Fulfillment of the Requirements

For the Degree of Doctor of Philosophy in

Chemistry

College of Arts and Sciences

University of South Carolina

2018

Accepted by:

Richard D. Adams, Major Professor

Natalia B. Shustova, Committee Member

Vitaly Rassolov, Committee Member

Timir Datta, Committee Member

Cheryl L. Addy, Vice Provost and Dean of the Graduate School

ACKNOWLEDGEMENTS

The undertaking of doctoral studies is not an easy task and requires the guidance and patience from the principal investigator. I express a deep sense of gratitude and sincere thankfulness to my advisor Prof. Richard Adams for allowing me to undertake my Ph.D. studies in his lab and for his invaluable guidance and constant encouragement throughout my time as a graduate researcher at the University of South Carolina. Prof. Adams has been a great influence on me as a researcher with his love for and vast knowledge of chemistry. He has also helped me mature as a person by showing me that hard work and diligence is required to be successful and didn't give up on me as a graduate student in his lab even when I struggled. And for that I can't thank him enough.

I would also like to thank the members of my research committee: Professors Natalia Shustova, Vitaly Rassolov, and Timir Datta for accepting to review my work and for taking the time to be there for all my comprehensive exams and dissertation defense. Thank you Prof. Rassolov for introducing me to computational chemistry and for advising me as an undergraduate at USC.

I would also like to thank the current and former member of the Adams research group who were crucial to my development as a chemistry researcher. I wish to thank Prof. Qiang Zhang and Dr. Yuwei Kan for introducing me to research in the laboratory as an undergraduate, Dr. Onn Wong and Dr. Gaya Elpitiya for training me in crystal structure solving and giving me research advice, Dr. Joseph Kiprotich, Poonam Dhull, Humaiara

Akter, Zhongwen Luo, Nutan Wakdikar, Meenal Kaushal and Morteza Maleki for being there for support and encouragement in and out of the lab and I wish each one of you luck as you continue your careers. Special recognition goes to Dr. Mark D. Smith for his help with crystal structures that were difficult to handle, Dr. Perry J. Pellechia and Helga J. Cohen for assistance with VT-NMR and other complex NMR studies and Dr. Mike Walla and Dr. William E. Cotham for technical support with mass spec.

The last group of people I would like to acknowledge are my family members. Without their constant support and encouragement, I would not be where I am here today. To my two brothers, Justin and Jacob, thank you being there to support me. To my Mom, you have always been there for me and have given me encouragement throughout this journey and I don't think I can ever repay you for all of your support. Your love and guidance kept me focused when times were tough. To my Dad, thank you for always believing in me and encouraging me to pursue all of my dreams. Even though you are not here today to see me finish my Ph.D, I know you would be proud of what I have accomplished and what I will accomplish in the future.

ABSTRACT

The current practical uses of hydrocarbons by industry are discussed in Chapter 1. Carbon-hydrogen (C-H) bond activation and selective functionalization by transition metal complexes is presented as a possible alternative for the upgrading of hydrocarbons. The comparison of carbon-gold (C-Au) bond activation to C-H bond activation based on isolobal principles by transition metal complexes is presented. The high nuclearity ruthenium cluster complexes Ru_6C and Ru_5C are presented and their early chemistry is discussed.

The reactions of high nuclearity carbido cluster complexes, $Ru_6C(CO)_{17}$ and $Ru_5C(CO)_{15}$, with PhAuNHC are presented in Chapter 2. The reaction of $Ru_6C(CO)_{17}$ with PhAuNHC yields the π-arene complex $Ru_6C(CO)_{14}[\eta^6\text{-PhAu(NHC)}]$, **2.3** that does not involve activation of the Au-C bond. The oxidative addition of the Au-C bond of PhAuNHC to $Ru_5C(CO)_{15}$ yielded two new cluster complexes: $Ru_5C(CO)_{14}(Ph)[\mu\text{-Au(NHC)}]$, **2.4** and $Ru_5C(CO)_{13}(\mu\text{–}\eta^2\text{-Ph})[\mu\text{-Au(NHC)}]$, **2.5**. Both **2.4** and **2.5** react with CO to yield the complex $Ru_5C(CO)_{14}(\mu\text{–}\eta^2\text{-O=CPh})[\mu\text{-Au(NHC)}]$, **2.6**, that contains a bridging benzoyl formed from the insertion of CO into the Ru-Ph bond.

The reaction of $Ru_5C(CO)_{15}$ with CH_3AuPPh_3 is reported in Chapter 3. Three hetero-bimetallic Ru_5CAu cluster complexes containing methyl ligands were isolated: $Ru_5(\mu_5\text{-C})(CO)_{14}(\mu\text{-}\eta^2\text{-O=CMe})[\mu\text{-Au}(PPh_3)]$, **3.5**; $Ru_5(\mu_5\text{-C})(CO)_{13}(\mu\text{-}\eta^2\text{-O=CMe})(Me)[\mu\text{-Au}_2(PPh_3)_2]$, **3.6**; $Ru_5(\mu_5\text{-C})(CO)_{14}(\mu\text{-}\eta^2\text{-O=CMe})(\eta^1\text{-O=CMe})[\mu\text{-}$

$Au_2(PPh_3)_2]$, **3.7**. The PPh_3 substituted complex $Ru_5(\mu_5\text{-}C)(CO)_{13}(PPh_3)(\mu\text{-}\eta^2\text{-}O{=}CMe)[\mu\text{-}Au(PPh_3)]$, **3.8**, was also isolated. Two nonmethyl complexes: $Ru_5(\mu_5\text{-}C)(CO)_{11}(\mu\text{-}CO)_3[\mu\text{-}Au(PPh_3)]_2$, **3.9**, and $Ru_5(\mu_5\text{-}C)(CO)_{11}(\mu\text{-}CO)_2[\mu\text{-}Au(PPh3)]_4$, **3.10** were also isolated. The synthesis, structures and interrelationships of these new complexes are described.

The products formed from the cluster opening reaction of $Ru_5C(CO)_{15}$ with benzoic acid are presented in Chapter 4. Two new isomeric Ru_5C open square pyramidal complexes: $Ru_5(C)(CO)_{14}(\eta^2\text{-}O_2CC_6H_5)(\mu\text{-}H)$, **4.2** and $Ru_5(C)(CO)_{14}(\mu\text{–}\eta^2\text{-}O_2CC_6H_5)(\mu\text{-}H)$, **4.3** were isolated that possess a benzoate ligand in η^2-chelating and $\mu\text{–}\eta^2$-bridging coordination modes, respectively. An equilibrium between the isomerization of the two benzoate isomers was established.

The studies of aldehydic C-H activation by $Ru_5C(CO)_{15}$ are introduced in Chapter 5. The reaction of $Ru_5C(CO)_{15}$ with benzaldehyde yielded two new complexes: $Ru_5(\mu_5\text{-}C)(CO)_{14}(\eta^2\text{-}O{=}CH(C_6H_4))(H)$, **5.2**, and $Ru_5(\mu_5\text{-}C)(CO)_{14}(\mu\text{-}\eta^2\text{-}O{=}CPh)(\mu\text{-}H)$, **5.3**. **5.2** possesses a η^2-chelating benzoyl ligand formed by C-H activation at the ortho position of the phenyl ring and **5.3** contains $\mu\text{-}\eta^2$-bridging benzoyl ligand formed from activation of the aldehydic C-H bond. Comparison studies of the reaction of $Ru_5(\mu_5\text{-}C)(CO)_{15}$ with cinnamaldehyde produced two analogous complexes: $Ru_5(\mu_5\text{-}C)(CO)_{14}(\eta^2\text{-}O{=}CHCH{=}CPh)(\mu\text{-}H)$, **5.4** and $Ru_5(\mu_5\text{-}C)(CO)_{14}[\mu\text{-}\eta^2\text{-}O{=}C(CH{=}CHPh)](\mu\text{-}H)$, **5.5**. Compounds **5.4** and **5.5** show similar differences in the site of C-H activation of cinnamaldehyde. The decomposition reactions of the coordinated acyl ligands in the product complexes are also presented.

The activation of formyl C-H bonds of aldehydes presented in chapter 5 is expanded on in Chapter 6 and looks at the activation of the formyl C-H bond of N,N-

dimethylformamide (DMF). The reaction of $Ru_5C(CO)_{15}$ with DMF yields two new Ru5C complexes that contain μ-η^2-bridging formamido ligands: $Ru_5(\mu_5\text{-}C)(CO)_{14}(\mu\text{-}\eta^2\text{-}O{=}CNMe_2)(\mu\text{-}H)$, **6.2**nand $Ru_5(\mu_5\text{-}C)(CO)_{13})(HN(Me_2)(\mu\text{-}\eta^2\text{-}O{=}CNMe_2)(\mu\text{-}H)$, **6.3**. The reaction of **6.3** with C_2H_2 yields the hydrocarbamoylation product $Ru_5(\mu_5\text{-}C)(CO)_{13}[\mu\text{-}\eta^3\text{-}O{=}CN(CH_3)_2CHCH](\mu\text{-}H)$, **6.4**, from coupling of the μ-η^2-bridging formamido ligand with C_2H_2 to form a μ-η^3-bridging acrylamido ligand. Placing complex **6.4** under an atmosphere of CO yields the CO addition product $Ru_5(\mu_5\text{-}C)(CO)_{14}[\eta^2\text{-}O{=}CN(CH_3)_2CH{=}CH](\mu\text{-}H)$, **6.6**. Under more forcing conditions of CO, reductive elimination of the η^2-chelating acrylamido ligand and the bridging hydride to yield N,N-dimethylacrylamide, effectively forming a catalytic cycle.

The investigations of olefinic C-H activation of substituted olefins with $Ru_5C(CO)_{15}$ are discussed in Chapter 7. The reaction of $Ru_5C(CO)_{15}$ with methyl acrylate yielded the new chelating acryloyl complex: $Ru_5(\mu_5\text{-}C)(CO)_{14}[\eta^2\text{-}O{=}CO(CH_3)CH{=}CH](\mu\text{-}H)$, **7.2**. The reaction of $Ru_5C(CO)_{15}$ with vinyl acetate yielded the new complex $Ru_5(\mu_5\text{-}C)(CO)_{14}[C(=CH_2)(O_2CMe)](\mu\text{-}H)$, **7.3**. The two C-H activated olefin complexes differ by the location of the C-H activation. Compound **7.2** is activated at the β-carbon of the olefin while **7.3** is activated at the α-carbon of the olefin.

The work in Chapter 8 is a continuation of the chemistry presented in Chapter 7. The functionalization of the activated olefinic C-H bonds of methyl acrylate, dimethylacrylamide, and vinyl acetate through the tail-to-tail coupling of a second equivalent of the olefin to the activated ligand in the complex was investigated. The reaction of the activated methyl acrylate **8.2** with Me_3NO and excess methyl acrylate yielded five new Ru_5C complexes of methyl acrylate: $Ru_5(\mu_5\text{-}C)(CO)_{13}[\mu\text{-}\eta^3\text{-}$

O=CO(Me)CHCH](μ-H), **8.6**, $Ru_5(\mu_5\text{-}C)(CO)_{13}[\eta^3\text{-}anti,anti\text{-}(Me)OC{=}O\text{-}C_3H_3\text{-}\eta^1\text{-}O{=}CO(Me)CH_2](\mu\text{-}H)$, **8.7**, $Ru_5(\mu_5\text{-}C)(CO)_{13}[\eta^3\text{-}anti,syn\text{-}(MeO_2C)CH_2C_3H_3\text{-}CH_2\text{-}\eta^1\text{-}O{=}C(OMe)](\mu\text{-}H)$, **8.8**, $Ru_5(\mu_5\text{-}C)(CO)_{12}[\mu\text{-}\eta^3\text{-}O{=}C(OMe)CH{=}CH][\eta^2\text{-}CH{=}CHCO_2Me](\mu\text{-}H)$, **8.9**, and $Ru_5(\mu_5\text{-}C)(CO)_{13}[\eta^3\text{-}syn,anti\text{-}(MeO_2C)C_3H_3\text{-}\eta^1\text{-}O{=}C(OMe)CH_2](\mu\text{-}H)$, **8.10** where complexes **8.7**, **8.8**, and **8.10** show carbon-carbon formation between methyl acrylate units. Reaction of the activated dimethylacrylamide ligand in **8.3** with additional dimethylacrylamide yielded two new coupled dimethylacrylamide complexes: $Ru_5(\mu_5\text{-}C)(CO)_{13}[\eta^3\text{-}syn,anti\text{-}Me_2NC{=}O\text{-}C_3H_3\text{-}\eta^1\text{-}O{=}CNMe_2CH_2](\mu\text{-}H)$, **8.11** and $Ru_5(\mu_5\text{-}C)(CO)_{13}[\eta^3\text{-}anti,syn\text{-}Me_2NC{=}O\text{-}C_3H_3\text{-}CH_2\text{-}\eta^1\text{-}O{=}CNMe_2](\mu\text{-}H)$, **8.12**. Two new hetero-coupled substituted olefin complexes, $Ru_5(\mu_5\text{-}C)(CO)_{12}[\mu\text{-}\eta^3\text{-}O{=}C(NMe_2)]CH{=}CH][\eta^2\text{-}CH{=}CHCO_2Me](\mu\text{-}H)$, **8.13** and $Ru_5(\mu_5\text{-}C)(CO)_{13}[\eta^3\text{-}anti,syn\text{-}MeO_2CCH_2\text{-}C_3H_3\text{-}\eta^1\text{-}O{=}C(NMe_2)](\mu\text{-}H)$, **8.14,** were obtained from the reaction of **8.3** with methyl acrylate. Reaction of activated vinyl acetate ligand in **8.5** with an additional equivalent of vinyl acetate in the presence of Me_3NO yielded a new uncoupled bis-vinyl acetate complex: $Ru_5(\mu_5\text{-}C)(CO)_{12}[\mu\text{-}\eta^2\text{-}(MeO_2C)CH{=}CH](\eta^3\text{-}CH_2{=}CHOC(=O)Me)(\mu\text{-}H)$, **8.15**.

TABLE OF CONTENTS

ACKNOWLEDGEMENTS iii

ABSTRACT v

LIST OF TABLES x

LIST OF FIGURES xi

CHAPTER 1: Introduction 1

CHAPTER 2: Phenyl–gold complexes of Ru_6 and Ru_5 carbonyl clusters 24

CHAPTER 3: Organometallic chemistry of pentaruthenium-gold carbonyl cluster complexes 53

CHAPTER 4: Open Pentaruthenium Cluster Complexes Formed from the Addition of Benzoic Acid to $Ru_5(C)(CO)_{15}$ 81

CHAPTER 5: CH Activations in Aldehydes in Reactions with $Ru_5(\mu_5\text{-}C)(CO)_{15}$ 97

CHAPTER 6: Formation of N,N-Dimethylacrylamide by a Multicenter Hydrocarbamoylation of C_2H_2 with N,N-Dimethylformamide Activated by $Ru_5(\mu_5\text{-}C)(CO)_{15}$ 123

CHAPTER 7: Substituent-Directed Activation of CH bonds in Activated Olefins by $Ru_5(\mu_5\text{-}C)(CO)_{15}$ 148

CHAPTER 8: Coupling of Activated Olefins by a Ru_5 Cluster Complex 163

APPENDIX A: Copyright Releases 207

LIST OF TABLES

Table 2.1 Crystallographic Data for Compounds **2.3** and **2.4** 37

Table 2.2 Crystallographic Data for Compounds **2.4** and **2.5**. 38

Table 3.1 Crystallographic Data for Compounds **3.5** and **3.6** 67

Table 3.2 Crystallographic Data for Compounds **3.7** and **3.8** 68

Table 3.3 Crystallographic Data for Compounds **3.9** and **3.10** 69

Table 4.1 Crystallographic Data for Compounds **4.2** and **4.3**. 90

Table 5.1. Crystallographic Data for Compounds **5.2** and **5.3** 109

Table 5.2. Crystallographic Data for Compounds **5.4** and **5.5** 110

Table 6.1. Crystallographic Data for Compounds **6.2, 6.3,** and **6.4** 135

Table 6.2. Crystallographic Data for Compounds **6.5** and **6.6** 136

Table 7.1. Crystallographic Data for Compounds **7.2** and **7.3** 155

Table 8.1. Crystallographic Data for Compounds **8.6** and **8.7** 186

Table 8.2. Crystallographic Data for Compounds **8.8, 8.9,** and **8.10** 187

Table 8.3. Crystallographic Data for Compounds **8.11** and **8.12** 188

Table 8.4. Crystallographic Data for Compounds **8.13, 8.14,** and **8.15** 189

LIST OF FIGURES

Figure 2.1. An ORTEP diagram of the molecular structure of Ru6C(CO)14[η6-PhAu(NHC)], **2.3** 39

Figure 2.2. An ORTEP diagram of the molecular structure of $Ru_5C(CO)_{14}(Ph)[\mu$-Au(NHC)], **2.4** 40

Figure 2.3. An ORTEP diagram of the molecular structure of $Ru_5C(CO)_{13}(\mu$-η^2-Ph)[μ-Au(NHC)], **2.5** 41

Figure 2.4. Variable temperature ^{1}H NMR spectra of **2.5** 42

Figure 2.5. A schematic of the proposed mechanism for the interchange of the ortho- and meta-hydrogen atoms on the bridging phenyl ligand in **2.5** 43

Figure 2.6. An ORTEP diagram of the molecular structure of $Ru_5C(CO)_{14}(\mu$-η^2O=CPh)[μ-Au(NHC)], **2.6** 44

Figure 3.1. A line drawing of compound **3.5** 70

Figure 3.2. An ORTEP diagram of the molecular structure of $Ru_5(\mu_5$-C)$(CO)_{13}(\mu$-η^2-O=CMe)(Me)[μ-$Au_2(PPh_3)_2$], **3.6** 71

Figure 3.3. An ORTEP diagram of the molecular structure of $Ru_5(\mu_5$-C)$(CO)_{14}(\mu$-η^2-O=CMe)(O=CMe)[μ-$Au_2(PPh_3)_2$], **3.7** 72

Figure 3.4 An ORTEP diagram of the molecular structure of $Ru_5(\mu^5$-C)$(CO)_{13}(\mu$-η^2-O=CMe)(PPh_3)[μ-Au(PPh_3)], **3.8** 73

Figure 3.5 An ORTEP diagram of the molecular structure of $Ru_5C(CO)_{11}(\mu$-CO$)_3[\mu$-Au(PPh_3)]$_2$, **3.9** 74

Figure 3.6 An ORTEP diagram of the molecular structure of $Ru_5C(CO)_{11}(\mu$-CO$)_2[\mu$-Au(PPh_3)]$_4$, **3.10** 75

Figure 4.1. Coordination modes of carboxylate ligands to metal atom 91

Figure 4.2. An ORTEP diagram of the molecular structure of $Ru_5(C)(CO)_{14}(\eta^2$-$O_2CC_6H_5)(\mu$-H), **4.2** 92

Figure 4.3. An ORTEP diagram of the molecular structure of $Ru_5(C)(CO)_{14}(\mu–\eta^2$-$O_2CC_6H_5)(\mu$-H), **4.3** 93

Figure 5.1. An ORTEP diagram of the molecular structure $Ru_5(\mu_5$-C)$(CO)_{14}(\eta^2$-O=CHPh)(μ-H), **5.2** 111

Figure 5.2. An ORTEP diagram of the molecular structure of $Ru_5(\mu_5$-C)$(CO)_{14}(\mu$-η^2-O=CPh)(μ-H), **5.3** 112

Figure 5.3. A line drawing for the molecular structure of $Ru_5(\mu_5$-C)$(CO)_{14}(\mu$-η^2-O=CPh)[μ-Au(NHC)] 113

Figure 5.4. Stacked plot of the decomposition of $Ru_5(\mu_5$-C)$(CO)_{14}(\mu$-η^2-O=CPh)(μ-H) 114

Figure 5.5. An ORTEP diagram of the molecular structure of $Ru_5(\mu_5$-C)$(CO)_{14}(\eta^2$-O=CHCH=CPh)(μ-H), **5.4**.....115

Figure 5.6. An ORTEP diagram of the molecular structure of $Ru_5(\mu_5$-C)$(CO)_{14}(\mu$-η^2-O=CCH=CHPh)(μ-H), **5.5**.....116

Figure 6.1. An ORTEP diagram of the molecular structure of $Ru_5(\mu_5$-C)$(CO)_{14}(\mu$-η^2-O=CN$(Me)_2$)(μ-H), **6.2** 137

Figure 6.2. An ORTEP diagram of the molecular structure of $Ru_5(\mu_5$-C)$(CO)_{14}(\mu$-η^2-O=CN$(Me)_2$)(HN$(Me)_2$(μ-H), **6.3**.....138

Figure 6.3. An ORTEP diagram of the molecular structure of $Ru_5(\mu_5$-C)$(CO)_{13}[\mu$-η^3-O=CN$(Me)_2$CHCH](μ-H), **6.4** 139

Figure 6.4. An ORTEP diagram of the molecular structure of $Ru_5(\mu_5$-C)$(CO)_{14}(\mu$-η^2-O=CN$(CH_3)_2$)(CH=CHNMe$_3$)(μ-H), **6.5**.....140

Figure 6.5. An ORTEP diagram of the molecular structure of $Ru_5(\mu_5$-C)$(CO)_{14}(\eta^2$-O=CN$(Me)_2$CH=CH)(μ-H), **6.6**.....141

Figure 7.1. An ORTEP diagram of the molecular structure of $Ru_5(\mu_5$-C)$(CO)_{14}[\eta^2$-O=CO(CH_3)CH=CH](μ-H), **7.2**.....156

Figure 7.2. An ORTEP diagram of the molecular structure of $Ru_5(\mu_5$-C)$(CO)_{14}(\eta^2$-O=C(CH_3)OC=CH_2)(μ-H), **7.3** 157

Figure 8.1. An ORTEP diagram of the molecular structure of $Ru_5(\mu_5$-C)$(CO)_{13}[\mu$-η^3-O=CO(Me)CHCH](μ-H), **8.6** 190

Figure 8.2. An ORTEP diagram of the molecular structure of $Ru_5(\mu_5$-C)$(CO)_{13}[\eta^3$-*anti*,*anti*-(Me)OC=O-C_3H_3-η^1-O=CO(Me)CH_2](μ-H), **8.7** 191

Figure 8.3. An ORTEP diagram of the molecular structure of $Ru_5(\mu_5\text{-}C)(CO)_{13}[\eta^3$-*anti*,*syn*-$(MeO_2C)CH_2C_3H_3\text{-}CH_2\text{-}\eta^1$-O=C(OMe)](μ-H), **8.8** 192

Figure 8.4. An ORTEP diagram of the molecular structure of $Ru_5(\mu_5\text{-}C)(CO)_{12}[\mu\text{-}\eta^3$-O=C(OMe)CH=CH][$\eta^2$-CH=$CHCO_2Me$](μ-H), **8.9** 193

Figure 8.5. An ORTEP diagram of the molecular structure of $Ru_5(\mu_5\text{-}C)(CO)_{13}[\eta^3$-*syn*,*anti*-$(MeO_2C)C_3H_3\text{-}\eta^1$-O=C(OMe)$CH_2$](μ-H), **8.10** 194

Figure 8.6. An ORTEP diagram of the molecular structure of $Ru_5(\mu_5\text{-}C)(CO)_{13}[\eta^3$-*syn*,*anti*-$Me_2NC$=O-$C_3H_3\text{-}\eta^1$-O=$CNMe_2CH_2$](μ-H), **8.11** 195

Figure 8.7. An ORTEP diagram of the molecular structure of $Ru_5(\mu_5\text{-}C)(CO)_{13}[\eta^3$-*anti*,*syn*-$Me_2NC$=O-$C_3H_3\text{-}CH_2\text{-}\eta^1$-O=$CNMe_2$](μ-H), **8.12**.....196

Figure 8.8. An ORTEP diagram of the molecular structure of $Ru_5(\mu_5\text{-}C)(CO)_{12}[\mu\text{-}\eta^3$-O=C($NMe_2$)]CH=CH][$\eta^2$-CH=$CHCO_2Me$](μ-H), **8.13** 197

Figure 8.9. An ORTEP diagram of the molecular structure of $Ru_5(\mu_5\text{-}C)(CO)_{13}[\eta^3$-*anti*,*syn*-$MeO_2CCH_2$ $C_3H_3\text{-}\eta^1$-O=C(NMe_2)](μ-H), **8.14**.....198

Figure 8.10. An ORTEP diagram of the molecular structure of $Ru_5(\mu_5\text{-}C)(CO)_{12}[\mu\text{-}\eta^2$-$(MeO_2C)$CH=CH]($\eta^3$-$CH_2$=CHOC(=O)Me)(μ-H), **8.15** 199

Figure 8.11. Stacked plot for the allyl isomerization of compound **8.7** at 80 °C in d_8-toluene followed by ^{1}H NMR. 200

Figure 8.12. Stacked plot for the allyl isomerization of compound **8.8** at 80 °C in d_8-toluene followed by ^{1}H NMR. 201

CHAPTER 1

Introduction

The ability to convert simple hydrocarbons into higher value commodity chemicals is of great importance to the chemical industry. The simplest alkanes, methane, ethane and propane, the major components of natural gas and petroleum, currently do have any practical routes for their conversion to higher valuable commodity chemicals directly. Combustion of light alkanes at high temperatures to utilize the energy content of the C-C and C-H bonds is still the predominate use of light alkanes which yields low value products carbon dioxide and water. With the potential adverse effects of increased greenhouse gas emissions from the combustion of hydrocarbons and limited natural resources, methods that utilize the ubiquitous C-H bonds of hydrocarbons efficiently and limit greenhouse gas emissions are highly sought after. Fischer-Tropsch chemistry at this time remains the major process for upgrading abundant low value light alkanes, where first the components of natural gas are converted to carbon monoxide and hydrogen (syn-gas) by the steam reforming of hydrocarbons shown in Scheme 1.1.[1]

$$CH_4 + H_2O \xrightarrow[+206\ kJ/mol]{Ni} CO + 3H_2$$

Scheme 1.1. Steam reformation of methane to generate syn-gas

The steam reformation of methane is an energy intensive process that on the industrial scale requires methane to be passed over a supported Ni/Al_2O_3 catalyst at high temperatures up to 850 °C. Methane can be converted to syngas without the presence of a catalyst but requires even higher temperature up to 2000 °C and proceeds through a radical reaction called homogeneous oxidation. The syngas mixture produced by steam reformation can subsequently be converted into longer hydrocarbon chains or higher value oxygenates, i.e. methanol, using Fischer-Tropsch chemistry (Scheme 1.2) that can then be used as liquid fuels or as precursors for other commodity products.[2] The mechanism for chain lengthening associated with the Fischer-Tropsch reaction is still debated but the overall process of first steam reformation of hydrocarbons and second Fischer-Tropsch chemistry represents an indirect process to functionalization.[3]

$$\underset{\text{(Syn gas)}}{CO + 3H_2} \xrightarrow[\text{-90.7 kJ/mol}]{\text{Cu/ZnO}} CH_3OH$$

Scheme 1.2. Fischer-Tropsch synthesis of methanol from syn-gas

Fluid catalytic cracking can be used to convert longer chain, higher molecular weight hydrocarbons into more valuable products such as olefins and lighter alkanes that can be used in the production of valuable polymers and as fuels (Scheme 1.3).[4] Due to the high demand of light olefins, steam cracking has become the highest energy consuming process in the chemical industry and contributes heavily to CO_2 emissions.[5]

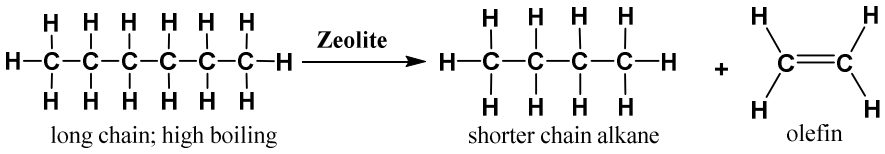

Scheme 1.3. Catalytic cracking of long chain hydrocarbons to form shorter chain hydrocarbons and olefins.

With the idea of developing new processes for the conversion of hydrocarbons into higher value chemicals under milder conditions that avoid the production of greenhouse gases, new technologies need to be developed that can compete with currently utilized industrial processes.

1.1 Transition Metal Catalyzed C-H Activation and Functionalization

Understanding the C-H bond properties of saturated and unsaturated hydrocarbons should help toward understanding their limited reactivity. Aliphatic and aromatic hydrocarbons are composed of strong and localized C-C and C-H bonds. The bond strength of the C-H bonds in methane is 105 kcal/mol and in benzene they are 110 kcal/mol.[6] Another key point in understanding the low reactivity of saturated hydrocarbons is the low polarity of C-H bonds because carbon and hydrogen possess nearly the same electronegativity (χ_C = 2.55; χ_H = 2.20). A molecular orbital explanation of saturated hydrocarbons show that they do not possess any low lying empty orbitals and no filled orbitals of high energy that can participate in chemical reactions making them relatively chemically inert compared to their unsaturated counterparts. After initial functionalization, another intrinsic drawback of the activation and functionalization of saturated hydrocarbons is the higher reactivity of the products which can lead to over oxidation to CO_2 or coke, making partial selective oxidations difficult.

Development of technologies to activate and functionalize ubiquitous C-H bonds to make new C-C, C-N, C-O, C-S, and C-X bonds directly, in particular of methane, is considered the "holy grail" process by academia and industry. The activation of aliphatic and aromatic C-H bonds by transition metal atoms has been highlighted in numerous studies.[7] The four general classes of C-H activation by transition metal complexes are oxidative addition, sigma-bond metathesis, electrophilic metalation, and Lewis base assisted deprotonation highlighted in Scheme 1.4.

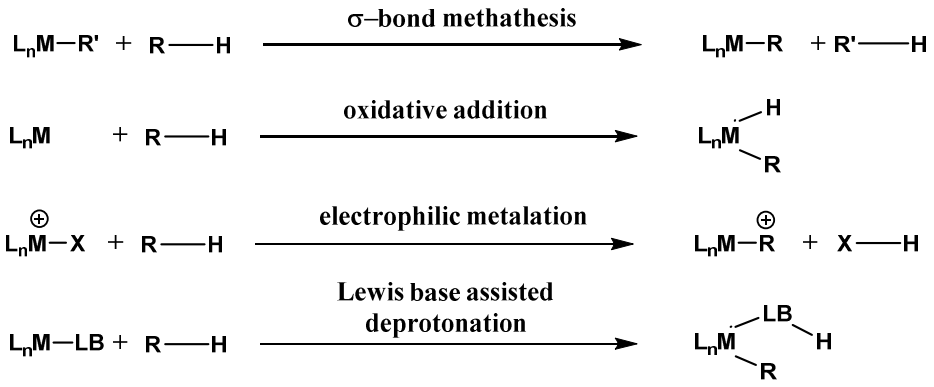

Scheme 1.4. Four general classes of C-H activation by a transition metal center.

Potentially, C-H activations by transition metal complexes can overcome the need for high temperatures and the addition of strong oxidants and acidic or basic reagents which generally are not compatible with functional groups that are present. This use of harsh conditions for C-H activation makes it impracticable in the use of complex natural product syntheses, hence the need for mild C-H activation technologies. Well known catalytic systems for the selective oxidation of hydrocarbons that proceed through the initial C-H activation of the hydrocarbon have already been developed Shilov[8] (Scheme 1.5) and Periana[9] (Scheme 1.6). Both systems invoke the use of Pt(II) complexes to electrophilically activate and functionalize hydrocarbon C-H bonds catalytically but both systems have

disadvantages. The Shilov system requires the use of stoichiometric amounts of Pt(IV) and the catalyst decomposes over time precipitating platinum metal. The Periana system overcomes the instability of the Pt(II) catalyst, but harsh reagents such as H_2SO_4 are required and the product is protected which requires further processing to produce a valuable product.

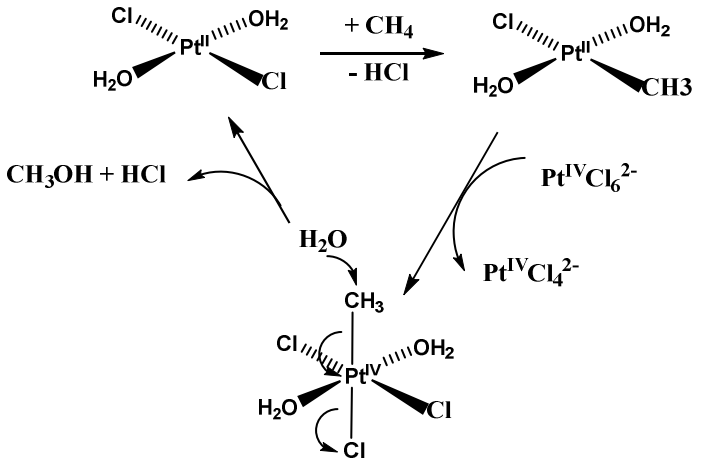

Scheme 1.5. Shilov catalytic oxidation of methane to methanol by Pt(II) catalyst.

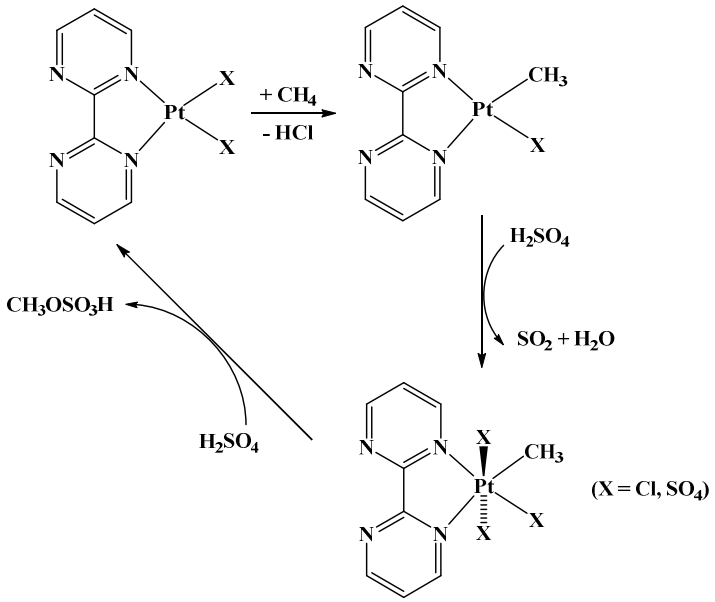

Scheme 1.6. Periana Catalytica catalytic oxidation of methane.

Developing catalytic C-H upgrading processes that proceed through initial oxidative addition of the C-H bond at the metal center could help alleviate problems associated with the electrophilic activation systems. Once activated, the selective functionalization of the activated hydrocarbon with benign oxidants (e.g. H_2O_2 or O_2) and the reductive elimination of the functionalized product to regenerate the catalyst in a catalytic cycle would represent an important step forward in the utilization of hydrocarbons (Scheme 1.7).[10]

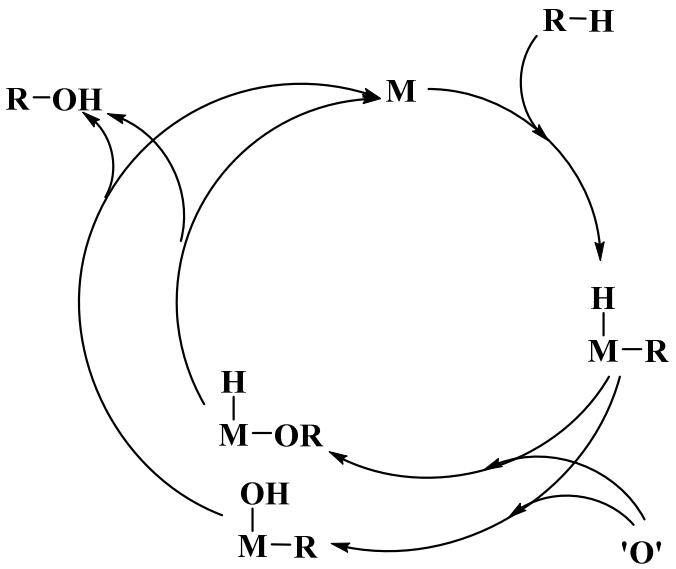

Scheme 1.7. Potential catalytic selective oxidation cycle initiated by oxidative addition of hydrocarbon to transition metal center.

The use of polynuclear transition metal cluster complexes for the activation of aromatic C-H bonds by oxidative addition of the C-H bond to the cluster has been studied as potential models for the activation and functionalization of C-H bonds at multinuclear metal sites and on metal surfaces. The reaction of $Os_3(CO)_{10}(NCMe)_2$ in refluxing benzene yields the doubly C-H activated complex $H_2Os_3(CO)_9(\mu_3\text{-}C_6H_4)$ and elimination of the

coordinated acetonitrile ligands (Scheme 1.8).[11] $H_2Os_3(CO)_9(\mu_3\text{-}C_6H_4)$ contains a triply bridging "benzyne" ligand and two hydrides that bridge two Os-Os bonds of the triosmium triangle.

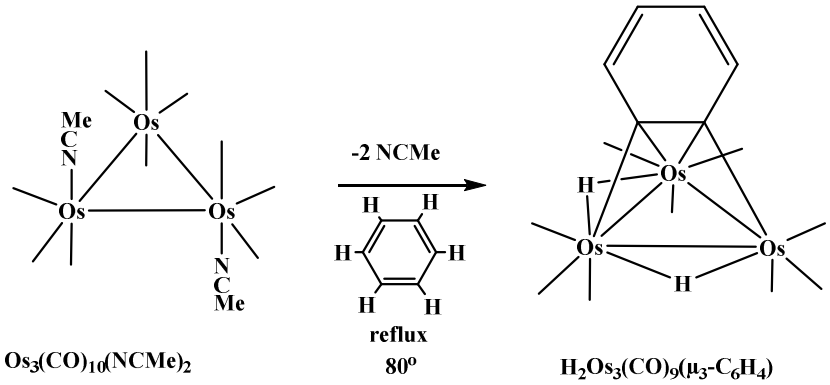

Scheme 1.8. Reaction of $Os_3(CO)_{10}(NCMe)_2$ with benzene yielding $H_2Os_3(CO)_9(\mu_3\text{-}C_6H_4)$.

The intermediate triosmium complex that contains a singly C-H activated η^1-bridging phenyl ligand with one bridging hydride has not been observed. An analogous species that replaces the bridging hydride with a bridging $AuPPh_3$ unit and contains a bridging phenyl ligand has been isolated by the Adams' group and is discussed in the next section of this introduction.

Recently it has been shown that the dirhenium complex $Re_2(CO)_9(\mu\text{-}H)(\mu\text{-}C_6H_5)$ can activate a C-H bond of naphthalene to yield the complex $Re_2(CO)_8(\mu\text{-}\eta^2\text{-}C_{10}H_7)$ (Scheme 1.9).[12] $Re_2(CO)_8(\mu\text{-}\eta^2\text{-}C_{10}H_7)$ was formed by the oxidative addition of the naphthalene C-H bond and reductive elimination of the bridging phenyl and hydrido ligand as benzene from the parent molecule.

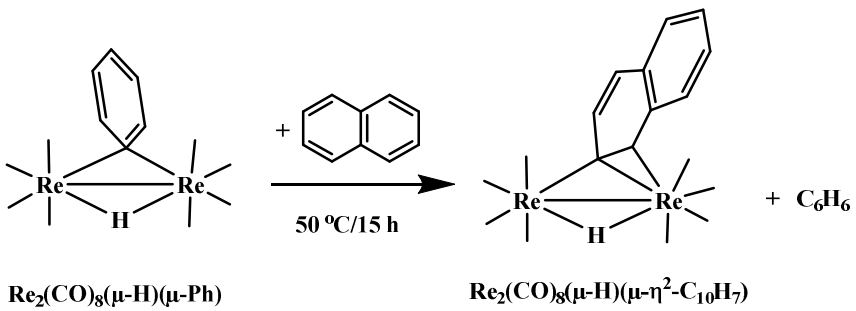

Scheme 1.9. Multi-center C-H activation of naphthalene by $Re_2(CO)_8(\mu\text{-}H)(\mu\text{-}Ph)$.

1.2 Carbon-Gold Activation by Transition Metal Carbonyl Clusters Guided by the Isolobality Principle

The first couple of chapters of this dissertation focus on the comparison of carbon-gold (C-Au) activation with C-H activation based on the isolobality concept. The isolobal principle, as described by Robert Burns Woodward and Roald Hoffmann, for which Hoffmann won the Nobel Prize, attempts to bridge the structure and bonding between inorganic, organometallic, and organic complexes and fragments.[13] The isolobal concept and its relation to gold chemistry has been described extensively in the review by Raubenheimer and Schmidbaur.[14] When comparing $[LAu]^+$ cation to proton $[H]^+$ and alkyl cations $[R]^+$, the frontier orbitals of all three species show similar symmetries and shapes along with comparable energies. Simple analogies between H and supported AuL can be seen in Scheme 1.10. Substitution of hydrogen atoms in molecular hydrogen and methane by supported AuL give the simplest case of the similarities between AuL and H. The use of NHCs as a supporting ligand for gold in AuL has made it possible to isolate H-AuL.[15] The LAu-AuL example has yet to be isolated at this time.

H—H
H—AuL
H_3C—AuL
LAu—AuL

Scheme 1.10. Isolobal analogies between H and supported AuL.

Structural similarities of metal-hydrido complexes and metal-$AuPPh_3$ have been examined for the monogold complexes, where the monogold formulas ($LAu\text{-}ML'_n$) closely resemble the monohydride complexes ($H\text{-}ML'_n$) (Scheme 1.11).

$HCo(CO)_4$	$PPh_3AuCo(CO)_4$
$HMn(CO)_5$	$PPh_3AuMn(CO)_5$
$HV(CO)_6$	$PPh_3AuV(CO)_6$

Scheme 1.11. Substitution of hydride ligand (H) with $AuPPh_3$ in monogold carbonyl complexes.

Differences arise when the dihydride complexes are compared to the digold complexes of $Fe(CO)_4(AuPPh_3)_2$ and $Fe(CO)_4(H)_2$ and the complexes of $Co(CO)_4(PPh_3)(AuPPh_3)_2$ and $Co(CO)_4H_2$ (Scheme 1.12).

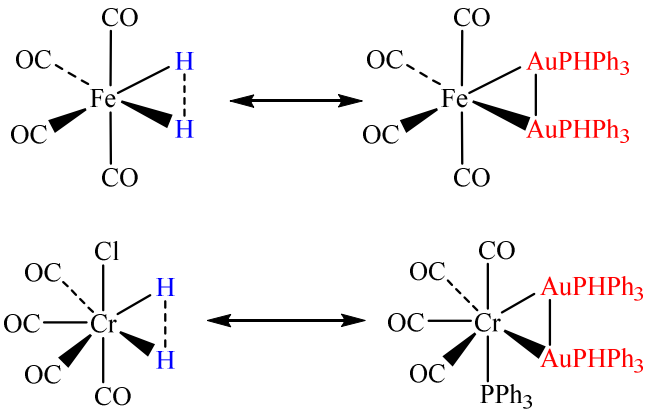

Scheme 1.12. Comparison of digold complexes to the analogous dihydride compounds.

The $AuPPh_3$ units in digold complexes tend to locate themselves in places of close proximity either by coordinating at cis positions at a common transition metal center or in neighboring positions on metal complexes. In the case of the differences between the Fe-H_2 and the Fe-Au_2 complex, the H-Fe-H angle is 100° while the Au-Fe-Au angle is 73° signifying that there is repulsion between the two H atoms and also attraction between the two Au atoms. The Au-Cr-Au angle in the complex $Co(CO)_4(PPh_3)(AuPPh_3)_2$ is 59.88° with a short Au-Au contact distance of 2.694 Å.

The Adams' group has recently investigated several examples of Phenyl-Gold (Ph-Au) and Methyl-Gold (CH_3-Au) activation by transition metal carbonyl clusters which can potentially serve as models for aromatic or aliphatic transformations at multinuclear metal sites. The introduction of gold to produce hetero-bimetallic complexes also produces enhanced catalytic activity that possesses greater catalytic activity than the monometallic counterparts. The reaction of $Os_3(CO)_{12}(NCMe)_2$ with $PhAuPPh_3$ yielded the hetero-bimetallic Os-$AuPPh_3$ carbonyl cluster complex $Os_3(CO)_{10}(\mu\text{-}C_6H_5)(\mu\text{-}AuPPh_3)$ by oxidative addition of the Ph-Au bond to the Os_3 cluster, where the phenyl and the $AuPPh_3$ unit coordinates to the cluster in an η^1-bridging fashion across the same Os-Os bond (Scheme 1.13).

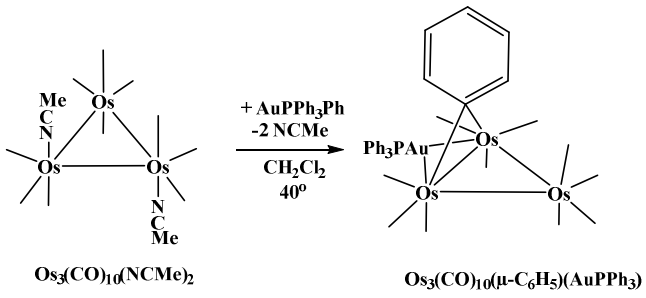

Scheme 1.13. Oxidative addition of Au-Ph bond to trisosmium cluster to form η^1-bridging phenyl ligand.

With the bridging phenyl and $AuPPh_3$ units acting as one-electron donors, the valence electron count for the Os_3 cluster is 46 electrons making the cluster formally unsaturated by two electrons. The unsaturation of the cluster was investigated by using DFT computational fragment analysis where examination of the fragments revealed π-donation from the ring to the cluster helps to relieve the unsaturation of the Os_3 cluster. Variable-temperature NMR studies of the η^1-bridging phenyl ligand revealed dynamic hindered rotation of the phenyl ligand about the metal-metal bond.[17] The η^1-bridging phenyl and η^1-bridging $AuPPh_3$ unit are coordinated in a proposed fashion to the speculated intermediate to the formation of the triply bridging benzyne ligand, where an η^1-bridging hydrido ligand would be in place of the $AuPPh_3$ unit.

Similar C-Au activations with polycyclic aromatics have been achieved from the reactions of $Os_3(CO)_{10}(NCMe)_2$ with NaphthylAuPPh$_3$ and (1-Pyryl)AuPPh$_3$ to give η^1-bridging naphthyl and pyryl ligands, respectively. Upon further heating, the η^1-bridging phenyl ligand was converted to η^3-bridging benzyne ligand accompanied by the loss of one CO from the Os_3 cluster to give the complex $HOs_3(CO)_9(\mu_3\text{-}\eta^2\text{-}C_6H_4)(AuPPh_3)$ (Scheme 1.14).

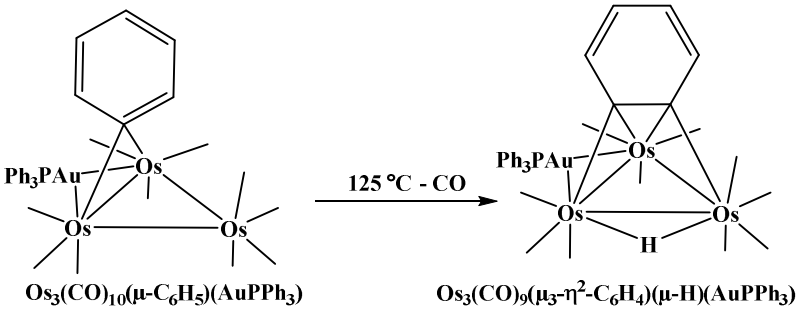

Scheme 1.14. Conversion of bridging phenyl to triply bridging benzyne on the Os_3 triangle.

The η^3-bridging benzyne ligand of $HOs_3(CO)_9(\mu_3\text{-}\eta^2\text{-}C_6H_4)(AuPPh_3)$ is analogous to the η^3-bridging benzyne ligand of $H_2Os_3(CO)_9(\mu_3\text{-}\eta^2\text{-}C_6H_4)(H)$ complex described by Johnson and Lewis from the reaction of $Os_3(CO)_{10}NCMe_2$ with benzene except for a η^1-bridging $AuPPh_3$ unit replacing one of the η^1-bridging hydrides.

The reaction of $Re_2(CO)_8[\mu\text{-}\eta^2\text{-}C(H)=C(H)^nBu](\mu\text{-}H)$ with $PhAuPPh_3$ yields the unsaturated complex $Re_2(CO)_8(\mu\text{-}AuPPh_3)(\mu\text{-}C_6H_5)$ after the oxidative addition of the Au-Ph bond across the loss of the $\mu\text{-}\eta^2$-bridging hexenyl ligand (Scheme 1.15).[12]

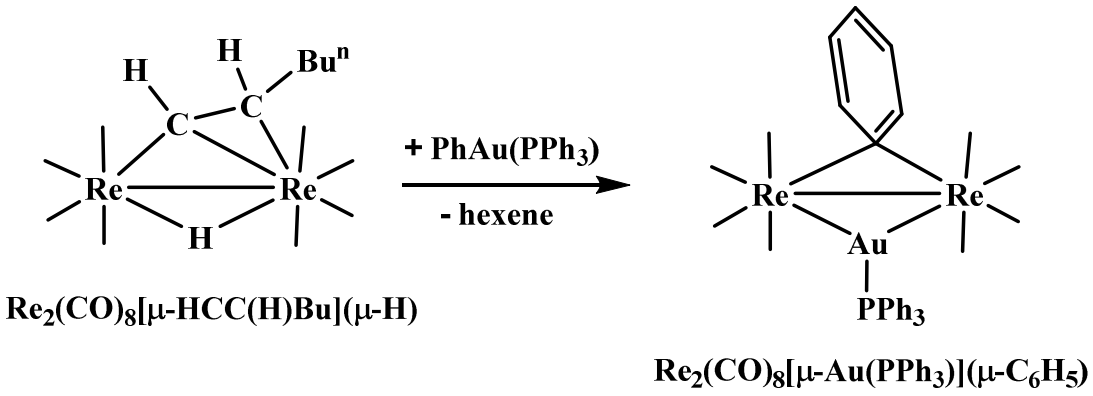

Scheme 1.15. Oxidative addition of Au-Ph bond to the dirhenium complex, $Re_2(CO)_8[\mu\text{-}\eta^2\text{-}C(H)=C(H)nBu](\mu\text{-}H)$.

The bridging $AuPPh_3$ unit of $Re_2(CO)_8(\mu\text{-}AuPPh_3)(\mu\text{-}C_6H_5)$ can be replaced by the treatment with $HSnPh_3$ to yield the complex $Re_2(CO)_8(\mu\text{-}H)(\mu\text{-}C_6H_5)$ that contains a bridging phenyl ligand and an analogous bridging hydride in the place of the $AuPPh_3$ unit, further highlighting the similar coordination modes of (H) and $AuPPh_3$ (Scheme 1.16).

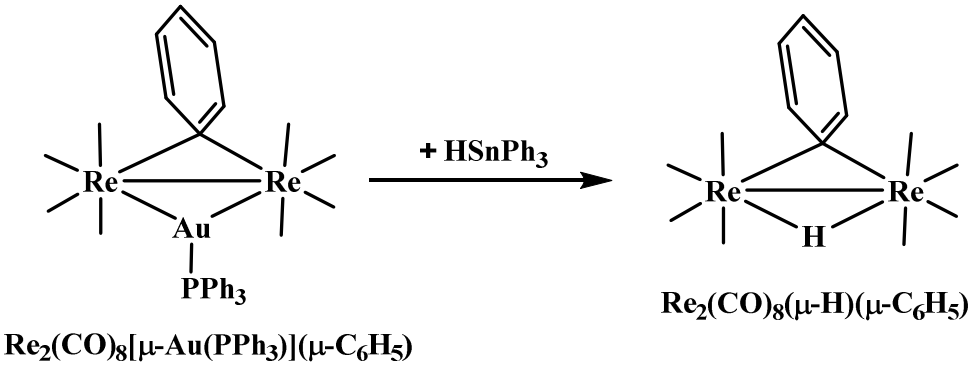

Scheme 1.16. Replacement of bridging $AuPPh_3$ with bridging H by $HSnPh_3$.

Transformations of methyl ligands were also investigated on the triosmium cluster by the oxidative addition of the C-Au bond of CH_3AuPPh_3 to the cluster. Reaction of the Os_3 cluster with $Os_3(CO)_{11}(NCMe)$ with CH_3AuPPh_3 yielded two new Os_3 cluster complexes $Os_3(CO)_{10}(\mu\text{-}O{=}CCH_3)(\mu\text{-}AuPPh_3)$ and $Os_3(CO)_9(\mu_3\text{-}CH)(\mu\text{-}H)_2(\mu\text{-}AuPPh_3)$, presumably through the proposed intermediate complex $Os_3(CO)_{11}(CH_3)(\mu\text{-}AuPPh_3)$ (Scheme 1.17).[18]

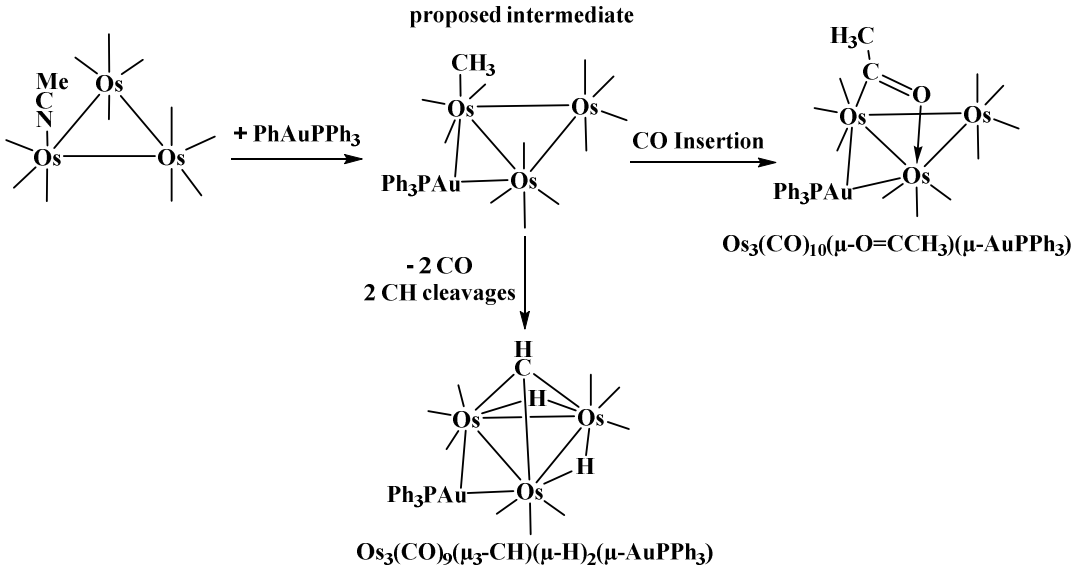

Scheme 1.17. Reaction of $Os_3(CO)_{11}(NCMe)$ with CH_3AuPPh_3 yielding complexes containing methyl derivatives.

CO insertion into the proposed terminally coordinated CH_3 intermediate, $Os_3(CO)_{11}(CH_3)(\mu\text{-}AuPPh_3)$ would yield the complex $Os_3(CO)_{10}(\mu\text{-}O{=}CCH_3)(\mu\text{-}AuPPh_3)$. Loss of two CO ligands and two successive C-H activations of the intermediate terminally coordinated CH_3 ligand leads to the triply bridging methylidyne ligand in the complex $Os_3(CO)_9(\mu_3\text{-}CH)(\mu\text{-}H)_2(\mu\text{-}AuPPh_3)$.

1.3 Syntheses and Reactivity of $Ru_6(\mu_6\text{-}C)(\mu\text{-}CO)(CO)_{16}$ and $Ru_5(\mu_5\text{-}C)(CO)_{15}$

To set the stage for this collection of work, a brief overview of the previously reported synthesis and chemistry of the transition metal carbonyl clusters highlighted in this dissertation is provided here. The high nuclearity clusters of $Ru_6(\mu_6\text{-}C)(CO)_{17}$ and $Ru_5(\mu_5\text{-}C)(CO)_{15}$, the latter being the main focus of this dissertation, syntheses were improved by Brian F. G. Johnson and Jack Lewis and the majority of the early chemistry of the clusters was investigated by them. The octahedral hexaruthenium carbido cluster, $Ru_6(\mu_6\text{-}C)(CO)_{17}$, was initially synthesized in low yield (18.7 %) by the thermal decomposition of triruthenium dodecacarbonyl, $Ru_3(CO)_{12}$, in nonane solvent, where the encapsulated carbido atom is presumed to originate from the reduction of a carbonyl (CO) ligand and carbon dioxide (CO_2) is released during the pyrolysis.[19] An improved synthesis was developed by Johnson and Lewis where $Ru_3(CO)_{12}$ is loaded into a high-pressure reactor, dissolved in octane solvent, and pressurized to 30 atm of ethylene and heated at 150 °C for 6 h.[20] Yields of 70% for $Ru_6(\mu_6\text{-}C)(CO)_{17}$ can be achieved by using this method as compared to the low yields (18.7%) produced by the previously reported pyrolysis of $Ru_3(CO)_{12}$. A slightly modified procedure that is used in the Adams' lab is shown in Scheme 1.18.

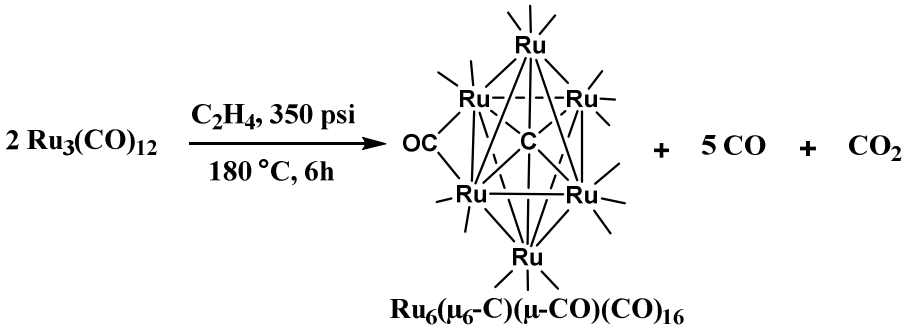

Scheme 1.18. Synthesis of the hexaruthenium carbido carbonyl cluster, $Ru_6(\mu_6\text{-}C)(\mu\text{-}CO)(CO)_{16}$.

The octahedral Ru_6C cluster consists of sixteen terminal carbonyl ligands and one μ-bridging carbonyl across one of the Ru-Ru bonds of the square of the octahedron. The encapsulated carbido carbon is bonded to all six Ru atoms of the Ru_6 cluster. With each carbonyl ligand contributing two electrons and the interstitial carbido carbon a four-electron donor, the total valence cluster electron count adds up to 86 electrons, which is consistent with an octahedral cluster of six metal atoms.[21] The Ru_6C cluster forms cluster complexes of arenes (e.g. benzene, toluene, mesitylene) to form η^6 π-arene complexes where the arene is predominately coordinated to one of the apical Ru atoms of the octahedron or as face bridging $\mu_3\text{-}\eta^2\text{:}\eta^2\text{:}\eta^2$ coordination modes of the arene have also been isolated (Scheme 1.19).[22]

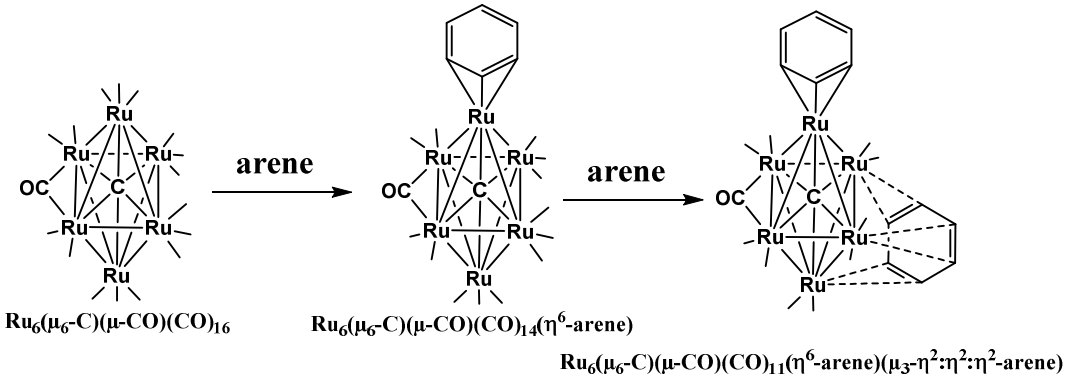

Scheme 1.19. Reactions of the Ru_6C cluster with arenes.

The Ru_6C cluster can be reduced to form its dianion by taking $Ru_6C(CO)_{17}$ in a KOH/MeOH solution to yield $[Ru_6C(CO)_{16}]^{2-}$.[20] The dianion readily reacts with electrophilic reagents such as gold phosphine cations that yield hetero-bimetallic Ru_6C-Au_2 clusters.[23]

Reaction of the hexaruthenium cluster $Ru_6C(CO)_{17}$ at 80 °C and 80 atm of CO for 4 h yields the very important pentaruthenium carbido cluster, $Ru_5(\mu_5\text{-}C)(CO)_{15}$, from the reduction of one of the apical Ru atoms yielding $Ru(CO)_5$ as a side product (Scheme 1.20).[24]

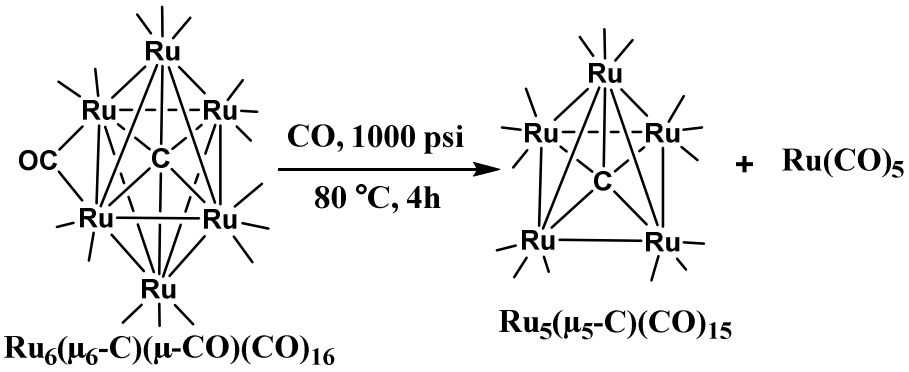

Scheme 1.20. Synthesis of the pentaruthenium carbido carbonyl cluster, $Ru_5(\mu_5\text{-}C)(CO)_{15}$, from $Ru_6C(CO)_{17}$.

The $Ru_5(\mu_5\text{-}C)(CO)_{15}$ cluster consists of a square pyramid of five ruthenium atoms with a carbido carbon that sits in the center of the square base of the pyramid and is bonded to all five ruthenium atoms. Assuming the carbido carbon acts as a four-electron donor and the fifteen linear COs as two-electron donors, the formal electron count comes to 74 valence electrons, which is consistent with a square pyramidal arragnement of five metal atoms. The square pyramidal cluster $Ru_5(\mu_5\text{-}C)(CO)_{15}$ has been shown to exhibit a remarkable chemistry based in its ability to add electron-donor ligands by a cluster opening cleavage of one its Ru-Ru bonds between the apical positioned Ru atom and one of the

basal positioned Ru atoms. When dissolved in a coordinating solvent, the Ru_5 cluster quickly reacts giving solvated adducts which can be visually observed by a solution color change from dark red to bright orange. For example, dissolving $Ru_5(\mu_5\text{-}C)(CO)_{15}$ in acetonitrile gives the compound $Ru_5(\mu_5\text{-}C)(CO)_{15}(MeCN)$ shown in Scheme 1.21.[24]

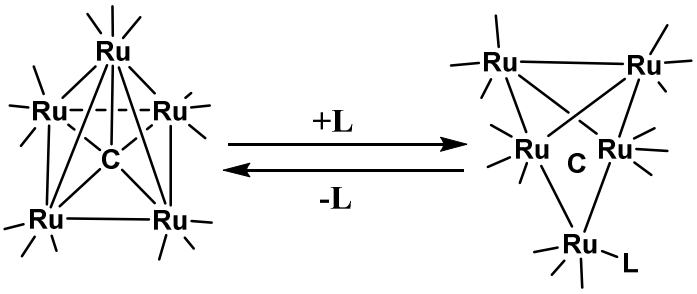

Scheme 1.21. Cluster opening cleavage of apical-to-basal Ru-Ru bond induced by coordination of donor ligands.

The structure of the solvated Ru_5 cluster can be described as that of a 'butterfly' of four ruthenium atoms with fifth ruthenium atom bridging what has been called the two 'wing tip' atoms of the butterfly. The carbido carbon serves to stabilize the open arrangement of the square pyramid and assists in the flexibility of the Ru_5C framework. The cluster valence electron count for an open square pyramid of five ruthenium atoms is 76 electrons. The reaction of the Ru_5 cluster in the presence of triethylsilane ($HSiEt_3$) under irradiation yields the open pentaruthenium square pyramidal cluster and be closed and reopened in a reversible fashion based on the loss and addition of CO shown in Scheme 1.22.[25]

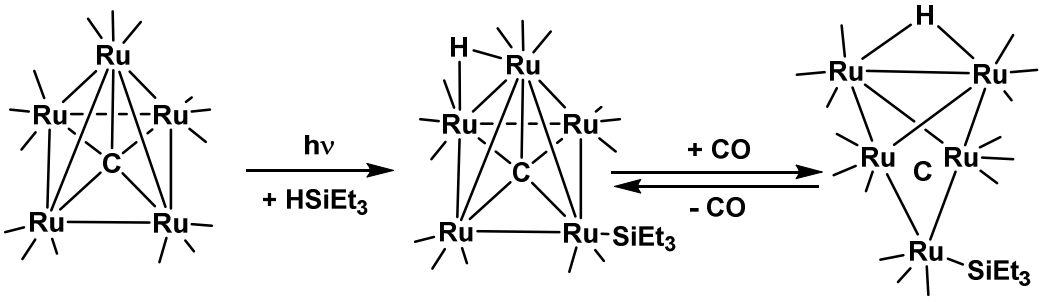

Scheme 1.22. Reaction of $Ru_5(\mu_5\text{-}C)(CO)_{15}$ with $HSiEt_3$. Reversible cluster closing and opening induced by the loss of CO ligands.

Carbonyl ligands of $Ru_5(\mu_5\text{-}C)(CO)_{15}$ can be substituted by phosphine ligands to give Ru_5C complexes of the formula $Ru_5(\mu_5\text{-}C)(CO)_{15-n}(PR_3)_n$ (n = 1 or 2 for PPh_3; n = 3 for $PMePh_2$). The monoanion of the Ru_5C cluster can be obtained by the reaction with NEt_4X (X = F, Cl, Br, or I) which yields open square pyramidal clusters of the formula $[Ru_5(\mu_5\text{-}C(CO)_{15}X]^-$. Treatment of the monoanion with H_2SO_4 gives the protonated neutral monohydrido Ru_5C complex, $Ru_5H(\mu_5\text{-}C(CO)_{15}X$. Reaction of the Ru_5C cluster with strong acid HX (X = Cl or Br) yields the monohydrido-complexes directly. Just as the octahedral Ru_6 cluster can be reduced to its dianion, the pentaruthenium Ru_5 cluster can also be reduced in a similar fashion by dissolving $Ru_5C(CO)_{15}$ in solution of KOH and methanol.[26] The dianion reacts with electrophilic reagents such as two equivalents of cations of gold phosphines $[AuPR_3][ClO_4]$ (PR_3 = PEt_3, PPh_3, or PMe_2Ph) at room temperature yielding $Ru_5C\text{-}Au_2$ hetero-bimetallic clusters of the formula $Ru_5C(CO)_{14}(AuPR_3)_2$. Reaction of $Ru_5C(CO)_{14}(AuPR_3)_2$ with CO at 80 atm and 60 C yields the butterfly complex $Ru_4C(CO)_{12}(AuPR_3)_2$ where one gold phosphine unit bridges across the 'wing-tips' and the other gold phosphine bridges the 'hinge' of the 'butterfly' (Scheme 1.24).[27]

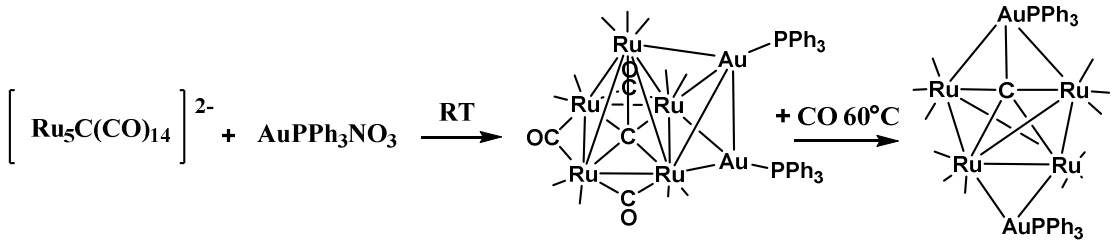

Scheme 1.23. Reaction of Ru_5C dianion with Au cation to yield the neutral digold Ru_5CAu_2 complex which reacts with CO to remove one Ru atom yielding a Ru_4CAu_2 complex.

Section 1.3 constitutes a brief review on the synthesis and early chemistry of the high nuclearity ruthenium carbido carbonyl clusters $Ru_6C(CO)_{17}$ and $Ru_5C(CO)_{15}$. The review by Takemoto and Matsuzaka gives a more recent review on the advancements of ruthenium carbide clusters including those made using the clusters Ru_6C and Ru_5C.[28]

1.4 Conclusions

With the adverse effects of increasing greenhouse gas emissions and limited natural resources, new techniques to produce fuels and commodity chemicals from hydrocarbons selectively and efficiently is much sought after. Current technologies used in industry to convert hydrocarbons to useful products require high temperatures and offer limited selectivity over the products formed. Transition metal complexes can potentially be used to selectively activate and functionalize carbon-hydrogen bonds at mild conditions without the use of harsh reagents. As a mimic to C-H activation, carbon-gold (C-Au) activation can be used to oxidatively add hydrocarbon fragments in the form of C_6H_5 and CH_3 to polynuclear transition metal carbonyl clusters and the transformations of the hydrocarbon fragments can then be studied. By understanding the chemistry of the high nuclearity clusters, $Ru_6(C)(CO)_{17}$ and $Ru_5(C)(CO)_{15}$, they can then be used to study the activations and transformation of C-Au and C-H bonds.

1.5 References

(1) (a) Rostrup-Nielsen, J. R.; Shested, J.; Nørskov, J. K. *Adv. Catal.* **2002**, 47, 65-139. (b) Rostrup-Nielsen, J. R., *Catalysis*, Springer, Berlin, Heildelberg, 1984, chapter 1, pp 1 – 117.

(2) (a) Fischer, F.; Tropsch, H. Brennst. *Chem*. **1923**, 4, 276-285. (b) Fischer, F.; Tropsch, H. Brennst. *Chem*. **1926**, 4, 97-104. (c) Maitlis, P. M.; Zanotti, V. *Chem. Comm.* **2009**, 0 (13), 1619-1634. Kim, J.; Lee, S.; Cho, K.; Na, K.; Lee, C.; Ryoo, R. *ACS Catal*. **2014**, 4, 3919-3927.

(3) (a) Kirste, B.; Kurreck, H. *J. Am. Chem. Soc*. **1980**, 102, 6181-6182. (b) Rostrup-Nielsen, J. R., *Advance in Catalysis*, Elsevier, Amsterdam, Netherlands, 2011, chapter 3, pp 127-186. (c) Filot, I. A. W.; van Santen; R. A.; Hensen, E. J. M. *Angew. Chem. Int. Ed.* **2014**, 53, 12746-12750. (d) Schweicher, J.; Bundhoo, A.; Kruse, N. *J. Am. Chem. Soc*. **2012**, 134, 16135-16138.

(4) (a) Rahimi, N.; Karimzadeh, R. *Appl. Catal. A.* **2011**, 398, 1-17. (b) Mokrani, T.; Scurrell, M. *Catal. Rev.* **2009**, 51, 1-145. (c) Ren, T.; Patel, M. K.; Blok, K. *Energy*. **2008**, 33, 817-833.

(5) Neelis, M.; Patel, M.; Blok, K.; Haije, W.; Bach, P. *Energy*. **2007**, 32, 1104-1123.

(6) Luom Y.-R.; *Comprehensive Handbook of Chemical Bond Energies*, CRC Press, Boca Ratón, Fl, 2007.

(7) (a) Balcells, D.; Clot, E.; Eisenstein, O., *Chem. Rev.*, **2010**, 110, 749–823. (b) Crabtree, R. H.; *J. Organomet. Chem*. **2004**, 689, 4083–4091. (c) Shi-lov, A. E.; Shul'pin, G. B.,

Chem. Rev. **1997**, 97, 2879-2932. (d) Labinger, J. A.; Bercaw, J. E., *Nature* **2002**, 417, 507–514. (e) Bergman R. G., *Nature* **2007**, 446, 391–393. (f) Caballero, A.; Pérez, P. J., *Chem. Soc. Rev.* **2013**, 42, 8809–8820. (g) Gunay, A; Theopold, K. H., *Chem. Rev*. **2010**, 110, 1060–1081. (h) Hall, C.; Perutz, R. N., *Chem. Rev*. **1996**, 96, 3125–3146. (i) Rudakov, E. S.; Shul'pin, G. B., *J. Organomet. Chem*. **2015**, 793, 4–16. (j) Labinger, J. A.; Bercaw, J. E., *J. Organomet. Chem*. **2015**, 793, 47–53. (k) Webb, J. R.; BolaÇo, T.; Gunnoe, T. B., *ChemSusChem* **2011**, 4, 37–49. (l) Lersch, M.; Tilset, M., *Chem. Rev.* **2005**, 105, 2471–2526. (m) Jones, W. D.; Feher, F. J., *Acc. Chem. Res*. **1989**, 22, 91-100 (n) Jones, W. D., *Acc. Chem. Res*. **2003**, 36, 140–146. (o) Koppaka, A.; Captain, B., *Inorg. Chem*. **2016**, 55, 2679−2681. (p) Wencel-Delord, J.; Dröge, T.; Liu, F.; Glorius, F. *Chem. Soc. Rev.* **2011**, 40, 4740-4761.

(8) Shilov, A. E.; Shulpin, G. B. Russ. *Chem. Rev.* **1987**, 56, 442-464. (b) Luinstra, G. A.; Wang, L.; Stahl, S. S.; Labinger, J. A.; Bercaw, J. E. *J. Organmet. Chem.* **1995**, 504, 75-91.

(9) (a) Periana. R. A. *Science* **1998**, 280, 560-564. (b) Hashiguchi, B. G.; Bischof, S. M.; Konnick, M. M.; Periana, R. A. *Acc. Chem. Res*. **2012**. 45. 885-898.

(10) Boisvert, L.; Goldberg, K. I. *Acc. Chem. Res*. **2012**, 45, 899-910.

(11) Goudsmit, R. J.; Johnson, B. F. G.; Lewis, J.; Raithby, P. R.; Rosales, M. J., *J. Chem. Soc., Dalton Trans.* **1983**, 2257−2261.

(12) Adams, R. D.; Rassolov, V.; Wong, Y. O., *Angew. Chem.* **2016**, 55, 1324-1327.

(13) (a) Hoffmann, R., *Angew. Chem., Int. Ed*. **1982**, 21, 711. (b) Elian, M.; Chen, M. M.-L.; Mingos, D. M. P.; Hoffmann, R. *Inorg. Chem.* **1976**, 15, 1148.

(14) Raubenheimer, H. G.; Schmidbaur, H. *Organometallics* **2012**, 31, 2507-2522.

(15) Tsui, E. Y.; Müller, P.; Gray, T. G.; Sadighi, J. P. *Organometallic*. **2005**, 24, 4503.

(16) Adams, R. D.; Rassolov, V.; Zhang, Q. *Organometallics*. **2013**, 32, 6368-6378.

(17) Adams, R. D.; Rassolov, V.; Zhang, Q. *Organometallics*. **2013**, 32, 1587-1590.

(18) Adams, R. D.; Chen, M.; Luo, Z.; Rassolov, V. *J. Organomet. Chem.* **2016**, 812, 95-107.

(19) Johnson, B. F. G.; Johnston, R. D.; Lewis, J., *Inorg. Phys. Theor*. **1968**, 0, 2865-2868.

(20) Johnson, B. F. G.; Lewis, J.; Sankey, S. W.; Wong, K.; McPartlin, M.; Nelson, W. J. H., *J. Organomet. Chem*. **1980**, 191, C3-C7.

(21) Mingos, D. M. P. *Acc. Chem. Res.* **1984**, 17, 311 – 319.

(22) (a) Dyson, P. J.; Johnson, B. F. G.; Lewis, J.; Martinelli, M.; Braga, D.; Grepioni, F. *J. Am. Chem. Soc*. (b) Braga, D.; Grepioni, F.; Parisini, E.; Dyson, P. J.; Blake, A. J.; Johnson, B. F. G. *J. Chem. Soc. Dalton Trans.* **1993**, 2951-2957. (c) Borchert, T.; Lewis, J.; Raithby, P. R.; Shields, G. P.; Wadepohl, H. *Inorganica Chimica Acta*, **1998**, 274, 201-209.

(23) Bunkhall, S. R.; Holden, H. D.; Johnson, B. F. G.; Lewis, J.; Pain, G. N.; Raithby, P. R.; Taylor, M. J. *J. Chem. Soc. Chem. Commun*. **1984**, 25.

(24) Johnson, B. F. G.; Lewis, J.; Nicholls, J. N.; Puga, J.; Raithby, P. R.; Rosales, M. J. *J. Chem. Soc. Dalton Trans.* **1983**, 277-290.

(25) Adams, R. D.; Captain, B.; Fu, W. *Organometallics.* **2000**, 19, 3670-3673.

(26) Johnson, B. F. G.; Lewis, J.; Nicholls, J N.; Puga, J.; Raithby, P. R.; Rosales, M. J.; Schroder, M.; Vargas, M. D. *J. Chem. Soc. Dalton Trans.,* **1983**, 0, 2447.

(27) Cowie, A. G.; Johnson, B. F. G.; Lewis, J.; Raithby, P. R. *J. Chem. Soc., Chem. Commun.*, **1984**, 0, 1710-1712.

(28) Takemoto, S.; Matsuzaka, H. *Coord. Chem. Rev.* **2012**, 256, 574-588.

CHAPTER 2

Phenyl–gold complexes of Ru_6 and Ru_5 carbonyl clusters [1]

[1] Adams, R. D.; Tedder, J.; Wong, Y. O. *J. Organomet. Chem.* **2015**, 795, 2-10.
Reprinted here with permission from publisher

2.1 Introduction

Interest in the organometallic chemistry of gold has grown rapidly following the discoveries that gold complexes exhibit high activity for variety of homogeneous transformations of hydrocarbons.[1,2] Catalytic transformations of organic compounds by gold clusters[3] and nanoparticles[4] have also attracted considerable interest. Certain bimetallic catalysts containing gold exhibit catalytic activity that is superior to that of pure gold.[5]

Bimetallic cluster complexes containing gold have been synthesized by a variety of methods.[6] In recent studies we have found that alkyl- and arylgoldphosphine compounds, such as $(PPh_3)AuR$, R = Me, Ph, Np, Py etc. can be conveniently, oxidatively added to activated 3rd row polynuclear metal carbonyl cluster complexes to yield metal carbonyl cluster complexes containing alkyl and aryl ligands with bridging gold phosphine groupings, e.g. Eqs. (2.1)–(2.3).[7-9] In some cases, the aryl ligands have adopted unusual bridging coordination modes that can result in interesting physical and chemical properties, such as hindered rotation about the metal–metal bond.[10]

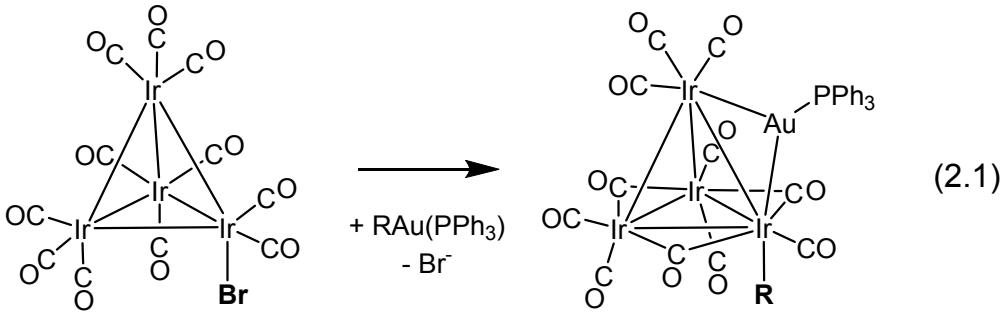

$[Ir_4(CO)_{11}Br]^-$ $Ir_4(CO)_{11}(R)[\mu\text{-}Au(PPh_3)]$, R = CH_3, C_6H_5, 2-$C_{16}H_9$ (2.1)

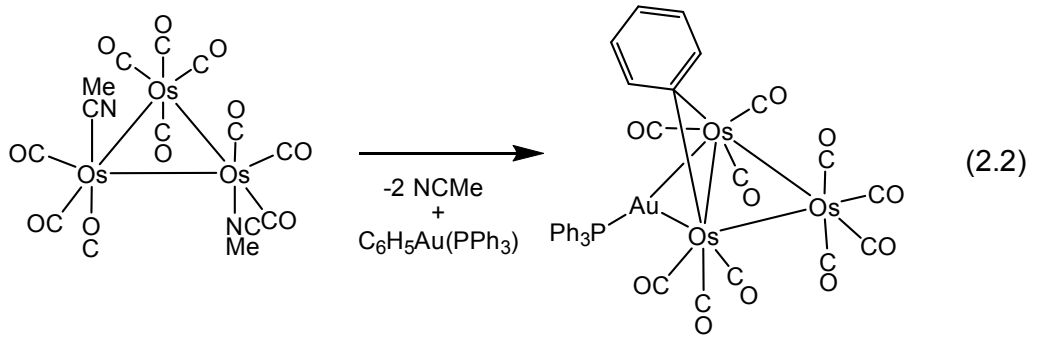

$Os_3(CO)_{10}(NCMe)_2$ $Os_3(CO)_{10}(\mu\text{-}C_6H_5)[\mu\text{-}Au(PPh_3)]$ (2.2)

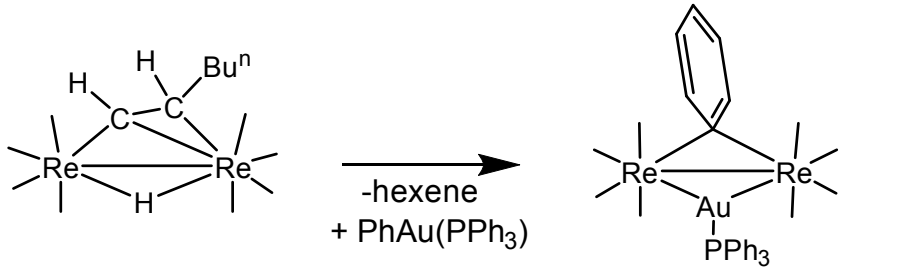

$Re_2(CO)_8[\mu\text{-}HCC(H)Bu](\mu\text{-}H)$ $Re_2(CO)_8[\mu\text{-}Au(PPh_3)](\mu\text{-}C_6H_5)$ (2.3)

We have now investigated the reactions of $Ru_6(C)(CO)_{17}$, **2.1** and $Ru_5(C)(CO)_{15}$, **2.2** with (NHC)AuPh, NHC = 1,3-bis(2,6-diisopropylphenyl-imidazol-2-ylidene). The reaction of **2.1** with (NHC)AuPh yielded the π-arene complex $Ru_6C(CO)_{14}[\eta^6$-PhAu(NHC)], **2.3** without cleavage of the Au–C bond. On the other hand, the reaction of **2.2** with (NHC)AuPh yielded the complexes $Ru_5C(CO)_{14}$(Ph)[μ-Au(NHC)], **2.4** and $Ru_5C(CO)_{13}(\mu\text{–}\eta^2$-Ph)[μ-Au(NHC)], **2.5** by oxidative-addition of the Au–C bond at the ruthenium atoms. Compounds **2.4** and **2.5** were found to react with CO at 1 atm to yield the CO insertion product $Ru_5C(CO)_{14}(\mu\text{–}\eta^2$-O═CPh)[μ-Au(NHC)], **2.6** that contains a bridging benzoyl ligand in an opened Ru_5 cluster complex. The synthesis, structures and interrelationships of these new complexes are described in this report.

2.2 Experimental Data

General Data

Reagent grade solvents were dried by the standard procedures and were freshly distilled prior to use. Infrared spectra were recorded on a Thermo Nicolet Avatar 360 FT-IR spectrophotometer. ^{1}H NMR spectra were recorded on a Varian Mercury 300 spectrometer operating at 300.1 MHz. Variable temperature ^{1}H NMR spectra were recorded on a Bruker AVANCE III spectrometer operating at 400 MHz. Mass spectrometric (MS) measurements were performed by a direct-exposure probe by using electron impact ionization (EI) for compound **2.3**. Positive/negative ion mass spectra were recorded on a Micromass Q-TOF instrument by using electrospray (ES) ionization for compounds **2.4**, **2.5**, and **2.6**. $Ru_3(CO)_{12}$ was obtained from STREM and was used without further purification. $Ru_6(C)(CO)_{17}$, **2.1**, and $Ru_5(C)(CO)_{15}$, **2.2** were prepared according to previously reported procedures.[11,12] 1,3-[Bis(2,6-diisopropylphenyl-imidazol-2-ylidene)]gold(I) chloride = (NHC)AuCl was obtained from STREM and was used without further purification. (NHC)AuPh was prepared from (NHC)AuCl by a slightly modified version of the reported procedure.[13] The (NHC)AuPh was verified spectroscopically by comparisons to that of the reported compound.[13] Product separations were performed by TLC in air on Analtech 0.25 mm silica gel 60 Å F254 glass plates.

Reaction of 2.1 with (NHC)AuPh

25 mg (0.023 mmol) of **2.1** was added to a 100 mL three-neck flask with a solution of 22.7 mg (0.034 mmol) of (NHC)AuPh in 25 mL of octane. After heating to reflux for 12 h, the solvent was removed in vacuo, and the product was then isolated by using TLC to yield 51.9 of $Ru_6C(CO)_{14}[\eta^6$-PhAu(NHC)], **2.3** (68% yield). Spectral data for **2.3**: IR

νCO (cm−1 in hexane): 2070(s), 2026(sh), 2019(s), 2000(w), 1990(w), 1978(m), 1965(w). ^{1}H NMR (CD_2Cl_2, in ppm) δ = 7.51 (t, 9 Hz, 2H, para CH–$(CH)_2$), 7.31 (d, 9 Hz, 4H, meta CH–$(CH)_2$), 7.20 (s, 2H, N$(CH)_2$), 5.24 (t, 6 Hz, 2H, meta-CH–$(CH)_2$–$(CH)_2$), 5.03 (t, 6 Hz, 1H, para-CH–$(CH)_2$–$(CH)_2$), 4.95 (d, 6 Hz, 2H, ortho-CH–$(CH)_2$–$(CH)_2$), 2.63 (sept, 6 Hz, 2H, CH–$(CH_3)_2$), 1.36 (d, 6 Hz, 12H, CH–$(CH_3)_2$), 1.19 (d, 6 Hz, 12H, CH–$(CH_3)_2$). Mass spec. EI/MS m/z. 1674.

Reaction of 2.2 with (NHC)AuPh

27 mg (0.028 mmol) of **2.2** was added to a 100 mL three-neck flask with a solution of 27.5 mg (0.041 mmol) of (NHC)AuPh in 25 mL of heptane. After refluxing for 3.5 h, the solvent was removed in vacuo, and the products were then isolated by using TLC to yield in order of elution: 11.4 mg of $Ru_5C(CO)_{13}$(μ–η^2-Ph)[μ-Au(NHC)], **2.5**, (26% yield), and 4.8 mg of $Ru_5C(CO)_{14}$(Ph)[μ-Au(NHC)], **2.4** (11% yield). Spectral data for **2.4**: IR νCO (cm−1 in hexane): 2056(s), 2043(m), 2024(m), 2016(s). ^{1}H NMR (CD_2Cl_2, in ppm) δ = 7.45 (t, 6 Hz, 2H, para CH–$(CH)_2$), 7.31 (d, 6 Hz, 4H, meta CH–$(CH)_2$), 7.13 (s, 2H, N$(CH)_2$), 6.88–6.91 (m, 2H, Ru–Ph), 6.65–6.67 (m, 3H, Ru–Ph), 2.76 (sept, 6 Hz, 4H, CH–$(CH_3)_2$), 1.37 (d, 6 Hz, 12H, CH–$(CH_3)_2$), 1.13 (d, 6 Hz, 12H, CH–$(CH_3)_2$). (EI+/MS: m/z 1574 (M+)). Spectral data for **2.5**: IR νCO (cm−1 in hexane): 2071(m), 2038(vs), 2024(s), 2013(vs) 2006(vs), 1987(w), 1974(w). ^{1}H NMR (at −55 °C, CD_2Cl_2, in ppm) δ = 8.20 (d, 8 Hz, 1H, ortho-Ru–Ph), 7.64 (t, 8 Hz, 1H, meta-Ru–Ph), 7.44 (t, 8 Hz, 2H, para CH–$(CH)_2$), 7.30 (d, 8 Hz, 4H, meta CH–$(CH)_2$), 7.21 (t, 8 Hz, 1H, para-Ru–Ph), 7.17 (s, 2H, N$(CH)_2$), 6.94 (t, 8 Hz, 1H, meta-Ru–Ph), 5.51 (dd, 8 Hz, 1H, ortho-Ru–Ph), 2.80 (sept, 8 Hz, 4H, CH–$(CH_3)_2$), 1.39 (d, 8 Hz, 12H, CH–$(CH_3)_2$), 1.15 (d, 8 Hz, 12H, CH–$(CH_3)_2$). EI+/MS: m/z 1545 (M+).

Reaction of 2.4 with CO

11.8 mg (0.0075 mmol) of **2.4** was dissolved in 20 mL of dichloromethane in a 100 mL three-neck flask. Reaction mixture was purged with CO at room temperature for 10 min. The solvent was removed in vacuo, and the products were then isolated by TLC to provide 8.6 mg (72% yield) of pure orange $Ru_5C(CO)_{14}$(μ–η2-OCPh)[μ-Au(NHC)], **2.6**. Spectral data for **2.6**: IR νCO (cm−1 in hexane): 2092(m), 2056(m), 2048(vs), 2030(s), 2018(w), 1998 (m), 1986(m). 1H NMR (CD_2Cl_2, in ppm) δ = 7.24–7.43 (m, 9H, para CH–$(CH)_2$), meta CH–$(CH)_2$, C–C_6H_5), 7.12 (s, 2H, N$(CH)_2$), 2.89 (sept, 6 Hz, 4H, CH–$(CH_3)_2$), 1.34 (d, 6 Hz, 12H, CH–$(CH_3)_2$), 1.15 (d, 6 Hz, 12H, CH–$(CH_3)_2$). EI+/MS: m/z 1602 (M+).

Reaction of 2.5 with CO

15.7 mg (0.010 mmol) of **2.5** was dissolved in 20 mL of dichloromethane in a 100 mL three-neck flask. Reaction mixture was purged with CO at room temperature for 30 min. The solvent was removed in vacuo, and the products were then isolated by TLC to provide 10.0 mg (61% yield) of **2.6**.

Thermal conversion of 2.6 to 2.5

8.6 mg (0.0054 mmol) of **2.6** was dissolved in 20 mL of octane in a 100 mL three-neck flask. Reaction mixture was heated to reflux for 30 min. The solvent was removed in vacuo, and the products were then isolated by TLC to provide 2.6 mg (31% yield) of **2.5**.

Transformations of 2.4 to 2.5

(a) Thermal. 10.2 mg (0.0065 mmol) of **2.4** was dissolved in 20 mL of heptane in a 50 mL three-neck flask. Reaction mixture was heated to reflux for 2.5 h. The solvent was removed in vacuo, and the products were then isolated by TLC to provide 5.2 mg (52% yield) of **2.5**.

(b) By irradiation. 19.0 mg (0.012 mmol) of **2.4** was dissolved in 20 mL of benzene in a 100 mL three-neck flask. A slow stream of nitrogen was allowed to flow through the flask and was irradiated using a tungsten lamp for 12.5 h. The solvent was removed in vacuo, and the product was then isolated by TLC to provide 4.1 mg (22% yield) of **2.5**.

Crystallographic analyses

Dark red single crystals of **2.3**, **2.4**, and **2.5** suitable for x-ray diffraction analyses were obtained by slow evaporation of solvent from an octane/benzene solvent mixture at room temperature. Orange single crystals of **2.6** suitable for x-ray diffraction analysis were obtained by slow evaporation of solvent from an octane/benzene mixture at room temperature. Each data crystal was glued onto the end of a thin glass fiber. X-ray intensity data were measured by using a Bruker SMART APEX CCD-based diffractometer by using Mo Kα radiation (λ = 0.71073 Å). The raw data frames were integrated with the SAINT+ program by using a narrow-frame integration algorithm.[14] Correction for Lorentz and polarization effects were also applied with SAINT+. An empirical absorption correction based on the multiple measurements of equivalent reflections was applied using the program SADABS.[14] All structures were solved by a combination of direct methods and difference Fourier syntheses, and refined by full-matrix least squares refinement on F^2 by

using the SHELXTL software package.[15] All nonhydrogen atoms were refined with anisotropic thermal parameters. All hydrogen atoms were placed in geometrically idealized positions and were included as standard riding atoms during the final least-squares refinements. Compounds **2.4** and **2.5** crystallized in the triclinic crystal system. The space group P-1 was assumed and confirmed by the successful solution and refinement of each structure. Compounds **2.3** and **2.6** crystallized in the monoclinic crystal system. The space groups $P2_1/n$ and $P2_1/c$, respectively, were identified uniquely on the basis of systematic absences observed in the intensity data. Crystal data, data collection parameters, and results for the analyses are listed in Table 2.1.

2.3 Results

The reaction of **2.1** with (NHC)AuPh in a solution in octane solvent heated to reflux for 12 h yielded the π-arene complex $Ru_6C(CO)_{14}[\eta^6$-PhAu(NHC)], **2.3** in 68% yield. Compound **2.3** was characterized by a combination of IR, mass spectrum, 1H NMR spectroscopy and a single-crystal X-ray diffraction analysis. An ORTEP diagram of the molecular structure of compound **2.3** is shown in Fig. 2.1. The structure of **2.3** is analogous to a number of other (arene)Ru_6C cluster complexes that have been structurally characterized except that the arene group in **2.3** contains a pendant Au(NHC) group.[16] The Ru–C distances to the coordinated phenyl ring, 2.215(5)–2.297(4) Å, (the longest is the bond to the gold substituted carbon atom) are similar to those of the other arene complexes, The Au1–C1 distance to the phenyl ring is 2.025(4) Å is similar to that of the uncoordinated parent molecule (NHC)AuPh, 2.01(3)–2.09(3).[17]

By contrast, no Au-arene coordinated complexes were obtained from the reaction of **2.2** with (NHC)AuPh. Instead, two new complexes $Ru_5C(CO)_{14}$(Ph)[μ-Au(NHC)], **2.4**

and $Ru_5C(CO)_{13}(\mu-\eta^2\text{-Ph})[\mu\text{-Au(NHC)}]$, **2.5** formed by oxidative-addition of the Au–C bond of the (NHC)AuPh at the ruthenium atoms were obtained in 11% and 26% yields, respectively, after refluxing a solution of **2.2** and (NHC)AuPh for 3.5 h in heptane solvent. Compound **2.4** can be converted to **2.5** by decarbonylation: 52% yield thermally and 22% yield by irradiation (tungsten lamp). Both compounds were characterized by a combination of IR, mass spec, 1H NMR and a single-crystal X-ray diffraction analyses. An ORTEP diagram of the molecular structure of **2.4** as found in the solid state is shown in Fig. 2.2.

Compound **2.4** consists of a square pyramidal cluster of five ruthenium atoms with a carbide ligand in the base of the square pyramid. This portion of the molecule is analogous to many other square pyramidal Ru_5C structures that have been reported previously.[18] An (NHC)Au group bridges the apical–basal Ru(1)–Ru(2) bond of the cluster. The Ru–Au bond distances in 4, Ru1–Au1 = 2.8083(5) Å, Ru2–Au1 = 2.8318(6) Å, are similar to those found in other gold-containing ruthenium cluster complexes: $Ru_6C(CO)_{16}[\mu\text{-Au}(PMePh_2)]_2$, 2.788(1) Å, 2.758(1) Å[19] and $Ru_5C(CO)_{13}(NO)[\mu\text{-Au}(PEt_3)]$, 2.792(2) Å, 2.748(2) Å[20]. There is a terminally coordinated σ-phenyl ligand located in an axial position on the basal ruthenium atom Ru(4) which is positioned on the opposite side of the cluster from the bridging gold atom. The Ru–C distance to the phenyl ligand, Ru(4)–C(2) = 2.091(7) Å is typical of an Ru–C σ-phenyl bond in ruthenium complexes, e. g. 2.096(3) Å in $Ru_3(CO)_5(Ph)(\mu_3\text{-PPhCH}_2\text{PPh}_2)(\mu_3\text{-}C_8H_8)$.[21] Interestingly, the Ru–Ru bond that lies approximately trans to this phenyl ligand, Ru1–Ru4 = 3.0072(7) Å, is the longest one in the cluster. This could be the result of a strong structural trans influence produced by the phenyl ligand. Compound **2.4** contains fourteen terminally-coordinated carbonyl ligands distributed as shown in Fig. 2.2. Assuming that the Ph ligand

and Au(NHC) group donate one electron each to the cluster, the cluster then contains 74 valence electrons which is precisely the number required for a square pyramidal cluster of five metal atoms.[22]

An ORTEP diagram of the molecular structure of **2.5** as found in the solid state is shown in Fig. 2.3. Compound **2.5** consists of a square pyramidal Ru_5C cluster similar to that of **2.4** with an (NHC)Au group bridging the same apical-basal Ru(1)–Ru(2) bond of the cluster. The Ru–Au bond distances, Ru1–Au1 = 2.7906(4) Å, Ru2–Au1 = 2.8338(4) Å, are also similar to those found in **2.4**. Compound **2.5** contains only thirteen carbonyl ligands. Formally, one CO ligand was lost from the atom Ru(3) in **2.4**. In order to make up for this loss electrons, the phenyl ligand has adopted an η^2-bridging coordination that involves a π-donation from the ring to Ru(3) and it thus serves as a three-electron donor. Ring atoms C(2) and C(3) are π-coordinated to Ru(3) and Ru3–C2 = 2.314(4) Å, Ru3–C3 = 2.387(4) Å, while C(2) remains σ-coordinated to Ru(4), Ru4–C2 = 2.082(4) Å. σ, π-coordinated bridging phenyl ligands have been reported previously.[23] Interestingly, the room temperature H NMR spectrum of **2.5** shows only one resonance, a triplet (1H), at 7.25 ppm for the σ, π-coordinated phenyl ligand. Suspecting dynamical activity for this ligand, a variable temperature (VT) study was undertaken. A stacked plot of the VT NMR spectra of **2.5** in the phenyl region of the spectrum is shown in Fig. 2.4.

At −55 °C, five resonances are observed at δ = 8.20 (dd, J_{H-H} = 8 Hz, 1H, ortho-Ph), 7.64 (t, J_{H-H} = 8 Hz, 1H, meta-Ru–Ph), 7.21 (t, J_{H-H} = 8 Hz, 1H, para-Ph), 6.94 (t, J_{H-H} = 8 Hz, 1H, meta-Ph), 5.51 (dd, J_{H-H} = 8 Hz, 1H, ortho-Ph). The doublets at 8.20 and 5.51 ppm are assigned to the two inequivalent ortho-hydrogens. The triplets at 7.64 and 6.94 ppm are assigned to the two inequivalent meta-hydrogens. The triplet at 7.21 ppm is assigned to the

para-hydrogen atom on the phenyl ring. As the temperature is raised the resonances at 8.20 and 5.51 ppm and 7.64 and 6.94 ppm broaden and collapse into the baseline. The resonance of the para-hydrogen atom at 7.21 ppm is unchanged throughout this temperature range. These observations can be explained by a dynamical exchange process. Unfortunately, efforts to obtain spectra in the fast exchange region were unsuccessful due to decomposition of the complex at the high temperatures required for this. However, assuming room temperature to be the approximate coalescence temperature, one can estimate that rate of exchange, and in turn, the activation energy for the process to be $\Delta G* = 13.7(2)$ kcal/mol.

A proposed mechanism for the exchange process is shown in Fig. 2.5. In this process the η^2-phenyl ligand is converted to a η^1-bridging ligand in the intermediate I. The phenyl ligand can then undergo a 180° rotation at the bridging carbon atom and then return to the bridging η^2-mode as represented in the equivalent structure **2.5′**. While the rotation of the η^1-bridging ligand in I is not expected to be unhindered, it has been shown in osmium cluster complexes it can occur readily on the ^{1}H NMR time scale.[10] There is also an alternative mechanism (not shown in the scheme) that would involve a shift of the bridging phenyl ligand to a terminal site such as that found in **2.4** accompanied by the creation of a vacant coordination site on the neighboring metal atom. After a 180° rotation, the phenyl ligand could move back to the bridging position to complete the exchange process. We think the creation of a vacant coordination site would be energetically less favorable than the process shown in Fig. 2.5 and thus prefer the one in Fig. 2.5.

When allowed to react with CO at 25 °C (1 atm), compounds **2.4** and **2.5** were converted to the new compound $Ru_5C(CO)_{14}(\mu\text{–}\eta^2\text{-OCPh})[\mu\text{-Au(NHC)}]$, **2.6** (72% yield in

10 min from **2.4**). Compound **2.6** was characterized by a combination of IR, mass spec, ^{1}H NMR and a single-crystal X-ray diffraction analyses. An ORTEP diagram of the molecular structure of **2.6** is shown in Fig. 2.6.

Compound **2.6** consists of an open Ru_5C cluster consisting of a carbide-bridged Ru_4 butterfly cluster with an (NHC)Au group bridging the hinge metal atoms Ru(1)–Ru(2) of the cluster. The fifth ruthenium atom, Ru(4), bridges the wingtip atoms Ru(3) and Ru(5) of the butterfly. The Ru – Au bond distances, Ru(1)–Au(1) = 2.8470(8) Å, Ru(2)–Au(1) = 2.8189(8) Å, are also similar to those found in **2.4** and **2.5**. Compound **2.6** contains fourteen linear carbonyl ligands distributed as shown in Fig. **2.6**. The most interesting ligand is the benzoyl group, Ph–C(1)–O(1), that bridges the nonbonded pair of ruthenium atoms Ru(1) and Ru(4). Atom C(1) is bonded to Ru(1), Ru1–C1 = 2.025(9) Å and the oxygen atom O(1) is bonded to Ru(4), Ru(4)–O(1) = 2.110(6) Å. The CO bond distance is 1.287(1) Å. Bridging-η^2-benzoyl ligands have been observed previously in open ruthenium carbonyl cluster complexes.[24] The metal atoms of the cluster of **2.6** contain a total of 76 valence electrons which is consistent with that of an "open" square pyramidal cluster of five metal atoms.[22]

2.4. Discussion and conclusions

It is well known that **2.1** reacts with arenes to yield η^6-arene complexes[16]; thus, the formation of **2.2** from the reaction of **2.1** with (NHC)AuPh is not too surprising, Scheme 2.1. The reaction of **2.2** with (NHC)AuPh proceeds formally by the oxidative addition of the Au–C bond of the gold complex to the cluster accompanied by the loss of CO ligands to yield **2.4** and **2.5**, respectively, Scheme 2.2. A number of years ago, Johnson and Lewis reported that **2.2** reacts with $Au(PPh_3)Cl$ by oxidative addition of the Au–Cl bond without

loss of CO to yield the open cluster complex $Ru_5C(CO)_{15}(Cl)[\mu\text{-}Au(PPh_3)]$, **2.7** having the chloro ligand on the bridging ruthenium atom, see Scheme 2.3.[25] Adams et al. have reported that $HSiEt_3$ can be oxidatively added to **2.2** to yield the two complexes, $Ru_5C(CO)_{15}(SiEt_3)(\mu\text{-}H)$ and $Ru_5C(CO)_{14}(SiEt_3)(\mu\text{-}H)$ which have open and closed cluster structures analogous to **2.7** and **2.4**, respectively, and these two silyl complexes can be interconverted by the addition and elimination of a CO ligand.[26] It is quite likely that **2.2** initially reacts with (NHC)AuPh in a cluster-opening first step, but it then loses CO to reform the Ru–Ru bond leaving the Ph ligand in an axial position on one of the basal Ru atoms to yield **2.4**.

When compound **2.4** is heated or irradiated, it eliminates CO and the phenyl ligand shifts to a bridging position and serves as a three-electron donor in order to preserve the 74 electron configuration as found in the compound **2.5**. Interestingly, compounds **2.4** and **2.5** both add CO to form the open cluster **2.6** containing the bridging benzoyl ligand. This process clearly involves the insertion of one CO ligand into the Ru–C bond of the phenyl ligand. Some ligand shifts and rearrangements will be required to produce the exact geometry found in **2.6**, but we think it would be premature to speculate about the nature of these rearrangements in absence of any additional information.

Table 2.1. Crystallographic Data for Compounds **2.3** and **2.4**

Compound	**2.3**	**2.4**
Empirical formula	$Ru_6AuO_{14}N_2C_{54}H_{48}$	$Ru_5AuO_{13}N_2C_{47}H_{41}$
Formula weight	1752.34	1544.13
Crystal system	Monoclinic	Triclinic
Lattice parameters		
a (Å)	10.5575(5)	11.2363(4)
b (Å)	19.4875(9)	13.9424(6)
c (Å)	28.5950(14)	18.3806(7)
α (deg)	90.00	68.160(10)
β (deg)	94.387(10)	79.165(10)
γ (deg)	90.00	76.284(10)
V (Å^3)	5865.9(5)	2580.69(17)
Space group	P 2(1)/n	P $\bar{1}$
Z value	4	2
ρ_{calc} (g / cm^3)	1.984	1.987
μ (Mo Kα) (mm^{-1})	4.056	4.319
Temperature (K)	294(2)	294(2)
$2\Theta_{max}$ (°)	56.26	56.54
No. Obs. (I > 2σ(I))	8521	5733
No. Parameters	702	621
Goodness of fit (GOF)	1.131	1.071
Max. shift in cycle	0.003	0.001
Residuals*: R1; wR2	0.0255; 0.0636	0.0256; 0.0646
Absorption Correction, Max/min	Multi-scan 1.000 / 0.688	Multi-scan 1.000 / 0.671
Largest peak in Final Diff. Map (e$^-$ / Å^3)	1.208	1.214

[a] $R = \Sigma_{hkl}(||F_{obs}|-|F_{calc}||)/\Sigma_{hkl}|F_{obs}|$; $R_w = [\Sigma_{hkl}w(|F_{obs}|-|F_{calc}|)^2/\Sigma_{hkl}wF^2_{obs}]^{1/2}$; $w = 1/\sigma^2(F_{obs})$; GOF = $[\Sigma_{hkl}w(|F_{obs}|-|F_{calc}|)^2/(n_{data} - n_{vari})]^{1/2}$.

Table 2.2. Crystallographic Data for Compounds **2.5** and **2.6.**

Compound	**2.5**	**2.6**
Empirical formula	$Ru_5AuO_{14}N_2C_{48}H_{41}$	$Ru_5AuO_{15}N_2C_{49}H_{41}$
Formula weight	1572.14	1600.15
Crystal system	Triclinic	Monoclinic
Lattice parameters		
a (Å)	10.4338(3)	18.5932(9)
b (Å)	13.9382(4)	17.4564(8)
c (Å)	19.4755(6)	17.6393(8)
α (deg)	80.528(10)	90.00
β (deg)	88.287(10)	104.049(10)
γ (deg)	73.320(10)	90.00
V (Å^3)	2675.68(14)	5553.9(4)
Space group	P $\bar{1}$	P 2(1)/c
Z value	2	4
ρ_{calc} (g / cm^3)	1.951	1.914
μ (Mo Kα) (mm^{-1})	4.169	4.020
Temperature (K)	294(2)	294(2)
$2\Theta_{max}$ (°)	56.36	56.38
No. Obs. (I > 2σ(I))	8845	6065
No. Parameters	639	657
Goodness of fit (GOF)	1.051	1.029
Max. shift in cycle	0.045	0.001
Residuals*: R1; wR2	0.0375; 0.1099	0.0461; 0.0876
Absorption Correction, Max/min	Multi-scan 1.000 / 0.624	Multi-scan 1.000 / 0.804
Largest peak in Final Diff. Map (e$^-$ / Å^3)	1.817	1.076

[a] $R = \Sigma_{hkl}(||F_{obs}| - |F_{calc}||)/\Sigma_{hkl}|F_{obs}|$; $R_w = [\Sigma_{hkl}w(|F_{obs}| - |F_{calc}|)^2/\Sigma_{hkl}wF^2_{obs}]^{1/2}$; $w = 1/\sigma^2(F_{obs})$; GOF = $[\Sigma_{hkl}w(|F_{obs}| - |F_{calc}|)^2/(n_{data} - n_{vari})]^{1/2}$.

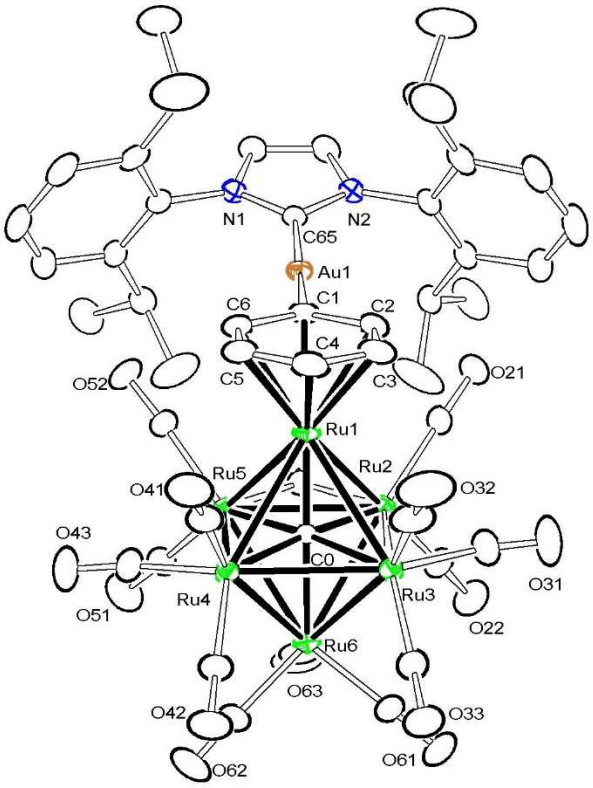

Figure 2.1. ORTEP diagram of the molecular structure of $Ru_6C(CO)_{14}[\eta^6$-PhAu(NHC)], **2.3**, showing 15% thermal ellipsoid probability. The hydrogen atoms are omitted for clarity. Selected interatomic bond distances (Å) are as follows: Ru1−C1 = 2.297(4), Ru1−C2 = 2.242(4), Ru1−C3 = 2.226(5), Ru1−C4 = 2.215(5), Ru1−C5 = 2.231(4), Ru1−C6 = 2.246(4), Ru1−Ru2 = 2.87780(5), Ru1−Ru3 = 2.8699(5), Ru1−Ru4 = 2.8797(5), Ru1−Ru5 = 2.8824(5), Ru2−Ru3 = 2.9352(5), Ru3−Ru4 = 2.8719(5), Ru4−Ru5 = 2.9342(5), Ru2−Ru5 = 2.8597(5), Ru2−Ru6 = 2.8383(5), Ru3−Ru6 = 2.8873(5), Ru4−Ru6 = 2.8916(5), Ru5−Ru6 = 2.8561(5), Au1−C1 = 2.025(4), Au1−C65 = 2.034(4), Ru1−C0 = 1.922(4), Ru2−C0 = 2.049(4), Ru3−C0 = 2.057(3), Ru4−C0 = 2.055(4), Ru5−C0 = 2.052(3), Ru6−C0 = 2.101(4).

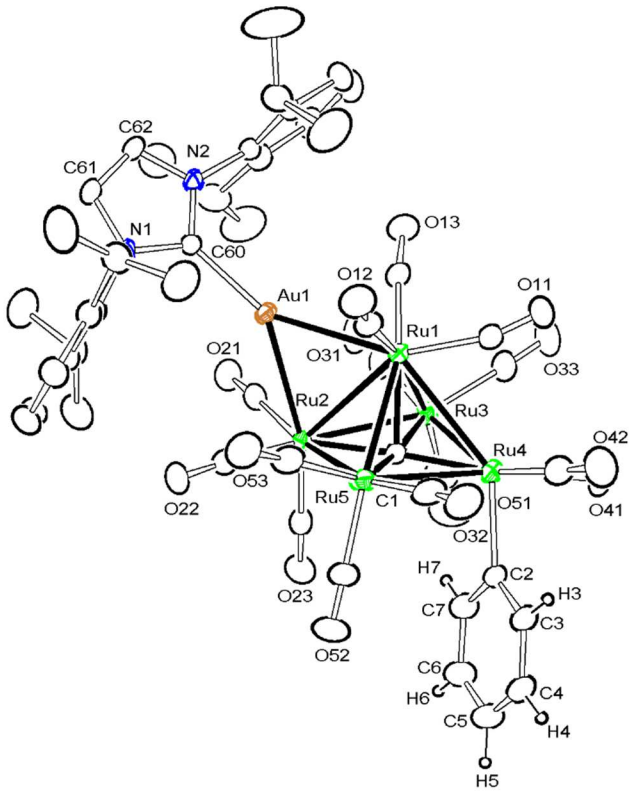

Figure 2.2. ORTEP diagram of the molecular structure of $Ru_5C(CO)_{14}(Ph)[\mu\text{-}Au(NHC)]$, **2.4** showing 20% thermal ellipsoid probability. The hydrogen atoms on the carbene ligand are omitted for clarity. Selected interatomic bond distances (Å) are as follows: Ru3−Ru4 = 2.8715(9), Ru1−Ru4 = 3.0072(7), Ru4−Ru5 = 2.8509(8), Ru2−Ru3 = 2.8573(7), Ru1−Ru3 = 2.7883(8), Ru1−Ru2 = 2.9526(7), Ru1−Ru5 = 2.8192(7), Ru2−Ru5 = 2.8526(9), Ru4−C2 = 2.091(7), Ru2−Au1 = 2.8318(6), Ru1−Au1 = 2.8083(5), Au1−C60 = 2.055(6), Ru1−C1 = 2.110(6), Ru2−C1 = 2.036(6), Ru3−C1 = 2.041(6), Ru4−C1 = 2.020(6), Ru5−C1 = 1.976(7).

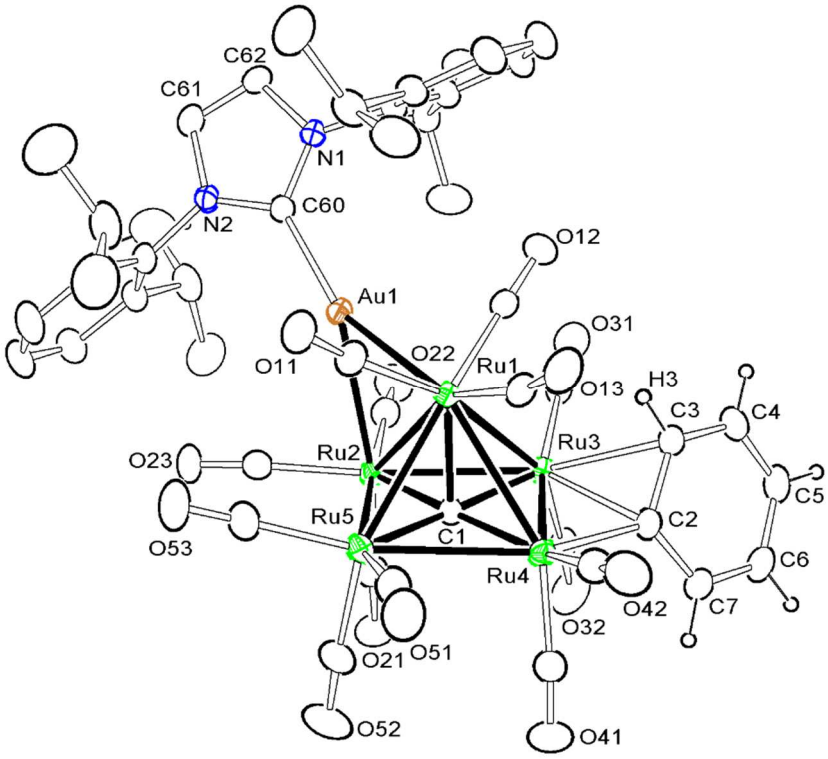

Figure 2.3. ORTEP diagram of the molecular structure of and $Ru_5C(CO)_{13}(\mu\text{-}\eta^2\text{-Ph})[\mu\text{-Au(NHC)}]$, **2.5** showing 20% thermal ellipsoid probability. The hydrogen atoms on the carbene ligand are omitted for clarity. Selected interatomic bond distances (Å) are as follows: Ru3−Ru4 = 2.7057(5), Ru1−Ru4 = 2.9308(5), Ru4−Ru5 = 2.8799(5), Ru2−Ru3 = 2.8477(5), Ru1−Ru3 = 2.8708(5), Ru1−Ru2 = 2.9375(5), Ru1−Ru5 = 2.8215(5), Ru2−Ru5 = 2.9052(5), Ru3−C2 = 2.314(4), Ru3−C3 = 2.387(4), Ru4−C2 = 2.082(4), C2−C3 = 1.425(6), Ru2−Au1 = 2.8338(4), Ru1−Au1 = 2.7906(4), Au1−C60 = 2.041(4), Ru1−C1 = 2.090(4), Ru2−C1 = 2.016(4), Ru3−C1 = 2.012(4), Ru4−C1 = 2.004(4), Ru5−C1 = 1.985(4).

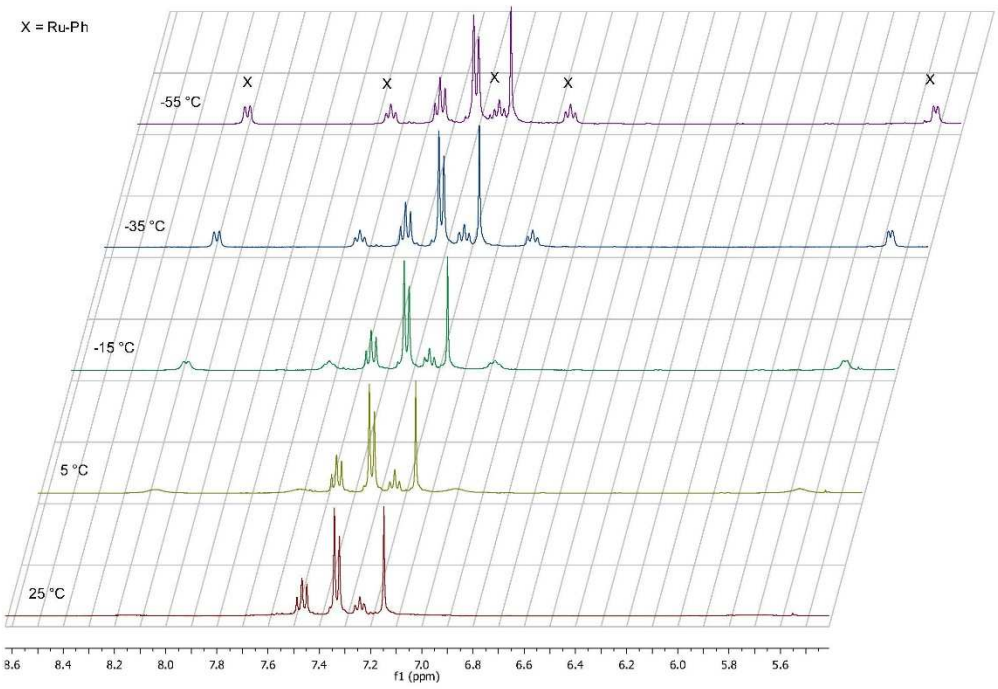

Figure 2.4. Variable temperature ^{1}H NMR spectra of **2.5** showing the temperature-dependent broadening of the resonances of the bridging phenyl ligand indicated by the label X.

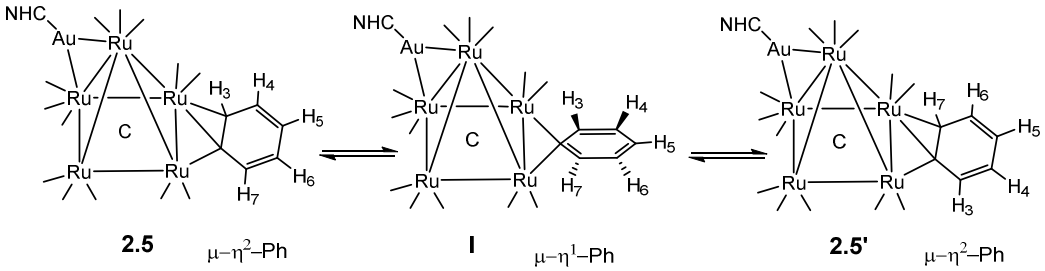

Figure 2.5. A schematic of the proposed mechanism for the interchange of the ortho- and meta-hydrogen atoms on the bridging phenyl ligand in **2.5**.

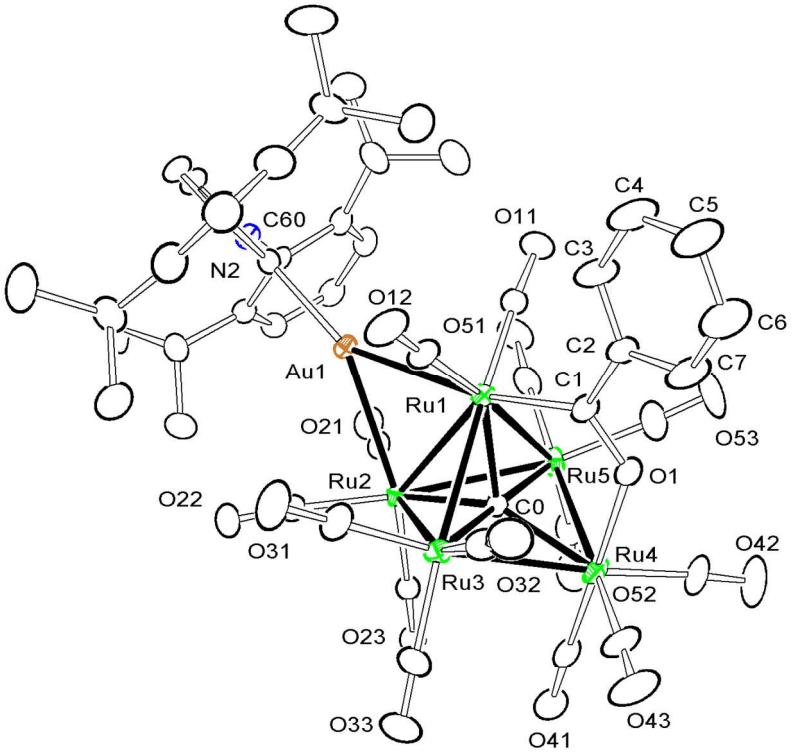

Figure 2.6. ORTEP diagram of the molecular structure of $Ru_5C(CO)_{14}(\mu\text{-}\eta^2O{=}CPh)[\mu\text{-}Au(NHC)]$, **2.6**, showing 10% thermal ellipsoid probability. The hydrogen atoms are omitted for clarity. Selected interatomic bond distances (Å) and angles (deg) are as follow: Ru3−Ru4 = 2.8588(12), Ru4−Ru5 = 2.8593(13), Ru2−Ru3 = 2.8846(10), Ru1−Ru3 = 2.8315(11), Ru1−Ru2 = 2.9361(10), Ru1−Ru5 = 2.8106(5), Ru2−Ru5 = 2.8690(11), Ru1−C1 = 2.025(9), Ru4−O1 = 2.110(6), O1−C1 = 1.287(10), C1−C2 = 1.499(13), Ru2−Au1 = 2.8189(8), Ru1−Au1 = 2.8470(8), Au1−C60 = 2.047(9), Ru1−C0 = 2.020(8), Ru2−C0 = 2.076(8), Ru3−C0 = 1.969(8), Ru4−C0 = 2.089(8), Ru5−C0 = 1.973(8), Ru1−C1−O1 = 121.7(7), Ru4−O1−C1 = 124.4(6), Ru1−Ru3−Ru4 = 77.12(3), Ru1−Ru5−Ru4 = 77.44(3), Ru1−C0−Ru4 = 119.4(4), C1−Ru1−C0 = 89.3(4).

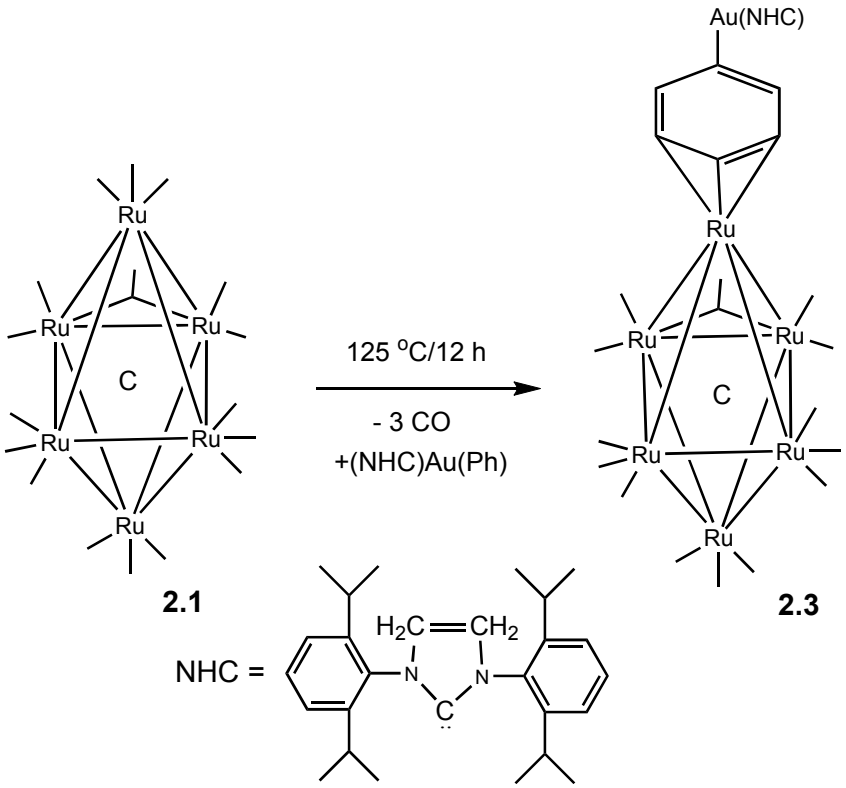

Scheme 2.1. A schematic of the reaction of **2.1** with (NHC)AuPh.

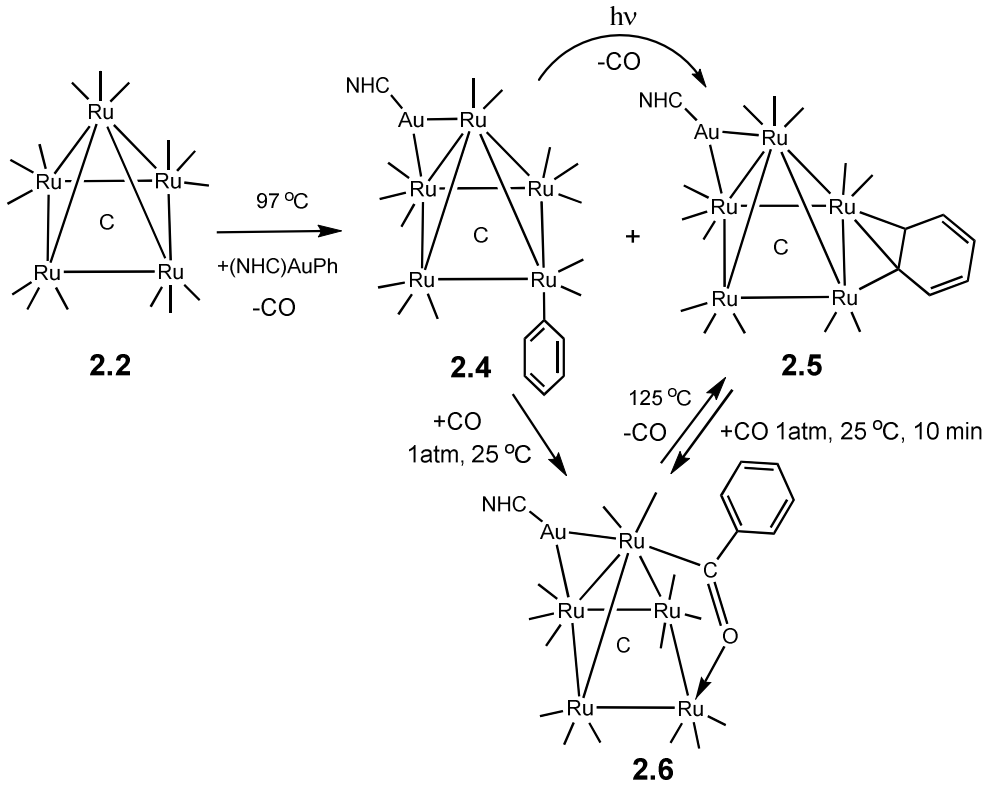

Scheme 2.2. A summary of the products obtained from the reaction of **2.2** with (NHC)AuPh.

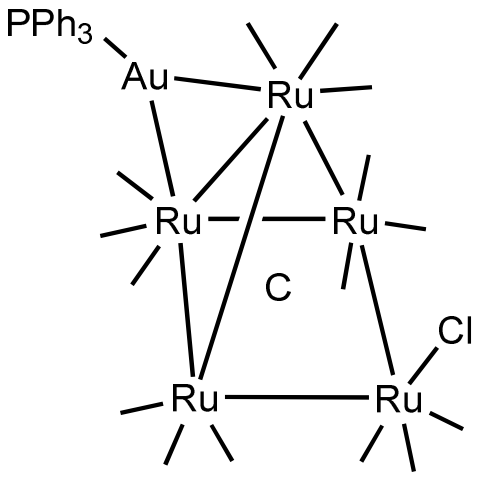

Scheme 2.3. A line structure of the molecular structure of compound **2.7**.

2.5 References

1) Hashmi, A. S. K. and Toste, F. D., *Modern Gold Catalyzed Synthesis*, *Eds.*, Wiley-VCH Publishers, Weinheim, Germany, 2012.

2) (a) Obradorsa, C.; Echavarren, A.M. *Chem. Commun.* **2014**, 50, 16 – 28. (b) Hashmi, A. S. K. *Chem. Rev.* **2007**, 107, 3180–3211. (c) Jiménez-Núñez, E.; Echavarren A. M. Chem. Commun. **2007**, 333–346; (d) Fürstner, A.; Davies, P. W. *Angew. Chem., Int. Ed.* **2007**, 46, 3410–3449; (e) Jiménez-Núñez, E.; Echavarren, A. M. *Chem. Rev*. **2008**, 108, 3326–3350; (f) Gorin, D. J.; Sherry B. D.; Toste. F. D. *Chem. Rev*. **2008**, 108, 3351–3378; (g) Fürstner, A. *Chem. Soc. Rev*. **2008**, 38, 3208–3221; (h) Shapiro, N.D.; Toste, F.D. *Synlett* **2010**, 675–691. (i) Patil, H.G. N. T.; Yamamoto, Y., *Chem. Rev*., **2008**, 108, 3395–3442; (j) Zhang, L., *Acc. Chem. Res*., **2014**, 47, 877 – 888; (k) Gaillard, S.; Cazin, C.S.J.; Nolan, S.P., *Acc. Chem. Res*. **2012**, 45, 778 – 787.

3) (a) Li, G.; R. Jin *Acc. Chem. Res.* **2013**, 46, 1749 – 1758. (b) Oliver-Meseguer, J.; Cabrero-Antonino, J.R.; Dominquez, I.; Leyva-Perea, A.; Corma, A. *Science* **2012**, 338, 1452 – 1455; (c) Lee, I.; Molina, L.M.; Lopez, M.J.; Alonso, J.A.; Hammer, B.; Lee,B.; Seifert, S.; Winans, R.E.; Elam, J.; Pellin, M.J.; Vajda, S. *Angew. Chem. int. Ed.* **2009**, 48, 1467 – 1471.

4) (a) Li, G.; Jin, R., *Acc. Chem. Res.,* **2013**, 46, 1749 – 1758; (b) Haruta, M., *Gold Bull.,* **2004**, 37, 27 – 36; (c) Haruta, M., *Catal. Today*, **1997**, 36, 153 – 166; (d) Haruta, M. *Appl. Catal. A: Gen.* **2001**, 222, 427 – 437; (e) Oliver-Meseguer, J.; Cabrero-Antonino, J.R.; Dominquez, I.; Leyva-Perea, A.; Corma, A. *Science*, **2012** 338, 1452 – 1455; (f) Hashmi, A.S.K.; Hutchings, G.J. *Angew. Chem. Int. Ed.* **2006**,

45, 7896 – 7936; (g) Della Pina, C.; Falletta, E.; Prati, L.; Rossi *Chem. Soc. Rev.* **2008**, 37, 2077 – 2095; (h) Lee, S.; Molina, L.M.; Lopez, M.J.; Alonso, J.A.; Hammer, B.; Lee, B.; Seifert, S.; Winans, R.E.; Elam, J.W.; Pellin, M.J.; Vajda, S. *Angew. Chem. int. Ed.* **2009**, 48, 1467 – 1471; (i) Herzing, A.A.; Kiely, C.J.; Carley, A.F.; Landon, P.; Hutchings, G.J. *Science* **2008**, 32, 1331 – 1335. (j) Zhang, L. *Acc. Chem. Res*. **2014**, 47, 877 – 888.

5) (a) Freakley, S.J.; He, Q.; Kiely, C.J.; Hutchings, G.J. *Catal. Lett.* **2015**, 145, 71 – 79; (b) Hutchings, G.J.; Kiely, C.J. *Acc. Chem. Res.* **2013**, 46, 1759 – 1772; (b) Hutchings, G.J. Catalysis *Today* **2014**, 238, 69–73; (c) Zhang, Y.; Cui, X.; Shi, F.; Deng, Y. *Chem. Rev.* **2012**, 112, 2467–2505; (d) Hutchings, G.J. *Chem. Commun.* **2008**, 1148 – 1164; (e) Lopez-Sanchez, J.A.; Dimitratos, N.; Glanvilla, N.; Kesavan, L.; Hammond, C.; Edwards, J.K.; Carley, A.F.; Kiely, C.; Hutchings, G.J. *Appl. Catal. A: Gen.* **2011**, 391, 400 – 406; (f) Enache, D.I.; Edwards, J.K.; Landon, P.; Solsona-Espriu, B.; Carley, A.F.; Herzing, A.A.; Watanabe, M.; Kiely, C.J.; Knight, D.W.; Hutchings, G.J. *Science* **2006**, 311, 362 – 365; (g) Miedziak, P.; Sankar, M.; Dimitratos, M.; Lopez-Sanchez, J.A.; Carley, A.F.; Knight, D.W.; Taylor, S.H.; Kiely, C.J.; Hutchings, G.J. *Catal. Today* **2011**, 164, 315–319; (h) Wang, R.; Zhiwei Wu Z.; Chen, C.; Zhangfeng Qin, Z.; Zhu, H.; Wang, H.; Wu, C.; Dong, W.; Fan, W.; Wang, J. *Chem. Commun.* **2013**, 49, 8250-8252; (i) Kesavan, L.; Tiruvalam, R.; Ab Rahim, M.H.; bin Saiman, M.I.; Enache, D.I.; Jenkins, R.L.; Dimitratos, N.; Lopez-Sanchez, J.A.; Taylor, S.H.; Knight, Kiely, C.J.; Hutchings, G.J. *Science* **2011**, 331, 195-199.

6) (a) Salter, I.D.in *Comprehensive Organometallic Chemistry II,* Abel, E. W.; Stone, F. G. A.; Wilkinson, G., Oxford, UK, 1995, 10, pp 255 – 322; (b) Salter, I. D. in *Metal Clusters in Chemistry*, Braunstein, P.; Oro, L. A.; Raithby, P. R., 1999, 1, pp 509-534; (c) Salter, I. D. *Adv. Organomet. Chem.* **1989**, 29, 249 – 343.

7) Adams, R.D.; Chen, M. *Organometallics* **2012**, 31, 6457−6465.

8) Adams, R.D.; Rassolov, V.; Zhang, Q. *Organometallics* **2013**, 32, 6368−6378.

9) Adams, R.D.; Rassolov, V.; Wong, Y.O. *Angew. Chem.* **2014**, 53, 11006 -11009.

10) Adams, R.D.; Rassolov, V.; Zhang, Q. *Organometallics* **2013**, 32, 1587 - 1590.

11) Johnson, B.F.G.; Lewis, J.; Sankey, S.; Wong, K.; McPartlin, M.; Nelson, W.J.H. *J. Organomet. Chem.* **1980**, 191, C3 – C7.

12) Johnson, B.F.G.; Lewis, J.; Nicholls, J.N.; Puga, J.; Raithby, P.R.; Rosales, M.J.; McPartlin, M.; Clegg, W. *J. Chem. Soc., Dalton Trans*. **1983**, 277 – 290.

13) Hashmi, A.S.K.; Ramamurthi, T.D.; Rominger, F. *J. Organomet. Chem*. **2009**, 694, 592–597.

14) SAINT+, version 6.2a, Bruker Analytical X-ray Systems, Inc., **2001**, Madison, WI.

15) G. M. Sheldrick, SHELXTL, version 6.1, Bruker Analytical X-ray Systems, Inc., Madison, WI, **1997**.

16) (a) Borchert, T.; Lewis, J.; Raithby, P.R.; Shields, G.P.; Wadepohl*, Inorg. Chim. Acta* **1998**, 274, 201 – 209; (b) Blake, A.J.; Johnson, B.F.G.; Reed, D.; Shephard, D.S. *J. Chem. Soc., Dalton Trans.* **1995**, 843 – 849; (c) Braga, D.; Grepioni, F.; Parisini, E.; Dyson, P.J.; Blake, A.J.; Johnson, B.F.G. *J. Chem. Soc., Dalton Trans.* **1993**, 2951 – 2957; (d) Johnson, B.F.G.; Shephard, D.S.; Braga, D.; Grepioni, F.; Parsons, S. *J. Chem. Soc., Dalton Trans.* **1997**, 3563 – 3569.

17) Gomez-Suarez, A.; Dupuy, S.; Slawin, Nolan, S.P. *Angew. Chem. Int. Ed.* **2013**, 52, 938 –942.

18) (a) Johnson, B.F.G.; Lewis, J.; Nicholls, J.N.; Puga, J.; Raithby, P.R.; Rosales, M.J.; McPartlin, M.; Clegg, W. *J. Chem.Soc., Dalton Trans*. **1983**, 277 – 290. (b) Burrow, R.A.; Farrar, D.H.; Hao, J.; Lough, A.; Mourad, O; Poe, A.J.; Zheng, Y., Polyhedron, **1998**, 17, 2907 – 2919.

19) Bunkhall, Holden, H.D.; Johnson, B.F.G.; Lewis, J.; Pain, G.N.; Raithby, P.R.; Taylor, M.J. *Chem. Commun*. **1984**, 25 – 27.

20) Henrick, K.; Johnson, B.F.G.; Lewis, J.; Mace, J.; McPartlin, M.; Morris, J. *Chem. Commun*. **1985**, 1617 – 1618.

21) Bruce, M.I.; Humphrey, P.A.; Skelton, B.W.; White, A.H. *J. Organomet. Chem*. **1996**, 526, 85 – 97.

22) Mingos, D.M.P. *Acc. Chem. Res.* **1984**, 17, 311 – 319.

23) (a) Adams, R.D.; Kan, Y.; Zhang, Q. *Organometallics* **2011**, 30, 328−333; (b) Farrugia, L.G.; Miles, A.D.; Stone, F.G.A. *J. Chem. Soc., Dalton Trans*. **1984**, 2415−2422; (c) Hoferkamp, L.A.; Rheinwald, G.; Stoeckli-Evans,H.; Suss-Fink, G. *Organometallics* **1996**, 15, 704−712; (d) Shima, T.; Suzuki, H. *Organometallics* **2005**, 24, 1703−1708 (e) Akita, M.; Hua, R.; Oku, T.; Tanaka, M.; Moro-oka, Y. *Organometallics* **1996**, 15, 4162 – 4177; (f) Alvarez, M.A., Garcia, M.E., Martinez, M.E., Ramos, A., Ruiz, M.A. *Organometallics* **2009**, 28, 6293−6307.

24) (a) Lugan, N., Lavigne, G.; Bonnet, J-J. *Inorg. Chem*. **1987**, 26, 585 – 590; (b) Kong, F.-S.; Wong, W.-T. *J. Chem. Soc. Dalton Trans.* **1999**, 2497 – 2510; (c)

Randles, M.D.; Willis, A.C.; Cifuentes, M.P.; Humphrey, M.G., J. Organomet. Chem., **2007**, 692, 4467 – 4472; (d) *J. Organomet. Chem*., **2004**, 689, 3426 – 3437.

CHAPTER 3

Organometallic chemistry of pentaruthenium-gold carbonyl cluster complexes[2]

[2] Adams, R. D.; Tedder, J. *J. Organomet. Chem.* **2017**, 829, 58-65.
Reprinted here with permission from publisher

3.1 Introduction

Over the years, there has been considerable interest in the synthesis and structures of transition metal carbonyl cluster complexes containing gold.[1] Recent studies of the organometallic chemistry of gold[2,3] have revealed a range of new catalytic transformations of organic compounds by gold clusters[4] and nanoparticles[5] and have provided a renewed interest in the organometallic chemistry of metal cluster complexes containing gold. A number of bimetallic catalysts containing gold have been shown to exhibit catalytic activity that is superior to that of pure gold catalysts.[6]

In recent studies, it has been shown that alkyl- and arylgold phosphine compounds, such as $(PPh_3)AuR$, R = Me, Ph, Np, Py etc. can be readily, oxidatively added to activated 3rd row polynuclear metal carbonyl cluster complexes to yield bimetallic cluster complexes containing alkyl and aryl ligands with bridging gold phosphine groupings, e.g. Eqs. (3.1)–(3.3).[7-9] In some cases, the aryl ligands have adopted unusual bridging coordination modes that can result in interesting physical and chemical properties, such as hindered rotation about the metal-metal bond.[10]

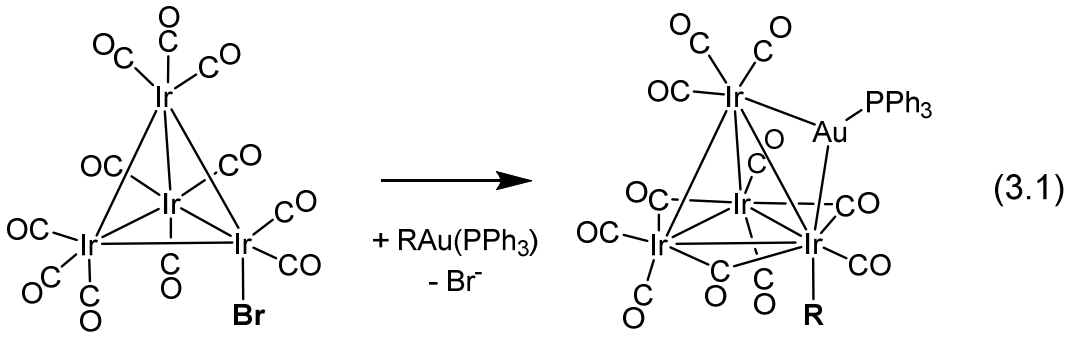

$[Ir_4(CO)_{11}Br]^-$ $Ir_4(CO)_{11}(R)[\mu\text{-}Au(PPh_3)]$, R = CH_3, C_6H_5, 2-$C_{16}H_9$ (3.1)

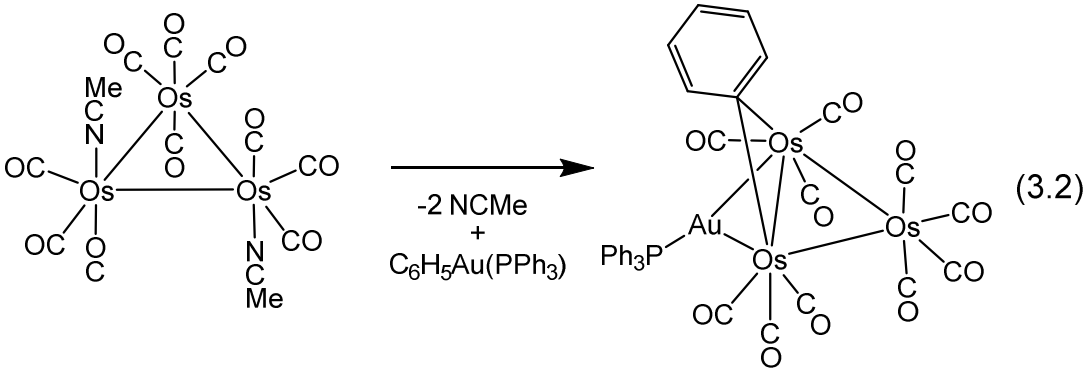

(3.2)

$Os_3(CO)_{10}(NCMe)_2$ $Os_3(CO)_{10}(\mu\text{-}C_6H_5)[\mu\text{-}Au(PPh_3)]$

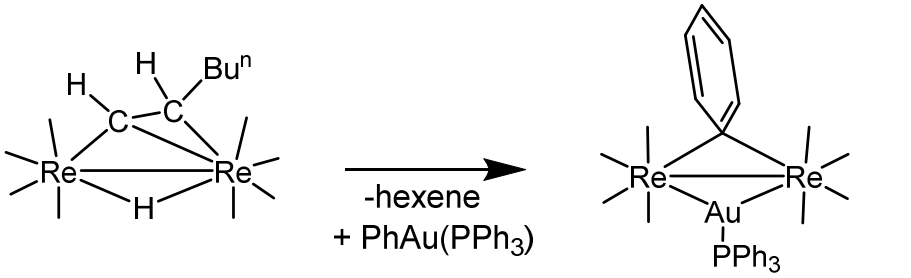

(3.3)

$Re_2(CO)_8[\mu\text{-}HCC(H)Bu](\mu\text{-}H)$ $Re_2(CO)_8[\mu\text{-}Au(PPh_3)](\mu\text{-}C_6H_5)$

We have also shown that $Ru_5(C)(CO)_{15}$, **3.1** reacts with PhAu(NHC), NHC = 1,3-bis(2,6-diisopropylphenyl-imidazol-2-ylidene) to yield the Ru_5AuC complexes: $Ru_5(C)(CO)_{14}(Ph)[\mu\text{-}Au(NHC)]$, **3.2** and $Ru_5(C)(CO)_{13}(\mu\text{-}\eta^2\text{-}Ph)[\mu\text{-}Au(NHC)]$, **3.3** by oxidative-addition of the Au-C phenyl bond at the ruthenium atoms. Compounds **3.2** and **3.3** were found to add CO at 1 atm to yield the CO insertion product $Ru_5(C)(CO)_{14}(\mu\text{-}\eta^2\text{-}O{=}CPh)[\mu\text{-}Au(NHC)]$, **3.4** that contains a bridging benzoyl ligand in an opened Ru_5 cluster complex, Scheme 3.1.[11] Osmium-gold complexes containing methyl groups were obtained from reactions by using $MeAu(PPh_3)$ with osmium carbonyl cluster complexes.[12]

We have now investigated the reactions of **3.1** with $MeAu(PPh_3)$. A series of methyl-containing Ru_5AuC complexes: $Ru_5(\mu_5\text{-}C)(CO)_{14}(\mu\text{-}\eta^2\text{-}O{=}CMe)[\mu\text{-}Au(PPh_3)]$, **3.5**;

$Ru_5(\mu_5\text{-}C)(CO)_{13}(\mu\text{-}\eta^2\text{-}O{=}CMe)(Me)[\mu\text{-}Au_2(PPh_3)_2]$, **3.6**; $Ru_5(\mu_5\text{-}C)(CO)_{14}(\mu\text{-}\eta^2\text{-}O{=}CMe)(\eta^1\text{-}O{=}CMe)[\mu\text{-}Au_2(PPh_3)_2]$, **3.7**, $Ru_5(\mu_5\text{-}C)(CO)_{13}(PPh_3)(\mu\text{-}\eta^2\text{-}O{=}CMe)[\mu\text{-}Au(PPh_3)]$, **3.8**, and nonmethyl complexes $Ru_5(\mu_5\text{-}C)(CO)_{11}(\mu\text{-}CO)_3[\mu\text{-}Au(PPh_3)]_2$, **3.9**[13], and $Ru_5(\mu_5\text{-}C)(CO)_{11}(\mu\text{-}CO)_2[\mu\text{-}Au(PPh3)]_4$, **3.10** have been obtained. The synthesis, structures and interrelationships of these new complexes are described in this report.

3.2 Experimental section

General data

All reactions were performed under an atmosphere of nitrogen unless indicated otherwise. Reagent grade solvents were dried by the standard procedures and were freshly distilled just prior to use. Infrared spectra were recorded on a Nicolet IS10 Mid-infrared FT-IR spectrophotometer. ^{1}H NMR spectra were recorded on a Varian Mercury 300 spectrometer operating at 300.1 MHz. Variable temperature ^{31}P NMR spectra were recorded on a Bruker AVANCE III spectrometer operating at 400 MHz for compounds **3.9** and **3.10**. Mass spectrometric (MS) measurements were performed by a direct-exposure probe by using electron impact ionization (EI) or electrospray ionization (ESI). $Ru_3(CO)_{12}$ and $MeAu(PPh_3)$ were purchased from STREM and were used without further purification. $Ru_5(\mu_5\text{-}C)(CO)_{15}$, **3.1**, was prepared according to a previously reported procedure.[14] Product separations were performed by TLC in air on Analtech 0.25 mm silica gel 60 Å F254 glass plates. Elemental analyses were performed by Galbraith Labs., Knoxville, TN.

Reaction of $Ru_5(\mu_5\text{-}C)(CO)_{15}$, 3.1 with $MeAuPPh_3$

39.0 mg (0.042 mmol) of **3.1** was added to a 50 mL three-neck flask with a solution of 22.7 mg (0.048 mmol) of $MeAu(PPh_3)$ in 20 mL of hexane. After heating to reflux for 1 h, the solvent was removed in vacuo, and the products were then isolated by using TLC

by using a hexane/methylene chloride solvent mixture to yield in order of elution: 17.7 mg of the known compound $Ru_5(\mu_5\text{-}C)(CO)_{14}(\mu\text{-}\eta^2\text{-}O{=}CMe)[\mu\text{-}Au(PPh_3)]$, **3.5** (30% yield)[15]; 24.0 mg of $Ru_5(\mu_5\text{-}C)(CO)_{13}(\mu\text{-}\eta^2\text{-}O{=}CMe)(Me)[\mu\text{-}Au_2(PPh_3)_2]$, **3.6** (31% yield); and 1.6 mg of $Ru_5(\mu_5\text{-}C)(CO)_{14}(\mu\text{-}\eta^2\text{-}O{=}CMe)(\eta^1\text{-}O{=}CMe)[\mu\text{-}Au_2(PPh_3)_2]$, **3.7** (2% yield). Spectral data for **3.5**: IR νCO (cm^{-1} in hexane): 2095(m), 2057(m), 2050(vs), 2033(m), 2018(w), 2001(m), 1989(m), 1947(w). ^1H NMR (CD_2Cl_2, in ppm) δ = 7.56–7.45 (m, 15H, $P(C_6H_5)_3$, 2.14 (s, 3H, $\mu\text{-}\eta^2\text{-}OCCH_3$). ^{31}P NMR (CD_2Cl_2, in ppm) δ = 68.4 (s, 1P, $P(C_6H_5)_3$. Mass spectrum (EI^+): 1385 ($M^+ - CO$). Spectral data for **3.6**: IR νCO (cm^{-1} in hexane): 2067(m), 2041(m), 2019(m), 2009(vs), 1991(vw), 1974(w). ^1H NMR (CD_2Cl_2, in ppm) δ = 7.42–7.20 (m, 15H, $(P(C_6H_5)_3)_2$, 2.39 (s, 3H, $\mu\text{-}\eta^2\text{-}OCCH_3$), 1.68 (s, 3H, CH_3). ^{31}P NMR (CD_2Cl_2, in ppm) δ = 62.0 (s, 2P, $P(C_6H_5)_3$. Mass spectrum (ESI^+): 1859 (M^+). Spectral data for **3.7**: IR νCO (cm^{-1} in dichloromethane): 2071(s), 2040(vs), 2025(s), 1990(w), 1973(m), 1926(vw). ^1H NMR (CD_2Cl_2, in ppm) δ = 7.42–7.21 (m, 15H, $(P(C_6H_5)_3)_2$, 2.66 (s, 3H, $OCCH_3$), 2.46 (s, 3H, $\mu\text{-}\eta^2\text{-}OCCH_3$). ^{31}P NMR (CD_2Cl_2, in ppm) δ = 61.9 (s, 2P, $(P(C_6H_5)_3)_2$).

Transformation of 3.5 to 3.6

20.6 mg (0.015 mmol) of **3.5** was added to a 50 mL three-neck flask containing a solution of 20 mg (0.042 mmol) of $MeAu(PPh_3)$ in 20 mL of hexane. After heating to reflux for 1.5 h, the solvent was removed in vacuo, and the products were then isolated by TLC by using a hexane/methylene chloride mixture to yield in order of elution 0.2 mg unreacted **3.5**, 1.4 mg $Ru_5(\mu_5\text{-}C)(CO)_{13}(PPh_3)(\mu\text{-}\eta2\text{-}O{=}CMe)[\mu\text{-}Au(PPh_3)]$, **3.8** (6% yield) and 10.6 mg (39% yield) **3.6**. Spectral data for **3.8**: IR νCO (cm^{-1} in hexane): 2067(m), 2040(vs), 2024(s), 1994(m), 1985(w), 1975(m), 1968(w), 1959(vw), 1939(vw). ^1H NMR (CD_2Cl_2,

in ppm) δ = 7.70–7.63 (m, 15H, Ru-P(C_6H_5)$_3$), 7.55–7.42 (m, 15, Au-(PC_6H_5)$_3$), 1.86 (s, 3H, CH_3). ^{31}P NMR (CD_2Cl_2, in ppm) δ = 67.7 (s, 1P), 31.4 (s, 1P). Elemental Anal. % Calc (% Found): C = 37.94 (38.15) and H = 2.02 (2.14).

Pyrolysis of 3.6

29.6 mg (0.016 mmol) of **3.6** was added to a 50 mL three-neck flask containing a solution benzene. The solution was heated to reflux for 1 h. The solvent was removed in vacuo, and the products were then isolated by TLC by using a hexane/methylene chloride mixture to yield in order of elution: 3.7 mg (16% yield) **3.5**, 10.4 mg of orange $Ru_5(\mu_5$-C)$(CO)_{11}(\mu$-CO)$_3[\mu$-Au(PPh_3)$]_2$, **3.9** (35% yield)[13] and 2.2 mg of grey-green $Ru_5(\mu_5$-C)$(CO)_{11}(\mu$-CO)$_2[\mu$-Au(PPh_3)$]_4$ **3.10**, (5% yield). Spectral data for **3.10**: IR ν CO (cm^{-1} in methylene chloride): 2027, 1984(s), 1936(w). ^{31}P NMR (CD_2Cl_2, -55 °C, in ppm) δ = 62.8 (s, 1P), 60.4 (s, 1P), 57.4 (s, 1P), 34.0 (s, 1P).

Synthesis of 3.7 by addition of CO to 3.6

13.7 mg (0.0070 mmol) of **3.6** was added to an NMR tube as a solution in CD_2Cl_2 solvent. The NMR tube was evacuated and then filled with CO to 1 atm. Solution was then stored under CO for 3 days at room temperature. The solvent was removed by a steady flow of nitrogen and the product was then isolated by TLC to provide 8.8 mg of **3.7** (63% yield) and 2.1 mg of unreacted **3.6**.

Formation of acetone by addition of CO to 3.6

11 mg (0.006 mmol) of **3.6** was dissolved in C_6D_6 and placed in a NMR tube. The solution was purged with CO and the mixture was placed in an oil bath at 80 °C for 23 h. A ^{1}H NMR spectrum taken at this time confirmed the formation of acetone. After removal

of the solvent, the products were isolated by TLC to provide 1.2 mg (14% yield) of **3.5**, 4.2 mg (43% yield) of **3.8**, 1.7 mg (16% yield) of the previously reported compound $Ru_5(\mu_5\text{-}C)(CO)_{11}(\mu\text{-}CO)_2[\mu\text{-}Au(PPh_3)]_2$, **3.9**[13], 0.4 mg (4%) of **3.6**, and 0.7 mg (6% yield) of **3.7**.

Thermal decarbonylation of 3.7

10.4 mg (0.006 mmol) of **3.7** was dissolved in toluene-d_8 and then placed to a NMR tube. The solution was heated at 60 °C for 23.5 h. The solvent was removed by a steady flow of N_2 and the products were then isolated by TLC to yield in order of elution: 1.0 mg (13% yield) of **3.5**, 0.3 mg (3% yield) of **3.8**, 2.8 mg (27% yield) of **3.6**, 0.1 mg (1% yield) of **3.9**, 0.4 mg (3% yield) of **3.10** and 0.6 mg (6%) of starting material **3.7**.

Synthesis of 3.8 by addition of PPh_3 to 3.5

19.4 mg (0.014 mmol) of **3.5** was added to a 50 mL three-neck flask with a solution of 7.2 mg (0.027 mmol) PPh_3 in 20 mL of hexane. After heating to reflux for 1.5 h, the solvent was removed in vacuo, and the product was then isolated by TLC to yield 17.1 mg (76% yield) of **3.8**.

Synthesis of 3.10 from 3.9 and $CH_3Au(PPh_3)$

10 mg (0.0050 mmol) of **3.9** was added to a 50 mL three-neck flask in 15 mL of heptane. 13 mg (0.029 mmol) of $CH_3Au(PPh_3)$ was added and the solution was heated at reflux for 3 h. The solvent was then removed in vacuo and the product was isolated by TLC to provide 1.3 mg of **3.10** (9% yield).

Crystallographic analyses

Red single crystals of **3.6** suitable for x-ray diffraction analysis were obtained by slow evaporation from a solution in hexane solvent at room temperature. Dark red crystals of **3.7** suitable for x-ray diffraction analyses were obtained by slow evaporation of solvent from a solution in a hexane/methylene chloride solvent mixture at room temperature. Orange crystals of **3.8** suitable for x-ray diffraction analyses were obtained by slow evaporation of solvent from a solution in hexane solvent at room temperature. Orange crystals of **3.9** suitable for x-ray diffraction analyses were obtained by slow evaporation of solvent from a solution in hexane solvent at room temperature. Dark brown crystals of **3.10** suitable for x-ray diffraction analyses were obtained by slow evaporation of solvent from a solution in a hexane/methylene chloride solvent mixture at room temperature. Each data crystal was glued onto the end of a thin glass fiber. X-ray intensity measurements were made by using a Bruker SMART APEX CCD-based diffractometer using Mo Kα radiation (λ = 0.71073 Å). The raw data frames were integrated with the SAINT + program by using a narrow-frame integration algorithm.[15] Corrections for Lorentz and polarization effects were also applied with SAINT^{+}. An empirical absorption correction based on the multiple measurements of equivalent reflections was applied by using the program SADABS.[15] All structures were solved by a combination of direct methods and difference Fourier syntheses, and refined by full-matrix least squares on F^2 by using the SHELXTL software package.[16] All non-hydrogen atoms were placed in geometrically idealized positions included as standard riding atoms during the least-squares refinements. Crystal data, data collection parameters, and results of the analyses are listed in Tables 3.1, 3.2, and 3.3. Compounds **3.6**, **3.7**, and **3.8** crystallized in the triclinic crystal system. The space group

P^{-}1 was assumed and confirmed by the successful solution and refinement of the structure. Compound **3.9** crystallized with two independent molecules in the asymmetric crystal unit. Compound **3.10** crystallized in the monoclinic crystal system. The space group P21/c was established by the systematic absences in the data and then confirmed by the successful solution and refinement of the structure. Crystal data, data collection parameters and results for the analyses are listed in Tables 3.1, 3.2, and 3.3.

Results

The reaction of **3.1** with $MeAu(PPh_3)$ provided two products: $Ru_5(\mu_5\text{-}C)(CO)_{14}(\mu\text{-}\eta^2\text{-}O{=}CMe)[\mu\text{-}Au(PPh_3)]$, **3.5** (30% yield) and $Ru_5(\mu_5\text{-}C)(CO)_{13}(\mu\text{-}\eta^2\text{-}O{=}CMe)(Me)[\mu\text{-}Au_2(PPh_3)_2]$, **3.6** (31% yield) in significant amounts, and one minor product $Ru_5(\mu_5\text{-}C)(CO)_{14}(\mu\text{-}\eta^2\text{-}O{=}CMe)(\eta1\text{-}O{=}CMe)[\mu\text{-}Au_2(PPh_3)_2]$, **3.7** (2% yield). All three products were characterized by a combination of IR, mass spectrum, ^{1}H NMR spectroscopy and a single-crystal X-ray diffraction analyses. Compound **3.6** can be obtained from **3.5** by reaction with $MeAu(PPh_3)$, see below. We have not tried to optimize the yields of **3.5** and **3.6** by changing the ratios of the reagents in the initial reaction, although one should certainly be able to increase the yield of **3.6** at the expense of **3.5** by increasing the amount of $CH_3Au(PPh_3)$ relative to the amount of **3.1**.

Compound **3.5** was obtained previously by Cowie et al. from the reaction of **3.1** with LiMe, followed by the addition of $ClAu(PPh_3)$.[15] The metrical parameters for **3.5** determined in our study are similar to those reported previously[15], see Supplementary Material. Compound **3.5** consists of an open Ru_5C cluster consisting of a carbide-bridged Ru_4 butterfly cluster with an $Au(PPh_3)$ group bridging the hinge metal atoms of the cluster and an acetyl ligand bridging the nonbonded pair of ruthenium atoms (Figure 3.1).

An ORTEP diagram of the molecular structure of **3.6** as found in the solid state is shown in Fig. 3.2. Compound **3.6** also consists of an opened Ru_5C cluster with an acetyl ligand, Me-C(14)-O(14), bridging the nonbonded pair of ruthenium atoms Ru(1) and Ru(4). Atom C(1) is bonded to Ru(1), Ru1-C14 = 2.046(8) Å and the oxygen atom O(1) is bonded to Ru(4), Ru(4)-O(14) = 2.106(6) Å. The C = O bond distance is 1.250(10) Å. Unlike **3.5**, compound **3.6** contains a single σ-coordinated methyl group on the bridging ruthenium atom Ru(4), Ru4-C1 = 2.309(15) Å. The resonance of the acetyl methyl group observed at δ = 2.39 in the ^{1}H NMR spectrum of **3.6** and the resonance of the σ-coordinated methyl group was found at 1.68 ppm. Most importantly, compound **3.6** contains two $Au(PPh_3)$ groups which are mutually bonded, Au1-Au2 = 2.8145(4) Å and are bonded to the Ru_4 portion of the cluster. Atom Au(1) is bonded to three Ru atoms, Ru1-Au1 = 2.7954(7) Å, Ru2-Au1 = 2.9153(7) Å, Ru5-Au1 = 3.0948(7) Å but the Ru(5)-Au(1) bond is significantly longer than the other two. Atom Au(2) is bonded to only two Ru atoms, Ru1-Au2 = 2.8349(7) Å, Ru2-Au2 = 2.8761(7) Å. The Ru3-Au2 distance of 3.798(1) Å is too long for a significant direct bonding interaction. The metal atoms of the cluster of **3.6** contain a total of 76 valence electrons which is consistent with that of an "open" square pyramidal cluster of five metal atoms.[18]

When **3.5** was allowed to react with $MeAuPPh_3$ in hexane solvent at reflux for 1.5 h, compound **3.6** was obtained in 39% yield together with a side product $Ru_5(\mu_5\text{-}C)(CO)_{13}(PPh_3)(\mu\text{-}\eta^2\text{-}O{=}CMe)[\mu\text{-}Au(PPh_3)]$, **3.8** in 6% yield obtained by substitution of a CO ligand of **3.5** by PPh_3. The PPh_3 was evidently derived from the added $MeAuPPh_3$. Compound **3.8** was synthesized independently and was fully characterized, see below.

An ORTEP diagram of the molecular structure of **3.7** as found in the solid state is shown in Fig. 3.2. Compound **3.7** is very similar to **3.6** except that it contains a second acetyl ligand, Me-C(42)-O(42), that is coordinated to Ru(4) in terminal η^1-coordination site in the location of the σ-methyl group in **3.6**, Ru4-C42 = 2.029(9) Å, C42-O42 = 1.171(12) Å. Other bond distances and angles are similar to those found in **3.6**. As expected, the methyl groups of the two acetyl groups in **3.7** exhibit separate resonances in the ^{1}H NMR spectrum, δ = 2.66 (s) and 2.46 (s).

Compound **3.7** was obtained initially in a low yield (2% yield) because its formation requires the addition of a molecule of CO. As expected, it was found that **3.7** can be obtained from **3.6** in a better yield (63%) by reaction of **3.6** with CO (1 atm) at room temperature, and so we believe it was formed in this way in the original reaction of 1 with MeAu(PPh_3). When heated to 60 °C for 23.5 h in a toluene solution, compound **3.7** eliminated CO, presumably from the terminally coordinated acetyl group, to regenerate **3.6** in 27% yield.

When **3.5** was allowed to react with PPh_3 in a hexane solution at reflux for 1.5 h, compound **3.8** was obtained in 76% yield. Compound **3.8** was characterized by a single-crystal X-ray diffraction analysis and an ORTEP diagram of its molecular structure as found in the solid state is shown in Fig. 3.3. The structure of **3.8** is very similar to that of compound **3.5** except that it contains a PPh_3 ligand coordinated to the bridging Ru atom Ru(4), Ru4-P2 = 2.417(2) Å in the place of one of the CO ligands in **3.5**. The acetyl ligand bridges the atoms Ru(1) and Ru(4) which are not mutually bonded, Ru1-C14 = 2.020(9) Å, Ru4-O14 = 2.124(6) Å and C14-O14 = 1.279(10) Å. The methyl resonance of the

bridging acetyl ligand occurs at δ = 1.86 in the ^{1}H NMR spectrum and there are two phosphorus resonances, δ = 67.7 (s), 31.4 (s) in the ^{31}P NMR spectrum.

When a solution of **3.6** in benzene solvent was heated to reflux for 1 h, two products that do not contain methyl groups $Ru_5(\mu_5\text{-}C)(CO)_{11}(\mu\text{-}CO)_3[\mu\text{-}Au(PPh_3)]_2$, **3.9** and $Ru_5(\mu_5\text{-}C)(CO)_{11}(\mu\text{-}CO)_2[\mu\text{-}Au(PPh_3)]_4$, **3.10** were obtained in 35% and 5% yields, respectively. Compound **3.9** was reported a number of years ago as a product of the reaction of the anion $[Ru_5(\mu_5\text{-}C)(CO)_{14}]^{2-}$ with $[AuPPh_3][C1O_4]$.[13] Compound **3.9** has not yet been structurally characterized crystallographically, so we have done that together with an X-ray diffraction structural analysis of compound **3.10** and both of these analyses are reported here.

An ORTEP diagram of the molecular structure of **3.9** as found in the solid state is shown in Fig. 3.4. Compound **3.9** contains a square pyramidal Ru_5C cluster with two mutually bonded $Au(PPh_3)$ groups bridging one triangular Ru_3 face Ru1-Ru2-Ru3 and an edge Ru2-Ru3 of the square pyramid, Au1-Au2 = 2.8817(5) Å. The compound contains fourteen carbonyl ligands; three of them are bridging ligands about the base of the Ru_5C square pyramid. The five ruthenium atoms in 9 contain a total of 74 valence electrons which is consistent with a square-pyramidal cluster, as observed.[17] The structure of 9 is very similar to that of the compound $Ru_5(\mu_5\text{-}C)(CO)_{14}[\mu\text{-}Au_2(Ph_2PCH_2CH_2PPh_2)]$ which contains a bridging $Ph_2PCH_2CH_2PPh_2$ ligand across the two gold atoms.[19]

An ORTEP diagram of the molecular structure of **3.10** is shown in Fig. 3.5. Compound **3.10** contains a square pyramidal cluster of five ruthenium atom with four $Au(PPh_3)$ groups. Two of the $Au(PPh_3)$ groups form a mutually bonded pair on the Ru1-Ru2-Ru3 face and Ru2-Ru3 edge of the square pyramid, Au1-Au2 = 2.8277(6) Å, similar to that found in **3.9**. An additional $Au(PPh_3)$ group, Au4, is found along the Ru4-Ru5 edge

of the Ru_5C square base and for the fourth $Au(PPh_3)$ group, atom Au3, is asymmetrically bonded across the square base and includes bonding to the interstitial carbido ligand C0, Ru2-Au3 = 3.1831(9) Å, Ru4-Au3 = 2.8963(8) Å, Ru5-Au3 = 2.8532(9) Å, Au3-C0 = 2.126(8) Å. The Ru3-Au3 distance, 3.387(8) Å, seems to be too long for a significant bonding interaction. The ^{31}P NMR spectrum of **3.10** exhibits four resonances, δ = 62.8 (s), 60.4 (s), 57.4 (s), and 34.0 (s) which is consistent with the structure found in the solid state. The five ruthenium atoms in **3.10** contain a total of 74 valence electrons which is consistent with the observed square-pyramidal cluster [18]. Compound 10 was also obtained directly from compound **3.9** in a low yield (9%) by reaction with $MeAu(PPh_3)$ in a heptane solution at reflux for 3 h.

Discussion

A summary of the reactions described in this report is given in Scheme 3.2. In this work we have shown that the reaction of **3.1** with $MeAu(PPh_3)$ yields two products, **3.5** and **3.6**, by the loss of CO from **3.1** and the oxidative addition of one and two equivalents $MeAu(PPh_3)$, respectively, to **3.1** in a cluster opening process. Both products contain a bridging acetyl ligand formed presumably by a CO insertion process involving in an unobserved precursor complex containing a σ-methyl ligand. A similar transformation was observed in the addition of CO to compound **3.2** to form **3.4**, the Ph homolog of **3.5**.[11] Compound **3.5** reacts with $MeAu(PPh_3)$ to form **3.6** which contains σ-methyl ligand and **3.6** adds CO accompanied by an insertion reaction to yield **3.7** which contains a terminally coordinated acetyl ligand. The formation of **3.7** is reversible and heating **3.7** leads to regeneration of **3.6** by CO elimination. Most interestingly, compound **3.6** also eliminates the acetyl ligand and the σ-methyl ligand in the form of acetone with addition of CO to

yield the digold compound **3.9**. Compound **3.9** can add two more $Au(PPh_3)$ groups and eliminate CO to yield the interesting tetragold complex **3.10**.

Conclusions

Methyl groups can be added to compound **3.1** by cluster opening reactions that oxidatively add the Au-C bond of $MeAu(PPh_3)$ to the ruthenium atoms under mild conditions. The $Au(PPh_3)$ group(s) are added as bridges across the ruthenium atoms. The methyl groups engage in facile CO insertion reactions leading to stable complexes containing bridging acetyl ligands and in one case, compound **3.6**, the acetyl ligand was combined with a methyl ligand to form acetone by reductive elimination.

Table 3.1. Crystallographic data for compounds **3.5** and **3.6**.

Compound	**3.5**	**3.6**
Empirical formula	$Ru5AuPO_{15}C_{35}H_{18}$	$Ru_5Au_2P_2O_{14}C_{53}H_{36}$
Formula weight	1411.78	1858.04
Crystal system	Monoclinic	Triclinic
Lattice parameters		
a (Å)	9.6245(3)	10.0683(3)
b (Å)	14.0955(4)	14.5070(4)
c (Å)	15.1564(5)	21.3998(6)
α (deg)	90.00	108.3630(10)
β (deg)	90.692(10)	91.2510(10)
γ (deg)	90.00	107.4400(10)
V ($Å^3$)	2056.0(11)	2806.72(14)
Space group	*P* n	*P* $\bar{1}$
Z value	2	2
ρ_{calc} (g / cm^3)	2.280	2.199
μ (Mo Kα) (mm^{-1})	5.449	6.635
Temperature (K)	294(2)	294(2)
$2\Theta_{max}$ (°)	50.06	50.06
No. Obs. (I > 2σ(I))	6799	9890
No. Parameters	515	687
Goodness of fit (GOF)	0.728	1.033
Max. shift in cycle	0.075	0.000
Residuals*: R1; wR2	0.0157; 0.0376	0.0375; 0.0837
Absorption Correction, Max/min	Multi-scan 1.000 / 0.578	Multi-scan 1.000 / 0.626
Largest peak in Final Diff. Map (e^- / $Å^3$)	0.260	1.049

* $R = \Sigma_{hkl}(||F_{obs}| - |F_{calc}||)/\Sigma_{hkl}|F_{obs}|$; $R_w = [\Sigma_{hkl}w(|F_{obs}| - |F_{calc}|)^2/\Sigma_{hkl}wF^2_{obs}]^{1/2}$; $w = 1/\sigma^2(F_{obs})$; $GOF = [\Sigma_{hkl}w(|F_{obs}| - |F_{calc}|)^2/(n_{data} - n_{vari})]^{1/2}$.

Table 3.2. Crystallographic data for compounds **3.7** and **3.8**.

Compound	**3.7**	**3.8**
Empirical formula	$Ru_5Au_2P_2O_{15}C_{54}H_{36}$	$Ru_5AuP_2O_{14}C_{52}H_{33}$
Formula weight	1886.05	1646.04
Crystal system	Triclinic	Triclinic
Lattice parameters		
a (Å)	10.0366(7)	10.5517(9)
b (Å)	14.8042(10)	15.1516(12)
c (Å)	21.6258(14)	17.1661(14)
α (deg)	71.2160(10)	92.095(2)
β (deg)	79.5360(10)	93.142(2)
γ (deg)	71.7660(10)	97.190(2)
V ($Å^3$)	2877.6(3)	2716.1(4)
Space group	$P\ \bar{1}$	$P\ \bar{1}$
Z value	2	2
ρ_{calc} (g / cm^3)	2.177	2.013
μ (Mo Kα) (mm^{-1})	6.474	4.167
Temperature (K)	294(2)	294(2)
$2\Theta_{max}$ (°)	50.06	50.06
No. Obs. (I > 2σ(I))	10150	9592
No. Parameters	705	668
Goodness of fit (GOF)	1.014	1.029
Max. shift in cycle	0.002	0.098
Residuals*: R1; wR2	0.0360; 0.0903	0.0494; 0.1149
Absorption Correction, Max/min	Multi-scan 1.000/0.693	Multi-scan 1.000 / 0.678
Largest peak in Final Diff. Map (e^- / $Å^3$)	1.251	1.901

* $R = \Sigma_{hkl}(||F_{obs}| - |F_{calc}||)/\Sigma_{hkl}|F_{obs}|$; $R_w = [\Sigma_{hkl}w(|F_{obs}| - |F_{calc}|)^2/\Sigma_{hkl}wF^2_{obs}]^{1/2}$; $w = 1/\sigma^2(F_{obs})$; GOF = $[\Sigma_{hkl}w(|F_{obs}| - |F_{calc}|)^2/(n_{data} - n_{vari})]^{1/2}$.

Table 3.2. Crystallographic data for compounds **3.9** and **3.10**.

Compound	**3.9**	**3.10**
Empirical formula	$Ru_5Au_2P_2O_{14}C_{51}H_{30}$	$Ru_5Au_4P_4O_{13}C_{86}H_{60}$
Formula weight	1847.50	2718.44
Crystal system	Monoclinic	Monoclinic
Lattice parameters		
a (Å)	51.2765(13)	24.2834(9)
b (Å)	14.5935(4)	12.9674(5)
c (Å)	35.3322(9)	27.0725(6)
α (deg)	90.00	90.00
β (deg)	122.533(10)	91.631(1)
γ (deg)	90.00	90.00
V (Å^3)	22290.4(10)	8521.5(6)
Space group	*C2/c*	$P2_1/c$
Z value	16	4
ρ_{calc} (g / cm^3)	2.202	2.199
μ (Mo Kα) (mm^{-1})	6.683	7.853
Temperature (K)	294(2)	294(2)
$2\Theta_{max}$ (°)	50.06	50.06
No. Obs. (I > 2σ(I))	19677	15072
No. Parameters	1345	979
Goodness of fit (GOF)	1.134	1.021
Max. shift in cycle	0.002	0.000
Residuals*: R1; wR2	0.0445; 0.0674	0.0430; 0.1039
Absorption Correction, Max/min	Multi-scan 0.4908 / 0.3488	Multi-scan 1.000 / 0.653
Largest peak in Final Diff. Map (e$^-$ / Å^3)	1.084	1.429

* $R = \Sigma_{hkl}(\,|\,|F_{obs}|-|F_{calc}|\,|)/\Sigma_{hkl}|F_{obs}|$; $R_w = [\Sigma_{hkl}w(|F_{obs}|-|F_{calc}|)^2/\Sigma_{hkl}wF^2_{obs}]^{1/2}$; $w = 1/\sigma^2(F_{obs})$; GOF = $[\Sigma_{hkl}w(|F_{obs}|-|F_{calc}|)^2/(n_{data}-n_{vari})]^{1/2}$.

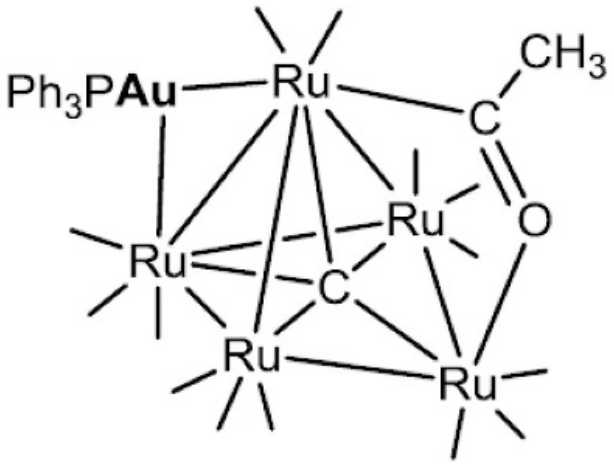

Figure **3.1**. A line drawing of compound **3.5**.

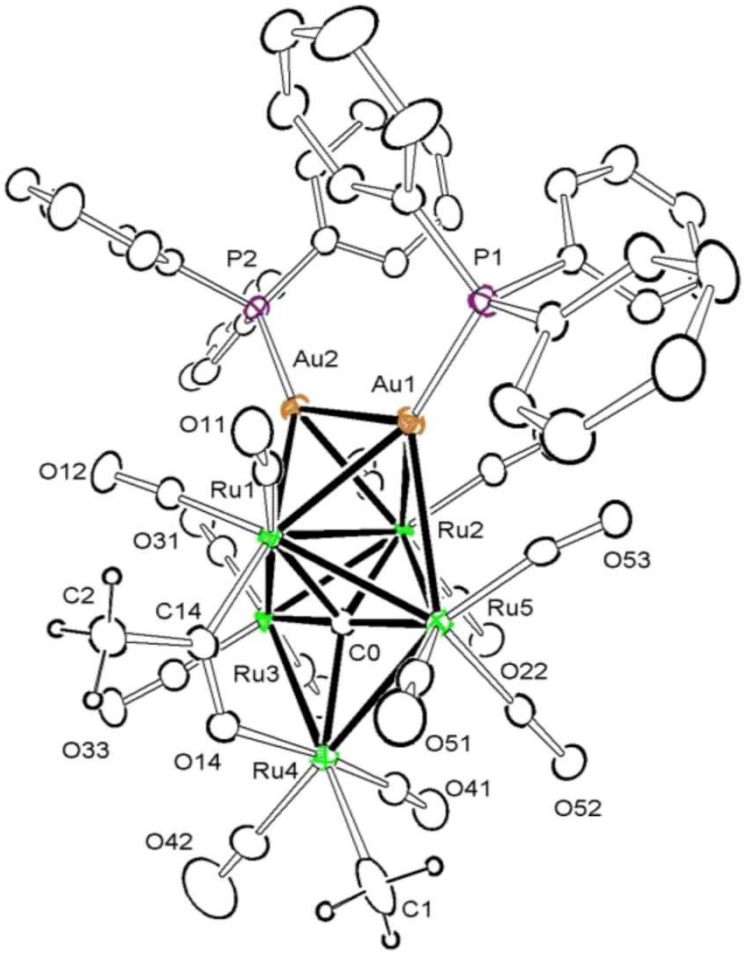

Figure 3.2. ORTEP diagram of the molecular structure of $Ru_5(\mu_5\text{-}C)(CO)_{13}(\mu\text{-}\eta^2\text{-}O{=}CMe)(Me)[\mu\text{-}Au_2(PPh_3)_2]$, **3.6**, showing 15% thermal ellipsoid probability. The hydrogen atoms of the PPh_3 ligands are omitted for clarity. Selected interactomic bond dstances (Å) are as follows: Ru1-Ru3 = 2.8447(9), Ru1-Ru5 = 2.9089(5), Ru1-Ru2 = 2.9913(9), Ru2-Ru5 = 2.8464(9) Ru2-Ru3 = 2.8651(10), Ru3-Ru4 = 2.9480(10), Ru4-Ru5 = 2.9342(10), Ru1-Au1 = 2.7954(7), Ru2-Au1 = 2.9153(7), Ru5-Au1 = 3.0948(7), Ru1-Au2 = 2.8349(7), Ru2-Au2 = 2.8761(7), Au1-Au2 = 2.8145(4), Ru4-O14 = 2.106(6), Ru4-C1 = 2.309(15), Ru1-C14 = 2.046(8), O14-C14 = 1.250(10), Ru1-C0 = 2.057(8), Ru2-C0 = 2.128(8), Ru3-C0 = 1.976(8), Ru4-C0 = 2.126(8), Ru5-C0 = 1.989(8).

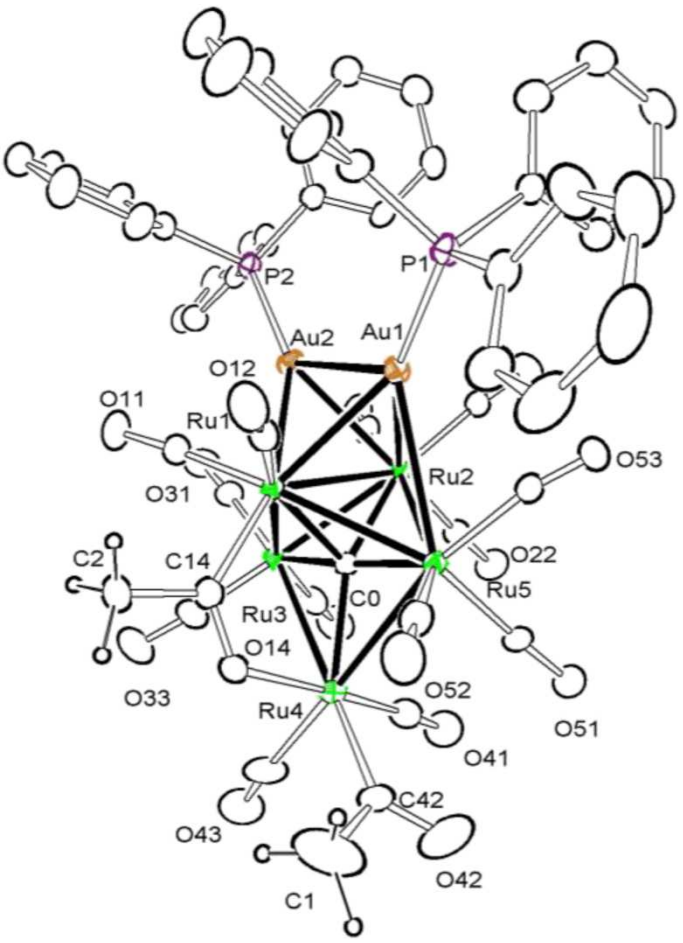

Figure 3.3. ORTEP diagram of the molecular structure of $Ru_5(\mu_5\text{-}C)(CO)_{14}(\mu\text{-}\eta^2\text{-}O{=}CMe)(O{=}CMe)[\mu\text{-}Au_2(PPh_3)_2]$, **3.7**, showing 15% thermal ellipsoid probability. The hydrogen atoms of the PPh3 ligands are omitted for clarity. Selected interactomic bond dstances (Å) are as follows: Ru1-Ru3 = 2.8240(8), Ru1-Ru5 = 2.9066(8), Ru1-Ru2 = 2.9891(8), Ru2-Ru5 = 2.8440(8) Ru2-Ru3 = 2.8600(9), Ru3-Ru4 = 2.9781(9), Ru4-Ru5 = 2.9502(9), Ru1-Au1 = 2.8011(7), Ru2-Au1 = 2.9258(6), Ru5-Au1 = 3.1476(6), Ru1-Au2 = 2.8241(6), Ru2-Au2 = 2.8505(6), Au1-Au2 = 2.8029(4), Ru4-O14 = 2.107(5), Ru4-C42 = 2.029(9), Ru1-C14 = 2.033(8), O14-C14 = 1.239(9), C42-C1 = 1.426(18), C42-O42 = 1.171(12), Ru1-C0 = 2.068(7), Ru2-C0 = 2.131(7), Ru3-C0 = 1.971(7), Ru4-C0 = 2.143(7), Ru5-C0 = 1.987(7).

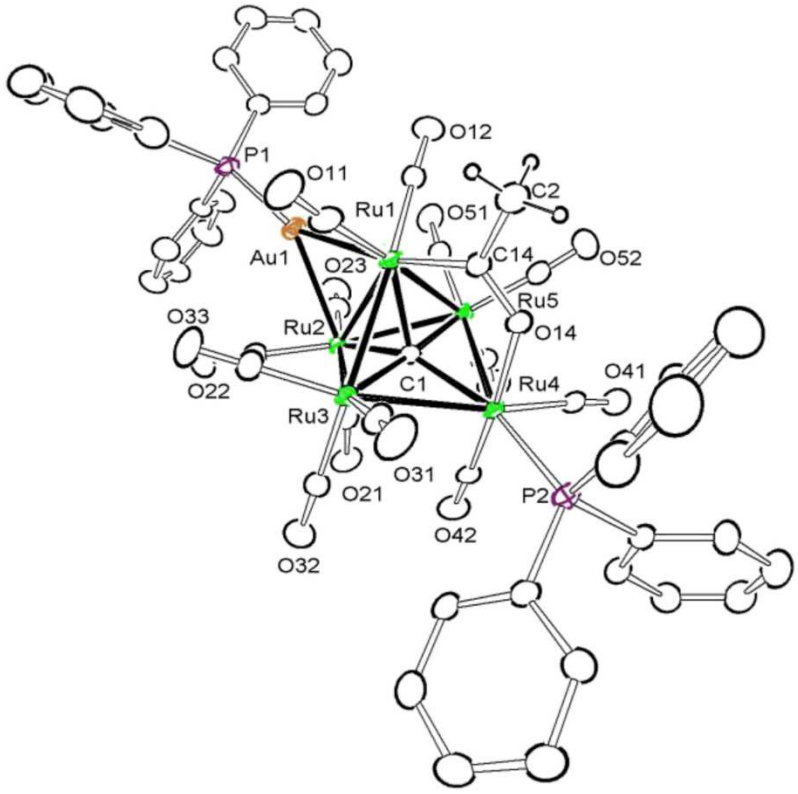

Figure 3.4. ORTEP diagram of the molecular structure of $Ru_5(\mu^5\text{-}C)(CO)_{13}(\mu\text{-}\eta^2\text{-}O{=}CMe)(PPh_3)[\mu\text{-}Au(PPh_3)]$, **3.8**, showing 15% thermal ellipsoid probability. The hydrogen atoms of the PPh_3 ligands are omitted for clarity. Selected interactomic bond dstances (Å) are as follows: Ru1-Ru3 = 2.8248(10), Ru1-Ru5 = 2.8119(11), Ru1-Ru2 = 2.9451(10), Ru2-Ru5 = 2.8668(11) Ru2-Ru3 = 2.8545(10), Ru3-Ru4 = 2.9494(10), Ru4-Ru5 = 2.8901(10), Ru1-Au1 = 2.7686(8), Ru2-Au1 = 2.7636(8), Ru4-P2 = 2.417(2), Ru4-O14 = 2.124(6), Ru1-C14 = 2.020(9), O14-C14 = 1.279(10), Ru1-C1 = 2.061(8), Ru2-C1 = 2.086(8), Ru3-C1 = 1.976(8), Ru4-C1 = 2.092(8), Ru5-C1 = 2.001(8).

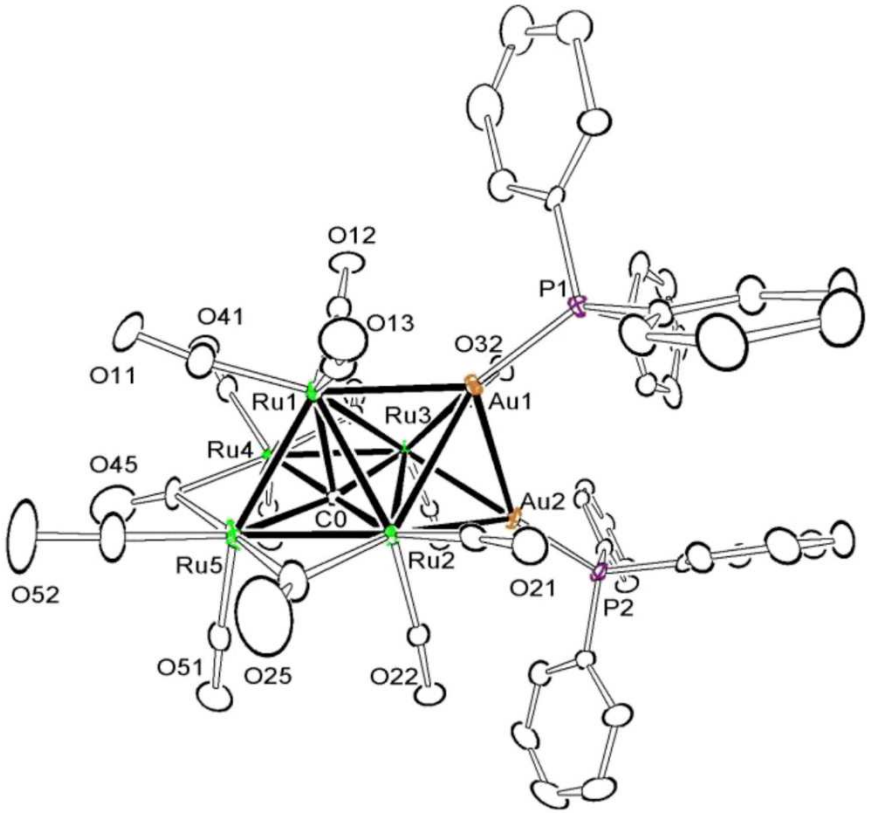

Figure 3.5. ORTEP diagram of the molecular structure of $Ru_5C(CO)_{11}(\mu\text{-}CO)_3[\mu\text{-}Au(PPh_3)]_2$, **3.9**, showing 15% thermal ellipsoid probability. The hydrogen atoms of the PPh_3 ligands are omitted for clarity. Selected interatomic bond distances (Å) are as follows: Ru1-Ru3 = 2.8892(9), Ru1-Ru5 = 2.8335(10), Ru1-Ru2 = 2.8632(10), Ru1-Ru4 = 2.8103(10), Ru2-Ru5 = 2.7361(10) Ru2-Ru3 = 3.0919(9), Ru3-Ru4 = 2.7819(9), Ru4-Ru5 = 2.7781(11), Ru1-Au1 = 2.7994(7), Ru2-Au1 = 2.9697(8), Ru3-Au1 = 2.8934(8), Ru2-Au2 = 2.7989(7), Ru3-Au2 = 2.7855(7), Au1-Au2 = 2.8817(5), Ru1-C0 = 2.179(8), Ru2-C0 = 1.996(8), Ru3-C0 = 2.007(8), Ru4-C0 = 2.055(8), Ru5-C0 = 2.036(8).

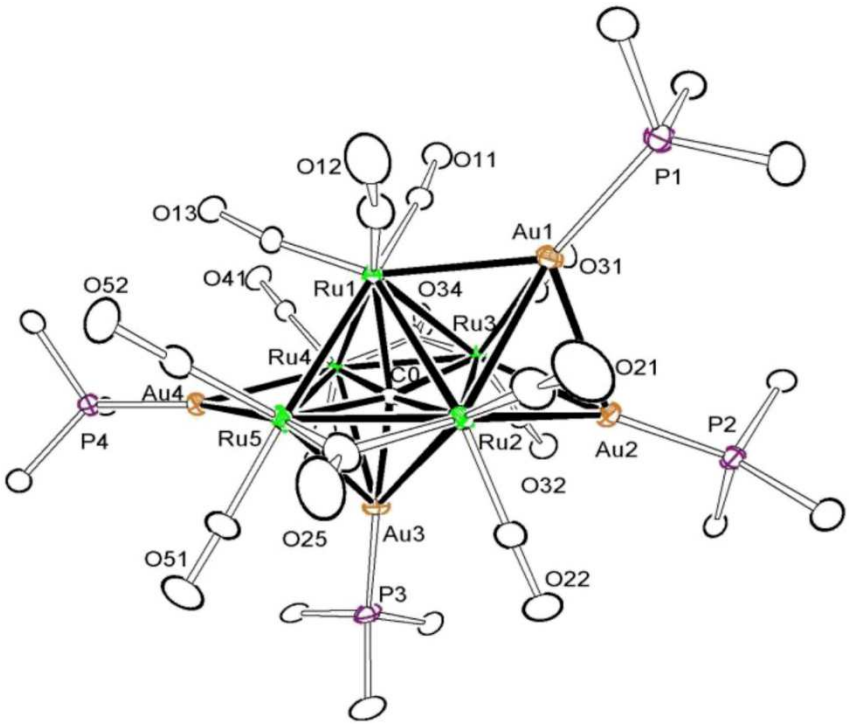

Figure 3.6. ORTEP diagram of the molecular structure of $Ru_5C(CO)_{11}(\mu\text{-}CO)_2[\mu\text{-}Au(PPh_3)]_4$, **3.10**, showing 15% thermal ellipsoid probability. The hydrogen atoms of the PPh_3 ligands are omitted for clarity. Selected interatomic bond distances (Å) are as follows: Ru1-Ru3 = 2.8495(10), Ru1-Ru5 = 2.8306(10), Ru1-Ru2 = 2.9243(11), Ru1-Ru4 = 2.8498(10), Ru2-Ru5 = 2.8148(11) Ru2-Ru3 = 3.0316(10), Ru3-Ru4 = 2.7968(10), Ru4-Ru5 = 3.0933(10), Ru1-Au1 = 2.8728(9), Ru2-Au1 = 2.8609(9), Ru3-Au1 = 2.9559(8), Ru2-Au2 = 2.7868(9), Ru3-Au2 = 2.8185(8), Ru2-Au3 = 3.1831(9), Ru4-Au3 = 2.8963(8), Ru5-Au3 = 2.8532(9), Ru4-Au4 = 2.7589(8), Ru5-Au4 = 2.7603(9), Au1-Au2 = 2.8277(6), Ru1-C0 = 2.136(8), Ru2-C0 = 2.047(8), Ru3-C0 = 2.097(8), Ru4-C0 = 2.081(8), Ru5-C0 = 2.104(8), Au3-C0 = 2.126(8).

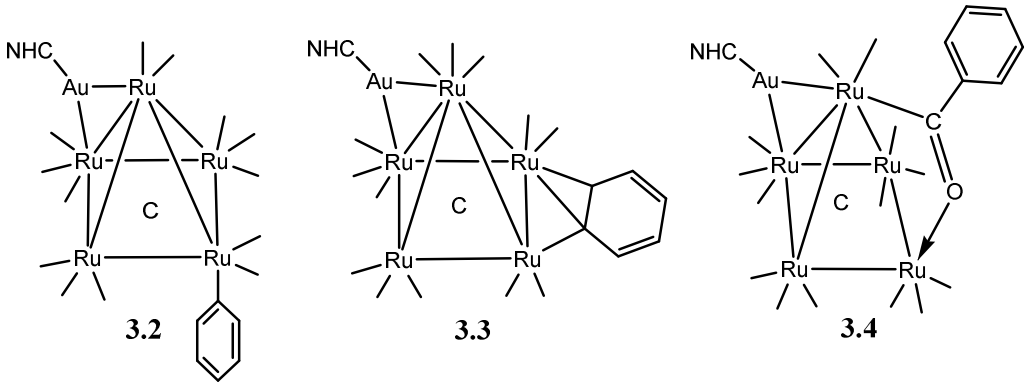

Scheme 3.1. Ru_5-Ph products from the reaction of $Ru_5C(CO)_{15}$ with PhAuNHC.

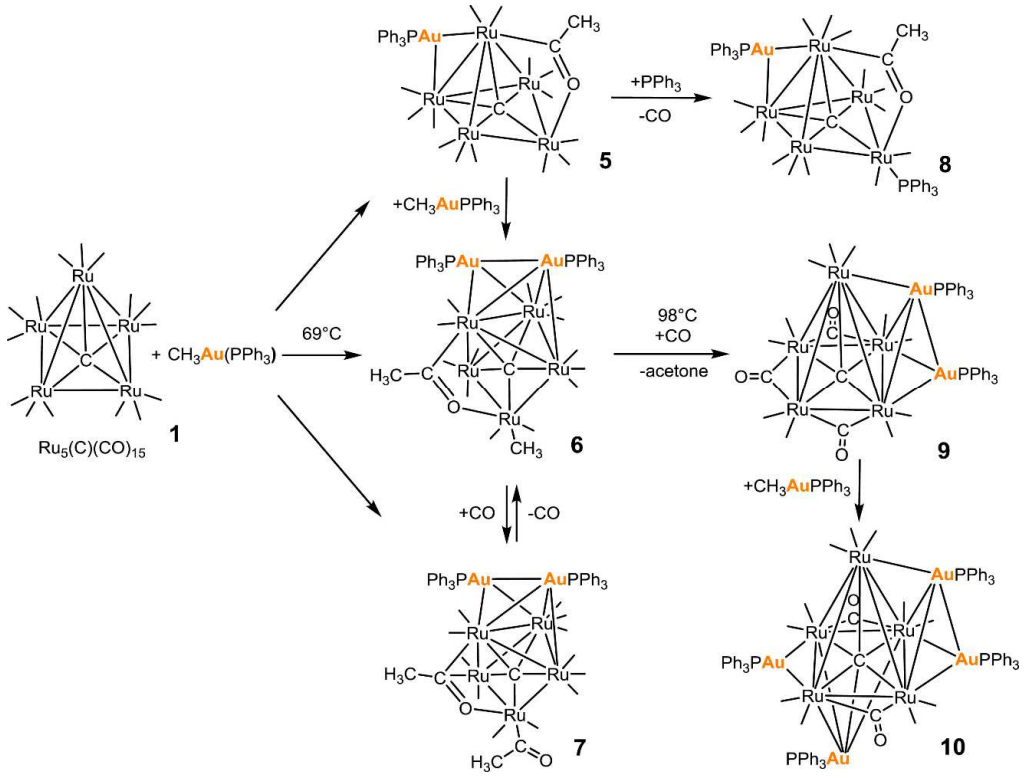

Scheme 3.2. Summary of the reaction of $Ru_5C(CO)_{15}$ with CH_3AuPPh_3.

3.5. References

1) (a) Salter, I.D. in *Comprehensive Organometallic Chemistry II,* Abel, E. W.; Stone, F. G. A.; Wilkinson, G., Oxford, UK, 1995, Vol. 10, Ch. 5, pp 255 – 322. (b) Salter, I.D. in *Metal Clusters in Chemistry*, Braunstein, P., Oro, L.A., Raithby, P.R., Eds. Wiley-VCH, Weinheim, 1999, Vol. 1, Ch.1.27, pp 509-534. (c) Salter, I.D., *Adv. Organomet. Chem.,* **1989**, 29, 249 – 343.

2) (a) Hashmi, A. S. K.; Toste, F. D., *Modern Gold Catalyzed Synthesis*, *Eds*, Wiley-VCH Publishers, Weinheim, Germany, 2012. (b) Kashmi, A.S.K.; Adams, R.D., Eds., *The Organometallic Chemistry of Gold*, *J. Organomet. Chem.*, 2015, 795, 1 – 77.

3) (a) Obradorsa, C.; Echavarren, A.M. *Chem. Commun*. **2014**, 50, 16 – 28; (b) Braun, I.; Asiri, A.M; Hashmi, A.S.K. *ACS Catal*. **2013**, 3., 1902−1907; (c) Hashmi, A.S.K. Chem. *Rev.* **2007**, 107, 3180–3211; (d) Jiménez-Núñez, E.; Echavarren, A.M. *Chem. Commun*. **2007**, 46, 333–346; (e) Fürstner, A.; Davies, P.W. *Angew. Chem., Int. Ed.* **2007**, 3410–3449; (f) Jiménez-Núñez, E.; Echavarren, A.M. *Chem. Rev*. **2008**, 108, 3326–3350; (g) Gorin, D.J.; Sherry, B.D.; Toste, F.D. *Chem. Rev*. **2008**, 108, 3351–3378; (h) Fürstner, A. *Chem. Soc. Rev*. 2009, 38, 3208–3221; (i) Shapiro, N.D.; Toste, F.D. *Synlett* **2010**, 675–691; (j) Patil, H.G.N.T.; Yamamoto,Y. *Chem. Rev*. **2008**, 108, 3395–3442; (k) Zhang, L. *Acc. Chem. Res*. **2014**, 47, 877 – 888; (l) Gaillard, S.; Cazin, C.S.J.; Nolan, S.P. *Acc. Chem. Res*. **2012**, 45, 778 – 787.

4) (a) Li, G.; Jin, R. *Acc. Chem. Res.* **2013**, 46, 1749 – 1758; (b) Oliver-Meseguer, J.; Cabrero-Antonino, J.R.; Dominquez, I.; Leyva-Perea, A.; Corma, A. *Science* **2012**, 338, 1452 – 1455; (c) Lee, S.; Molina, L.M.; Lopez, M.J.; Alonso, J.A.; Hammer, B.;

Lee, B., Seifert, S.; Winans, R.E.; Elam, J.W.; Pellin, M. J.; Vajda, S. *Angew. Chem. Int. Ed.* **2009**, 48, 1467-1471.

5) (a) Li, G.; Jin, R. *Acc. Chem. Res.* **2013**, 46, 1749 – 1758; (b) Haruta, M. *Gold Bull* **2004**, 37, 27 – 36; (c) Haruta, M. *Catal. Today* **1997**, 36, 153 – 166; (d) Haruta, M. *Appl. Catal. A: Gen.* **2001**, 222, 427 – 437; (e) Hashmi, A.S.K.; Hutchings, G.J. *Angew. Chem. Int. Ed.* **2006**, 45, 7896 – 7936; (f) Della Pina, C.; Falletta, E.; Prati, L.; Rossi, M. *Chem. Soc. Rev.* **2008**, 37, 2077 – 2095; (g) Herzing, A.J.; Kiely, C.J.; Carley, A.F.; Landon, P.; Hutchings, G.J. *Science* **2008**, 37, 1331 – 1335; (i) Zhang, L. *Acc. Chem. Res*. **2014**, 47, 877 – 888.

6) (a) Freakley, S.J.; He, Q.; Kiely, C.J.; Hutchings, G.J. *Catal. Lett.* **2015**, 145, 71 – 79; (b) Hutchings, G.J.; Kiely, C.J. *Acc. Chem. Res.* **2013**, 46, 1759 – 1772; (b) Hutchings, G.J. *Catalysis Today* **2014**, 238, 69–73; (c) Zhang, Y.; Cui, X.; Shi, F.; Deng, Y. *Chem. Rev.* **2012**, 112, 2467–2505; (d) Hutchings, G.J. *Chem. Commun.* **2008**, 1148 – 1164; (e) Lopez-Sanchez, J.A.; Dimitratos, N.; Glanvilla, N.; Kesavan, L.; Hammond, C.; Edwards, J.K.; Carley, A.F.; Kiely, C.; Hutchings, G.J. *Appl. Catal. A: Gen.* **2011**, 391, *400* – 406; (f) Enache, D.I.; Edwards, L.K.; Landon, P.; Solsona-Espriu, B.; Carley, A.F.; Herzing, A.A.; Watanabe, M.; Kiely, C.J.; Knight, D.W.; Hutchings, G.J. *Science* **2006**, 311, 362 – 365; (g) Miedziak, P.; Sankar, M.; Dimitratos, M.; Lopez-Sanchez, J.A.; Carley, A.F.; Knight, D.W.; Taylor, S.H.; Kiely, C.J.; Hutchings, G.J. *Catal. Today* **2011**, 164, 315–319; (h) Wang, R.; Zhiwei, Z.; Wu, Z.; Chen, C., Zhangfeng Qin, Z; Zhu, H.; Wang, G.; Wang, H.; Wu, C.; Dong, W.; Fan, W.; Wang, J.; *Chem. Commun.* **2013**, 49, 8250-8252; (i) Kesavan, L.; Tiruvalam, R.; Ab Rahim, M.H.; bin Saiman, M.I.; Enache, D.I.; Jenkins, R.L.; Dimitratos, N.;

Lopez-Sanchez, J.A.; Taylor, S.H.; Knight, D..W.; Kiely, C.J.; Hutchings, G.J. *Science* **2011**, 331, 195-199; (j) Chinchilla, L.E.; Olmos, C.M.; Villa, A.; Carlsson, A.; Prati, L.; Chen, X.; Blanco, G.; Calvino, J.J.; Hungría, A.B. *Catal. Today* **2015**, 253, 178–189.

7) Adams, R.D.; Chen, M. *Organometallics* **2012**, 31, 6457−6465.

8) Adams, R.D.; Rassolov, V.; Zhang, Q. *Organometallics* **2013**, 32, 6368−6378.

9) Adams, R.D.; Rassolov, V.; Wong, Y.O. *Angew. Chem.* **2014**, 53, 11006 -11009.

10) Adams, R.D.; Rassolov, V.; Zhang, Q. *Organometallics* **2013**, 32, 1587 - 1590.

11) Adams, R.D.; Tedder, J.; Wong, Y.O. *J. Organomet. Chem.* **2015**, 795, 2 – 10.

12) (a) Adams, R.D.; Luo, Z.; Chen, M.; Rassolov, V. *J. Organomet. Chem.* **2016**, 812, 95 – 107; (b) Adams, R.D.; Luo, Z. *J. Organomet. Chem.* **2016**, 812, 108 – 114.

13) Cowie, A.G.; Johnson, B.F.G.; Lewis, J; Raithby, P.R. *J. Chem. Soc., Chem. Commun.*, **1984**, 1710 – 1712.

14) Johnson, B.F.G.; Lewis, J.; Nicholls, J.N.; Puga, J.; Raithby, P.R.; Rosales, M.J.; McPartlin, M.; Clegg, W. *J. Chem. Soc., Dalton Trans*. **1983**, 277 – 290.

15) SAINT+, version 6.2a, Bruker Analytical X-ray Systems, Inc., Madison, WI, **2001**.

16) G. M. Sheldrick, SHELXTL, version 6.1, Bruker Analytical X-ray Systems, Inc., Madison, WI, **1997**.

17) Mingos, D.M.P. in *The Chemistry of Metal Cluster Complexes,* Shriver, D.F., Kaesz, H.D., and Adams, R.D., Eds. VCH Pub. 1990, Ch. 2, pp 40.

18) Amoroso, A. J.; Edwards, A.J.; Johnson, B.F.G.; Lewis, J; Al-Mandhary, M.R.; Raithby, P.R.; Saharan, V.P.; Wong, W.-T. *J. Organomet. Chem*. **1993**, 443, C11 – C13.

CHAPTER 4

Open Pentaruthenium Cluster Complexes Formed from the Addition of Benzoic Acid to $Ru_5(C)(CO)_{15}$[3]

[3] Adams, R. D.; Smith, M.; Tedder, J. *J. Clust. Sci.* **2017**, 28, 695-702.
Reprinted here with permission from publisher

4.1 Introduction

The square pyramidal cluster compound $Ru_5(C)(CO)_{15}$, **4.1** has been shown to exhibit a remarkable chemistry based on its ability to add ligands by a cluster opening cleavage of one of its Ru–Ru bonds between the apical positioned Ru atom and one of the basal positioned Ru atoms, e.g., Eq. (4.1).[1] Compound **4.1** also reacts with $(Ph_3P)AuCl$ or HCl by oxidative addition processes by a similar cleavage of a Ru–Ru bond in the cluster, e.g., Eq. (4.2).[2] Adams et al. obtained open and closed Ru_5 clusters formed by the addition of $HSiEt_3$ to **4.1** see Eq. (4.3).[3] These two products could be interconverted by the addition and elimination of CO.

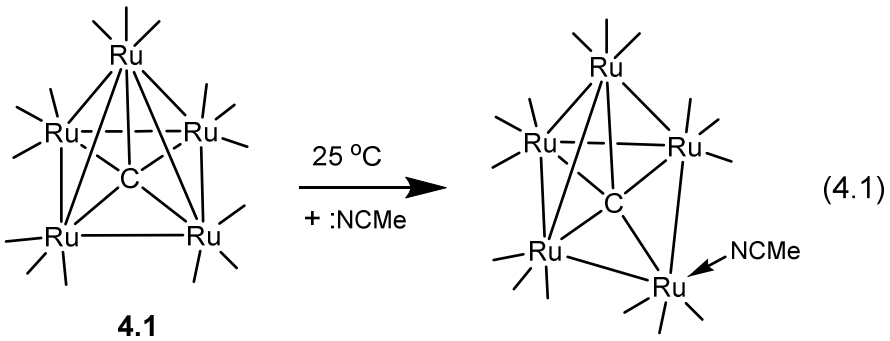

4.1 (4.1)

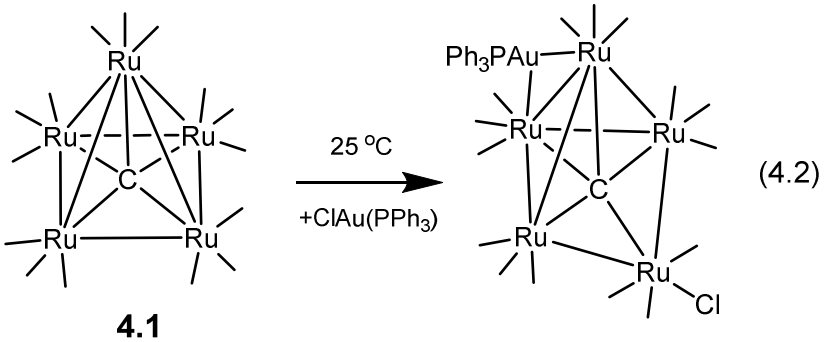

4.1 (4.2)

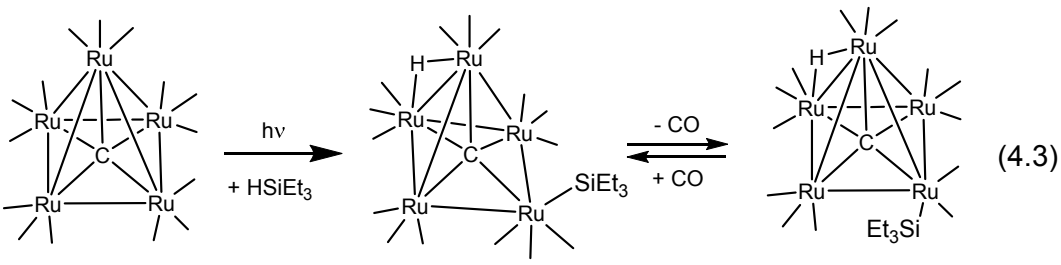

(4.3)

4.1 $Ru_5(C)(CO)_{15}(SiEt_3)(\mu\text{-}H)$ $Ru_5(C)(CO)_{14}(SiEt_3)(\mu\text{-}H)$

Carboxylate ligands are able to coordinate to metal atoms in η^1-mondentate A, η^2-chelate B and μ–η^2-bridging modes, C (Figure 4.1).

We have now investigated the reaction of **4.1** with benzoic acid, $C_6H_5CO_2H$, and have obtained two new complexes, $Ru_5(C)(CO)_{14}(\eta 2\text{-}O_2CC_6H_5)(\mu\text{-}H)$, **4.2** and $Ru_5(C)(CO)_{14}(\mu\text{–}\eta_2\text{-}O_2CC_6H_5)(\mu\text{-}H)$, **4.3** that are formed by an addition of benzoic acid to the Ru_5 cluster by a process that involves an opening of the cluster and the loss of one of its CO ligands. Compounds **4.2** and **4.3** have been characterized structurally by single-crystal X-ray diffraction analyses.

4.2 Experimental Section

General Data

All reactions were performed under an atmosphere of nitrogen. Reagent grade solvents were dried by standard procedures and were freshly distilled prior to use. Infrared spectra were recorded on a Thermo Scientific Nicolet IS10. ^{1}H NMR for **4.2** spectra was recorded on a Varian Mercury 300 spectrometer operating at 300.1 MHz. ^{1}H NMR for **4.3** spectra was recorded on a Bruker Avance III spectrometer operating at 400.2 MHz. Mass spectrometric (MS) measurements were performed by a direct-exposure probe by using electron impact (EI) ionization for the compounds **4.2** and **4.3**. $Ru_3(CO)_{12}$ was obtained

from STREM and was used without further purification. $Ru_5(C)(CO)_{15}$, **4.1**, was prepared according to previously reported procedure.[4] Benzoic acid ($C_6H_5CO_2H$) was obtained from Sigma-Aldrich and was used without further purification. Product separations were performed by TLC in air on Analtech 0.25 mm silica gel 60 Å F254 glass plates.

Reaction of 4.1 with $C_6H_5CO_2H$

39.3 mg (0.042 mmol) of **4.1** was added to a 50 mL three-neck flask with a solution of 15.2 mg (0.012 mmol) of $C_6H_5CO_2H$ in 20 mL of octane. After heating for 7 h at 80 °C, the solvent was removed in vacuo, and the products were then isolated by TLC with a hexane/CH_2Cl_2 solvent mixture to provide in order of elution: 19.2 mg of $Ru_5(C)(CO)_{14}(\eta^2$-$O_2CC_6H_5)(\mu$-H), **4.2** (44 % yield) and 4.6 mg of $Ru_5(C)(CO)_{14}(\mu$–η^2-$O_2CC_6H_5)(\mu$-H), **4.3** (11 % yield). Spectral data for **4.2**: IR vCO (cm^{-1} in hexane): 2103(w), 2074(s), 2063(s), 2057(sh), 2040(m), 2029(m), 2006(m), 1981(w). ^{1}H NMR (CD_2Cl_2, in ppm) δ = 7.81 (d, $J_{H–H}$ = 7.2 Hz, 2H), 7.52 (t, $J_{H–H}$ = 7.2 Hz, 1H), 7.38 (t, $J_{H–H}$ = 7.2 Hz, 2H), −22.42 (s, 1H, hydride). EI/MS m/z, M^+ = 1032 and the isotope distribution is consistent with the presence of five ruthenium atoms. Spectral data for 3: IR vCO (cm^{-1} in hexane): 2106(w), 2090(vw), 2078(m), 2055(m), 2048(w), 2032(m), 2022(w), 2010(w), 1996(w), 1981(w). 1H NMR (CD_2Cl_2, in ppm) δ = 7.49 (d, $J_{H–H}$ = 7.6 Hz, 2H), 7.36 (t, $J_{H–H}$ = 7.6 Hz, 1H), 7.24 (t, $J_{H–H}$ = 7.6 Hz, 2H), −28.03 (s, 1H, hydride). EI/MS m/z, M^+ = 1032 and the isotope distribution is consistent with the presence of five ruthenium atoms.

Determination of the Equilibrium Ratio Between 4.2 and 4.3

(a) 17.8 mg (0.017 mmol) of pure 4.2 was dissolved in d_8-toluene and placed in an NMR tube. The solution was then heated to 95 °C for 21 h. After this time, the hydride resonances were integrated and the ratio of compounds **4.2**/**4.3** was then 1/1.54.

(b) 7.4 mg (0.0072 mmol) of pure **4.3** was dissolved in deuterated toluene and placed in an NMR tube. The solution was then heated to 95 °C for 21 h. After this time, the hydride resonances were integrated and the ratio of compounds **4.2**/**4.3** was then 1/1.54.

Crystallographic Analyses

Yellow crystals of **4.2** suitable for X-ray diffraction analyses were obtained by slow evaporation of solvent from a solution in hexane solvent at room temperature. Orange single crystals of **4.3** suitable for X-ray diffraction analysis were obtained by slow evaporation of solvent from a solution in hexane solvent at room temperature. Each data crystal was glued onto the end of a thin glass fiber. X-ray intensity measurements were made by using a Bruker SMART APEX CCD-based diffractometer using Mo Kα radiation (λ = 0.71073 Å). The raw data frames were integrated with the SAINT+ program by using a narrow-frame integration algorithm.[5] Corrections for Lorentz and polarization effects were also applied with SAINT+. An empirical absorption correction based on the multiple measurements of equivalent reflections was applied by using the program SADABS.[5] All structures were solved by a combination of direct methods and difference Fourier syntheses, and refined by full-matrix least squares on F2 by using the SHELXTL software package.[6] The hydride ligands were located and refined in both analyses. All remaining non-hydrogen atoms were placed in geometrically idealized positions included as standard

riding atoms during the least-squares refinements. Crystal data, data collection parameters, and results of the analyses are listed in Table 4.1. Compound **4.2** crystallized in the triclinic crystal system. The space group $P\ \bar{1}$ was assumed and confirmed by the successful solution and refinement of the structure. Compound **4.3** crystallized in the monoclinic crystal system. The space group P2(1)/c was established by the systematic absences in the data and then confirmed by the successful solution and refinement of the structure.

4.3 Results and Discussions

Two products $Ru_5(C)(CO)_{14}(\eta^2\text{-}O_2CC_6H_5)(\mu\text{-}H)$, **4.2** (44 % yield) and $Ru_5(C)(CO)_{14}(\mu\text{–}\eta^2\text{-}O_2CC_6H_5)(\mu\text{-}H)$, **4.3** (11 % yield) have been isolated from the reaction of **4.1** with benzoic acid ($C_6H_5CO_2H$) in a solution in octane solvent after heating to 80 °C for 7 h. Compound **4.2** can be partially converted to **4.3** in 55 % yield by heating to 98 °C for 4 h, and **4.3** can be converted partially back to **4.2** by similar heating. Compound **4.2** appears to be the one formed first in the reaction, because it is present in the highest yields early in the reaction period, but based on the 1.54/1.0 (**4.3**/**4.2**) equilibrium ratio, **4.3** the more stable of the two products.

Both products have been characterized IR, ^{1}H NMR and mass spectral analysis and structurally by single-crystal X-ray diffraction analysis. An ORTEP diagram of the molecular structure of **4.2** is shown in Fig. 4.2. The molecule consists of a cluster of five ruthenium atoms arranged in the form of a Ru_4 butterfly tetrahedron with the fifth Ru atom bridging the wingtips of the butterfly tetrahedron. There is a carbido ligand in the center of the cluster and a chelating benzoate ligand, type B, coordinated to bridging ruthenium atom Ru(4). The compound contains one hydrido ligand, H(1), which was found in a bridging

position across the Ru(1)–Ru(2) bond, Ru(1)–Ru(2) = 2.8522(5) Å. Its resonance was observed at δ = −22.42 in its ^{1}H NMR spectrum. The Ru–Ru and Ru–C distances to the carbido ligand are similar to those in other open Ru5C carbonyl cluster complexes.[1,2] The Ru–O distances to the chelating benzoate ligand, Ru(4)–O(1) = 2.131(3) Å, Ru(4)–O(2) = 2.169(3) Å, are similar to those of other chelating benzoate ligands coordinated to ruthenium atoms.[7-10] Compound **4.2** contains 14 linear terminally coordinated CO ligands distributed as shown in Fig. 4.2.

An ORTEP diagram of the molecular structure of **4.3** is shown in Fig. 4.3. Compound **4.3** also contains an open Ru-bridged butterfly cluster of five ruthenium atoms similar to that of **4.2** and a benzoate ligand, but in this case the η^2-benzoate ligand bridges two of the Ru atoms, Ru(1) and Ru(4). The Ru–O distances to the benzoate ligand are slightly shorter than those in **4.2**, Ru1–O1 = 2.1251(18) Å and Ru4–O2 = 2.1280 (18) Å. There are many examples of carboxylate bridged pairs of ruthenium atoms,[11] but there are only a few examples of benzoate ligands bridging pairs of Ru atoms that are not mutually bonded.[12] The hydrido ligand bridges the Ru(1)–Ru(2) bond, 2.8328(3) Å. Its ^{1}H NMR resonance is found at an unusually high field value, δ = −28.03. The Ru–Ru and Ru–C distances to the carbido ligand are similar to those found in **4.1** and **4.2**.

4.4 Conclusions

A summary of the reactions studied in this report is shown Scheme 4.1. Compound **4.2** was formed by a cluster-opening addition of benzoic acid to compound **4.1**. One CO ligand was eliminated from **4.1** in the reaction and thus the benzoate ligand adopted a η^2-chelating coordination in which it serves as a three-electron donor to the metal atoms. The carboxylate hydrogen atom, which serves as a one-electron donor, was shifted to the cluster

and adopted a bridging position across the hinge bond of the Ru_4 butterfly tetrahedral portion of the cluster. Overall, the five ruthenium atoms in compound **4.2** contain a total of 76 valence electrons and thus each metal atom formally achieves an 18 electron configuration.[13] The ruthenium atoms in compound **4.1** contain only 74 electrons and it contains the well-known square pyramidal structural arrangement of the five metal atoms. The formation of **4.2** and **4.3** from **4.1** leads to a net increase in the cluster valence electron count by two electrons. This requires the cleavage of one Ru–Ru bond which turns out to be one of the bonds between the apical Ru atom and one of the Ru atoms in the square base. A similar transformation was observed in the addition of NCMe to **4.1**, see Eq. (4.1).

Compounds **4.2** and **4.3** exist in an equilibrium in solution **4.3**/**4.2** = 1.54 at equilibrium at 95 °C, so **4.2** can be partially converted to the more stable product **4.3** that contains a bridging η^2-bridging benzoate ligand that also serves as a three-electron donor and vice versa. If **4.2** truly is a precursor to **4.3** as the evidence suggests, then the cluster-opening addition of benzoic acid to **4.1** proceeds by the addition of one its oxygen atoms to one of the Ru atoms in the base of the square pyramidal cluster of **4.1**, analogous to the addition of other donors, e.g., Eq. (4.1). Loss of a CO ligand from that same Ru atom would then allow the second oxygen atom to become coordinated to this metal atom and this would complete the formation of compound **4.2**. The transformation of **4.2** to **4.3** requires one of the benzoate oxygen atoms to shift to one of the ruthenium atoms in the hinge of the carbide-bridged Ru_4 butterfly tetrahedron portion of the molecule. This shift would require an accompanying series of shifts of CO ligands, not shown in the scheme (probably by intramolecular terminal–bridge–terminal rearrangements) around the cluster from ruthenium atom to which the carboxylate oxygen atom was added, Ru(1), to the ruthenium

atom from which the carboxylate oxygen atom departed, Ru(4), because Ru(1) loses a CO ligand and Ru(4) gains a CO ligand in the course of the transformation of the benzoate from a chelating ligand to bridging ligand, see Fig. 4.2. The interconversions of carboxylate ligands between chelating and bridging coordination sites are not common, but have been observed previously.[14]

Table 4.1. Crystallographic data for compounds **4.2** and **4.3**.

Compound	**4.2**	**4.3**
Empirical formula	$Ru_5O_{16}C_{22}H_6$	$Ru_5O_{16}C_{22}H_6$
Formula weight	1031.62	1031.62
Crystal system	Triclinic	Monoclinic
Lattice parameters		
a (Å)	9.6985(4)	9.5167(2)
b (Å)	15.7434(7)	15.8466(3)
c (Å)	20.1885(9)	19.2889(4)
α (deg)	103.56(10)	90.00
β (deg)	96.49(10)	92.84
γ (deg)	91.92(10)	90.00
V (Å^3)	2971.6(2)	2905(10)
Space group	$P\ \bar{1}$	$P2_1/c$
Z value	4	4
ρ_{calc} (g / cm^3)	2.31	2.36
μ (Mo Kα) (mm^{-1})	2.55	2.61
Temperature (K)	294(2)	294(2)
$2\Theta_{max}$ (°)	50.06	50.04
No. Obs. (I > 2σ(I))	10501	5125
No. Parameters	783	392
Goodness of fit (GOF)	1.10	1.066
Max. shift in cycle	0.002	0.001
Residuals*: R_1; wR_2 (2σ(I))	0.0260; 0.0652	0.0182; 0.0425
Absorption Correction, Max/min	Multi-scan 1.000 / 0.775	Multi-scan 1.000 / 0.877
Largest peak in Final Diff. Map (e$^-$/Å^3)	0.715	0.314

* $R = \Sigma_{hkl}(\,|\,|F_{obs}|-|F_{calc}|\,|)/\Sigma_{hkl}|F_{obs}|$; $R_w = [\Sigma_{hkl}w(|F_{obs}|-|F_{calc}|)^2/\Sigma_{hkl}wF^2_{obs}]^{1/2}$; $w = 1/\sigma^2(F_{obs})$; GOF = $[\Sigma_{hkl}w(|F_{obs}|-|F_{calc}|)^2/(n_{data} - n_{vari})]^{1/2}$.

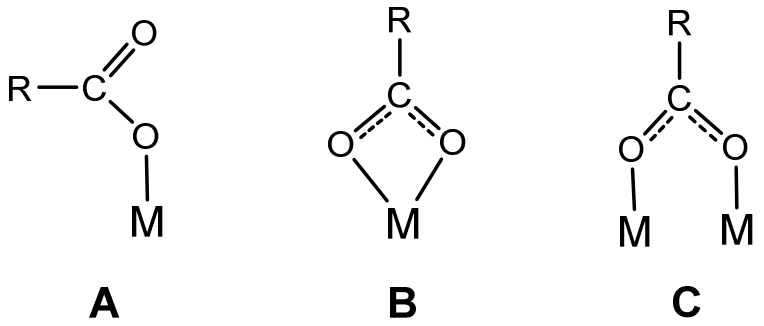

Figure 4.1. Coordination modes of carboxylate ligand to metal atom.

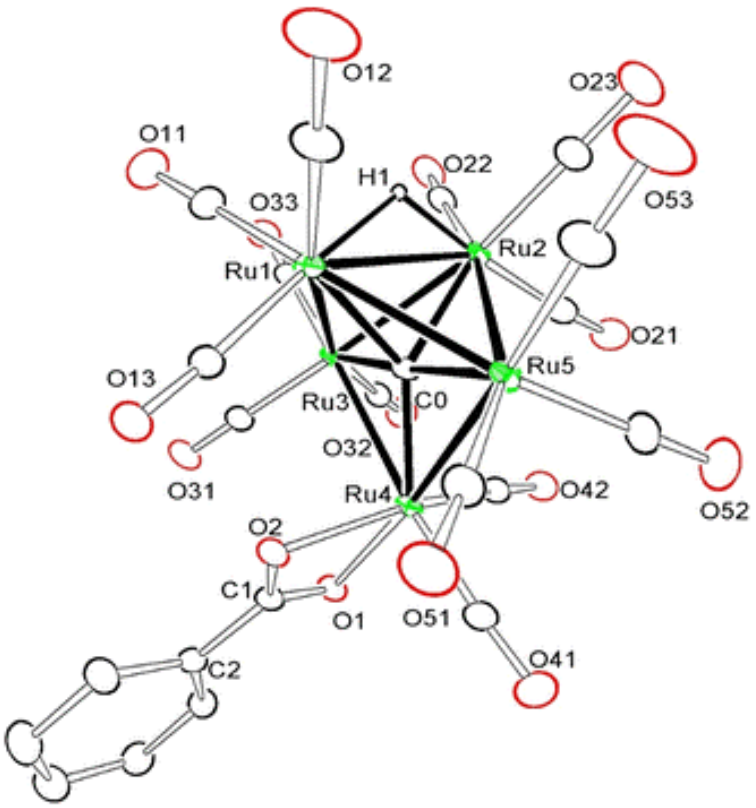

Figure 4.2. An ORTEP diagram of the molecular structure of compound **4.2** showing 15% probability thermal ellipsoid. The hydrogen atoms on the phenyl ring are omitted for clarity. Selected interactomic bond dstances (Å) and bond angles (°) are as follows: Ru1-Ru3 = 2.8476(4), Ru1-Ru5 = 2.8487(5), Ru1-Ru2 = 2.8522(5), Ru2-Ru5 = 2.8423(4) Ru2-Ru3 = 2.8607(4), Ru3-Ru4 = 2.9140(5), Ru4-Ru5 = 2.8657(5), Ru1-H1 = 1.58(3), Ru2-H1 = 1.58(4), Ru4-O1 = 2.131(3), Ru4-O2 = 2.169(3), O1-C1 = 1.275(5), O2-C1 = 1.270(4), C1-C2 = 1.482(5), Ru1-C0 = 2.107(4), Ru2-C0 = 2.107(3), Ru3-C0 = 1.962(4), Ru4-C0 = 2.046(4), Ru5-C0 = 1.984(4), O2-C1-O1 = 117.2(4).

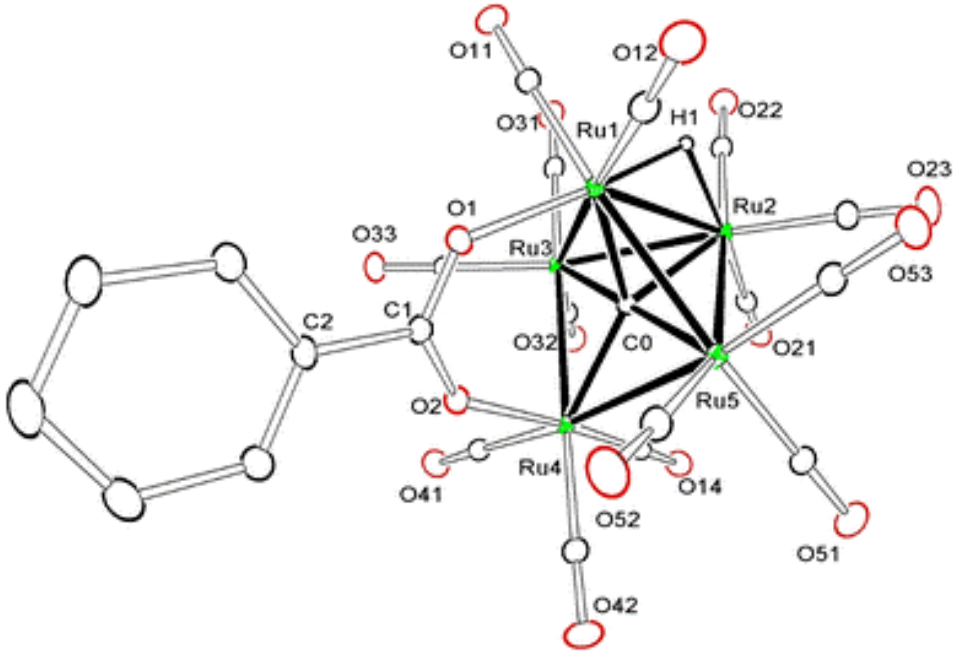

Figure 4.3. An ORTEP diagram of the molecular structure of **4.3**, showing 15% thermal ellipsoid probability. The hydrogen atoms on the phenyl ring are omitted for clarity. Selected interactomic bond distances (Å) are as follows: Ru1-Ru2 = 2.8328(3), Ru(1)-Ru(3) = 2.8486(3), Ru1-Ru5 = 2.8504(3) Ru2-Ru3 = 2.8480(3), Ru2-Ru5 = 2.8775(3), Ru3-Ru4 = 2.8754(3), Ru4-Ru5 = 2.8694(3), Ru1-H1 = 1.61(3), Ru2-H1 = 1.90(3), Ru1-O1 = 2.1251(18), Ru4-O2 = 2.1280(18), O2-C1 = 1.259(3), O1-C1 = 1.252(3), C1-C2 = 1.502(4), Ru1-C0 = 2.043(2), Ru2-C0 = 2.092(2), Ru3-C0 = 1.971(2), Ru4-C0 = 2.091(2), Ru5-C0 = 1.967(2). Bond angle (°) of O1-C1-O2 = 128.0(3).

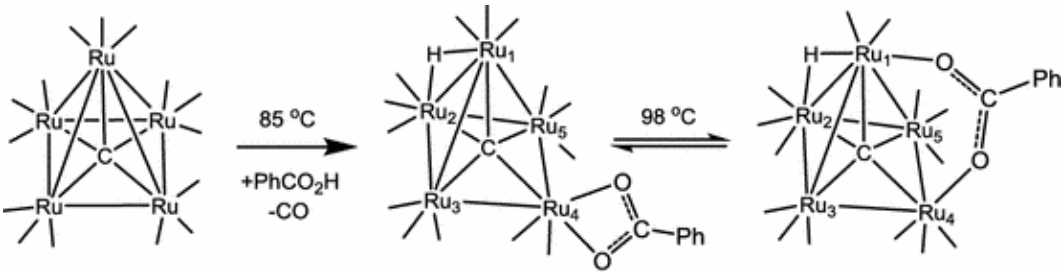

Scheme 4.1. Reaction of Ru5C(CO)15, **4.1**, with benzoic acid to yield complexes **4.2** and **4.3** that are in a dynamic equilibrium with each other.

4.5 References

1. Johnson, B.F.G.; Lewis, J.; Nicholls, J.N.; Puga, J.; Raithby, P.R.; Rosales, M.J.; McPartlin M.; Clegg, W. *J. Chem. Soc., Dalton Trans.* ***1983,*** 277 – 290.
2. Johnson, B.F.G.; Lewis, J.; Nicholls, J.N.; Puga, J.;Whitmire, K.H. *J. Chem. Soc., Dalton Trans* ***1983,*** 787 – 797.
3. Adams, R.D.; Captain, B.; Fu, W. *Organometallics* **2000***, 19*, 3670 - 3673.
4. Farrar, D.H.; Jackson, P.F.; Johnson, B.F.G.; Lewis, J.; Nicholls, J.N.; McPartlin, M. *J. Chem. Soc., Chem. Commun.* **1981**,415 - 416.
5. SAINT^{+} Version 6.2a. Bruker Analytical X-ray System, Inc., Madison, WI, USA, **2001**.
6. G. M. Sheldrick (**1997**). SHELXTL Version 6.1: Bruker Analytical X-ray Systems, Inc., Madison, WI, USA.
7. Groves, B.R.; Arbuckle, D.I.; Essoun, E.; Lundrigan, T.L.; Wang, R.; Aquino, M.A.S. *Inorg. Chem*. **2013**, *52*, 11563 − 11572.
8. Sorkau, A.; Schwarzer, K.; Wagner, C.; Poetsch, E.; Steinborn, D. *J. Mol. Catal. A: Chem*. **2004** *224*, 105 – 109.
9. Smith, E.F.; Pridmore, N.E.; Whitwood, A.C.; Lynam, J.M. *Organometallics* **2014***,* 33, 7260 – 7269.
10. Lian Lu; X., Ng; S.Y.; Vittal, J.J.; Tan, G.K.; Goh. L.Y.; Hor, T.S.A. *J. Organomet. Chem.* **2003***, 688*, 100 – 111.
11. Aquino, M.A.S. *Coord. Chem. Rev*. **1998**, 170, 141 – 202.
12. Mikata, Y.; Takeshita,N.; Miyazu, *T.;* Miyata, Y.; Tanase, T.; Kinoshita, *I.;* Ichimura, A.; Mori, *W.;* Takamiza, S.; Yano, S. *J. Chem. Soc., Dalton Trans*. **1998**, 1969 – 1972.

13. Mingos, D. M. P.; Wales, D. J., in *Introduction to Cluster Chemistry*, Prentice Hall Pub., Englewood Cliffs, NJ, 1990, Ch. 2.

14. Janssen, F.F.B.J.; Peters, L.C.J.M.; Schlebos, P.P.J.; Smits, J.M.M.; de Gelder, R.; Rowan, A.E. *Inorg. Chem*. **2013**, *52*, 13004 − 13013.

CHAPTER 5

CH Activations in Aldehydes in Reactions with $Ru_5(\mu_5\text{-}C)(CO)_{15}$[4]

[4] Adams, R. D.; Akter, H.; Tedder, J.; *J. Organomet. Chem.* **2018**, *In Review*.

5.1 Introduction

The ability to activate and functionalize C-H bonds to produce higher-value organic chemicals is of great importance to the chemical industry. Accordingly, the activation and functionalization of C-H bonds by metal complexes has received considerable research attention in recent years. Most studies have been focused on the activation of aliphatic[1] and aromatic[2] C-H bonds. The activation of aldehydic C-H bonds has received considerable attention and is a key step in reactions known generally as the hydroacylation of alkenes and alkynes that are catalyzed by transition metal complexes (eq. 1).[3]

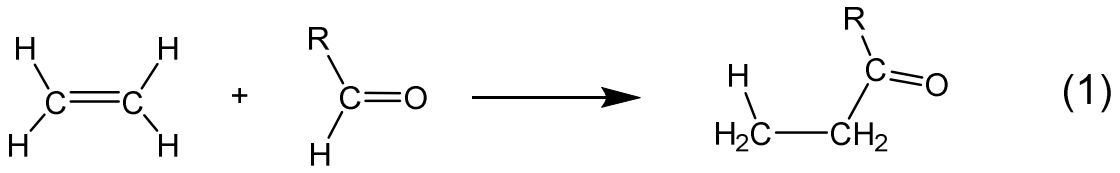

(1)

The oxidative addition of aldehydic C-H bonds to a metal complex will yield a metal complex **I** containing acyl and hydrido ligands that can undergo further transformations such as decarbonylation with subsequent formation of C-H bonds to yield a RH product by reductive elimination[4], or by coupling with an unsaturated substrate, e. g. C_2H_4, to yield a ketone by hydroacylation[5], (eq. 2).

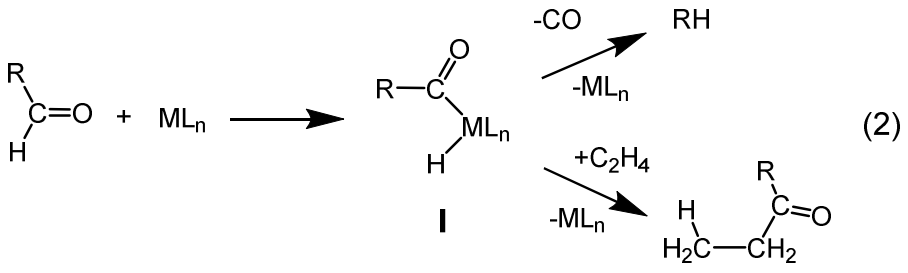

(2)

The competing decarbonylation process can significantly limit the usefulness of the more valuable hydroacylation reaction.

In recent studies, we have shown that the pentaruthenium cluster complex $Ru_5(\mu_5\text{-}C)(CO)_{15}$, **5.1**, is able to activate the formyl C-H bond of N,N-dimethylformamide to yield the complex $Ru_5(\mu_5\text{-}C)(CO)_{14}(\mu\text{-}\eta^2\text{-}O{=}CN(CH_3)_2)(\mu\text{-}H)$ that contains a bridging formamido $\eta^2\text{-}O{=}CN(CH_3)_2$ ligand formed by opening of the Ru_5C square pyramid cluster of metal atoms via oxidative addition of the formyl C-H bond, eq. (3).[6]

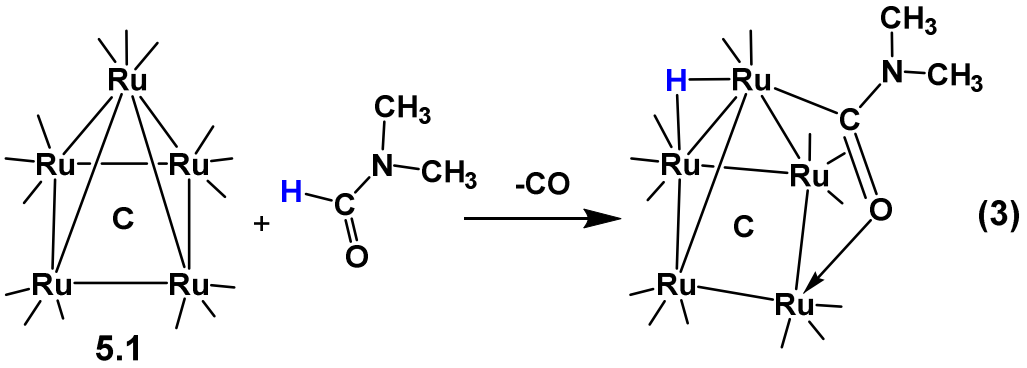

(3)

We have now investigated the reactions of **5.1** with a series of selected aldehydes: benzaldehyde, cinnamaldehyde, furfural and 5-hydroxymethylfurfural, and have observed some similar cluster opening C – H bond activations at the formyl functional groups and in some cases C – H activations on neighboring aryl and olefinic substitutents. Herein we report on our new studies of the activation of aldehydic C-H bonds by the cluster complex **5.1**.

5.2 Experimental Section

General Data

All reactions were performed under an atmosphere of nitrogen. Reagent grade solvents were dried by standard procedure and were freshly distilled prior to use. Infrared spectra were recorded on a Thermo Scientific Nicolet IS10. ^{1}H NMR spectra was recorded

on a Varian Mercury 300 spectrometer operating at 300.1 MHz. Mass spectrometric (MS) measurements were performed by a direct-exposure probe by using electron impact (EI) ionization. $Ru_3(CO)_{12}$ was obtained from STREM and was used without further purification. $Ru_5(\mu_5\text{-}C)(CO)_{15}$, **5.1** was prepared from $Ru_3(CO)_{12}$ according to a previously reported procedure.[7] Benzaldehyde, C_6H_5CHO, was obtained from Sigma-Aldrich and was purified by trap-to-trap distillation techniques prior to use. Trans-cinnamaldehyde, $C_6H_5CH{=}CHCHO$, was obtained from Sigma Aldrich and was used without any further purification. Furfural was purchased from Sigma Aldrich and was used without further purification. 5-Hydroxymethyl-2-furaldehyde (5-Hydroxymethylfurfural) was purchased from Sigma Aldrich and was used without further purification. Product separations were performed by TLC in air on Analtech 0.25 mm and 0.50 mm silica gel 60 Å F254 glass plates and silica gel column chromatography on silica gel 60, 0.606 -0.2 mm (70 – 230 mesh).

Reaction of $Ru_5(\mu_5\text{-}C)(CO)_{15}$, 5.1, with Benzaldehyde at 98 ˚C

49.9 mg (0.053 mmol) of **5.1** was added to a 50 mL three-neck flask with a solution of 30 µL of benzaldehyde in 20 mL of degassed heptane. After heating for 13 h at 98 ˚C, the solvent was removed in vacuo, and the products were then isolated by TLC with a hexane/methylene chloride solvent mixture to provide in order of elution: 2.7 mg of $Ru_5(\mu_5\text{-}C)(CO)_{14}(\eta^2\text{-}O{=}CH(C_6H_4))(\mu\text{-}H)$, **5.2** (5% yield), and 22.3 mg of $Ru_5(\mu_5\text{-}C)(CO)_{14}(\mu\text{-}\eta^2\text{-}O{=}CPh)(\mu\text{-}H)$, **5.3** (41% yield). Spectral data for **5.2**: IR νCO (cm^{-1} in hexane): 2096(w), 2066(s), 2056(vs), 2048(m), 2034(w), 2022(w), 2018(sh), 2013(sh), 1995(w), 1989(w), 1974(vw). ^1H NMR (CD_2Cl_2, in ppm) δ = 9.28 (s, 1H, C(**H**)=O), 8.37 (d, $^3J_{H\text{-}H}$ = 8 Hz, 1H, C**H**$(CH)_2$CH), 8.00 (d, $^3J_{H\text{-}H}$ = 8 Hz, 1H, C**H**$(CH)_2$CH), 7.55 (t, $^3J_{H\text{-}H}$ = 7 Hz, 1H,

CH(C**H**)$_2$CH), 7.30 (t, $^3J_{H-H}$ = 7 Hz, 1H, CH(C**H**)$_2$CH), -22.36 (s, 1H, hydride). EI/MS *m*/*z*. 1015. The isotope distribution pattern is consistent with the presence of five ruthenium atoms. Spectral data for **5.3:** IR νCO (cm^{-1} in hexane): 2105(w), 2077(s), 2060(vs), 2053(m), 2033(m), 2017(m), 2012(sh), 2003(w), 1993(w), 1972(w). ^{1}H NMR (CD_2Cl_2, in ppm) δ = 7.46-7.29 (m, 5H, O=C(C$_6$**H$_5$**)), -20.96 (s, 1H, hydride). EI/MS *m*/*z*. 1015. The isotope distribution pattern is consistent with the presence of five ruthenium atoms.

Reaction of Ru$_5$(μ$_5$-C)(CO)$_{15}$, 5.1, with trans-cinnamaldehyde at 98 ˚C

39.9 mg (0.043 mmol) of **5.1** was added to a 100 mL three-neck flask with a solution of 100 μL of C_6H_5CH=CHCHO in 25 mL of degassed heptane. After heating for 13 h at 98 ˚C, the solvent was removed *in vacuo*, and the products were then isolated by TLC with a hexane/methylene chloride solvent mixture to provide in order of elution: 2.6 mg of Ru$_5$(μ$_5$-C)(CO)$_{14}$(η^2-O=CHCH=CPh)(μ-H), **5.4** (6% yield), and 8.1 mg of Ru$_5$(μ$_5$-C)(CO)$_{14}$(μ-η^2-O=CCH=CHPh)(μ-H), **5.5** (18% yield). Spectral data for **5.4**: IR νCO (cm^{-1} in hexane): 2097(w), 2068(s), 2058(vs), 2049(m), 2036(w), 2024(sh), 2020(w), 1997(w), 1990(w), 1981(vw). ^{1}H NMR (CD_2Cl_2, in ppm) δ = 8.715 (d, 1H, $^3J_{H-H}$ = 0.6 Hz, O=C**H**CH=CPh), 7.52-7.40 (m, 5H, O=CHCH=C**Ph**), 7.091 (d, 1H, $^3J_{H-H}$ = 0.6 Hz, O=CHC**H**=CPh), -22.34 (s, 1H, hydride). EI/MS *m*/*z*. 1042. The isotope distribution pattern is consistent with the presence of five ruthenium atoms. Spectral data for **5.5**: IR νCO (cm^{-1} in hexane): 2104(w), 2077(s), 2059(vs), 2052(m), 2033(m), 2016(m), 2011(sh), 2002(w), 1983(vw), 1974(vw), 1969(vw). ^{1}H NMR (CD_2Cl_2, in ppm) δ = 7.49-7.34 (m, 5H, CCH=CH(C$_6$**H$_5$**)), 6.86 (d, 1H, $^3J_{H-H}$ = 15 Hz, CC**H**=CHPh), 6.65 (d, 1 H, $^3J_{H-H}$ = 15 Hz, CCH=C**H**Ph), -20.82 (s, 1H, hydride). EI/MS *m*/*z*. 1042. The isotope distribution pattern is consistent with the presence of five ruthenium atoms.

Decomposition of $Ru_5(\mu_5\text{-}C)(CO)_{14}(\mu\text{-}\eta^2\text{-}O{=}CPh)(\mu\text{-}H)$ at 105 °C

10.9 mg (0.0107 mmol) of **5.3** was added to a NMR tube in deuterated toluene solution. After heating for 10.25 h at 105°C in a thermostatted oil bath. Benzene formation was observed in the H NMR spectrum. The solvent was removed *in vacuo* and the products were then isolated by column chromatography on silica gel by using a hexane/methylene chloride mixture which yielded 4.9 mg (49% yield) of **5.1**. The presence of benzene was confirmed by ^{1}H NMR spectroscopy.

Thermal Decomposition of 5.4 at 105 °C

6.0 mg (0.0058 mmol) of **5.4** was added to a NMR tube in deuterated toluene solution. After heating for 17 h at 105°C in a thermostated oil bath. The solvent was removed *in vacuo*, and the products were then isolated by TLC with a hexane/methylene chloride mixture to provide in order of elution: 0.6 mg (11.1% yield) of **5.1**, 0.8 mg (13.3% yield) of **4**, 0.6 mg (10% yield) of **5.5**. The presence of trans-cinnmaldehyde was confirmed by ^{1}H NMR spectroscopy.

Thermal Decomposition of 5.5 at 105 °C

15.5 mg (0.0149 mmol) of **5.5** was added to a NMR tube in deuterated toluene solution. After heating for 13 h at 105°C in a thermostatted oil bath. Formation of styrene was observed in the ^{1}H NMR spectrum. The solvent was removed in vacuo, and the products were then isolated by column chromatography on silica gel by using a hexane/methylene chloride mixture which yielded 9.3 mg (67% yield) of **5.1**. Formation of styrene was observed in the ^{1}H NMR spectrum.

Crystallographic Analyses

Single crystals of compounds **5.2-5.5** suitable for X-ray diffraction analyses were obtained by slow evaporation of solvent from solutions of the pure compounds in hexane solvent at room temperature. Each data crystal for compounds **5.2-5.5** was glued onto the end of a thin glass fiber. X-ray intensity data for compounds **5.2-5.5** was measured by using a Bruker SMART APEX CCD-based diffractometer by using Mo Kα radiation (λ = 0.71073 Å). The raw data frames were integrated with the SAINT+ program by using a narrow frame integration algorithm.[8] Correction for Lorentz and polarization effects were also applied with SAINT+. An empirical absorption correction based on the multiple measurements of equivalent reflections was applied by using the program SADABS was applied in each analysis.[8] All structures were solved by a combination of direct Methods and difference Fourier syntheses, and refined by full-matrix least squares refinement on F^2 by using the SHELXTL software package.[11] All non-hydrogen atoms were refined with anisotropic thermal parameters. All hydrogen atoms were placed in geometrically idealized positions and were included as standard riding atoms during the final least-squares refinements with C-H distances fixed at 0.96 Å. The hydrido ligands bonded to the metal atoms in compounds **5.2-5.5** were located and refined in each analysis. Compounds **5.3**, **5.4**, **and 5.5** crystallized in the monoclinic crystal system. The space group $P2_1/c$ was identified for compound **5.4** based on the systematic absences observed in the intensity data. The space group $P2_1/n$ was identified for compound **5.3** on the basis of systematic absences observed in the intensity data. The space group *P*c or *P*2/c was identified for compound **5.5** on the basis of systematic absences observed in the intensity data. The centrosymmetric group *P*2/c was chosen and confirmed by successful structure refinement.

Compound **5.5** contains two independent formula equivalents of the complex in the asymmetric crystal unit. Both molecules have similar molecular structures. Compound **5.2** crystallized in the triclinic crystal system. The space group P-1 was chosen for compound **5.2** and confirmed by successful structure refinement of each structure. Crystal data, data collection parameters, and results of the refinements for each analysis are listed in Table 5.1 in the Supporting Information.

5.3 Results and Discussion

The reaction of **5.1** with benzaldehyde at 98 °C for 13 h yielded two new pentaruthenium carbido cluster compounds: $Ru_5(\mu_5\text{-}C)(CO)_{14}(\eta^2\text{-}O{=}CH(C_6H_4))(H)$, **5.2**, (5% yield), and $Ru_5(\mu_5\text{-}C)(CO)_{14}(\mu\text{-}\eta^2\text{-}O{=}CPh)(\mu\text{-}H)$, **5.3**, (41% yield). Compounds 5.**2** and **5.3** were both characterized by IR, and ^{1}H NMR spectroscopy, mass spectrometry and single-crystal X-ray diffraction analyses. An ORTEP diagram of the molecular structure of 5.**2** is shown in Figure 5.1. Compound **5.2** contains a chelating, ortho-metallated benzaldehyde ligand coordinated to an open Ru_5C cluster. The cluster can be described as a Ru_4C butterfly cluster that is bridged at the wingtips by a fifth Ru atom, Ru(4). The chelating ortho-metallated benzaldehyde ligand is coordinated by the oxygen atom of the aldehyde oxygen atom and one of the ortho-positioned carbon atoms of the phenyl ring that was formed by an oxidative addition of the C-H bond to the metal atom. It serves as a three electron donor to the metal atom Ru4. The hydrogen atom became a hydrido ligand and is located on the Ru1 – Ru2 bond of Ru_4 butterfly cluster portion of the cluster, Ru1 – H1 = 1.72(5) Å, Ru2 – H1 = 1.83(5) Å, δ = -22.36. Having a total of fourteen terminal CO ligands distributed as shown in Figure **5.1**, compound **5.2** contains a total of 76 cluster valence

electrons which is consistent with that of an 'open' Ru_5C square pyramidal cluster of five metal atoms.[7,12]

Compound **5.3** is an isomer of **5.2**. An ORTEP diagram of the molecular structure of **5.3** as found in the solid state is shown in Figure **5.2**. Compound **5.3** contains an O=C-coordinated, η^2-bridging benzoyl ligand across the open edge of a Ru wingtip-bridged Ru_4C cluster similar to that found in **5.2**. The acyl carbon atom C1 is bonded to Ru1 and to oxygen atom O1 bonded to Ru4, Ru1-C1 = 2.062(5) Å, Ru4-O1 = 2.114(4) Å, C1-O1 = 1.258(6) Å. The hydrido ligand bridges the hinge metal atoms Ru1 and Ru2, Ru1 – H1 = 1.78(2) Å, Ru2 – H1 = 1.81(2) Å, δ = -20.96.

Compound **5.3** is structurally similar to the compound $Ru_5(\mu_5\text{-}C)(CO)_{14}(\mu\text{-}\eta^2\text{-}O{=}CPh)[\mu\text{-}Au(NHC)]$ that was obtained by the addition of CO to the compound $Ru_5(\mu_5\text{-}C)(CO)_{14}(\mu\text{-}\eta^2\text{-}O{=}CPh)(\mu\text{-}Au(NHC))$ except that this one contains a bridging Au(NHC) group in the place of the hydride ligand in **5.3**(Figure 5.3).[13]

With fourteen CO ligands, compound **5.3** also contains a total of 76 electrons which is consistent with that of an 'open' Ru_5C square pyramidal cluster of five metal atoms.[7,12] When compound **5.3** was heated to 105°C for 10.25 h the benzoyl ligand was decarbonylated with formation of benzene confirmed by ^1H NMR spectroscopy and reformation of **5.1** in 49% yield (Figure 5.4).

It has been shown that **5.1** readily reacts with donors, such as $N{\equiv}CCH_3$ by ligand addition by using the lone pair of electrons on the N atom to yield the opened Ru_5 cluster in the complex $Ru_5(\mu_5\text{-}C)(CO)_{15}(NCCH_3)$ without the loss of a CO ligand, see Scheme 1.[7]

It is proposed that similar reaction of **5.1** with benzaldehyde at the oxygen atom could produce a similar cluster opening intermediate **I** by the coordination of the oxygen atom to one of the ruthenium atoms in the base of the square pyramid, see Scheme 2. From that intermediate the reaction diverges to give the two different products. The formation of **5.2** could occur by the loss of a CO ligand from the metal atom Ru4 followed by oxidative addition of one of the ortho CH bonds on the phenyl ring to Ru4. Alternatively, the formation of **5.3** could occur by the loss of a CO ligand from Ru5 or Ru3 followed by the oxidation addition of the formyl CH bond to the metal which loses the CO ligand, see Scheme 2.

In additional studies, we examined the reaction of **5.1** with trans-cinnamaldehyde. Two new products: $Ru_5(\mu_5\text{-}C)(CO)_{14}(\eta^2\text{-}O{=}CHCH{=}CPh)(\mu\text{-}H)$, **5.4** in 6% yield and $Ru_5(\mu_5\text{-}C)(CO)_{14}[\mu\text{-}\eta^2\text{-}O{=}C(CH{=}CHPh)](\mu\text{-}H)$, **5.5** in 18% yield were obtained when a solution of **5.1** with trans-cinnamaldehyde in a heptane solvent was heated to reflux (98 °C) for 13 h. Compounds **5.4** and **5.5** were both characterized by single crystal X-ray diffraction analyses and ORTEP diagrams of their molecular structures are shown in Figures 5.5 and 5.6.

Compound **5.4** consists of an open Ru_5C cluster similar to that found in compound **5.2**, but it contains a metallated, chelating η^2-cinnamoyl ligand,O=CHCH=CPh coordinated to the metal atom Ru4. The cinnamoyl ligand is coordinated by the oxygen atom of the aldehyde group and the β-carbon atom C3 of the olefin group which has undergone C – H bond activation at Ru4 to form a five membered metallacyclic ring, Ru4-C3 = 2.069(5) Å, Ru4-O1 = 2.117(3) Å, C1-O1 = 1.253(7) Å. There is a hydrido ligand bridging the two hinge metal atoms Ru1 and Ru2, Ru1 – H1 = 1.74(6) Å, Ru2 – H1 =

1.92(6) Å, δ = -22.34. With the chelating cinnamoyl acting as a three-electron ligand and the bridging hydride as a one-electron ligand, the total electron count for the Ru_5 cluster is 76 electrons which is consistent with that of an opened square-pyramidal cluster, as observed. Compound **5.4** can be converted to **5.5** when heated to 105 ^{o}C for 17 h in a toluene-d_8 solution, but the formation of free cinnamaldehyde in the NMR solution suggests that the transformation is not an intramolecular one, but may involve reduction elimination of cinnamaldehyde from **5.4** followed by an oxidative-readdition of cinnamaldehyde to the cluster to form **5.5**.

Compound **5.5** is analogous in structure to that of compound **5.3** consisting of an open Ru_5C cluster with a bridging O=C-coordinated, η^2-O=CH=CPh, cinnamoyl ligand in place of the bridging benzoyl ligand observed in **5.3**. The hydrogens of the alkene are coordinated trans to each other across the C=C bond and was confirmed by ^{1}H NMR spectroscopy, 6.86 (d, $^3J_{H-H}$ = 15 Hz), 6.65 (d, $^3J_{H-H}$ = 15 Hz). There is a hydrido ligand H1 bridging the two hinge Ru atoms of the Ru_4C portion of the cluster, Ru1 – H1 = 1.72(5) Å, Ru2 – H1 = 1.83(5) Å, δ = -20.82. Compound **5.5** contains a total of 76 electrons which is consistent with that of an opened square-pyramidal cluster. When compound **5.5** was heated to 105 °C for 13 h in toluene solvent, the cinnamoyl ligand was decarbonylated with formation of free styrene detected by H NMR spectroscopy and compound **5.1** was regenerated in 67% yield.

5.4 Conclusions

A summary of the reactions and products studied in this work are shown in Scheme 5.3. We have shown that **5.1** possesses the ability to activate the formyl C-H bond and certain aromatic and alkenyl CH bonds in selected aldehydes via reactions that lead to an

opening of the square pyramidal cluster of **5.1** by cleavage of one of the apical-basal Ru – Ru bonds.

The reaction of **5.1** with benzaldehyde and cinnamaldehyde yields μ-η^2 bridging benzoyl and cinnamoyl ligands, respectively, that bridge an opened apical-basal Ru-Ru bond formed from a two-electron donation of the carbonyl oxygen of the aldehyde to a basal Ru atom and C-H activation at the apical Ru. A minor, ortho-metalated product was formed from the reaction of **5.1** with benzaldehyde with the C-H activation occurring ortho to the formyl group of the phenyl ring to yield a η^2-chelating group, O=CH(C_6H_5). In the reaction of **5.1** with trans-cinnamaldehyde, a secondary product is formed by C-H activation at the β C-H bond to the formyl group of the alkene to yield a chelating ligand, O=CHCH=CPh. The decomposition of the bridging acyl groups led to reductive decarbonylation of the bridging acyl to regeneration of **5.1**. The functionalization of the activated formyl C-H bond of aldehydes by $Ru_5(\mu_5\text{-}C)(CO)_{15}$, **5.1** with unsaturated compounds could lead to the functionalization of alkenes and alkynes in a manner similar to that observed in the reaction of **5.1** with *N*,*N*-dimethylformamide and C_2H_2.[6]

Table 5.1. Crystal data, data collection parameters for compounds **5.2** and **5.3**.

Compound	**5.2**	**5.3**
Empirical formula	$Ru_5O_{15}C_{22}H_6$	$Ru_5O_{15}C_{22}H_6$
Formula weight	1015.62	1015.62
Crystal system	Triclinic	Monoclinic
Lattice parameters		
a (Å)	9.1318(5)	9.1215(4)
b (Å)	9.5301(5)	33.5654(14)
c (Å)	18.1201(10)	9.3979(4)
α (deg)	95.1760(10)	90.00
β (deg)	90.6190(10)	102.7440(10)
γ (deg)	114.4890(10)	90.00
V (Å^3)	1427.20(13)	2806.4(2)
Space group	*P*-1	$P2_1/n$
Z value	2	4
ρ_{calc} (g / cm^3)	2.363	2.404
μ (Mo Kα) (mm^{-1})	2.655	2.700
Temperature (K)	294(2)	294(2)
$2\Theta_{max}$ (°)	50.06	50.04
No. Obs. (I > 2σ(I))	5036	4953
No. Parameters	387	383
Goodness of fit (GOF)	1.156	1.363
Max. shift in cycle	0.005	0.000
Residuals*: R1; wR2	0.0297; 0.0807	0.0282; 0.0703
Absorption Correction, Max/min	Multi-scan 1.000/0.763	Multi-scan 1.000 / 0.780
Largest peak in Final Diff. Map (e$^-$ / Å^3)	2.103	1.651

*$R1 = \Sigma_{hkl}(||F_{obs}|-|F_{calc}||)/\Sigma_{hkl}|F_{obs}|$; $wR2 = [\Sigma_{hkl}w(|F_{obs}|-|F_{calc}|)^2/\Sigma_{hkl}wF^2_{obs}]^{1/2}$; $w = 1/\sigma^2(F_{obs})$; $GOF = [\Sigma_{hkl}w(|F_{obs}|-|F_{calc}|)^2/(n_{data} - n_{vari})]^{1/2}$.

Table 5.2. Crystal data, data collection parameters for compounds **5.4** and **5.5**.

Compound	**4**	**5**
Empirical formula	$Ru_5O_{15}C_{24}H_8$	$Ru_5O_{15}C_{24}H_8$
Formula weight	1041.65	1041.65
Crystal system	Monoclinic	Monoclinic
Lattice parameters		
a (Å)	20.9891(16)	33.0556(14)
b (Å)	10.3020(8)	10.1112(4)
c (Å)	14.9411(11)	19.1485(8)
α (deg)	90.00	90.00
β (deg)	109.8950(10)	106.7310(10)
γ (deg)	90.00	90.00
V (Å^3)	3037.9(4)	6129.1(4)
Space group	$P2_1/c$	$P2/c$
Z value	4	8
ρ_{calc} (g / cm^3)	2.278	2.258
μ (Mo Kα) (mm^{-1})	2.498	2.476
Temperature (K)	294(2)	294(2)
$2\Theta_{max}$ (°)	50.06	56.60
No. Obs. (I > 2σ(I))	5368	15206
No. Parameters	401	803
Goodness of fit (GOF)	1.264	1.088
Max. shift in cycle	0.001	0.005
Residuals*: R1; wR2	0.0272; 0.0784	0.0410; 0.1003
Absorption Correction, Max/min	Multi-scan 1.000/0.793	Multi-scan 1.000/0.771
Largest peak in Final Diff. Map (e$^-$ / Å^3)	0.588	0.491

*$R1 = \Sigma_{hkl}(||F_{obs}| - |F_{calc}||)/\Sigma_{hkl}|F_{obs}|$; $wR2 = [\Sigma_{hkl}w(|F_{obs}| - |F_{calc}|)^2/\Sigma_{hkl}wF^2_{obs}]^{1/2}$; $w = 1/\sigma^2(F_{obs})$; $GOF = [\Sigma_{hkl}w(|F_{obs}| - |F_{calc}|)^2/(n_{data} - n_{vari})]^{1/2}$.

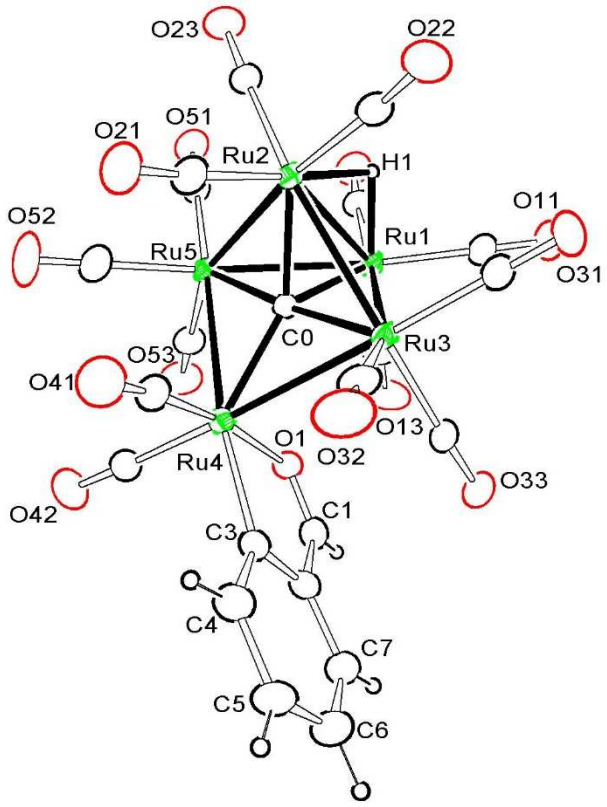

Figure 5.1. ORTEP diagram of the molecular structure of $Ru_5(\mu_5\text{-}C)(CO)_{14}(\eta^2\text{-}O{=}CHPh)(\mu\text{-}H)$, **5.2**, showing 20% thermal ellipsoid probability. Selected interatomic bond distances (Å) are as follows: Ru1-Ru3 = 2.8364(6), Ru1-Ru5 = 2.8468(6), Ru1-Ru2 = 2.8396(5), Ru2-Ru5 = 2.8409(5), Ru2-Ru3 = 2.8531(5), Ru3-Ru4 = 2.9529(6), Ru4-Ru5 = 2.9566(6), Ru1-H1 = 1.72(5), Ru2-H1 = 1.83(5), Ru4-C3 = 2.067(5), Ru4-O1 = 2.129(4), C1-C2 = 1.463(9), C2-C3 = 1.416(8), C1-O1 = 1.241(7), Ru1-C0 = 2.138(4), Ru2-C0 = 2.128(4), Ru3-C0 = 1.969(4), Ru4-C0 = 2.109(4), Ru5-C0 = 1.960(4).

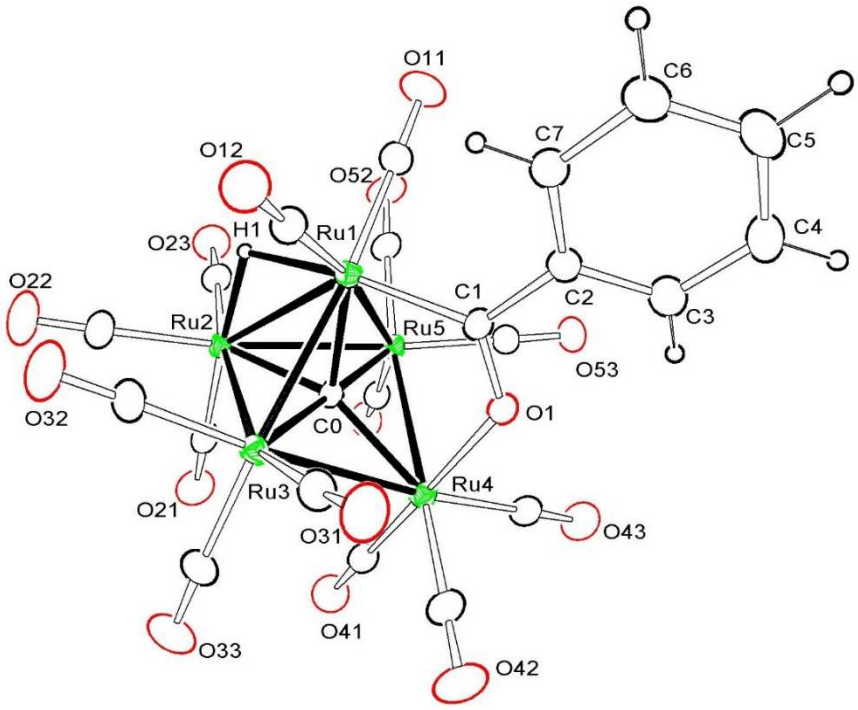

Figure 5.2. ORTEP diagram of the molecular structure of $Ru_5(\mu_5\text{-}C)(CO)_{14}(\mu\text{-}\eta^2\text{-}O{=}CPh)(\mu\text{-}H)$, **5.3**, showing 20% thermal ellipsoid probability. Selected interatomic bond distances (Å) are as follows: Ru1-Ru3 = 2.8126(6), Ru1-Ru5 = 2.8415(6), Ru1-Ru2 = 2.9104(6), Ru2-Ru5 = 2.8655(6), Ru2-Ru3 = 2.8711(6), Ru3-Ru4 = 2.8671(6), Ru4-Ru5 = 2.8930(6), Ru1-H1 = 1.78(2), Ru2-H1 = 1.81(2), Ru1-C1 = 2.062(5), Ru4-O1 = 2.114(4), C1-O1 = 1.258(6), C1-C2 = 1.494(7), Ru1-C0 = 2.034(5), Ru2-C0 = 2.096(5), Ru3-C0 = 1.965(5), Ru4-C0 = 2.079(5), Ru5-C0 = 1.983(5).

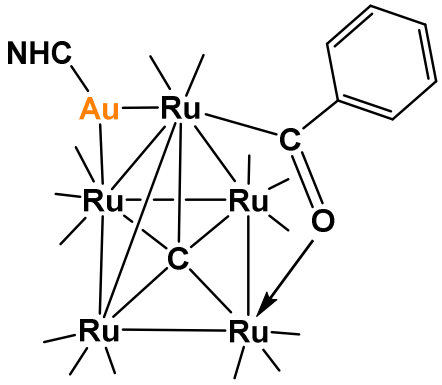

$Ru_5(\mu_5\text{-}C)(CO)_{14}(\mu\text{-}\eta^2\text{-}O{=}CPh)[\mu\text{-}Au(NHC)]$

Figure 5.3. Line drawing for the molecular structure of $Ru_5(\mu_5\text{-}C)(CO)_{14}(\mu\text{-}\eta^2\text{-}O{=}CPh)(\mu\text{-}Au(NHC))$.

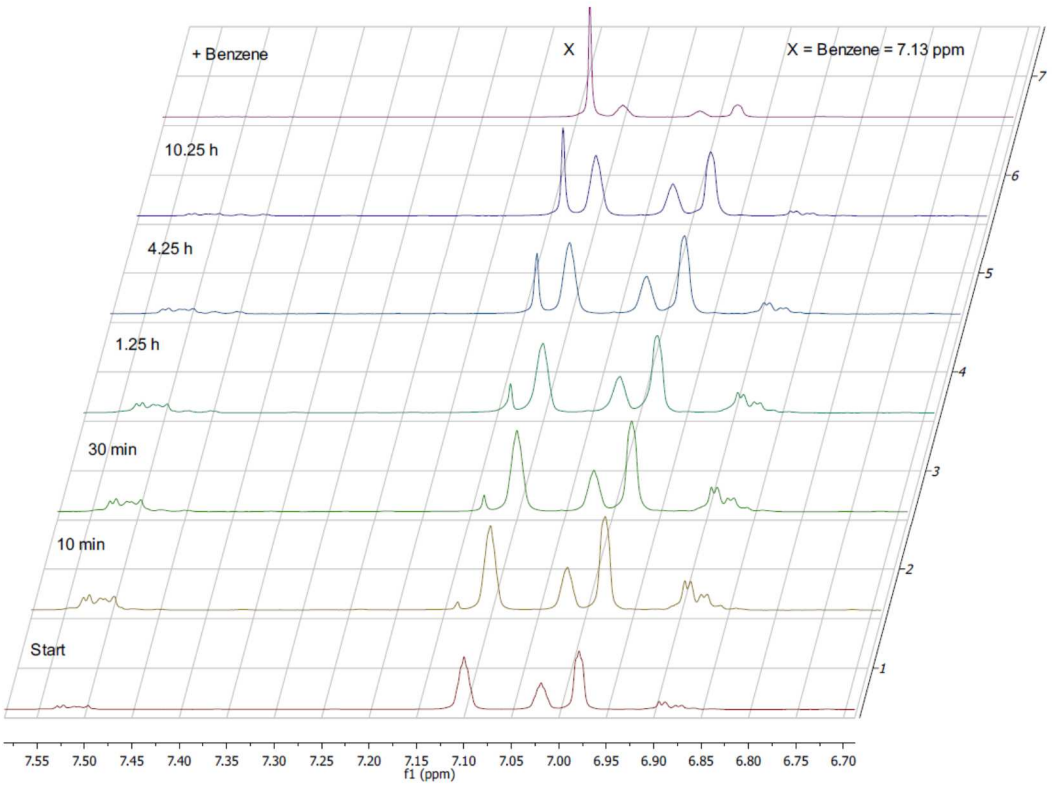

Figure 5.4. Stacked plot of the decomposition of $Ru_5(\mu_5\text{-}C)(CO)_{14}(\mu\text{-}\eta^2\text{-}O{=}CPh)(\mu\text{-}H)$ at 105 °C for 10.25 h showing the formation of benzene.

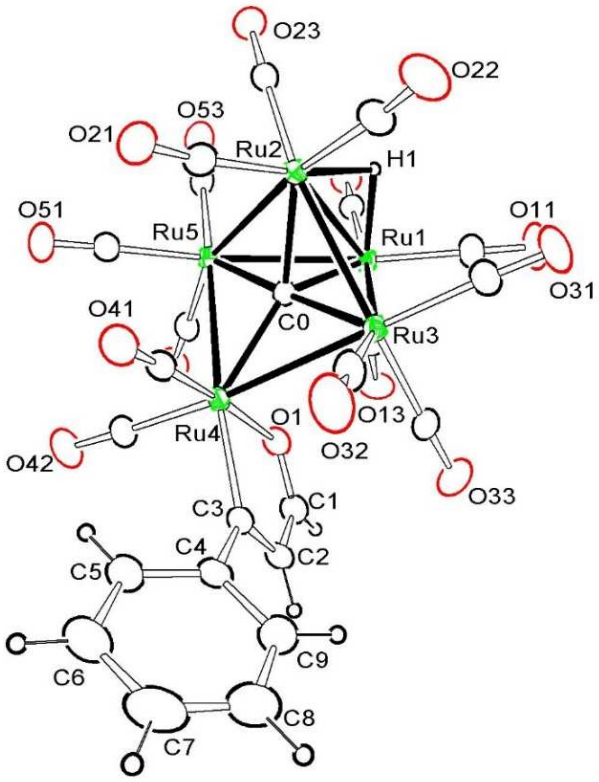

Figure 5.5. ORTEP diagram of the molecular structure of $Ru_5(\mu_5\text{-}C)(CO)_{14}(\eta^2\text{-}O{=}CHCH{=}CPh)(\mu\text{-}H)$, **5.4**, showing 20% thermal ellipsoid probability. Selected interatomic bond distances (Å) are as follows: Ru1-Ru3 = 2.8389(6), Ru1-Ru5 = 2.8627(5), Ru1-Ru2 = 2.8353(6), Ru2-Ru5 = 2.8437(5) Ru2-Ru3 = 2.8717(6), Ru3-Ru4 = 2.9289(5), Ru4-Ru5 = 2.9388(6), Ru1-H1 = 1.74(6), Ru2-H1 = 1.92(6), Ru4-C3 = 2.069(5), Ru4-O1 = 2.117(3), C1-O1 = 1.253(7), C1-C2 = 1.400(8), C2-C3 = 1.355(7), Ru1-C0 = 2.116(4), Ru2-C0 = 2.104(4), Ru3-C0 = 1.965(4), Ru4-C0 = 2.133(5), Ru5-C0 = 1.959(4).

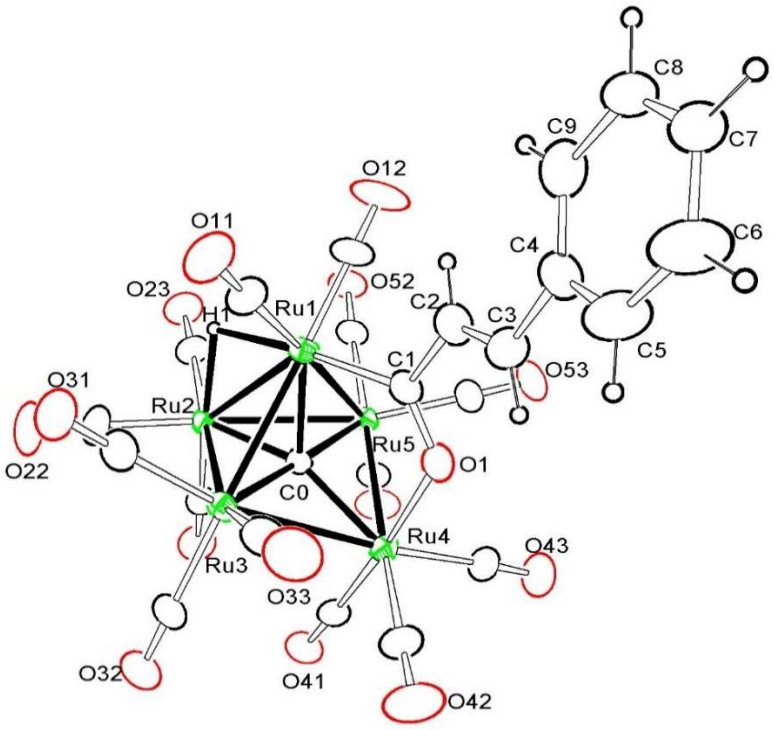

Figure 5.6. ORTEP diagram of the molecular structure of $Ru_5(\mu_5\text{-}C)(CO)_{14}(\mu\text{-}\eta^2\text{-}O{=}CCH{=}CHPh)(\mu\text{-}H)$, **5.5** showing 20% thermal ellipsoid probability. Selected interatomic bond distances (Å) are as follows: Ru1-Ru3 = 2.8186(6), Ru1-Ru5 = 2.8210(5), Ru1-Ru2 = 2.8977(6), Ru2-Ru5 = 2.8752(6) Ru2-Ru3 = 2.8751(6), Ru3-Ru4 = 2.8655(6), Ru4-Ru5 = 2.8769(6), Ru1-H1 = 1.95(7), Ru2-H1 = 1.80(7), Ru1-C1 = 1.992(6), Ru4-O1 = 2.128(4), C1-O1 = 1.273(7), C1-C2 = 1.498(8), C2-C3 = 1.256(10), Ru1-C0 = 2.049(4), Ru2-C0 = 2.098(5), Ru3-C0 = 1.974(4), Ru4-C0 = 2.065(5), Ru5-C0 = 1.972(4).

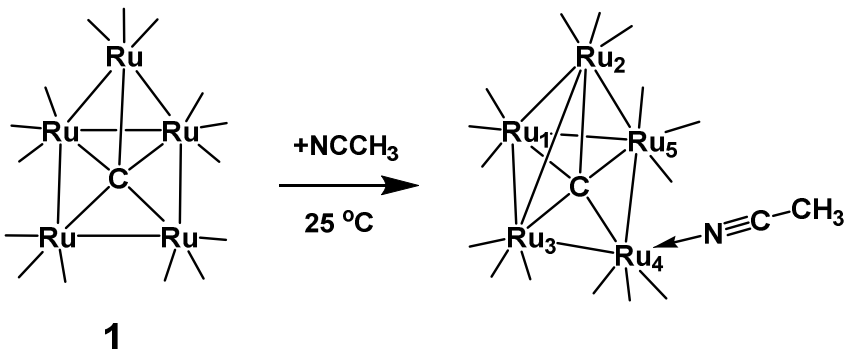

1

Scheme 5.1. A schematic of the cluster opening addition of $NCCH_3$ to compound **5.1**.

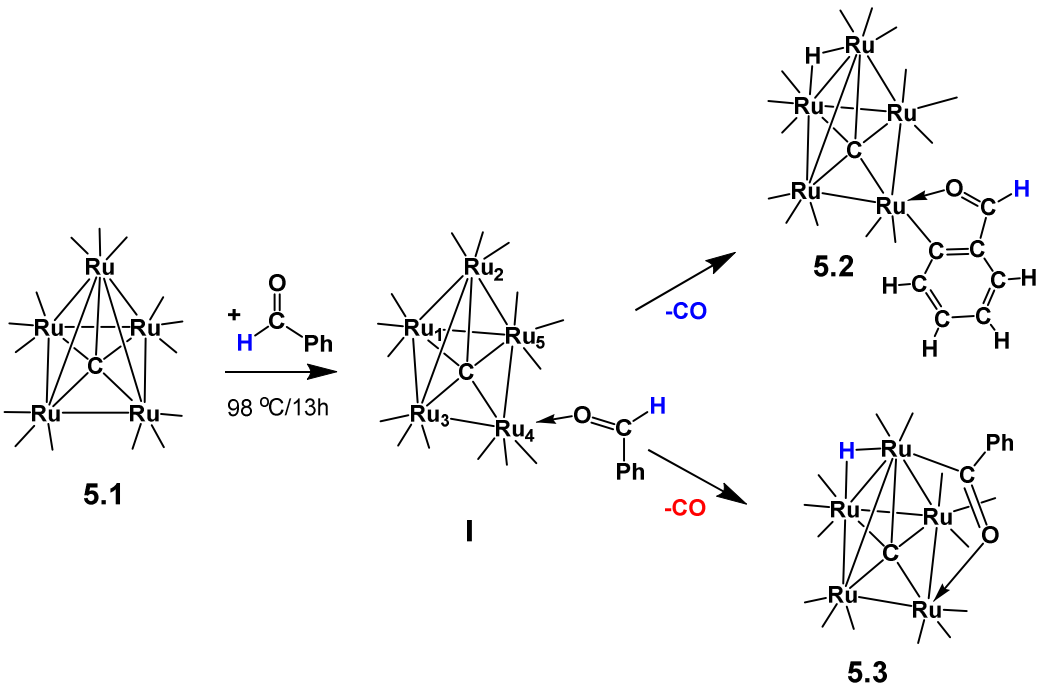

Scheme 5.2. A schematic for CH activation reactions in benzaldehyde by **5.1**.

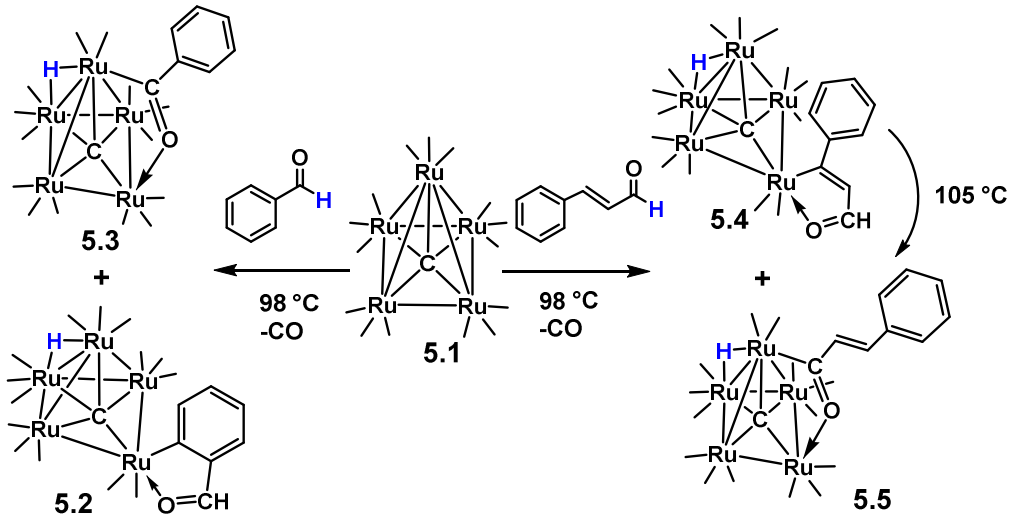

Scheme 5.3. Products formed by the oxidative addition of aldehydes to **5.1**.

5.5 References

(1) (a) Yang, Y.; Lan, J.; You, J. *Chem. Rev*. **2017**, 117, 8787−8863; (b) Eisenstein, O.; Milani, J.; Perutz, R.N. *Chem. Rev*. **2017**. 117, 8710−8753; (c) Xiao-Song Xue, X.-S.; Ji, P.; Zhou B.; Cheng, J.-P. *Chem. Rev*. **2017**, 117, 8622−8648; (d) Balcells, D.; Clot, E.; Eisenstein, O. *Chem. Rev.* **2010**, 110, 749–823; (e) Crabtree, R.H. *J. Organomet. Chem.* **2004**, 689, 4083–4091; (f) Shilov, A.E.; Shul'pin, G.B. *Chem. Rev.* **1997**, 97, 2879-2932; (g) Labinger, J.A.; Bercaw, J.E. *Nature* **2002**, 417, 507–514; (h) Bergman, R.B. *Nature,* **2007**, 446, 391-393. (i)Gunay, A; Theopold, K.H. *Chem. Rev.* **2010**, 42, 1060–1081; (j) Hal, C.; Perutz, R.N. *Chem. Rev.* **1996**, 96, 3125–3146; (k) Rudakov, E.S.; Shul'pin, G.B. *J. Organomet. Chem.* **2015**, 793, 4–16; (l) Labinger, J.A.; Bercaw, J.E. *J. Organomet. Chem.* **2015**, 793, 47–53; (m) Webb, J.R.; BolaCo, T.; Gunnoe, T.B. *ChemSusChem.* **2011** 4, 37–49.

(2) (a) Lersch, M.; Tilset, M. *Chem. Rev.* **2005**, 105, 2471–2526; (b) Jones, W.D.; Feher, F.J. *Acc. Chem. Res.* **1989**, 22, 91-100; (c) Jones, W.D. *Acc. Chem. Res.* **2003**, 36, 140–146; (d) Koppaka, A.; Captain, B. *Inorg. Chem.* **2016**, 55, 2679−2681; (e) Adams, R.D.; Rassolov, V.; Wong, Y.O. *Angew. Chem. int. Ed.* **2016**, 55 1324–1327.

(3) (a) Willis, M.C.; M.S. *Chem. Rev.* **2010**, 110, 725–748; (b) Coxon, T.J.; Fernández, M.; Barwick-Silk, J.; McKay, A.I.; Britton, L.E.; Weller, A.S.; Willis, M.C. *J. Am. Chem. Soc*. **2017**, 137, 10142−10149; (c) Kondo, T.; Akazome, M.; Tsuji, Y.; Watanabe, Y. *J. Org. Chem.* **1990**, 55, 1286-1291; (d) Kondo, T.; Hiraishi, N.; Morisaki, Y.; Wada, K.; Watanabe, Y.; Mitsudo, T. *Organometallics* **1998**, 17, 2131-2134; (e)Dyker, G. *Angew. Chem., Int. Ed* **1999**, 38, 1698-1712; (f) Jun, C.-

H.; Moon, C.W.; Lee, D.-Y. *Chem, Eur. J.* **2002**, 8, 2423-2428; (g) Willis, M.C.; McNally, S.J.; Beswick, P.J. *Angew. Chem., Int. Ed.* **2004**, 43, 340-340; (h) Lochow, C.F; Miller, R.G. *J. Am. Chem. Soc.* **1976**, 98, 1281-1283; (i) Tanaka, K.; Fu, G.C. *J. Am. Chem. Soc.* **2001**, 123, 11492-11493; (j) Tanaka, M.; Sakai, K.; Suemune, H. *Org. Chem.* **2003**, 7, 353-367.

(4) (a) Suggs, J.W. *J. Am. Chem. Soc.***1978**, 100, 640-641; (b) Saunder, M; Kates, M.R. *J. Am. Chem. Soc.* **1978**, 100, 7083-7085; (c) Beck, C.M.; Rathmill, S.E.; Park, Y.J.; Chen, J.R.; Crabtree, R.H.; Liable-Sands, L.M.; Rheingold, A. L. *Organometallics* **1999**, 18, 5311-5317; (d) Kreis, M.; Palmelund, A.; Bunch, L.; Madsen, R. *Adv. Synth. Catal.* **2006**, 348, 2148-2154; (e) Fristrup, P.; Kreis, M.; Palmelund, A.; Northby, P.O.; Madsen, R.J. *J. Am. Chem. Soc.* **2008**, 130, 5206-5215.

(5) (a) Campbell Jr. R.E.; Lochow, C.F.; Vora, K.P.; Miller, R.G. *J. Am. Chem. Soc.* **1980**, 102, 5824 – 5830; (b) Campbell Jr., R.E.; Miller, R.G. *J. Organomet. Chem.* **1980**, 186, C27 – C31; (c) Fairlie, D.; Bosnich, B. *Organometallics* **1988**, 7, 946 – 954; (d) Moxham, G.L.; Randell-Sly, H.E.; Brayshaw, S.K.; Woodward, R.L.; Weller, A.S.; Willis, M.C. *Angew. Chem., Int. Ed.* **2006**, 45, 7618 – 7622; (e) Moxham, G.L.; Randell-Sly, H.E.; Brayshaw, S.K.; Weller, A.S.; Willis, M.C. *Chem. Eur. J.*, **2008**, 14, 8383 - 8397.

(6) Adams, R.D.; Tedder, J.D. *Inorg. Chem.* **2018**, 57, 5707 – 5710.

(7) Johnson, B.F.G.; Lewi, J.; Nicholls, J.; Puga, J.; Raithby, P.R.; Rosales, M.J.; McPartlin, M.; Clegg, W. *J. Chem. Soc. Dalton Trans.***1983**, 277-290.

(8) Saint+, Version 6.2a, Bruker Analytical X-ray System, Inc, Madison, WI, **2001**.

(11) Sheldrick, G. M. SHELXTL, Version 6.1, Bruker Analytical X-ray Systems, Inc, Madison, WI, **1997**.

(12) (a) Johnson, B.F.G.; Lewis, J.; Nicholls, J.N.; Pruga, J.; Whitmire, K.H. *J. Chem. Soc. Dalton Trans.* **1981**, 787-797; (b) Adams, R.D.; Captain, B.; Fu, W. *Organometallics* **2000**, 19, 3670-3673; (c) Adams, R.D.; Smith, M.; Tedder, J. *J Clust Sci* **2017**, 28, 695-702.

(13) Adams, R.D.; Tedder, J.; Wong, Y.O. *J. Organomet. Chem.*, **2015**, 795, 2-10.

CHAPTER 6

Formation of N,N-Dimethylacrylamide by a Multicenter Hydrocarbamoylation of C_2H_2 with N,N-Dimethylformamide Activated by $Ru_5(\mu_5\text{-}C)(CO)_{15}$[5]

[5] Adams, R. D.; Tedder, J. D; *Inorg. Chem.* **2018**, 57, 5707-5710.
Reprinted here with permission from publisher

6.1 Introduction

Acrylamides, like other acryloyl-compounds, are precursors to a range of valuable polymers.[1] As a result, the syntheses of these acryloyl-compounds have received considerable attention.[2] We have now found that dimethylacrylamide can be obtained by the hydrocarbamoylation of C_2H_2 by dimethylformamide DMF (eq. 6.1) in a series of reactions facilitated by the activation of the formyl CH bond of DMF by the cluster complex $Ru_5(\mu_5\text{-}C)(CO)_{15}$, **6.1**.

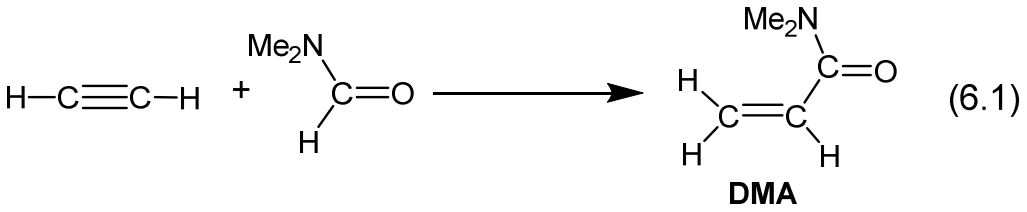

(6.1)

While the activation of C-H bonds by metal atoms has received much attention in recent years, most studies have been focused on the activation of aliphatic[3] and aromatic[4] CH bonds. Although it has not been as well studied, the activation of formyl C-H bonds has led to useful examples of the hydroacylations (eq. 6.2)[5], hydroesterifications (eq. 6.3)[6] and hydrocarbamoylations (eq. 6.4)[7] of olefins and alkynes by metal complexes.

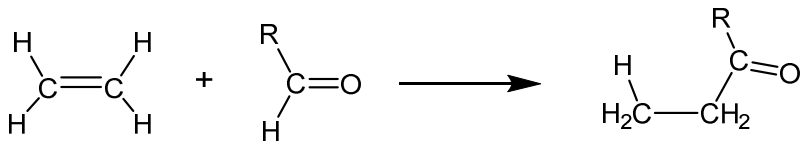

(6.2)

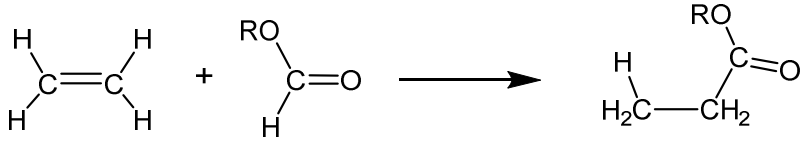

(6.3)

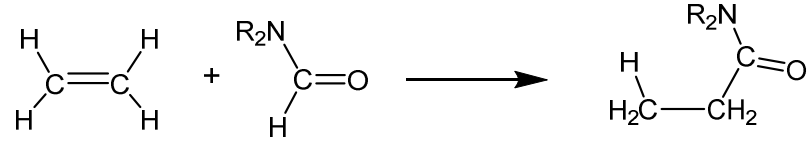

(6.4)

In recent studies we have found that the dinuclear rhenium complex $Re_2(CO)_8[\mu\text{-}\eta^2\text{-}C(H)=C(H)Bu^n](\mu\text{-}H)$ reacts with N,N-dimethylformamide (DMF) by elimination of 1-hexene and activation of the formyl CH bond to yield the complexes $Re_2(CO)_8(\mu\text{-}\eta^2\text{-}O=CNMe_2)(\mu\text{-}H)$ and $Re_2(CO)_7(NHMe_2)(\mu\text{-}\eta^2\text{-}O=CNMe_2)(\mu\text{-}H)$, both of which contain a bridging N,N-dimethylformamido ligand, see Scheme 6.1.[8]

6.2 Experimental

General Data

All reactions were performed under an atmosphere of nitrogen. Reagent grade solvents were dried by standard procedure and were freshly distilled prior to use. Infrared spectra were recorded on a Thermo Scientific Nicolet IS10. ^1H NMR spectra was recorded on a Varian Mercury 300 spectrometer operating at 300.1 MHz. Mass spectrometric (MS) measurements were performed by a direct-exposure probe by using electron impact (EI) ionization. $Ru_3(CO)_{12}$ was obtained from STREM and was used without further purification. $Ru_5(\mu_5\text{-}C)(CO)_{15}$, **6.1** was prepared from $Ru_3(CO)_{12}$ according to a previously reported procedure[9]. N,N-Dimethylformamide, $(Me)_2NC(O)H$, (DMF) was obtained from Sigma-Aldrich and was used without further purification. Dimethylamine ($HNMe_2$) was obtained in a 2.0 M solution in tetrahydrofuran from Sigma Aldrich and was used without any further purification. Trimethylamine N-oxide was purchased from Sigma Aldrich and was used without further purification. Product separations were performed by TLC in air on Analtech 0.25 mm and 0.50 mm silica gel 60 Å F254 glass plates.

Reaction of $Ru_5(\mu_5\text{-}C)(CO)_{15}$, 6.1, with DMF at 80 ˚C

55.0 mg (0.059 mmol) of **6.1** was added to a 50 mL three-neck flask with a solution of 100 µL of DMF in 20 mL of degassed benzene. After heating for 4 h at 80 ˚C, the solvent was removed in vacuo, and the products were then isolated by TLC with a hexane/methylene chloride solvent mixture to provide in order of elution: 36.9 mg of $Ru_5(\mu_5\text{-}C)(CO)_{14}(\mu\text{-}\eta^2\text{-}O{=}CN(Me)_2)(\mu\text{-}H)$, **6.2** (64% yield), and 1.8 mg of $Ru_5(\mu_5\text{-}C)(CO)_{14}(\mu\text{-}\eta^2\text{-}O{=}CN(Me)_2)(HN(Me)_2(\mu\text{-}H)$, **6.3** (3% yield). Spectral data for **6.2**: IR νCO (cm^{-1} in hexane): 2103(w), 2076(s), 2057(vs), 2051(m), 2030(m), 2013(m), 2004(w), 1998(w), 1989(vw), 1961(vw). ^1H NMR (CD_2Cl_2, in ppm) δ = 3.22 (s, 3H, $N(Me)_2$), 2.46 (s, 3H, N(Me)2), -21.47 (s, 1H, hydride). EI/MS *m*/*z*. 983. M^+-CO = 955. M^+-2CO = 927. The isotope distribution is consistent with the presence of five ruthenium atoms. Spectral data for **6.3:** IR νCO (cm^{-1} in hexane): 2088(w), 2051(s), 2043(m), 2029(vs), 2010(vw), 1997(w), 1991(w), 1965(w), 1957(w), 1948(vw). ^1H NMR (CD_2Cl_2, in ppm) δ = 3.63 (broad, 1H, **H**-$N(Me)_2$), 3.27 (s, 3H, $N(Me)_2$), 3.21 (d, 6 Hz, 3H, H-N(Me)2), 3.05 (d, 6 Hz, 3H, H-$N(Me)_2$), 2.52 (s, 3H, $N(Me)_2$), -21.99 (s, 1H, hydride). EI/MS *m*/*z*. M^+ = 1000. The isotope distribution is consistent with the presence of five ruthenium atoms.

Reaction of $Ru_5(\mu_5\text{-}C)(CO)_{14}(\mu\text{-}\eta^2\text{-}O{=}CN(Me)_2)(\mu\text{-}H)$, 6.2, with DMF at 98 ˚C

11.2 mg (0.011 mmol) of **6.2** was added to a 50 mL three-neck flask with a solution of 50 µL of DMF in 20 mL degassed heptane. After heating for 8 h at 98 C, the solvent was removed in vacuo, and the products were then isolated by TLC with a hexane/CH_2Cl_2 solvent mixture to provide in order of elution: 2.1 mg starting material, **6.2**, and 8.1 mg (71% yield) of **6.3**.

Reaction of $Ru_5(\mu_5\text{-}C)(CO)_{15}$, 6.1, with $HNMe_2$ at 80 ˚C

51.4 mg (0.055 mmol) of **6.1** was added to a 50 mL three-neck flask with a solution of 200 µL of $HNMe_2$ in 20 mL of degassed benzene. After heating for 8.5 h at 80 ˚C, the solvent was removed in vacuo, and the products were then isolated by TLC with a hexane/Methylene chloride solvent mixture to provide in order of elution: 6.6 mg (12% yield) of **6.2** and 7.5 mg (14% yield) of **6.3**.

Decomposition of $Ru_5(\mu_5\text{-}C)(CO)_{14}(\mu\text{-}\eta^2\text{-}O{=}CN(Me)_2)(\mu\text{-}H)$, 6.2, at 125 °C

14.3 mg (0.015 mmol) of **6.2** was added to a 100 mL three-neck flask in 20 mL of degassed octane. After heating for at 125 ˚C, the solvent was removed in vacuo, and the products were then isolated by TLC with a hexane/Methylene chloride solvent mixture to provide in order of elution: 1.1 mg (8% yield) of **6.1**. $Ru_5C(CO)_{15}$, **6.1**, decomposes during TLC reducing the amount of recoverable product.

Reaction of $Ru_5(\mu_5\text{-}C)(CO)_{14}(\mu\text{-}\eta^2\text{-}O{=}CN(Me)_2)(HN(Me)_2)(\mu\text{-}H)$, 6.3, with C_2H_2 at 70 °C

25.0 mg (0.025 mmol) of **6.3** was added to a 50 ml three-neck flask in 20 ml of degassed benzene. A slow purge of C_2H_2 was then passed through the solution for 5 h at 70 °C. The solvent was removed in vacuo and the products were then isolated by TLC with a hexane/Methylene chloride solvent mixture to provide in order of elution: 0.8 mg (3% yield), **6.2**, and 1.4 mg (6% yield) of $Ru_5(\mu_5\text{-}C)(CO)_{13}[\mu\text{-}\eta^3\text{-}O{=}CN(Me)_2CHCH](\mu\text{-}H)$, **6.4**, and 2.8 mg (11% recovered) of starting material **6.3**. Spectral data for **6.4**: IR νCO (cm^{-1} in hexane) 2090(m), 2061(vs), 2044(vs), 2034(vs), 2023(m), 2012(m), 2005(sh), 1996(vw), 1989(w), 1985(w), 1966(vw). ^1H NMR (CD_2Cl_2, in ppm) δ = 10.51 (d, 6 Hz, 1H, Ru-C(**H**)=C(H)-C), 4.75 (d, 6 Hz, 1H, Ru-C(H)=C(**H**)-C), 3.06 (s, 3H, $N(Me)_2$), 2.59 (s, 9H,

$N(ME)_3$), -22.03 (s, 1H, hydride). EI/MS *m/z*, M^+=981. Isotope distribution is consistent with the presence of five Ru atoms.

Reaction of $Ru_5(\mu_5\text{-}C)(CO)_{14}(\mu\text{-}\eta^2\text{-}O{=}CN(CH_3)_2)(\mu\text{-}H)$, 6.2, with Me_3NO and C_2H_2 at Room Temperature

27.9 mg (0.028 mmol) of **6.2** was added to a 50 mL three-neck flask with a solution of 3.2 mg Me_3NO in 20 mL of degassed benzene and was stirred for 30 min. A slow purge of C_2H_2 was then passed through the solution for 4 h until the IR showed no signs of starting material. The solvent was removed in vacuo and the products were then isolated by TLC with a hexane/methylene chloride solvent mixture to provide in order of elution: 1.1 mg starting material, **6.2**, and 19.6 mg (66% yield) of $Ru_5(\mu_5\text{-}C)(CO)_{14}(\mu\text{-}\eta^2\text{-}O{=}CN(CH_3)_2)(CH{=}CHNMe_3)(\mu\text{-}H)$, **6.5**. Spectral data for **6.5**: IR νCO (cm^{-1} in methylene chloride) 2076(m), 2038(vs), 2030(vs), 2016(s), 1999(sh), 1973(m), 1923(w). ^{1}H NMR (CD_2Cl_2, in ppm) δ = 8.25 (d, 14 Hz, 1H, Ru-C(H)=C(H)-N), 5.90 (d, 14 Hz, 1H, Ru-C(H)=C(H)-N), 3.25 (s, 3H, $N(CH_3)_2$), 3.22 (s, 9H, $N(CH_3)_3$), 2.55 (s, 3H, $N(CH_3)_2$), -22.07 (s, 1H, hydride).

Reaction of $Ru_5(\mu_5\text{-}C)(CO)_{13}[\mu\text{-}\eta^3\text{-}O{=}CN(Me)_2CHCH](\mu\text{-}H)$, 6.4, with CO at Room Temperature

13.2 mg (0.013 mmol) of **6.4** was added to a 50 mL three-neck flask in 20 mL of degassed hexane. A slow purge of CO was then passed through the solution for 22 h until the IR showed no signs of starting material. The solvent was removed in vacuo and the products were then isolated by TLC with a hexane/Methylene chloride solvent mixture to provide in order of elution: 5.1 mg (38% yield) of $Ru_5(\mu_5\text{-}C)(CO)_{14}(\eta^2\text{-}$

O=CN(Me)$_2$CH=CH)(μ-H), **6.6,** and 0.6 mg of starting material, **6.4**. Spectral data for **6.6**: IR νCO (cm^{-1} in hexane) 2095(w), 2064(s), 2053(vs), 2045(m), 2032(w), 2019(w), 2015(sh), 1991(w), 1986(w), 1970(vw). ^{1}H NMR (CD_2Cl_2, in ppm) δ = 10.18 (d, 8 Hz, 1H, Ru-C(**H**)=C(H)-C), 6.96 (d, 8 Hz, 1H, Ru-C(H)=C(**H**)-C), 3.06 (s, 3H, N(Me), 2.77 (s, 3H, N(Me), -22.23 (s, 1H, hydride). EI/MS *m*/*z*. 1009. (M^+ – 2CO) = 953. The isotope distribution is consistent with the presence of five ruthenium atoms.

Decarbonylation of Ru$_5$(μ$_5$-C)(CO)$_{14}$(η^2-O=CN(Me)$_2$CH=CH)(μ-H), 6.6, at 125 °C

17.7 mg (0.018 mmol) of **6.6** was added to a 50 mL three-neck flask in 20 mL of degassed octane. After heating for 1 h at 125 °C, the solvent was removed in vacuo, and the products were then isolated by TLC with a hexane/Methylene chloride solvent mixture to provide in order of elution: 2.0 mg starting material, **6.6**, and 8.9 mg (52% yield) of **6.4**.

Reaction of Ru$_5$(μ$_5$-C)(CO)$_{14}$(η^2-O=CN(Me)$_2$CH=CH)(μ-H), 6.6, with CO 125 °C

24.8 mg (0.025 mmol) of **6.6** was dissolved in 1.5 mL d_8-toluene and was placed in a high-pressure reactor glass vial. The glass vial was enclosed in a high-pressure reaction vessel, pressurized with CO three times then degassed, and finally filled 400 psi. The high-pressure reaction vessel was placed in an oil bath set to 125 °C for 3 h. After heating, the CO gas was released from the reaction vessel and an NMR was taken of the solution which confirmed the presence of N,N-dimethylacrylamide. The solution was then blown dry by passing a fast stream of nitrogen over the solution. The product was then isolated by TLC with a hexane/Methylene chloride solvent mixture to give 16.3 mg (71% yield) of **6.1**.

Crystallographic Analyses

Single crystals of compounds **6.2-6.6** suitable for X-ray diffraction analyses were obtained by slow evaporation of solvent from solutions of the pure compounds in hexane solvent at room temperature. Each data crystal was glued onto the end of a thin glass fiber. X-ray intensity data for compounds **6.3**, **6.4**, **6.5**, and **6.6** was measured by using a Bruker SMART APEX CCD-based diffractometer by using Mo Kα radiation (λ = 0.71073 Å). The raw data frames were integrated with the SAINT + program by using a narrowframe integration algorithm [10]. Correction for Lorentz and polarization effects were also applied with SAINT+. An empirical absorption correction based on the multiple measurements of equivalent reflections was applied by using the program SADABS were applied in each analysis [10]. X-ray intensity data for compound **6.2** was measured by using a Bruker D8 QUEST diffractometer equipped with a PHOTON-100 CMOS area detector and an Incoatec microfocus source (Mo Kα radiation, λ = 0.71073 Å).[11] The data collection strategy consisted of three 180° ω-scans at different φ settings and one 360° φ-scan, with a scan width per image of 0.5°. The crystal-to-detector distance was 4.0 cm and each image was Measured for 5 s in shutterless mode. The average reflection redundancy was 9.6. The raw area detector data fraMes were reduced, scaled and corrected for absorption effects using the SAINT[11] and SADABS[12] programs All structures were solved by a combination of direct Methods and difference Fourier syntheses, and refined by full-matrix least squares refinement on F^2 by using the SHELXTL software package [13]. All non-hydrogen atoms were refined with anisotropic thermal parameters. All hydrogen atoms were placed in geometrically idealized positions and were included as standard riding atoms during the final least-squares refinements with C-H distances fixed at 0.96 Å. The hydride ligands

bonded to the metal atoms in **6.2**, **6.3**, **6.4**, **6.5**, and **6.6** were located and refined in each analysis. Compounds **6.2** and **6.3** crystallized in the monoclinic crystal system. The space group $P2_1/c$ was identified for compound **6.2** on the basis of systematic absences observed in the intensity data. Compound **6.2** contains three independent formula equivalents of the complex in the asymmetric crystal unit. All three molecules have similar molecular structures. The space group $P2_1/n$ was identified for compound **6.3** on the basis of systematic absences observed in the intensity data. The space group P 2(1)/n was identified for compound **6.3** on the basis of systematic absences observed in the intensity data. Compounds **6.4**, **6.5**, and **6.6** crystallized in the triclinic crystal system. The space group P-1 was chosen for compounds **6.4** and **6.6** and was confirmed by successful structure refinement. Compound **6.6** contains two independent formula equivalents of the complex in the asymmetric crystal unit. Both molecules have similar molecular structures. Crystal data, data collection parameters, and results for the analyses are listed in Table 6.1.

Discussion

We have now found that the square-pyramidal pentaruthenium carbonyl complex $Ru_5(\mu_5\text{-}C)(CO)_{15}$, **6.1**[9] reacts with DMF by activation of the formyl CH bond to yield the new dimethylformamido complex $Ru_5(\mu_5\text{-}C)(CO)_{14}(\mu\text{-}\eta^2\text{-}O{=}CNMe_2)(\mu\text{-}H)$, **6.2** (64% yield) and a minor, but important coproduct $Ru_5(\mu_5\text{-}C)(CO)_{13})(HN(Me_2)(\mu\text{-}\eta^2\text{-}O{=}CNMe_2)(\mu\text{-}H)$, **6.3** (3% yield). Both compounds were characterized by IR, ^{1}H NMR and single-crystal X-ray diffraction analyses and ORTEP diagrams of the molecular structures of **6.2** and **6.3** are shown in Figures 6.1 and 6.2, respectively. Both compounds contain a hydrido ligand that bridges the Ru1 – Ru2 bond on both complexes; δ = -21.47 and δ = -21.99 in the ^{1}H NMR spectrum of **6.2** and **6.3**, respectively, and a bridging

dimethylformamido ligand formed by the cleavage of the formyl CH bond of the DMF and their addition to the Ru_5 cluster. One Ru – Ru bond in the cluster was cleaved upon the addition and the μ-η^2-O=C-dimethylformamido ligand to the cluster in each compound and bridges the opened edge of the Ru_5 cluster. Compound **6.3** contains a $NHMe_2$ ligand on one of the metal atoms, Ru4, in the place of one of the terminal CO ligands in **6.2**. Compound **6.3** was also obtained from **6.2** (71% yield) by reaction with an additional quantity of DMF at 98 °C for 8 h and also by a direct reaction of **6.1** with $NHMe_2$. The $NHMe_2$ ligand was presumably formed by a decarbonylation of the DMF. Other metal complexes have also been shown to decarbonylate DMF via pathways that involve an initial activation of the formyl C-H bond.[14]

Most interestingly, complex **6.3** was found to react with C_2H_2 under a slow purge (1 atm) at 80 °C for 4.5 h to yield the new complex $Ru_5(\mu_5\text{-}C)(CO)_{13}[\mu\text{-}\eta^3\text{-}O{=}CN(CH_3)_2CHCH](\mu\text{-}H)$, **6.4**, 5% yield. Compound **6.4** was characterized crystallographically and an ORTEP diagram if its molecular structure is shown in Figure 6.3. Compound **6.4** contains a dimethylformamido-substituted μ-η^2-vinyl ligand that bridges the Ru3 – Ru4 edge of the open Ru_5C cluster by the carbon atoms C2 and C3, Ru3-C2 = 2.262(4) Å, Ru3-C3 = 2.186(4) Å. The formamido group is coordinated to Ru4 by its oxygen atom O1, Ru4-O1 = 2.114(2) Å. This unusual ligand was formed by a C-C coupling of the C_2H_2 to the C-end of the bridging formamido ligand in **6.3**.

To potentially improve the yield of the synthesis of **6.4**, compound **6.2** was reacted with acetylene at room temperature in the presence of Me_3NO to aid in the elimination of CO ligands from the cluster. Coupling between the activated DMF and the C_2H_2 was not observed as was the case with **6.4**, but 19.6 mg (66% yield) of the new zwitterionic

compound $Ru_5(\mu_5\text{-}C)(CO)_{14}(\mu\text{-}\eta^2\text{-}O{=}CN(CH_3)_2)(CH{=}CHNMe_3)(\mu\text{-}H)$, **6.5**, was obtained. An ORTEP diagram of the molecular structure of **6.5** is shown in Fig 6.4. Compound **6.5** retains the η^2-bridging formamido ligand and the bridging hydrido ligand, δ = -22.07, from the parent cluster, **6.2**. Replacing one carbonyl ligands at the non-bonded metal atom Ru4 is the new terminally coordinated zwitterionic ligand ($^{-}CH{=}CHN^{+}Me3$); Ru4 – C4 = 2.074(4) Å, C4 – C5 = 1.280(5), C5 – N2 = 1.506(5). The zwitterionic ligand is formed from the coupling of acetylene with presumably the trimethylamine (NMe_3) residue released after the oxidation of one of the CO ligands to CO_2. C4 of the zwitterionic ligand is formally an anion making the zwitterion a two-electron donor ligand bringing the electron count to 76 for the cluster (Scheme 6.2).

When treated with CO at 1 atm/25 ^{o}C, a CO adduct of **6.4**, $Ru_5(\mu_5\text{-}C)(CO)_{14}[\eta^2\text{-}O{=}CN(CH_3)_2CH{=}CH](\mu\text{-}H)$, **6.6**, was formed in 38% yield. An ORTEP diagram of the molecular structure of **6.6** is shown in Figure 6.4. Compound **6.6** contains a chelating η^2-dimethylformamido-substituted vinyl ligand coordinated to Ru4 by the amido oxygen atom O1, Ru4 – O1 = 2.155(3) Å and the terminal olefin carbon atom C3, Ru4 – C3 = 2.034(5) Å, C2 – C3 = 1.330(8) Å. Compound **6.6** was converted back to **6.4** (52% yield) by thermal decarbonylation (125 ^{o}C, 1h) with complete restoration of π-coordination of the C=C unit of the formamido-substituted vinyl ligand.

Most interestingly, when treated with CO under more forcing conditions (400 psi, 125 °C for 3h), DMA was released from **6.6 (**confirmed by ^{1}H NMR spectral analysis) and compound **6.1** was formed in 71% yield.

Conclusions

The sequence of transformations is overall tantamount to the hydrocarbamoylation of C_2H_2 by DMF eq. (6.1). Although the regeneration of **1** in the final step formally closes what could be considered as a "catalytic" cycle, Scheme 6.3, the reaction is not yet effectively catalytic because of certain low yield transformations, such as **6.3** to **6.4**, and the use of reagents, such as CO, which effectively inhibit the second loop through the cycle that requires additional reactions with DMF. Efforts to develop an effective catalytic process are in progress.

Table 6.1. Crystal data, data collection parameters for compounds **6.2**, **6.3**, and **6.4**.

Compound	**6.2**	**6.3**	**6.4**
Empirical formula	$Ru_5NO_{15}C_{18}H_7$	$Ru_5N_2O_{14}C_{19}H_{14}$	$Ru_5NO_{14}C_{19}H_9$
Formula weight	982.60	999.67	980.62
Crystal system	Monoclinic	Monoclinic	Triclinic
Lattice parameters			
a (Å)	24.373(3)	9.6142(10)	9.5384(8)
b (Å)	9.6742(11)	18.3396(18)	9.7674(8)
c (Å)	35.490(4)	16.4624(16)	15.3895(13)
α (deg)	90.00	90.00	84.825(2)
β (deg)	99.173(3)	95.964(2)	86.703(2)
γ (deg)	90.00	90.00	71.155(2)
V ($Å^3$)	8261.1(15)	2886.9(5)	1350.8(2)
Space group	$P2_1/c$	$P2_1/n$	P-1
Z value	12	4	2
ρ_{calc} (g / cm^3)	2.370	2.300	2.411
μ (Mo Kα) (mm^{-1})	2.748	2.622	2.798
Temperature (K)	298(2)	294(2)	294(2)
$2\Theta_{max}$ (°)	50.06	50.04	50.04
No. Obs. (I > 2σ(I))	14607	5112	4772
No. Parameters	1139	369	366
Goodness of fit (GOF)	1.227	1.174	1.087
Max. shift in cycle	0.005	0.000	0.001
Residuals*: R1; wR2	0.0284; 0.0496	0.0594; 0.1323	0.0325; 0.0865
Absorption Correction, Max/min	Multi-scan 0.262/0.180	Multi-scan 1.000 / 0.720	Multi-scan 1.000/0.701
Largest peak in Final Diff. Map (e^- / $Å^3$)	0.491	1.025	1.136

*$R1 = \Sigma_{hkl}(||F_{obs}|-|F_{calc}||)/\Sigma_{hkl}|F_{obs}|$; $wR2 = [\Sigma_{hkl}w(|F_{obs}|-|F_{calc}|)^2/\Sigma_{hkl}wF^2_{obs}]^{1/2}$; $w = 1/\sigma^2(F_{obs})$; $GOF = [\Sigma_{hkl}w(|F_{obs}|-|F_{calc}|)^2/(n_{data} - n_{vari})]^{1/2}$.

Table 6.2. Crystal data, data collection parameters for compounds **6.5** and **6.6**.

Compound	**6.5**	**6.6**
Empirical formula	$Ru_5N_2O_{14}C_{22}H_{18}$	$Ru_5NO_{15}C_{20}H_9$
Formula weight	1039.73	1008.63
Crystal system	Monoclinic	Triclinic
Lattice parameters		
a (Å)	9.7962(3)	9.1572(4)
b (Å)	17.8847(5)	9.5670(4)
c (Å)	18.6161(5)	37.3960(16)
α (deg)	90.00	83.555(1)
β (deg)	103.521(10)	84.617(1)
γ (deg)	90.00	62.147(1)
V (Å^3)	3171.08(16)	2875.1(2)
Space group	*P* 2(1)/c	*P*-1
Z value	4	4
ρ_{calc} (g / cm^3)	2.178	2.330
μ (Mo Kα) (mm^{-1})	2.391	2.635
Temperature (K)	291(2)	294(2)
$2\Theta_{max}$ (°)	50.06	50.06
No. Obs. (I > 2σ(I))	5604	10114
No. ParaMeters	405	768
Goodness of fit (GOF)	1.065	1.338
Max. shift in cycle	0.306	0.017
Residuals*: R1; wR2	0.0227; 0.0472	0.0300; 0.0622
Absorption Corr., Max/min	Multi-scan 0.563/0.464	Multi-scan 1.000/0.725
Largest peak in Final Diff. Map (e$^-$ / Å^3)	0.695	0.419

*$R1 = \Sigma_{hkl}(||F_{obs}| - |F_{calc}||)/\Sigma_{hkl}|F_{obs}|$; $wR2 = [\Sigma_{hkl}w(|F_{obs}| - |F_{calc}|)^2/\Sigma_{hkl}wF^2_{obs}]^{1/2}$; $w = 1/\sigma^2(F_{obs})$; $GOF = [\Sigma_{hkl}w(|F_{obs}| - |F_{calc}|)^2/(n_{data} - n_{vari})]^{1/2}$.

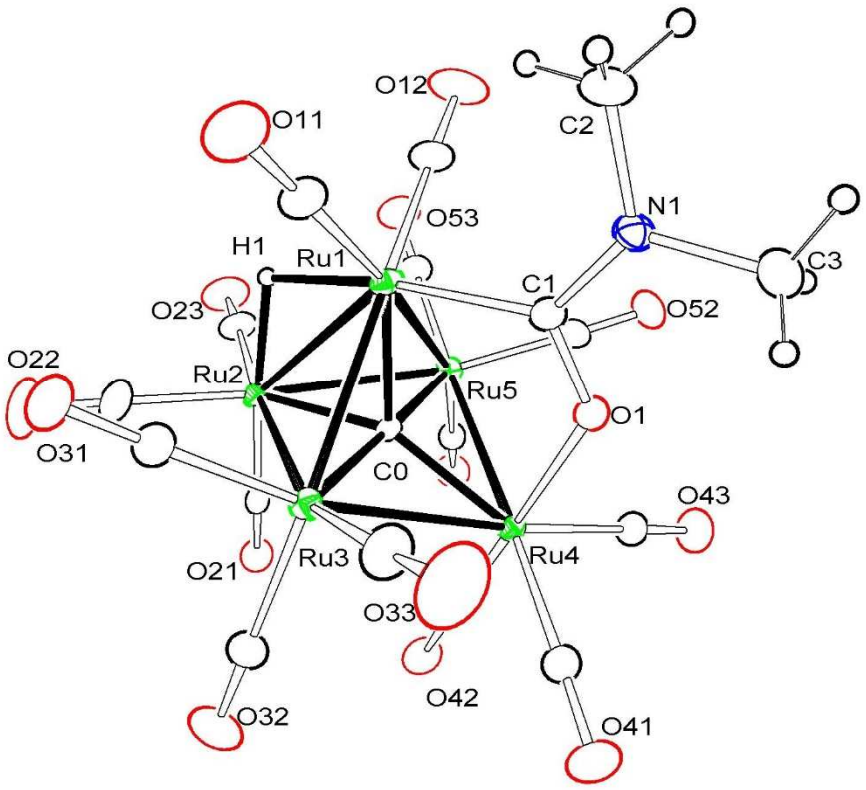

Figure 6.1. ORTEP diagram of the molecular structure of $Ru_5(\mu_5\text{-}C)(CO)_{14}(\mu\text{-}\eta^2\text{-}O{=}CN(Me)_2)(\mu\text{-}H)$, **6.2**, showing 15% thermal ellipsoid probability. Selected interatomic bond distances (Å) are as follows: Ru1-Ru3 = 2.8349(6), Ru1-Ru5 = 2.8265(5), Ru1-Ru2 = 2.8890(5), Ru2-Ru5 = 2.8588(5) Ru2-Ru3 = 2.8606(6), Ru3-Ru4 = 2.8690(5), Ru4-Ru5 = 2.8760(5), Ru1-H1 = 1.79(5), Ru2-H1 = 1.80(5), Ru1-C1 = 2.067(4), Ru4-O1 = 2.100(3), C1-O1 = 1.280(5), Ru1-C0 = 2.042(4), Ru2-C0 = 2.097(4), Ru3-C0 = 1.964(4), Ru4-C0 = 2.067(4), Ru5-C0 = 1.974(4).

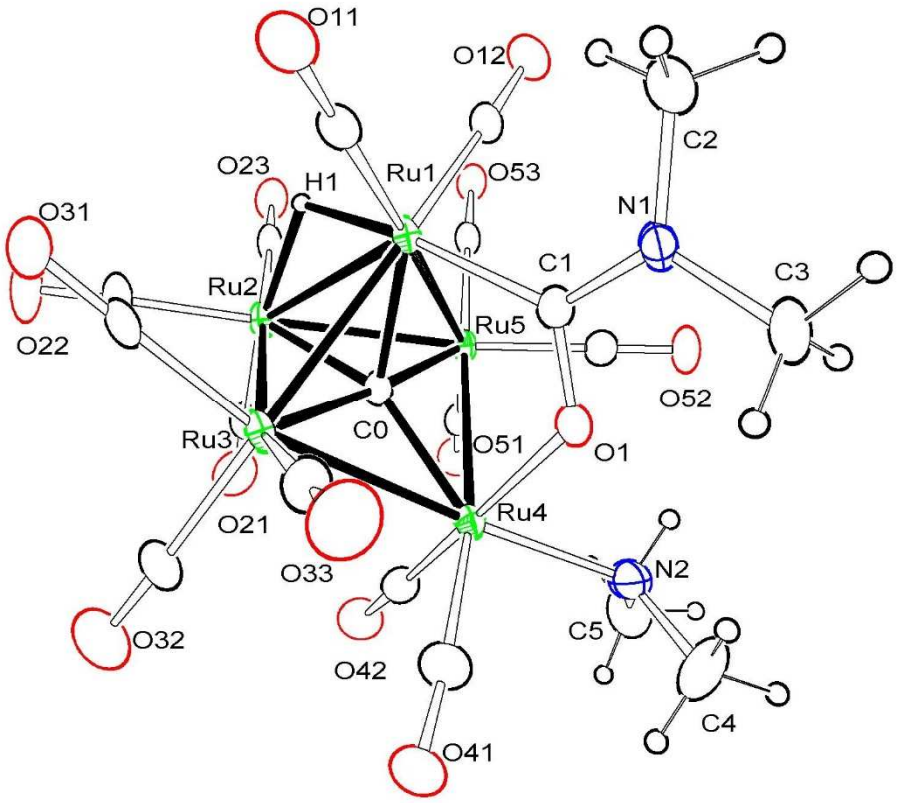

Figure 6.2. ORTEP diagram of the molecular structure of $Ru_5(\mu_5\text{-}C)(CO)_{14}(\mu\text{-}\eta^2\text{-}O{=}CN(Me)_2)(HN(Me)_2(\mu\text{-}H)$, **6.3**, showing 20% thermal ellipsoid probability. Selected interatomic bond distances (Å) are as follows: Ru1-Ru3 = 2.8087(11), Ru1-Ru5 = 2.8184(11), Ru1-Ru2 = 2.8950(11), Ru2-Ru5 = 2.8544(11) Ru2-Ru3 = 2.8541(12), Ru3-Ru4 = 2.8776(12), Ru4-Ru5 = 2.9049(12), Ru1-H1 = 1.77(8), Ru2-H1 = 1.82(8), Ru4-N2 = 2.201(11), Ru1-C1 = 2.072(10), Ru4-O1 = 2.090(7), C1-O1 = 1.299(12), Ru1-C0 = 2.057(9), Ru2-C0 = 2.099(9), Ru3-C0 = 2.007(9), Ru4-C0 = 2.029(10), Ru5-C0 = 1.967(9).

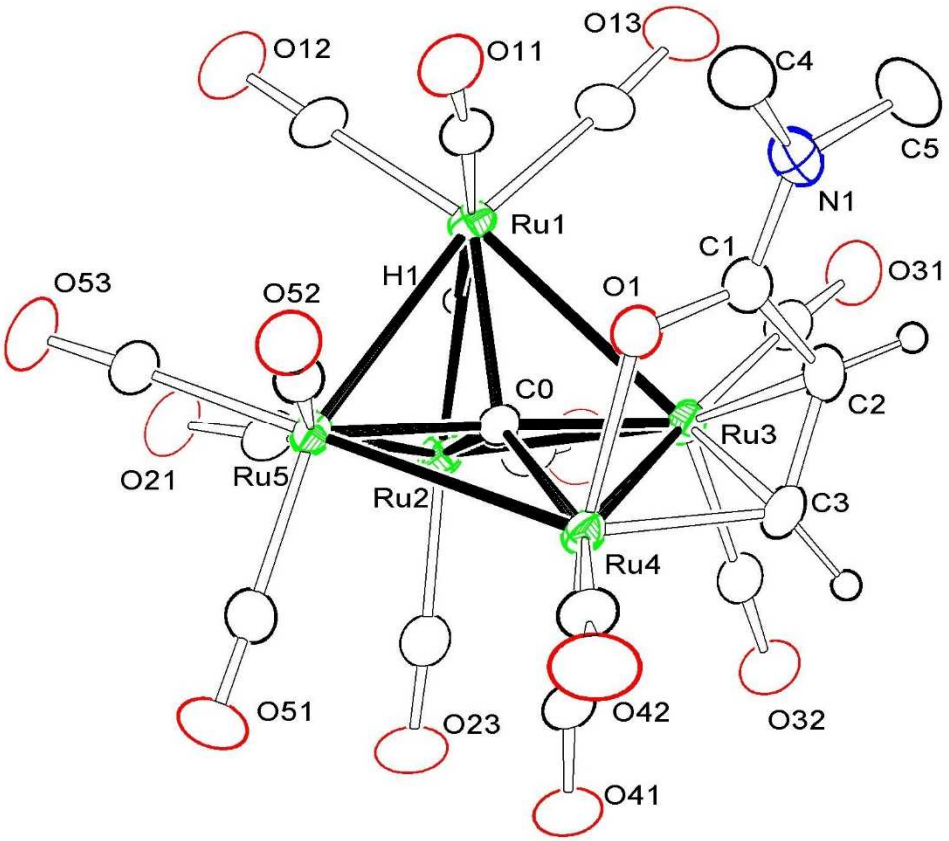

Figure 6.3. ORTEP diagram of the molecular structure of $Ru_5(\mu_5\text{-}C)(CO)_{13}[\mu\text{-}\eta^3\text{-}O{=}CN(Me)_2CHCH](\mu\text{-}H)$, **6.4**, showing 25% thermal ellipsoid probability. Methyl hydrogen atoms have been omitted for clarity. Selected interatomic bond distances (Å) are as follows: Ru1-Ru3 = 2.9491(5), Ru1-Ru5 = 2.8531(5), Ru1-Ru2 = 2.8248(5), Ru2-Ru5 = 2.8986(5) Ru2-Ru3 = 2.8409(5), Ru3-Ru4 = 2.7279(5), Ru4-Ru5 = 3.0092(5), Ru1-H1 = 1.70(6), Ru2-H1 = 1.60(6), Ru4-C3 = 2.013(4), Ru4-O1 = 2.114(2), Ru3-C2 = 2.262(4), Ru3-C3 = 2.186(4), C1-O1 = 1.264(5), C1-C2 = 1.454(6), C2-C3 = 1.408(6), Ru1-C0 = 2.109(4), Ru2-C0 = 2.105(4), Ru3-C0 = 1.980(4), Ru4-C0 = 2.112(4), Ru5-C0 = 1.942(3).

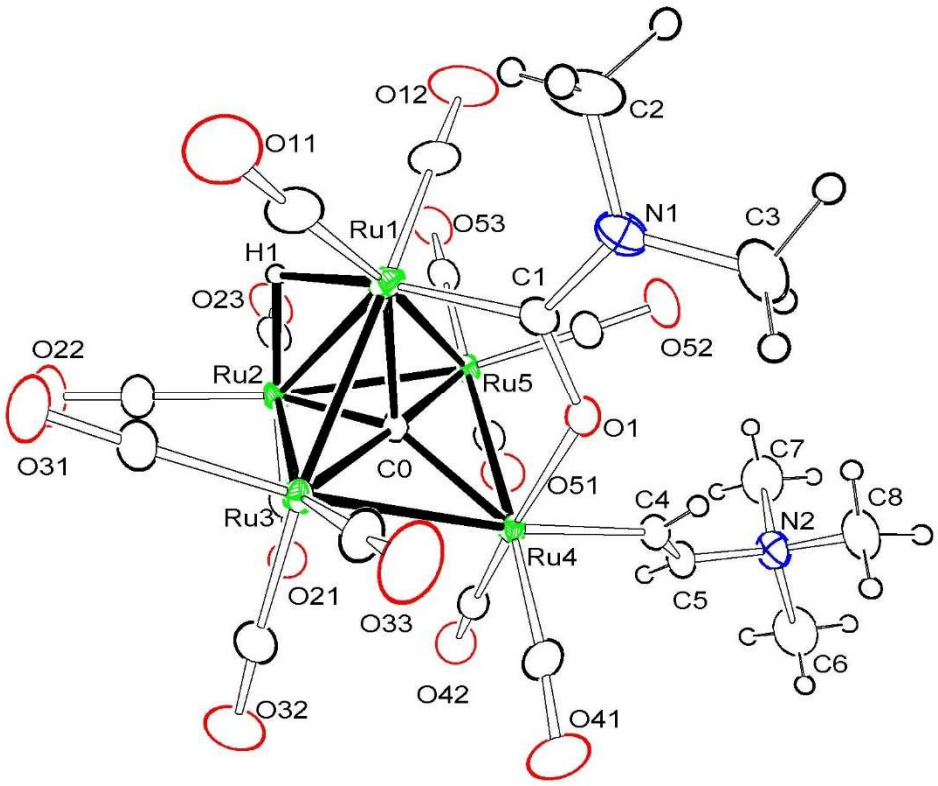

Figure 6.4. ORTEP diagram of the molecular structure of $Ru_5(\mu_5\text{-}C)(CO)_{14}(\mu\text{-}\eta^2\text{-}O{=}CN(CH_3)_2)(CH{=}CHNMe_3)(\mu\text{-}H)$, **6.5**, showing 20% thermal ellipsoid probability. Selected interatomic bond distances (Å) are as follow: Ru1-Ru3 = 2.8177(4), Ru1-Ru5 = 2.8275(4), Ru1-Ru2 = 2.9579(4), Ru2-Ru5 = 2.8635(4) Ru2-Ru3 = 2.8479(4), Ru3-Ru4 = 2.9146(4), Ru4-Ru5 = 2.9087(4), Ru1-H1 = 2.08(2), Ru2-H1 = 1.96(2), Ru4-C4 = 2.074(4), Ru1-C1 = 2.089(4), Ru4-O1 = 2.114(2), C1-O1 = 1.276(4), C4-C5 = 1.280(5), C5-N2 = 1.506(5), Ru1-C0 = 2.071(3), Ru2-C0 = 2.101(3), Ru3-C0 = 1.982(3), Ru4-C0 = 2.068(3), Ru5-C0 = 1.979(3).

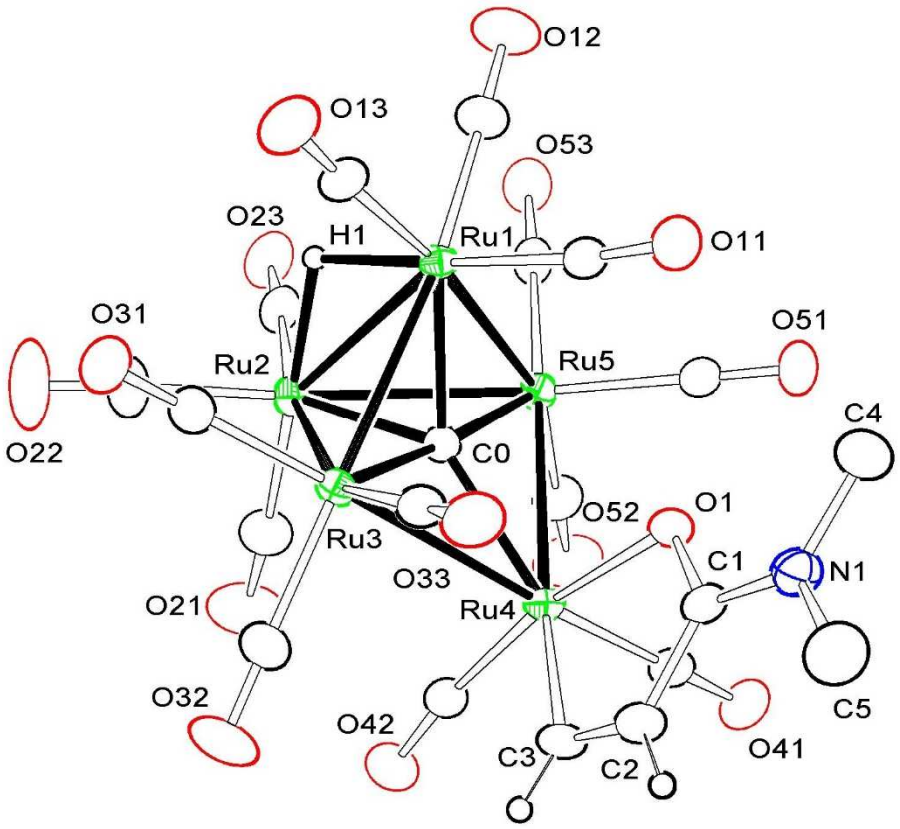

Figure 6.5. ORTEP diagram of the molecular structure of $Ru_5(\mu_5\text{-}C)(CO)_{14}(\eta^2\text{-}O{=}CN(Me)_2CH{=}CH)(\mu\text{-}H)$, **6.6**, showing 20% thermal ellipsoid probability. Methyl hydrogen atoms have been omitted for clarity. Selected interatomic bond distances (Å) are as follows: Ru1-Ru3 = 2.8437(5), Ru1-Ru5 = 2.8301(5), Ru1-Ru2 = 2.8458(5), Ru2-Ru5 = 2.8471(5) Ru2-Ru3 = 2.8706(5), Ru3-Ru4 = 2.9501(5), Ru4-Ru5 = 2.9549(5), Ru1-H1 = 1.66(4), Ru2-H1 = 1.79(4), Ru4-C3 = 2.034(5), Ru4-O1 = 2.155(3), C1-O1 = 1.282(5), C1-C2 = 1.452(7), C2-C3 = 1.330(8), Ru1-C0 = 2.126(4), Ru2-C0 = 2.118(4), Ru3-C0 = 1.952(4), Ru4-C0 = 2.139(4), Ru5-C0 = 1.963(4).

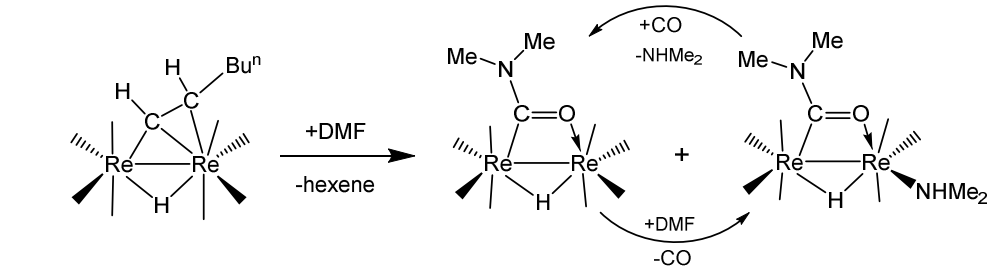

$Re_2(CO)_8[\mu\text{-}\eta^2\text{-}C(H)=C(H)Bu^n](\mu\text{-}H)$ $Re_2(CO)_8(\mu\text{-}\eta^2\text{-}O=CNMe_2)(\mu\text{-}H)$ $Re_2(CO)_7(NHMe_2)(\mu\text{-}\eta^2\text{-}O=CNMe_2)(\mu\text{-}H)$

Scheme 6.1. Formyl activation of DMF by $Re_2(CO)_8[\mu\text{-}\eta^2\text{-}C(H)=C(H)Bu^n](\mu\text{-}H)$.

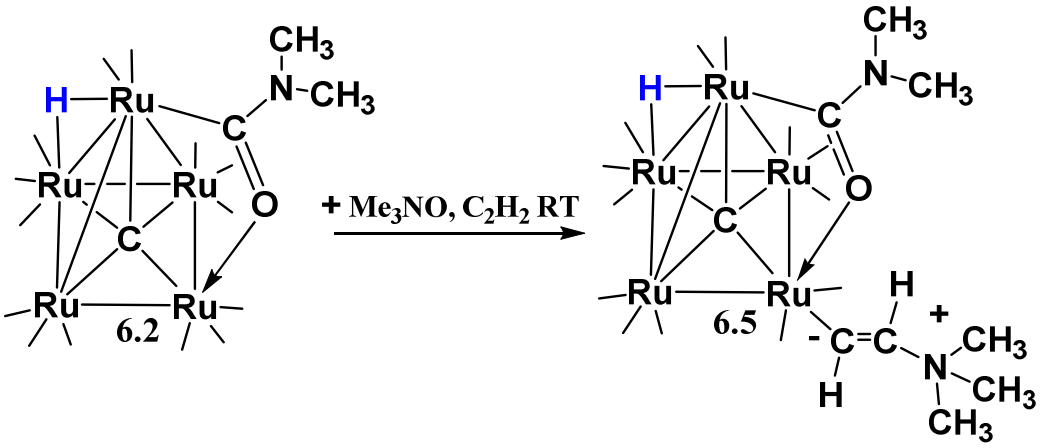

Scheme 6.2. Reaction of **6.2** with C_2H_2 in the presence of Me_3NO at room temperature to form complex **6.5**.

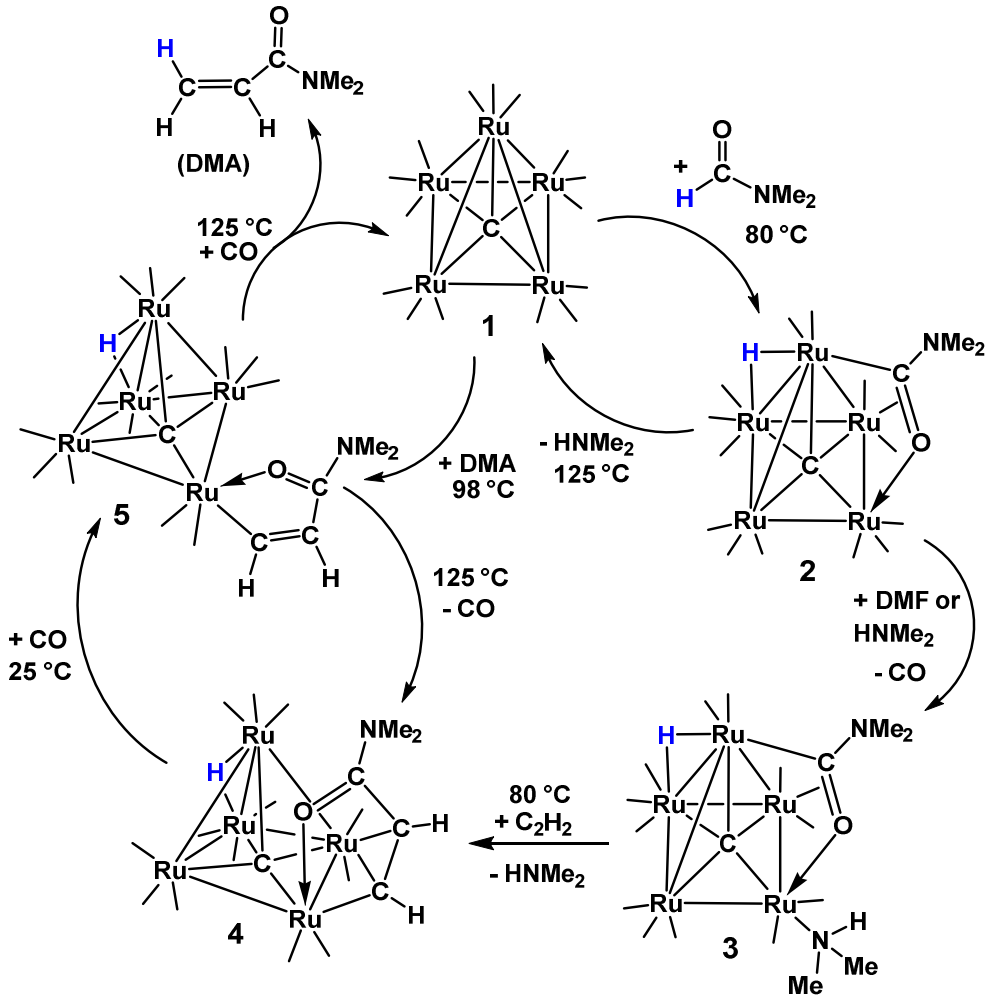

Scheme 6.3. Potential catalytic cycle for the formation of N,N-dimethylacrylamide from DMF and C_2H_2.

6.5 References

[1] (a) Rzaev, Z. M. O.; Dincer, S.; Piskin, E. *Prog. Polym. Sci*. **2007**, *32*, 534–595. (b) Hill, A.; Candau, F.; Selb, Joseph, J. *Macromolecules* **1993**, *26*, 4521-4532.

[2] (a) Mecking, S; Johnson, L. K.; Wang, L.; Brookhart, M. *J. Am. Chem. Soc.* **1998**, *120,* 888 – 899; (b) Wayland, B. B.; Poszmik, G.; Mukerjee, S. L. *J. Am. Chem. Soc.* **1994***, 116,* 7943-7944; (c) Kobayashi, M.; Nagasawa, T.; Yamada, H. *Trends in Biotech.* **1992**, 10, 402 – 408. (c) Yamada, H.; Kobayashi, M. *Biosci. Biotech. Biochem.* **1996**, *60*, 1391-1400; (d) Friedman, M. *J. Agric. Food Chem.* 2003**,** *51,* 4504-4526.

[3] (a) Balcells, D.; Clot, E.; Eisenstein, O. *Chem. Rev.* **2010**, *110,* 749–823. (b) Crabtree, R. H. *J. Organomet. Chem*. **2004**, *689*, 4083–4091; (c) Shilov, A. E.; Shul'pin, G. B. *Chem. Rev*. **1997**, *97*, 2879-2932; (d) Labinger, J. A.; Bercaw, J. E. *Nature* **2002**, *417*, 507–514; (e) Bergman R. G. *Nature* **2007**, 446, 391–393; (f) Caballero, A.; Pérez, P. J. *Chem. Soc. Rev.* **2013**, 42, 8809–8820; (g) Gunay, A.; Theopold, K. H. *Chem. Rev.* **2010**, 110, 1060–1081; (h) Hall, C.; Perutz, R. N. *Chem. Rev*. **1996**, 96, 3125–3146; (i) Rudakov, E. S.; Shul'pin, G. B. *J., Organomet. Chem.* **2015**, 793, 4–16; (j) Labinger, J. A.; Bercaw, J. E. *J. Organomet. Chem.* **2015**, *793*, 47–53; (k) Webb, J. R.; BolaÇo, T.; Gunnoe, T. B. *Chem Sus Chem.* **2011**, 4, 37–49.

[4] (a) Lersch, M.; Tilset, M. *Chem. Rev*. **2005**, 105, 2471–2526; (b) Jones, W.D.; Feher, F.J. *Acc. Chem. Res.* **1989**, 22, 91-100; (c) Jones, W.D. *Acc. Chem. Res*. **2003**, 36, 140–146. (d) Koppaka, A.; Captain, B. *Inorg. Chem*. **2016**, 55, 2679−2681; (e) Adams, R.D.; Rassolov, V.; Wong, Y.O. *Angew. Chem. int. Ed.* **2016**, 55 1324–1327.

[5] (a) Marder, T.B.; Roe, D.C.; Milstein, D. *Organometallics* **1988**, 7, 1451-1453; (b) Kondo, T.; Akazome, M.; Tsuji, Y.; Watanabe, Y. *J. Org. Chem.* **1990**, 55, 1286-1291. (c) Kondo, T.; Hiraishi, N.; Morisaki, Y.; Wada, K.; Watanabe, Y.; Mitsudo, T. *Organometallics* **1998**, 17, 2131-2134; (d) Dyker, G. *Angew. Chem., Int. Ed*. **1999**, 38, 1698-1712; (e) Jun, C.-H.; Moon, C.W.; Lee, D.-Y. *Chem, Eur. J.* **2002**, 8, 2423-2428; (f) Willis, M.C.; McNally, S.J.; Beswick, P.J. *Angew. Chem., Int. Ed.* **2004**, 43, 340-340; (g) Lochow, C. F.; Miller, R. G. *J. Am. Chem. Soc*. **1976**, 98, 1281-1283; (h) Tanaka, K.; Fu, G.C. *J. Am. Chem. Soc*. **2001**, 123, 11492-11493; (i) Sato, Y.; Oonishi, Y.; Mori, M. *Angew. Chem., Int. Ed.* **2002**, *41*, 1218-1221; (j) Tanaka, M.; Sakai, K.; Suemune, H.; Curr. *Org. Chem*., **2003**. 7, 353-367. (k) Kakiuchi, F.; Chatani, N. *Top.Organomet. Chem*. 2004, 11, 45-79.

[6] (a) Isnard, P.; Denise, D.; Sneeden, R.P.A.; Cognion, J.M.; Durual, P. J. *Organomet. Chem.* **1983**, 256, 135–139; (b) Profir, I.; Beller, M.; Fleischer, I. *Org. Biomol. Chem*. **2014**, 12, 6972–6976; (c) Legrand, C.; Castanet, Y.; Mortreux, Petit *J. Chem .Soc. Chem. Commun.* **1994**, 1173-1174; (d) Park, E.J.; Lee, J.M.; Han, H.; Chang, S. *Org. Lett.* **2006**, 8, 4355-4358.

[7] (a) Miyazaki, Y.; Yamada, Y.; Nakao, Y.; Hiyama, T. *Chem. Lett*. **2012**, 298-300; (b) Ko, S.; Han, H.; Chang, S. *Org. Lett.,* **2003**, 5, 2687-2690 (c) Nakao, Y.; Idei, H.; Kanyiva, K.S.; Hiyama, T. *J. Am. Chem. Soc.* **2009**, 131, 5070–5071; (d) Armanino, N.; Carreira, E.M. *J. Am. Chem. Soc.* **2013**, 135, 6814–6817; (e) Kondo, T.; Okada, T.; Mitsudo *Organometallics* **1999**, 18, 4123-4127; (f) Tsuji,Y.; Yoshii, S.; Ohsumi, T.; Kondo,T.; Watanabe, Y. *J. Organomet. Chem*. **1987**, 331, 379-385.

[8] Adams, R. D.; Dhull, P. *J. Organomet Chem.* **2017**, *849-850*, 228–232, https://doi.org/10.1016/j.jorganchem.2017.03.009.

[9] Johnson, B. F. G.; Lewis, J.; Nicholls, J. N.; Puga, J.; Raithby, P.R.; Rosales, M. J.; McPartlin, M.; Clegg, W. *J. Chem. Soc. Dalton Trans*. **1983**, 277 – 290.

[10] Saint+, Version 6.2a, Bruker Analytical X-ray System, Inc, Madison, WI, **2001**.

[11] APEX3 Version **2016**.5-0 and SAINT Version 8.34A. Bruker AXS, Inc. Madison, WI, USA.

[12] SADABS Version **2016**/2. Krause, L., Herbst-Irmer, R., Sheldrick G.M. & Stalke D. *J. Appl. Cryst*. **2015**, 48, 3-10.

[13] G.M. Sheldrick, SHELXTL, Version 6.1, Bruker Analytical X-ray Systems, Inc, Madison, WI, **1997**.

[14] (a) Ishida, T.; Mizobe, Y.; Tanase, T.; Hidai, M. *J. Organomet. Chem.* **1991**, *409*, 355-365; (b) Coalter, III, J.N.; Huffman, J. C.; Caulton, K. G. *Organometallics* **2000**, *19*, 3569-3578; (c) Graham, P. M.; Mocella, C. J.; Sabat, M.; Harman, W. D. *Organometallics* **2005**, *24*, 911-919; (d) Varshavsky, Y. S.; Cherkasova, T. G. *J. Organomet. Chem*. **2007**, *692*, 887-893.

CHAPTER 7

Substituent-Directed Activation of CH bonds in Activated Olefins by $Ru_5(\mu_5\text{-}C)(CO)_{15}$[6]

[6] Adams, R. D.; Smith, M. D.; Tedder, J. D; *Eur. J. Inorg. Chem.* **2018**, 2984-2986.
Reprinted here with permission from publisher

7.1 Introduction

Interest in olefin coupling reactions, such as oxidative olefination[1] and related olefinic homo- and cross-coupling reactions[2] that are predicated on the activation of alkenyl CH bonds continues to grow. In recent studies, we have found that the square pyramidal pentaruthenium cluster complex, $Ru_5(\mu_5\text{-}C)(CO)_{15}$, **7.1**[3] is able to activate the formyl CH bond in dimethylformamide by a cluster opening C-H oxidative addition to the Ru_5 cluster with formation of a bridging formamido ligand, eq.(7.1).[4]

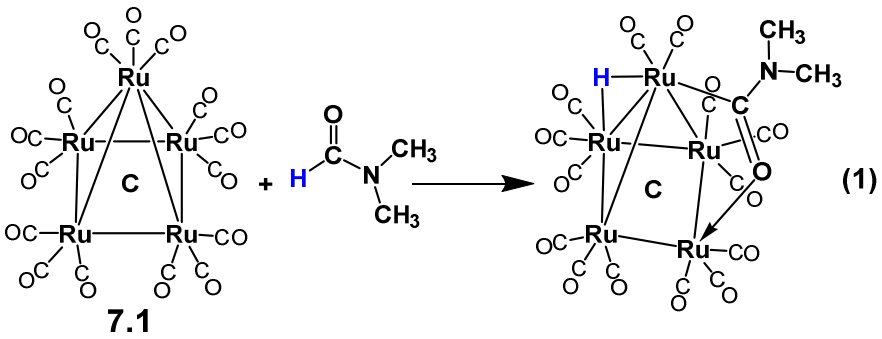

We have now found that **7.1** is also able to activate CH bonds readily in certain substituted olefins and in addition have found that the nature of the substituent on the alkene can play an important, if not decisive role, in determining the location of the CH bond activation site.

7.2 Experimental Section

General Data

All reactions were performed under an atmosphere of nitrogen. Reagent grade solvents were dried by standard procedure and were freshly distilled prior to use. Infrared spectra were recorded on a Thermo Scientific Nicolet IS10. ^{1}H NMR spectra was recorded on a Varian Mercury 300 spectrometer operating at 300.1 MHz. Mass spectrometric (MS) measurements were performed by a direct-exposure probe by using electron impact (EI)

ionization. $Ru_3(CO)_{12}$ was purchased from STREM and was used without further purification. $Ru_5(\mu_5\text{-}C)(CO)_{15}$, **7.1**, was prepared by using $Ru_3(CO)_{12}$ according to the previously reported procedure.[3] Vinyl acetate was obtained from Sigma-Aldrich and was used without further purification. Product separations were performed by TLC in air on Analtech 0.25 mm and 0.50 mm silica gel 60 Å F254 glass plates.

Reaction of $Ru_5(\mu_5\text{-}C)(CO)_{15}$, 7.1, with Methyl Acrylate at 80 ˚C

48.2 mg (0.051 mmol) of **7.1** was added to a 50 mL three-neck flask in 25 mL of degassed benzene with 700 µL of methyl acrylate. After heating for 48 h at 80 °C, the solvent was removed in vacuo, and the products were then isolated by TLC with a hexane/methylene chloride mixture to provide in the order of elution: 20.5 mg (40% yield) of $Ru_5(\mu_5\text{-}C)(CO)_{14}[\eta^2\text{-}O{=}CO(CH_3)CH{=}CH](\mu\text{-}H)$, **7.2**. Spectral data for **7.2**: IR νCO (cm^{-1} in hexane) 2097(w), 2066(s), 2056(s), 2049(s), 2036(w), 2022(m), 2018(sh), 2014(sh), 1995(sh), 1991(m), 1976(w). ^1H NMR (CD_2Cl_2, in ppm) δ = 10.18 (d, 8 Hz, 1H, Ru-C(H)=C(H)-C), 6.96 (d, 8 Hz, 1H, Ru-C(H)=C(H)-C), 3.65 (s, 3H, $O{=}COCH_3$), -22.181 (s, 1H, hydride). EI/MS m/z. M+ = 995.5. The isotope distribution pattern is consistent with the presence of five ruthenium atoms.

Reaction of $Ru_5(\mu_5\text{-}C)(CO)_{15}$, 7.1, with Vinyl Acetate at 80 ˚C

50.6 mg (0.054 mmol) of **7.1** was added to a 50 mL three-neck flask in 25 mL of degassed benzene with 350 µL of vinyl acetate. After heating for 42 h at 80 °C, the solvent was removed in vacuo, and the products were then isolated by TLC with a hexane/methylene chloride mixture to provide 33.2 mg (62% yield) of $Ru_5(\mu_5\text{-}C)(CO)_{14}(\eta^2\text{-}O{=}C(CH_3)OC{=}CH_2)(\mu\text{-}H)$, **7.3**. Spectral data for **7.3**: IR νCO (cm^{-1} in hexane) 2097(w), 2066(s), 2057(vs), 2050(m), 2036(w), 2023(sh), 2019(w), 2013(sh),

1996(w), 1990(w), 1986(sh), 1980(vw). ^{1}H NMR (CD_2Cl_2, in ppm) δ = 5.65 (d, 2.4 Hz, 1H, Ru-C=CH_2), 5.06 (d, 2.7 Hz, 1H, Ru-C=CH_2), 2.09 (s, 3H, O=C(CH_3)), -22.369 (s, 1H, hydride). EI/MS m/z. M+ = 995.5. The isotope distribution pattern is consistent with the presence of five ruthenium atoms.

Crystallographic Analyses

Single crystals of compounds **7.2** and **7.3** suitable for X-ray diffraction analyses were obtained by slow evaporation of solvent from solutions of the pure compounds in benzene/heptane solvent at room temperature. X-ray intensity data for compounds **7.2** and **7.3** was measured by using a Bruker D8 QUEST diffractometer equipped with a PHOTON-100 CMOS area detector and an Incoatec microfocus source (Mo Kα radiation, λ = 0.71073 Å).2 The data collection strategy for **7.2** consisted of three 180° ω-scans at different φ settings, with a scan width per image of 0.5°. The crystal-to-detector distance was 4.5 cm and each image was measured for 24 s. The average reflection redundancy to 2θ max was 6.1. The data collection strategy for **7.3** consisted of six 180° ω-scans at different φ settings and two 360° φ-scans at different ω angles, with a scan width per image of 0.5°. The crystal-to-detector distance was 5.0 cm and each image was measured for 2 s with the detector operated in shutterless mode. The raw area detector data frames were reduced, scaled and corrected for absorption effects using the SAINT[5] and SADABS[6] programs. All structures were solved by a combination of direct methods and difference Fourier syntheses, and refined by full-matrix least squares refinement on F2 by using the SHELXTL software package.[7] All non-hydrogen atoms were refined with anisotropic thermal parameters. The hydride ligands bonded to the metal atoms in **7.2** and **7.3** were located and refined in each analysis. All other hydrogen atoms were placed in

geometrically idealized positions and were included as standard riding atoms during the final least-squares refinements with C-H distances fixed at 0.96 Å. Compound **7.2** crystallized in the monoclinic crystal system. The space group P21/n was identified for compound **7.2** on the basis of systematic absences observed in the intensity data. Compound **7.2** was found to be disordered about two conformations and was modeled for with 70% comprising the major component (a) and 30% comprising the minor component (b). Compound **7.3** crystallized in the triclinic crystal system. The space group P-1 was assumed for compound **7.3** and was confirmed by successful structure solution and refinement. Crystal data, data collection parameters, and results for the analyses are listed in Table 7.1.

7.3 Results and Discussion

The reaction of **7.1** with methylacrylate, CH_2=CHC(=O)OMe, in benzene solvent at reflux for 48 h provided the new compound $Ru_5(\mu_5\text{-}C)(CO)_{14}[\eta^2\text{-}O{=}CO(CH_3)CH{=}CH](\mu\text{-}H)$, **7.2** in 40 % yield. Compound **7.2** was characterized by a combination of IR, ^{1}H NMR, mass spectrometry and single-crystal X-ray diffraction analyses. An ORTEP diagram of the molecular structure of **7.2** is shown in Figure 7.1. Compound **7.2** contains an open Ru_5C cluster with a chelating acryloyl, CH=CHC(=O)OMe, ligand coordinated to the Ru4 atom that was dislodged from the base of the square pyramidal Ru_5 cluster of **7.1**. The hydrogen atom became the hydrido ligand, H1, δ = -22.18, that bridges the Ru1 – Ru2 hinge bond of the remaining Ru4 group of metal atoms. The acryloyl ligand is coordinated to the alkenyl carbon atom C1a, Ru4 – C1a = 2.054(5) Å, and the carbonyl oxygen atom O1a, Ru4 – O1a = 2.158(5) Å. There is a double bond between the carbon atoms C1a and C2a, C1a – C2a = 1.303(7) Å. Most likely,

compound **7.2** was formed in two steps: (1) by a cluster opening addition of the carbonyl oxygen atom to one of the basal Ru atoms, Ru4, in **7.1** which was then followed by (2) loss of CO and an oxidative addition of a CH bond on the β-carbon atom of the methylacrylate ligand which leads to the formation of a very stable five-membered ring accompanied by migration of the hydrogen atom to the Ru1 – Ru2 bond, see Scheme 7.1. It is known that simple donors, such as NCMe, can open the cluster in **7.1** by a Ru – Ru bond cleavage process.[3]

There are a number of examples of alkyl acryloyl-substituted metal complexes containing similar five-membered chelate ring systems, but all of these complexes appear to have been synthesized by the insertion of a carboxylate acetylene into the metal-hydrogen bond of a metal complex.[8] Compound **7.2** contains fourteen carbonyl ligands and has a total of 76 valence electron and thus all metal atoms formally obey the 18 electron rule.

Interestingly, the reaction of **7.1** with vinyl acetate also yielded an opened Ru5 cluster complex containing a CH activated vinyl group, $Ru_5(\mu_5\text{-}C)(CO)_{14}[C(=CH_2)OCOMe](\mu\text{-}H)$, **7.3**, (62 % yield) after heating for 42 h in benzene solvent at reflux, but in this product the CH activation site occurred exclusively at the α-carbon atom of the vinyl group. An ORTEP diagram of the molecular structure of **7.3** is shown in Figure 7.2. Like **7.2**, compound **7.3** contains a chelating acetate-substituted vinyl ligand coordinated to one ruthenium atom in a five-membered metallacycle in an open Ru_5 cluster. There is one hydrido ligand on the Ru1 - Ru2 bond, δ = -22.37. The vinyl group is bonded to Ru4 through the α-carbon atom C1 of the vinyl group, Ru4 – C1 = 2.035(4) Å. The acetate group is also coordinated to Ru4 through the carbonyl oxygen atom O1, Ru4

– O1 = 2.124(3) Å. The exo-cyclic C – C bond, C1 – C4, is a double bond, C1 – C4 = 1.272(6) Å. Although there are a number of reports of metal complexes containing alkenyl acetate ligands,[9] none of these complexes were obtained by reactions of a metal complex with an alkenyl acetate. Compound **7.3** contains fourteen carbonyl ligands and has a total of 76 valence electron and all metal atoms formally obey the 18 electron rule.

7.4 Conclusions

We have confirmed the first examples of olefinic CH bond activation in methylacrylate and vinylacetate by a metal complex by using crystallographic structural characterizations. The reactions proceed by cluster-opening processes which are believed to be facilitated by coordination of the substituent on the olefin. This is followed by a CH bond activaton step leading to the formation of a five-membered metallacycle. The site of CH bond activation in the olefin is determined by the number of atoms in the substituent that are included in the ring, see Scheme 7.2.

Table 7.1. Crystal data, data collection parameters for compounds **7.2** and **7.3**.

Compound	**7.2**	**7.3**
Empirical formula	$Ru_5O_{16}C_{19}H_6$	$Ru_5O_{16}C_{19}H_6$
Formula weight	995.59	995.59
Crystal system	Monoclinic	Triclinic
Lattice parameters		
a (Å)	9.3688(3)	9.0847(2)
b (Å)	15.8209(6)	9.7485(3)
c (Å)	18.6237(7)	16.3407(4)
α (deg)	90.00	73.229(1)
β (deg)	100.761(1)	81.945(1)
γ (deg)	90.00	81.421(1)
V (Å^3)	2711.91(17)	1362.89(7)
Space group	*P* 2_1/n	*P* -1
Z value	4	2
ρ_{calc} (g / cm^3)	2.438	2.426
μ (Mo Kα) (mm^{-1})	2.794	2.780
Temperature (K)	100(2)	299(2)
$2\Theta_{max}$ (°)	54.522	59.926
No. Obs. (I > 2σ(I))	6263	4801
No. Parameters	356	366
Goodness of fit (GOF)	1.015	1.145
Max. shift in cycle	0.001	0.001
Residuals*: R1; wR2	0.0287; 0.0417	0.0198; 0.0557
Absorption Correction,	Multi-scan	Multi-scan
Max/min	0.9462/0.7304	0.7460/0.591
Largest peak in Final Diff. Map (e$^-$ / Å^3)	0.777	0.580

*$R1 = \Sigma_{hkl}(||F_{obs}| - |F_{calc}||)/\Sigma_{hkl}|F_{obs}|$; $wR2 = [\Sigma_{hkl}w(|F_{obs}| - |F_{calc}|)^2/\Sigma_{hkl}wF^2_{obs}]^{1/2}$; $w = 1/\sigma^2(F_{obs})$; $GOF = [\Sigma_{hkl}w(|F_{obs}| - |F_{calc}|)^2/(n_{data} - n_{vari})]^{1/2}$.

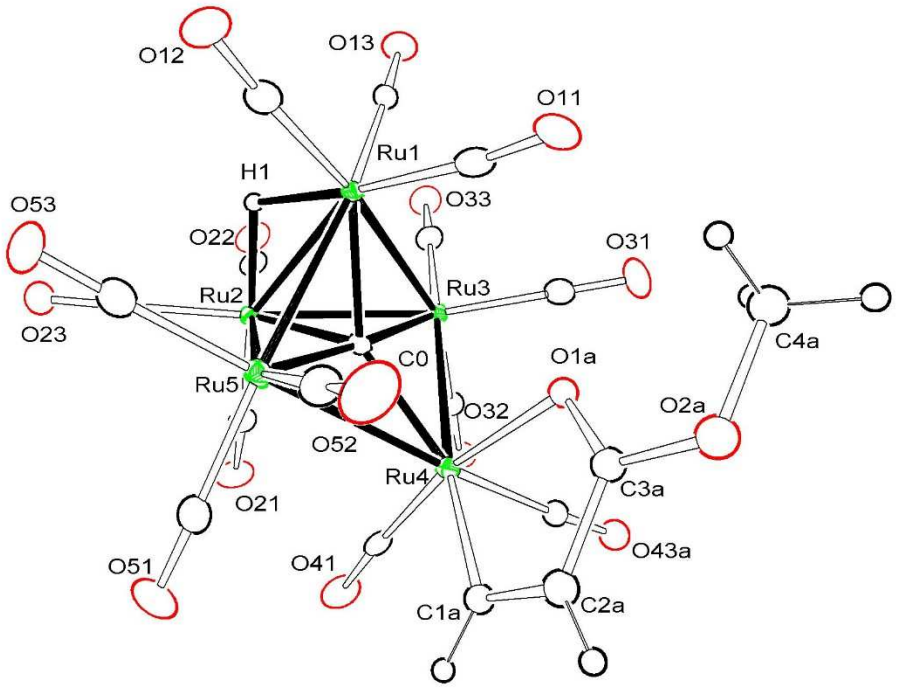

Figure 7.1. An ORTEP diagram of the molecular structure of $Ru_5(\mu_5\text{-}C)(CO)_{14}[\eta^2\text{-}O{=}CO(CH_3)CH{=}CH](\mu\text{-}H)$, **7.2**, showing 30% thermal ellipsoid probability. Selected interatomic bond distances (Å) are as follows: Ru1-Ru3 = 2.8405(4), Ru1-Ru5 = 2.8442(4), Ru1-Ru2 = 2.8335(4), Ru2-Ru5 = 2.8550(4) Ru2-Ru3 = 2.8501(4), Ru3-Ru4 = 2.9313(4), Ru4-Ru5 = 2.9388(4), Ru1-H1 = 1.74(3), Ru2-H1 = 1.77(3), Ru4-O1a = 2.158(5), Ru4-C1a = 2.054(5), C1a-C2a = 1.303(7), C2a-C3a = 1.447(6), C3a-O1a = 1.264(6), Ru1-C0 = 2.114(3), Ru2-C0 = 2.119(3), Ru3-C0 = 1.964(3), Ru4-C0 = 2.115(3), Ru5-C0 = 1.959(3).

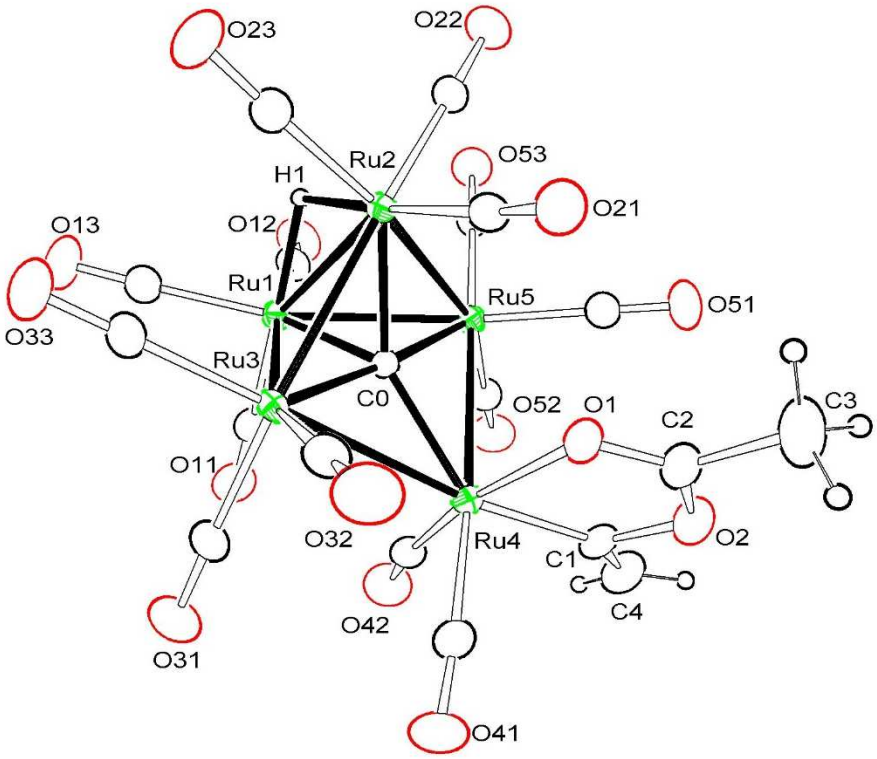

Figure 7.2. An ORTEP diagram of the molecular structure of $Ru_5(\mu_5\text{-}C)(CO)_{14}(\eta^2\text{-}O{=}C(CH_3)OC{=}CH_2)(\mu\text{-}H)$, **7.3**, showing 25% thermal ellipsoid probability. Selected interatomic bond distances (Å) are as follows: Ru1-Ru3 = 2.8469(4), Ru1-Ru5 = 2.8472(4), Ru1-Ru2 = 2.8412(4), Ru2-Ru5 = 2.8392(4) Ru2-Ru3 = 2.8340(4), Ru3-Ru4 = 2.9436(4), Ru4-Ru5 = 2.9432(6), Ru1-H1 = 1.81(4), Ru2-H1 = 1.71(4), Ru4-O1 = 2.124(3), Ru4-C1 = 2.035(4), C1-C4 = 1.272(6), C1-O2 = 1.486(5), O2-C2 = 1.327(5), C2-O1 = 1.215(5), Ru1-C0 = 2.115(3), Ru2-C0 = 2.118(3), Ru3-C0 = 1.968(3), Ru4-C0 = 2.116(3), Ru5-C0 = 1.955(3).

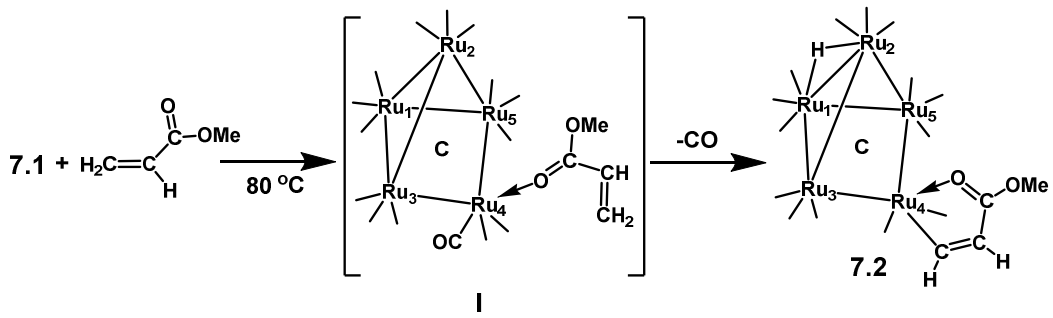

Scheme 7.1. Reaction of **7.1** with methyl acrylate at 80 °C.

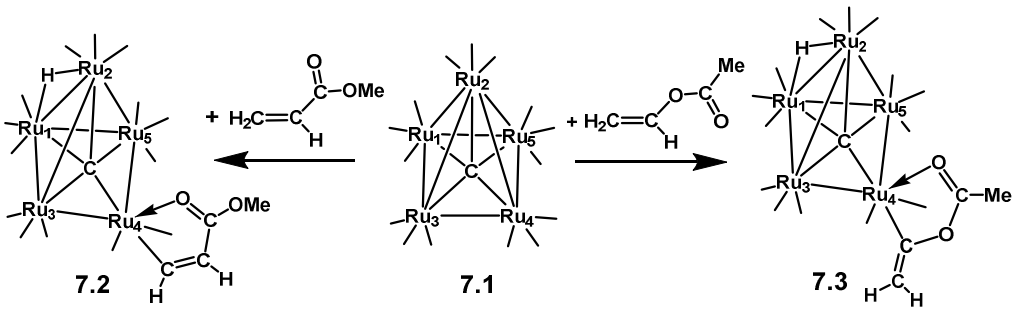

Scheme 7.2. Summary of the C-H activation reactions of substituted olefins with **7.1**.

7.5 References

[1] (a) Hu, H.; Zhang, X.-F.; Yang, Y.-H.; Xu, T.-P.; Loh *J. Am. Chem. Soc*. **2015**, 137, 3169−3172; (b) Hatamoto,Y.; Sakaguchi, S.; Ishii, Y. *Org. Lett*. **2004**, 6, 4623 – 4625; (c) Besset, T.; . Kuhl, N.; Patureau, F.W.; Glorius, F. *Chem. Eur. J.* **2011**, 17, 7167 – 7171; (d) Xu, Y.-H.; Lu, T.-P.; Loh *J. Am. Chem. Soc*. **2009**, 131, 1372–1373; (e) Yu, H.; Jin, W.; Ch. Sun, Chen, J.; Du, W.; He, S.; Yu, Z. *Angew. Chem. int. Ed.* **2010**, 122, 5928 – 5933; (f) Al-Maksoud, W.; Djakovitch, L.; Jahjah, M.; Pinel, C. *Sci. China Chem*. **2010**, 53, 1927 – 1931; (g) McKinney, R.J.; Colton, M.C. *Organometallics* **1986**, 5, 1080-1085; (h) Xu, Y.-H.; Loh, T.-P. *Chem. Eur. J.* **2012**, 18, 13284 – 13287; (i) Zhang, Y.; Cui, Z.; Li, Z.; Liu, Z.-Q. *Org. Lett.* **2012**, 14, 1838 – 1841; (j) Wen, Z.-K.; Xu, Y.-H.; Loh, T.-P. *Chem. Sci.* **2013**, 4, 4520 – 4524; (k) Zhang, J.; Loh, T.-P. *Chem. Commun.* **2012**, 48, 11232 – 11234; (l) Boultadakis-Arapinis, M.; Hopkinson, M.N.; Glorius, F. *Org. Lett*. **2014**, 16, 1630 – 1633; (m) Liu, M.; Yang, P.; Karunananda, M.K.; Wang, Y.; Liu, P., Engle, K.M. *J. Am. Chem. Soc.* **2018**, ASAP, DOI: 10.1021/jacs.8b02124; (n) O'Duill, M.L.; Matsuura, R.; Wang, Y.; Turnbull, Gurak, Jr., J.A.; Gao, D.-W.; Lu, G.; Liu, P.; Engle, K.M. *J. Am. Chem. Soc.* **2017**, 139, 15576-15579.

[2] (a) Takahama, Y.; Shibata, Y.; Tanaka, K. *Chem. Eur. J.* **2015**, 21, 9053 – 9056; (b) Grimster, N.P.; Gauntlett, C.; Godfrey, C.R.A.; Gaunt, M.J. *Angew. Chem. Int. Ed.* **2005**, 44, 3125 – 3129; (c) Mochida, S.; Hirano, K.; Satoh, T.; Miura, M. *J. Org. Chem*. **2009**, 74, 6295–6298; (d) Yu, H.; Jin, W.; Sun, C.; Chen, J.; Du, W.; He, S.; Yu, Z. *Angew. Chem. Int. Ed*. **2010**, 49, 5792 – 5797; (e) Sato, T.; Kakiuchi, F.; Chatani, N.; Murai, S. *Chem. Lett*. **1998**, 27, 893 – 894; (f) Gooßen, L.J.; Rodriguez, N. *Angew. Chem. Int. Ed.* **2007**, 46, 7544 – 7546; (g) Simon, M.-O.; Martinez, R.; Genet, J.-P.; Darses, S. *Adv. Synth.*

Catal. **2009**, 351, 153 – 157; (h) Tsujita, H.; Ura, Y.; Matsuki, S.; Wada, K.; Kenji, T.; Mitsudo, T.; Kondo *Angew. Chem. Int. Ed.* **2007**, 46, 5160 –5163; (i) Pertici, P.; Ballantini, V.; Salvadori, P.; Bennet, M.A. *Organometallics* **1995**, 14, 2565 – 2569; (j.) Tkatchenko, I.; Neibecker, D.; Grenouillet, P. *Organometallics* **1984**, 3, 1130 - 1132.

[3] Johnson, B.F.G.; Lewis, J.; Nicholls, J.N.; Puga, J.; Raithby, P.R.; Rosales, M.J.; McPartlin, M.; Clegg, W. *J. Chem. Soc. Dalton Trans*. **1983**, 277 – 290.

[4] Adams, R.D.; Tedder, J.D. *Inorg. Chem*. **2018**, 57, 5707-5710.

[5] SADABS Version 2016/2. Krause, L., Herbst-Irmer, R., Sheldrick G.M. & Stalke D. J. Appl. Cryst. **2015**, 48, 3-10.

[6] SADABS Version 2016/2. Krause, L., Herbst-Irmer, R., Sheldrick G.M. & Stalke D. *J. Appl. Cryst*. **2015**, 48, 3-10.

[7] G.M. Sheldrick, SHELXTL, Version 6.1, Bruker Analytical X-ray Systems, Inc, Madison, WI, **1997**.

[8] (a) Chen, J.; Huang, Z.-A.; Hua, Y.; Zhang, H.; Xia, H. *Organometallics* **2015**, 34, 340-347; (b) Zhao, Q.; Cao, X.-Y.; Wen, T.B.; Xia, H. *Chem. Asian J.* **2013**, 8, 269 – 275; (c). Bianchini,C.; Innocenti,P.; Masi, D.; Meli, A.; Sabat, M. *Organometallics* **1986**, 5, 72 – 78; d) Bohanna, C.; Buil, M.L.; Esteruelas, M.A.; Onate, E.; Valero, C. *Organometallics* **1999**, 18, 5176 – 5179; (e) Almeida, S.S.P.; Duarte, M.T.; Ribeiro, L.M.D.; Gormley, ., Galvao, A.M.; Da Silva, J.J.R.F.; Pombeiro,A.J.L. *J. Organomet. Chem.* **1996**, 524, 63 – 66; (f) Li, X.; Vogel, T.; Incarvito, C.D.; Crabtree, R.H. *Organometallics* **2005**, 24, 62 – 76.

[9] (a) Esteruelas, M. A.; Lahoz, F. J.; Lopez, A. M.; Ofiate, E.; Oro, L. A. *Organometallics* **1994**, 13, 1669-1678; (b) Chin, C. S.; Kim, M.; Lee, M. K.; Lee, H. *Organometallics* **2003**, 22(16), 3239–3244; (c) Sanford, M. S.; Valdez, M. R.; Grubbs, R. H. *Organometallics* **2001**, 20, 5455-5463; (d) Kawano, H.; Masaki, Y.; Matsunaga, T.; Hiraki, K.; Onishi, M.; Tsubomura, T. *J. Organomet. Chem.* **2000**, 601, 69 – 77.

CHAPTER 8

Coupling of Activated Olefins by a Ru_5 Cluster Complex[7]

[7] Adams, R. D.; Smith, M. D.; Tedder, J. D; *Manuscript in Progress*.

8.1 Introduction

The coupling of olefins by the formation of carbon – carbon bonds mediated by metal complexes is of great interest. The dimerization and oligomerization of simple olefins like ethylene yields higher-value olefins for use in the synthesis of new polymers, fuels and chemicals.[1-4] The coupling of activated olefins, such as acrylates, acrylamides, acrylonitrile and vinyl acetate, also leads to valuable polymers.[5, 6] Dimers of acrylates and acrylamides have been sought for use as precursors to adipic acid which is used in the synthesis of nylon-6,6.[5-12]

The mechanisms for C – C bond forming in the tail-to-tail dimerization of activated olefins fall broadly into three categories. These are often referred to as (1) the insertion/β-elimination mechanism, eq. (8.1)[5]; (2) oxidative coupling via metallacyclic intermediates followed by a β-elimination (βE), eq. (8.2)[6, 7, 13]; and (3) the C-H activation mechanism involving a vinyl-hydride intermediate followed by alkene insertion into the M – H bond and a C – C bond forming reductive elimination (RE), eq. (8.3)[7, 14].

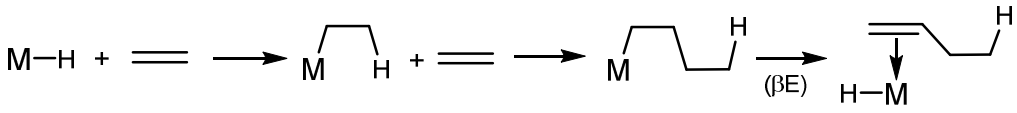

(8.1)

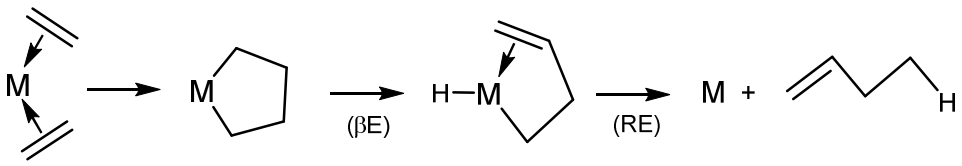

(8.2)

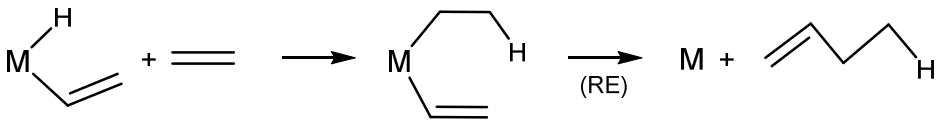

(8.3)

A related insertion-reductive elimination mechanism has been proposed for the formation of muconates eq. (8.4), observed for coupling of certain activated olefins by a palladium acetate catalyst.[15]

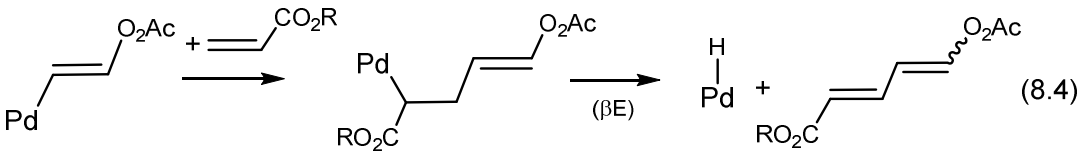

Substituted olefins like alkyl acrylates readily engage in CH activation at the vinyl group which is sometimes facilitated by coordination of the ester group.[16-18]

In recent studies we have discovered that the pentaruthenium cluster complex $Ru_5(CO)_{15}(\mu_5\text{-}C)$, **8.1** is able to activate the formyl CH bond in dimethylformamide[19] and certain aldehydes[20] to form opened Ru_5 cluster complexes containing η^2-C=O bridging acyl ligands e.g. eq. (8.5).

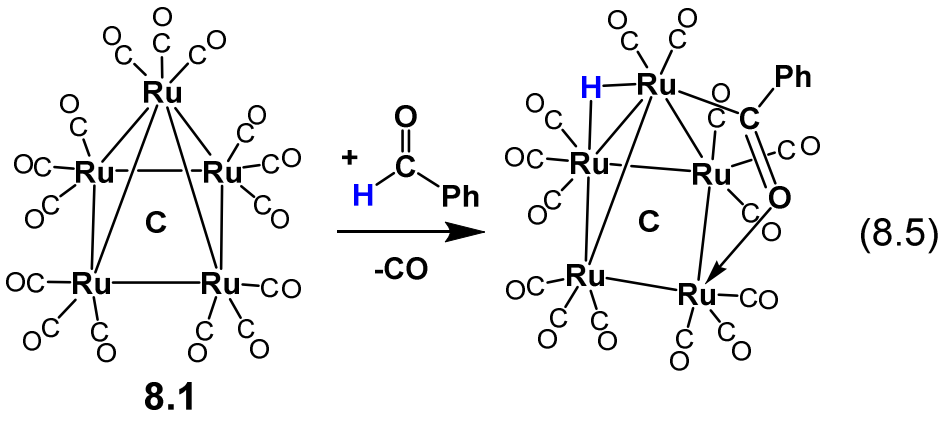

In an effort to pursue our studies of the activation of the activated olefins: methyl acrylate, N,N-dimethylacrylamide and vinyl acetate by pentaruthenium cluster complex $Ru_5(CO)_{15}(\mu_5\text{-}C)$, **8.1** we have investigated their potential for olefin coupling reactions. A pattern of CH activation on the vinyl group, the location of which is dependent of the

identity of the vinyl substituent, combined with C – C bond forming coupling reactions at the metal atoms has been observed and is described in this chapter. A preliminary report of this work has been published.[18]

8.2 Experimental Section

General Data

All reactions were performed under an atmosphere of nitrogen. Reagent grade solvents were dried by standard procedure and were freshly distilled prior to use. Infrared spectra were recorded on a Thermo Scientific Nicolet IS10. ^{1}H NMR spectra for compounds **8.6**, **8.9**, **8.13**, **8.14**, and **8.15** were recorded on a Varian Mercury 300 spectrometer operating at 300.1 MHz. ^{1}H NMR spectra for compounds **8.7**, **8.8**, **8.10**, **8.11**, and **8.12** were recorded on a Bruker AVANCE III spectrometer operating at 400 MHz. Mass spectrometric (MS) measurements were performed by a direct-exposure probe by using electron impact (EI) ionization. $Ru_3(CO)_{12}$ used to make $Ru_5(\mu_5\text{-}C)(CO)_{15}$ was obtained from STREM and was used without further purification. $Ru_5(\mu_5\text{-}C)(CO)_{15}$, **8.1**, was prepared according to previously reported procedure.[21] N,N-dimethylacrylamide (DMA), vinyl acetate and trimethylamine-N-oxide were obtained from Sigma-Aldrich and were used without further purification. Product separations were performed by TLC in air on Analtech 0.25 mm and 0.50 mm silica gel 60 Å F254 glass plates.

Reaction of $Ru_5(\mu_5\text{-}C)(CO)_{15}$, 8.1 with DMA at 98 ˚C.

25.2 mg (0.027 mmol) of **8.1** was added to a 50 mL three-neck flask in 20 mL of degassed heptane with 8 µL of DMA. After heating for 6.5 h at 98 °C, the solvent was removed *in vacuo*, and the products were then isolated by TLC by using a hexane/methylene chloride

mixture to provide in the order of elution: 8.0 mg (29% yield) of $Ru_5(\mu_5\text{-}C)(CO)_{14}[\eta^2\text{-}O{=}CN(Me)_2CH{=}CH](\mu\text{-}H)$, **8.3** and 1.2 mg (5% yield) of $Ru_5(\mu_5\text{-}C)(CO)_{13}(\mu\text{-}\eta^3\text{-}O{=}CNMe_2C(H)CH)(\mu\text{-}H)$, **8.4**. Compound **8.4** was obtained previously from the reaction of $Ru_5(\mu_5\text{-}C)(CO)_{13}(\mu\text{-}\eta^2\text{-}O{=}CNMe_2)(HNMe_2)](\mu\text{-}H)$ with C_2H_2 and compound **8.3** can be obtained by the carbonylation of **8.3** at room temperature.[19]

Reaction of $Ru_5(\mu_5\text{-}C)(CO)_{14}[\eta^2\text{-}O{=}C(OMe)CH{=}CH](\mu\text{-}H)$, 8.2, with Methyl Acrylate and Trimethylamine N-oxide at 25 °C.

39.8 mg (0.040 mmol) of **8.2** was added to a 50 mL three-neck flask in 20 mL of degassed hexane with 300 µL of methyl acrylate and 16 mg (0.21 mmol) of Trimethylamine N-oxide. The synthesis for **8.2** was reported in Chapter 7 as compound **7.2** After stirring for 20 h at room temperature, the solvent was removed *in vacuo*, and the products were then isolated by TLC by using a hexane/methylene chloride mixture to provide in the order of elution: 2.7 mg (7% yield) of starting material, **8.2**, 3.3 mg (8% yield) of $Ru_5(\mu_5\text{-}C)(CO)_{13}[\mu\text{-}\eta^3\text{-}O{=}CO(Me)CHCH](\mu\text{-}H)$, **8.6**, 3.6 mg (8% yield) of of $Ru_5(\mu_5\text{-}C)(CO)_{13}[\eta^3\text{-}$*anti*,*anti*$\text{-}(Me)OC{=}O\text{-}C_3H_3\text{-}\eta^1\text{-}O{=}CO(Me)CH_2](\mu\text{-}H)$, **8.7**, 5.6 mg (13% yield) of $Ru_5(\mu_5\text{-}C)(CO)_{13}[\eta^3\text{-}$*anti*,*syn*$\text{-}(MeO_2C)CH_2C_3H_3\text{-}CH_2\text{-}\eta^1\text{-}O{=}C(OMe)](\mu\text{-}H)$, **8.8**, 2.8 mg (7% yield) of $Ru_5(\mu_5\text{-}C)(CO)_{12}[\mu\text{-}\eta^3\text{-}O{=}C(OMe)CH{=}CH][\eta^2\text{-}CH{=}CHCO_2Me](\mu\text{-}H)$, **8.9**, and 3.7 mg (9% yield) of $Ru_5(\mu_5\text{-}C)(CO)_{13}[\eta^3\text{-}$*syn*,*anti*$\text{-}(MeO_2C)C_3H_3\text{-}\eta^1\text{-}O{=}C(OMe)CH_2](\mu\text{-}H)$, **8.10**. Spectral data for **8.6**: IR νCO (cm^{-1} in hexane) 2094(w), 2064(s), 2056(w), 2048(vs), 2038(s), 2026(w), 2017(w), 2002(vw), 1989(w), 1970(vw). ^1H NMR (CD_2Cl_2, in ppm) δ = 10.59 (d, $^3J_{H\text{-}H}$ = 5 Hz, 1H, Ru-C(**H**)=C(H)-C), 4.57 (d, $^3J_{H\text{-}H}$ = 5 Hz, 1H, Ru-C(H)=C(**H**)-C), 3.55 (s, 3H, OMe), 2.77, -22.02 (s, 1H, hydride). EI/MS *m*/*z*. 967.5. The isotope distribution is consistent with the presence of five ruthenium atoms. Spectral data

for **8.7**: IR νCO (cm^{-1} in hexane) 2090(w), 2060(s), 2051(vs), 2036(w), 2019(m), 2006(w), 1993(vw), 1985(vw), 1970(vw). ^1H NMR (CD_2Cl_2, in ppm) δ = 5.71 (t, $^3J_{H-H}$ = 8 Hz, 1H, C-C(H_2)-C(**H**)-C(H)-C(H)), 5.22 (d, $^3J_{H-H}$ = 8 Hz, 1H, C-C(H_2)-C(H)-C(H)-C(**H**)), 4.32 (t, $^3J_{H-H}$ = 8 Hz, 1H, C-C(H_2)-C(H)-C(**H**)-C(H)), 3.59 (s, 3H, OMe), 3.41 (dd, $^3J_{H-H}$ = 8 Hz, $^2J_{H-H}$ = 20 Hz, 1H, C-C(**H_2**)-C(H)-C(H)-C(H)), 3.37 (s, 3H, OMe), 3.15 (dd, $^2J_{H-H}$ = 20 Hz, 1H, C-C(**H_2**)-C(H)-C(H)-C(H)), -22.12 (s, 1H, hydride). EI/MS *m*/*z*. 1053.6. The isotope distribution is consistent with the presence of five ruthenium atoms. Spectral data for **8.8**: IR νCO (cm^{-1} in hexane) 2090(w), 2060(m), 2051(vs), 2036(w), 2019(m), 2005(w), 1993(vw), 1985(vw), 1970(vw). ^1H NMR (CD_2Cl_2, in ppm) δ = 5.48 (d, $^3J_{H-H}$ = 7 Hz, 1H, C-C(**H**)-C(H)-C(H)-C(H_2), 5.09 (dd, $^3J_{H-H}$ = 7 Hz, $^3J_{H-H}$ = 11 Hz, 1H, C-C(H)-C(**H**)-C(H)-C(H_2), 3.96 (dd, $^3J_{H-H}$ = 4 Hz, $^2J_{H-H}$ = 16 Hz, 1H, C-C(H)-C(H)-C(H)-C(**H_2**), 3.78 (s, 3H, OMe), 3.41, (s, 3H, OMe), 3.39 (td, $^3J_{H-H}$ = 4 Hz, $^3J_{H-H}$ = 11 Hz, 1H, C-C(H)-C(H)-C(**H**)-C(H_2), 3.14 (dd, $^3J_{H-H}$ = 10 Hz, $^2J_{H-H}$ = 16 Hz, 1H, C-C(H)-C(H)-C(H)-C(**H_2**), -22.43 (s, 1H, hydride). ESI/MS m^+/z. 1054.3. Spectral data for **8.9**: IR νCO (cm^{-1} in hexane) 2093(m), 2066(vs), 2050(s), 2032(m), 2026(m), 2017(w), 2004(vw), 1997(w), 1992(sh). ^1H NMR (CD_2Cl_2, in ppm) δ = 11.17 (d, $^3J_{H-H}$ = 5 Hz, 1H, Ru-C(**H**)=C(H)), 4.46 (d, $^3J_{H-H}$ = 5 Hz, 1H, Ru-C(H)=C(**H**)), 4.03 (dd, $^3J_{H-H}$ = 8 Hz, $^3J_{H-H}$ = 11 Hz, 1H, C(H_2)=C(**H**)), 3.83 (s, 3H, OMe), 3.81 (d, $^3J_{H-H}$ = 11 Hz, 1H, C(**H_2**)=C(H)), 3.41 (s, 3H, OMe), 2.34 (d, $^3J_{H-H}$ = 8 Hz, 1H, C(**H_2**)=C(H)), -20.92 (s, 1H, hydride). EI/MS *m*/*z*. 1025.4. The isotope distribution is consistent with the presence of five ruthenium atoms. Spectral data for **8.10**: IR νCO (cm^{-1} in hexane) 2090(w), 2060(s), 2051(vs), 2037(w), 2020(m), 2002(w), 1994(vw), 1986(vw), 1974(vw), 1970(vw), 1966(vw). ^1H NMR (CD_2Cl_2, in ppm) δ = 5.45 (t, $^3J_{H-H}$ = 8 Hz, 1H, C-C(H_2)-C(**H**)-C(H)-C(H), 5.35 (dd, $^3J_{H-H}$ = 4 Hz, $^3J_{H-H}$ = 12 Hz, 1H,

C-C(H₂)-C(H)-C(**H**)-C(H), 3.86 (s, 3H, OMe), 3.49 (s, 3H, OMe), 3.42 (dd, $^3J_{H-H}$ = 8 Hz, $^2J_{H-H}$ = 20 Hz, 1H, C-C(**H₂**)-C(H)-C(H)-C(H), 2.80 (d, $^3J_{H-H}$ = 12 Hz, 1H, C-C(H₂)-C(H)-C(H)-C(**H**), 2.69 (d, $^2J_{H-H}$ = 20 Hz, 1H, C-C(**H₂**)-C(H)-C(H)-C(H), -22.16 (s, 1H, hydride). EI/MS *m*/*z*. 1054.4. The isotope distribution is consistent with the presence of five ruthenium atoms.

Reaction of Ru₅(μ₅-C)(CO)₁₄(η²-O=CN(Me)₂CH=CH)(μ-H), 8.3, with DMA at 80 ˚C.

22.3 mg (0.022 mmol) of **8.3** was added to a 50 mL three-neck flask in 20 mL of degassed benzene with 200 μL of DMA. After heating for 11.5 h at 98 °C, the solvent was removed *in vacuo*, and the products were then isolated by TLC by using a hexane/methylene chloride mixture to provide in the order of elution: 3.2 mg (14% yield) of starting material **8.3**, 4.7 mg (22% yield) of **8.4**, 4.3 mg (18% yield) of $Ru_5(\mu_5\text{-}C)(CO)_{13}[\eta^3\text{-}syn,anti\text{-}Me_2NC{=}O\text{-}C_3H_3\text{-}\eta^1\text{-}O{=}CNMe_2CH_2](\mu\text{-}H)$, **8.11**, and 5.2 mg (22% yield) of $Ru_5(\mu_5\text{-}C)(CO)_{13}[\eta^3\text{-}anti,syn\text{-}Me_2NC{=}O\text{-}C_3H_3\text{-}CH_2\text{-}\eta^1\text{-}O{=}CNMe_2](\mu\text{-}H)$, **8.12**. Spectral data for **8.11**: IR νCO (cm^{-1} in dichloromethane) 2087(m), 2059(s), 2044(vs), 2032(sh), 2014(m), 1973(w). ^1H NMR (CD_2Cl_2, in ppm) δ = 5.48 (d, $^3J_{H-H}$ = 7 Hz, 1H, C-C(**H**)-C(H)-C(H)-C(H₂)), 4.96 (dd, $^3J_{H-H}$ = 7 Hz; $^3J_{H-H}$, = 11 Hz, 1H, C-C(H)-C(**H**)-C(H)-C(H₂), 4.04 (dd, $^3J_{H-H}$ = 4 Hz; $^2J_{H-H}$ = 16 Hz, 1H, C-C(H)-C(H)-C(H)-C(**H₂**), 3.31 (td, $^3J_{H-H}$ = 4 Hz; $^3J_{H-H}$ = 10 Hz, 1H, C-C(H)-C(H)-C(**H**)-C(H₂), 3.14 (s, 3H, N(ME)₂), 3.11 (s, 3H, N(ME)₂), 3.01 (dd, $^3J_{H-H}$ = 10 Hz; $^2J_{H-H}$ = 16 Hz, 1H, C-C(H)-C(H)-C(H)-C(**H₂**), 2.99 (s, 3H, N(Me₂), 2.44 (s, 3H, NMe₂), -22.43 (s, 1H, hydride). EI/MS *m*/*z*. 1082. The isotope distribution is consistent with the presence of five ruthenium atoms. Spectral data for **8.12**: IR νCO (cm^{-1} in dichloromethane) 2086(m), 2056(s), 2044(vs), 2032(sh), 2014(m), 1973(w). ^1H NMR (CD_2Cl_2, in ppm) δ = 5.54 (mm, 2H, C-C(H)-C(**H**)-C(**H**)-C(H₂)), 3.28 (dd, $^3J_{H-H}$ = 8 Hz, $^2J_{H-H}$ = 19 Hz, 1H, C-

C(H)-C(H)-C(H)-C(**H**$_2$)), 3.24 (s, 3H, NMe)$_2$), 3.17 (d, $^3J_{H-H}$ = 10 Hz, 1H, C-C(**H**)-C(H)-C(H)-C(H$_2$)), 3.05 (s, 3H, NMe$_2$), 2.80 (s, 3H, NMe$_2$), 2.71 (d, $^2J_{H-H}$ = 19 Hz, 1H, C-C(H)-C(H)-C(H)-C(**H**$_2$)), 2.57 (s, 3H, NMe$_2$), -22.23 (s, 1H, hydride). EI/MS *m*/*z*. 1081. The isotope distribution is consistent with the presence of five ruthenium atoms.

Reaction of Ru$_5$(μ$_5$-C)(CO)$_{14}$(η^2-O=CN(Me)$_2$CH=CH)(μ-H), 8.3, with Methyl Acrylate at 80 ˚C

20.4 mg (0.020 mmol) of **3** was added to a 50 mL three-neck flask in 25 mL of degassed benzene with 600 μL of methyl acrylate. After heating for 46 h at 80 °C, the solvent was removed *in vacuo*, and the products were then isolated by TLC by using a hexane/methylene chloride mixture to provide in the order of elution: 0.7 mg (3% yield) of **8.2**, 4.0 mg (20% yield) of starting material **8.3**, 0.4 mg (2% yield) of **8.4**, 0.7 mg (3% yield) of Ru$_5$(μ$_5$-C)(CO)$_{12}$[μ-η^3-O=C(NMe$_2$)]CH=CH][η^2-CH=CHCO$_2$Me](μ-H), **8.13**, and 6.5 mg (30% yield) of Ru$_5$(μ$_5$-C)(CO)$_{13}$[η^3-*anti*,*syn*-MeO$_2$CCH$_2$ C$_3$H$_3$-η^1-O=C(NMe$_2$)](μ-H), **8.14**. Spectral data for **8.13**: IR νCO (cm^{-1} in hexane) 2090(m), 2063(vs), 2046(s), 2028(m), 2024(sh), 2014(w). ^{1}H NMR (CD$_2$Cl$_2$, in ppm) δ = 11.14 (d, $^3J_{H-H}$ = 5 Hz, 1H, Ru-C(**H**)=C(H)-C), 4.61 (d, $^3J_{H-H}$ = 5 Hz, 1H, Ru-C(H)=C(**H**)-C), 4.01 (dd, $^3J_{H-H}$ = 8 Hz, $^3J_{H-H}$ = 11 Hz, 1H, C(H$_2$)-C(**H**)), 3.8 (s, 3H, O(Me)), 3.73 (d, $^3J_{H-H}$ = 11 Hz, 1H, C(**H**$_2$)-C(H)), 3.0 (s, 3H, NMe$_2$), 2.4 (s, 3H, NMe$_2$), 2.31 (d, $^3J_{H-H}$ = 8 Hz, 1H, C(**H**$_2$)-C(H)), -20.947 (s, 1H, hydride). EI/MS *m*/*z*. 1009. (M – 2CO) 953. Spectral data for **8.14**: IR νCO (cm^{-1} in hexane) 2089(w), 2061(s), 2048(vs), 2035(w), 2019(m), 2006(vw), 1990(vw), 1979(w), 1967(vw), 1948(vw). ^{1}H NMR (CD$_2$Cl$_2$, in ppm) δ = 5.49 (d, $^3J_{H-H}$ = 7 Hz, 1H, C-C(**H**)-C(H)-C(H)-C(H$_2$), 4.97 (dd, $^3J_{H-H}$ = 7 Hz, $^3J_{H-H}$ = 11 Hz, 1H, C-C(H)-C(**H**)-C(H)-C(H$_2$), 3.92 (dd, $^3J_{H-H}$ = 4 Hz, $^2J_{H-H}$ = 16 Hz, 1H, C-C(H)-C(H)-C(H)-C(**H**$_2$), -

22.23 (s, 1H, hydride). EI/MS *m*/*z*. 1066.7. The isotope distribution is consistent with the presence of five ruthenium atoms.

Reaction of $Ru_5(\mu_5\text{-}C)(CO)_{14}[\eta^2\text{-}O{=}C(Me)OC{=}CH_2](\mu\text{-}H)$, 8.5, with Vinyl Acetate and Trimethylamine N-oxide at Room Temperature.

23.0 mg (0.023 mmol) of **8.5** was added to a 50 mL three-neck flask in 25 mL of degassed hexane with 250 μL of vinyl acetate and 11 mg (0.15 mmol) of trimethylamine N-oxide. The synthesis for **8.5** was reported in Chapter 7 as compound **7.3**. After stirring at room temperature for 15.5 h, the solvent was removed *in vacuo*, and the products were then isolated by TLC by using a hexane/methylene chloride solvent mixture to provide in the order of elution: 0.6 mg (3% yield) of $Ru_5(\mu_5\text{-}C)(CO)_{12}[\mu\text{-}\eta^2\text{-}(MeO_2C)CH{=}CH](\eta^3\text{-}CH_2{=}CHOC(=O)Me)(\mu\text{-}H)$, **8.15**. Spectral data for **8.15**: IR νCO (cm^{-1} in hexane) 2088(w), 2063(s), 2045(vs), 2026(w), 2012(m), 2009(vw), 1992(vw), 1982(vw). ^1H NMR (CD_2Cl_2, in ppm) δ = 10.51 (d, ^3J = 9 Hz, 1H, O-C(H)=C(**H**)-Ru), 6.92 (dd, ^3J = 5 Hz, ^3J = 7 Hz, 1H, O-C(H)=C(**H₂**), 6.06 (d, ^3J = 9 Hz, 1H, O-C(**H**)=C(H)-Ru), 3.66 (t, ^3J = 5 Hz, 1H, O-C(H)=C(**H₂**), 3.34 (dd, ^3J = 5 Hz, ^3J = 7 Hz, 1H, O-C(H)=C(**H₂**), 2.13 (s, 3H, C=O(Me), 1.72 (s, 3H, C=O(Me), -21.40 (s, 1H, hydride). EI/MS *m*/*z*. 1025.3. The isotope distribution is consistent with the presence of five ruthenium atoms.

Isomerization of Compound 8.7 at 80 °C

4.7 mg (0.004 mmol) of **8.7** was added to a NMR tube in 1.5 mL of d_8-toluene. After heating for 34 h at 80 °C in a temperature-controlled silicone oil bath, the solution was allowed to cool and the solvent was removed by a fast stream of nitrogen, and the products

were then isolated by TLC with a hexane/methylene chloride mixture to provide 3.0 mg (64% yield) of **8.10**.

Isomerization of Compound 8.8 at 80 °C

3.6 mg (0.003 mmol) of **8.8** was added to a NMR tube in 1.5 mL of d_8-toluene. After heating for 25 h at 80 °C in a temperature-controlled silicone oil bath, the solution was allowed to cool and the solvent was removed by a fast stream of nitrogen, and the products were then isolated by TLC with a hexane/methylene chloride mixture to provide 2.6 mg (72% yield) of **8.10**.

Crystallographic Analyses

Single crystals of compounds **8.6-8.15** suitable for X-ray diffraction analyses were obtained by slow evaporation of solvent from solutions of the pure compounds. X-ray intensity data for compounds **8.10** and **8.12** was measured by using a Bruker SMART APEX CCD-based diffractometer by using Mo Kα radiation (λ = 0.71073 Å). The raw data frames were integrated with the SAINT+ program by using a narrow frame integration algorithm.[22] Correction for Lorentz and polarization effects were also applied with SAINT+. An empirical absorption correction based on the multiple measurements of equivalent reflections was applied by using the program SADABS were applied in each analysis.[24] X-ray intensity data for compounds **8.6-8.9**, **8.11** and **8.13-8.15** were measured by using a Bruker D8 QUEST diffractometer equipped with a PHOTON-100 CMOS area detector and an Incoatec microfocus source (Mo Kα radiation, λ = 0.71073 Å).[23] The data collection strategy for compound **8.11** consisted of four 180° ω-scans at different φ settings and one 360° φ-scan, with a scan width per image of 0.6°. The crystal-to-detector distance

was 5.0 cm and each image was measured for 2 s in shutterless mode. The average reflection redundancy was 10.3. The data collection strategy for compound **8.6** consisted of five 180° ω-scans at different φ settings and two 360° φ-scan, with a scan width per image of 0.5°. The crystal-to-detector distance was 5.0 cm and each image was measured for 5 s in shutterless mode. The average reflection redundancy was 11.0. for several crystals screened for compound **8.6**, all were found to be non-merohedral twins with two components. For a typical crystal, approximately 80-85% of reflections could be fit to one domain, with the remainder belonging to the minor domain. Upon solution and refinement, relatively high *R*-values ($R1 > 5.5\%$), large residual electron density peaks and a pattern of $F_{obs} >> F_{calc}$ for reflections with poorest agreement was observed following normal location and anisotropic refinement all non-hydrogen atoms These observations are consistent with twinning of the data crystal, suggested during crystal screening. The best twin refinement was achieved using an HKLF-5 format file constructed using the TwinRotMat function in PLATON.[25] The derived twin law is (0.375 0 0.625 / 0 -1 0 / 1.375 0 -0.375), corresponding to a two-fold rotation around the reciprocal [101] direction. The major twin domain volume fraction refined to 0.818(1). The data collection strategy for compound **8.7** consisted of four 180° ω-scans at different φ settings and two 360° φ-scan, with a scan width per image of 0.6°. The crystal-to-detector distance was 5.0 cm and each image was measured for 2 s in shutterless mode. The average reflection redundancy was 14.7. The data collection strategy for compound **8.8** consisted of three 180° ω-scans at different φ settings and two 360° φ-scan, with a scan width per image of 0.5°. The crystal-to-detector distance was 6.0 cm and each image was measured for 3 s in shutterless mode. The average reflection redundancy was 9.5. The data collection strategy for compound **8.9** consisted of four 180°

ω-scans at different φ settings and two 360° φ-scans at different ω angles, with a scan width per image of 0.5°. The crystal-to-detector distance was 5.0 cm and each image was measured for 40 s in shutterless mode. The average reflection redundancy was 19.2. The data collection strategy for compound **8.13** consisted of four 180° ω-scans at different φ settings and two 360° φ-scans at different ω angles, with a scan width per image of 0.5°. The crystal-to-detector distance was 5.0 cm and each image was measured for 20 s. The average reflection redundancy was 12.7. The data collection strategy for compound **8.14** consisted of four 180° ω-scans at different φ settings and two 360° φ-scans at different ω angles, with a scan width per image of 0.5°. The crystal-to-detector distance was 5.0 cm and each image was measured for 3 s in shutterless mode. The average reflection redundancy was 10.4. The data collection strategy for compound **8.15** consisted of seven 180° ω-scans at different φ settings and two 360° φ-scans at different ω angles, with a scan width per image of 0.5°. The crystal-to-detector distance was 5.0 cm and each image was measured for 1 s in shutterless mode. The average reflection redundancy was 8.3. The raw area detector data frames were reduced, scaled and corrected for absorption effects using the SAINT[22] and SADABS[24] programs All structures were solved by a combination of direct methods and difference Fourier syntheses, and refined by full-matrix least squares refinement on F^2 by using the SHELXTL software package.[25] All non-hydrogen atoms were refined with anisotropic thermal parameters. All hydrogen atoms were placed in geometrically idealized positions and were included as standard riding atoms during the final least-squares refinements with C-H distances fixed at 0.96 Å. The hydride ligands bonded to the metal atoms in compounds **8.6-8.15** were located and refined in each analysis. Compounds **8.11**, **8.6**, **8.7**, **8.8**, **8.10**, **8.13**, and **8.14** crystallized in the monoclinic

crystal system. The space group *P*2(1)/c was identified for compounds **8.11, 8.7, 8.10, 8.13**, and **8.14** on the basis of systematic absences observed in the intensity data. Compounds **8.11** and **8.10** contains two independent formula equivalents of the complex in the asymmetric crystal unit. Both independent molecules for compounds **8.11** and **8.10** have similar molecular structures. The space group *P* 2(1)/n was identified for compounds **8.6** and **8.8** on the basis of systematic absences observed in the intensity data. Compounds **8.12** and **8.9** crystallized in the orthorhombic crystal system. The space group *P*bcn was identified for compound **8.7** on the basis of systematic absences observed in the intensity data. The space group *P*bca was identified for compound **8.9** on the basis of systematic absences observed in the intensity data. Compound **8.15** crystallized in the triclinic crystal system. The space group *P*-1 was chosen for compound **8.15** and was confirmed by successful structure refinement. Compound **8.15** contains two independent formula equivalents of the complex in the asymmetric crystal unit. The two independent molecules found within the asymmetric unit are mirror images of each other. Crystal data, data collection parameters, and results for the analyses are listed in Tables 8.1, 8.2, 8.3 and 8.4.

8.3 Results and Discussion

The synthesis and characterizations of compounds **8.2** and **8.5** are discussed in Chapter 7. The reaction of **8.1** with N,N-dimethylacrylamide (DMA), CH_2=C(H)C(=O)NMe_2, in heptane solvent at reflux (98 °C) for 6.5 h yielded two products: $Ru_5(\mu_5\text{-}C)(CO)_{14}[\eta^2\text{-}O{=}CNMe_2CH{=}CH](\mu\text{-}H)$, **8.3** in 29% yield and $Ru_5(\mu_5\text{-}C)(CO)_{13}\{\mu\text{-}\eta^3\text{-}(O{=}CNMe_2)CHCH](\mu\text{-}H)$, **8.4** in 5% yield, eq. (6). Compound **8.4** was obtained previously from the reaction of the formamido complex $Ru_5(\mu_5\text{-}C)(CO)_{13}(\mu\text{-}\eta^2\text{-}O{=}CNMe_2)(HNMe_2)](\mu\text{-}H)$ with C_2H_2 and compound **8.3** can be obtained from the

addition of CO to **8.4** and compound **8.4** can be obtained by the decarbonylation of **8.3** by heating to 125° C.[19] Scheme 8.1 provides a review of the previously synthesized C-H activated substituted olefins by the Ru_5C cluster **8.1**.

Carbon-carbon coupling reactions of the activated olefins were studied on the Ru_5C cluster. The reaction of **8.2** with Me_3NO and an excess of methyl acrylate at room temperature for 20 h yielded five new Ru_5C complexes containing methyl acrylate: $Ru_5(\mu_5\text{-}C)(CO)_{13}[\mu\text{-}\eta^3\text{-}O{=}CO(Me)CHCH](\mu\text{-}H)$, **8.6** in 8% yield, $Ru_5(\mu_5\text{-}C)(CO)_{13}[\eta^3\text{-}anti,anti\text{-}(Me)OC{=}O\text{-}C_3H_3\text{-}\eta^1\text{-}O{=}CO(Me)CH_2](\mu\text{-}H)$, **8.7** in 8% yield, $Ru_5(\mu_5\text{-}C)(CO)_{13}[\eta^3\text{-}anti,syn\text{-}(MeO_2C)CH_2C_3H_3\text{-}CH_2\text{-}\eta^1\text{-}O{=}C(OMe)](\mu\text{-}H)$, **8.8** in 13% yield, $Ru_5(\mu_5\text{-}C)(CO)_{12}[\mu\text{-}\eta^3\text{-}O{=}C(OMe)CH{=}CH][\eta^2\text{-}CH{=}CHCO_2Me](\mu\text{-}H)$, **8.9** in 7% yield, and $Ru_5(\mu_5\text{-}C)(CO)_{13}[\eta^3\text{-}syn,anti\text{-}(MeO_2C)C_3H_3\text{-}\eta^1\text{-}O{=}C(OMe)CH_2](\mu\text{-}H)$, **8.10** in 9% yield, three of which show tail-to-tail coupling, **8.7**, **8.8**, and **8.10** of the methyl acrylate units.

Compounds **8.6-8.10** were characterized by a combination of IR, ^1H NMR, mass spectrometry and single-crystal X-ray diffraction analyses. An ORTEP diagram of the molecular structure for compound **8.6** is shown in Figure 8.1. Compound **8.6** is analogous to **8.4** that was formed from the reaction of $Ru_5(\mu_5\text{-}C)(CO)_{13}(HNMe_2)(\mu\text{-}\eta^2\text{-}O{=}CNMe_2)(\mu\text{-}H)$ and C_2H_2.

Compound **8.6** is open square pyramidal Ru_5C cluster that contains a CO_2Me substituted $\mu\text{-}\eta^2$-vinyl ligand that bridges the Ru3-Ru4 bond by the vinyl carbon atoms C2 and C3 which are π–bonded to Ru3 and σ-bonded to Ru4, Ru3-C2 = 2.287(4) Å, Ru3-C3 = 2.205(4) Å, Ru4-C3 = 2.022(4) Å. A hydrido ligand, δ = -22.02, bridges the 'hinge' metal atoms Ru1 and Ru2 of the Ru_4 butterfly cluster portion of the molecule, Ru1-H1 = 1.75(4) Å, Ru2-H1 = 1.76(5) Å. The ester group is coordinated to Ru4 by its carbonyl oxygen atom

O1, Ru4-O1 = 2.182(3) Å. With thirteen terminal carbonyl ligands, each acting as two-electron donors, the bridging methylacryloyl ligand as a five-electron donor, and the bridging hydride as a one-electron donor, the total valence cluster electron count for the metal atoms is 76 which is consistent with the observed structure an open square pyramidal cluster of five metal atoms.

Compounds **8.7**, **8.8**, and **8.10** are isomers formed by a tail-to-tail coupling of two methyl acrylate groups at the wingtip bridging Ru atom of the butterfly, Ru4. An ORTEP diagram of the molecular structure of **8.7** is shown in Figure 8.2. Compound **8.7** is an open square pyramidal cluster containing thirteen linear terminal carbonyl ligands and a bridging hydride, Ru1-H1 = 1.59(7) Å, Ru2-H1 = 1.72(7) Å, δ = -22.12. The most interesting portion of **8.7** is a η^3-allylic $(MeO_2C)CH_2C_3H_3$-CH_2-η^1-O=C(OMe) ligand. Atoms C2, C3, and C4 represent the coordinated allyl portion of this ligand which was formed by the tail-to-tail coupling of two methyl acrylate molecules at the carbon atoms C3 and C4, C3-C4 = 1.396(9) Å, C2-C3 = 1.419(9) Å, on the bridging metal atom Ru4, Ru4-C2 = 2.225(6) Å, Ru4-C3 = 2.175(6) Å, 2.258(6) Å. The two substituents are coupled in an *anti,anti* conformation where the three H atoms of the η^3-allyl are cis to each other, $^3J_{H\text{-}H}$ = 8 Hz.

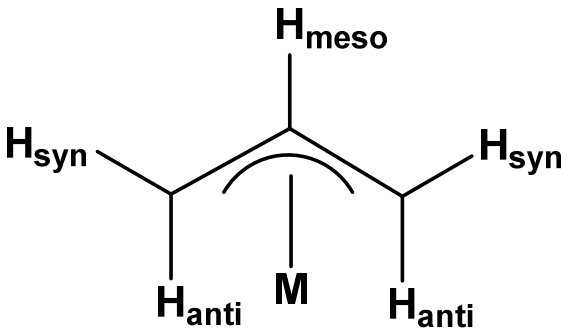

There is a five-membered ring composed of the atoms Ru4-O2-C6-C5-C4 that contains a methylene group at the C5 location, $^2J_{H\text{-}H}$ = 20 Hz, for the inequivalent H atoms

on it. This group was presumably formed by a metal mediated hydrogen shift from the β-carbon to the α-carbon of one of the methyl acrylate units, see below.

An ORTEP diagram of **8.8** is shown in Figure 8.3. Compound **8.8** is an isomer of **8.7** in which the two methyl acrylate units are coupled to form an η^3-*anti,syn*-$(MeO_2C)CH_2C_3H_3CH_2$-η^1-O=C(OMe) ligand, C3-C4 = 1.401(3) Å, C4-C5 = 1.418(3) Å, at the bridging Ru atom Ru4, Ru4-C3 = 2.228(2) Å, Ru4-C4 = 2.180(2), Å, Ru4-C5 = 2.192(2). The H atoms bonded to carbon atoms C3 and C4 are trans to one another, $^3J_{H-H}$ = 11 Hz, while the H atoms of C4 and C5 are cis oriented, $^3J_{H-H}$ = 7 Hz, in the η^3-allyl portion of the ligand. The methylene location in **8.8** is not contained in a ring as found in **8.7**.

An ORTEP diagram of **8.10** is shown in Figure 8.4. The two methyl acrylate units of **8.10** are coupled to form a substituted allyl group $(MeO_2C)C_3H_3$-η^1-O=C(OMe)CH_2 in an in an η^3-*syn,anti*-conformation, C2-C3 = 1.422(8) Å, C3-C4 = 1.393(7) Å, at the bridging Ru atom Ru4, Ru4-C2 = 2.235(5) Å, Ru4-C3 = 2.191(5) Å, 2.255(5) Å. The H atoms of C3 and C4 of **8.10** have a trans relationship, $^3J_{H-H}$ = 12 Hz, while the H atom of C2 is cis to the H atom of C3, $^3J_{H-H}$ = 8 Hz. The methylene group C5 is contained within five-membered ring of atoms Ru4-O2-C6-C5-C4 formed by coordination of the oxygen atom O2 to Ru4, Ru4-O2 = 2.197(3) Å.

An ORTEP diagram of the molecular structure of **8.9** is shown in Figure 8.5. Compound **8.9** contains an open Ru_5C cluster with two methyl acrylate ligands that that are not coupled to each other. One of the methyl acrylate fragments, C1-C2, is coordinated in a μ-η^2-bridging fashion to metal atoms Ru3 and Ru4, Ru3-C2 = 2.260(5) Å, Ru3-C1 = 2.149(5) Å, Ru4-C1 = 2.027(5) Å similar to that as found in compound **8.6**. Ru4 is also coordinated to the CO_2Me group by the oxygen atom O1, Ru4-O1 = 2.196(3) Å. The other

methyl acrylate ligand is a coordinated in an η^2-π-fashion by the olefinic carbon atoms C4 and C5 to the Ru atom, Ru4, Ru4-C4 = 2.173(5) Å, Ru4-C5 = 2.176(5) Å, of the open Ru_5C cluster. Compound **8.9** also contains a bridging hydrido ligand across the hinge metal atoms Ru1 and Ru2, Ru1-H10 = 1.72(6) Å, Ru2-H10 = 1.66(5) Å, δ = -20.92. With twelve terminal carbonyl ligands, a five-electron μ-η^3-acryloyl ligand, a π-bonded methyl acrylate ligand, and a bridging hydride ligand, the cluster contains a total valence electron count at the metal atoms of 76 electrons, as expected for an open square pyramidal cluster of five metal atoms.

The reaction of the activated olefin, N,N-dimethylacrylamide, with **8.3** was also investigated. The reaction of **8.3** with excess dimethylacrylamide at 98 °C for 11.5 h yielded two new tail-to-tail coupled dimethylacrylamide complexes: $Ru_5(\mu_5\text{-}C)(CO)_{13}[\eta^3$-*syn*,*anti*-$Me_2NC{=}O\text{-}C_3H_3\text{-}\eta^1\text{-}O{=}CNMe_2CH_2](\mu\text{-}H)$, **8.11** in 18% yield and $Ru_5(\mu_5\text{-}C)(CO)_{13}[\eta^3$-*anti*,*syn*-$Me_2NC{=}O\text{-}C_3H_3\text{-}CH_2\text{-}\eta^1\text{-}O{=}CNMe_2](\mu\text{-}H)$, **8.12** in 22% yield. An ORTEP diagram of the molecular structure of **8.11** is shown in Figure 8.6. The structure of **8.11** is analogous to that of the coupled methyl acrylate complex **8.10** except that **8.11** is formed from the coupling of two dimethylformamido-substituted vinyl ligands. Compound **8.11** contains a tail-to-tail coupled η^3-*syn*,*anti*-$(Me_2NC{=}O)C_3H_3(\eta^1\text{-}O{=}CNMe_2CH_2)$ allylic ligand, C2-C3 = 1.406(6) Å, C3-C4 = 1.399(6) Å, that is coordinated to the bridging metal atom Ru4, Ru4-C2 = 2.260(4) Å, Ru4-C3 = 2.177(4) Å, of the open Ru_5C cluster. A hydrido ligand spans the hinge metal atoms Ru1 and Ru2, Ru1-H1 = 1.77(4) Å, Ru2-H1 = Å, δ = -22.43.

An isomer of **8.11**, **8.12** was also isolated and fully characterized structurally. An ORTEP diagram of the molecular structure of **8.12** is shown in Figure 8.7. The molecular

structure of **8.12** is analogous to that of **8.8** except the allylic ligand in **8.12** is formed by the coupling of two dimethylacrylamide ligands through the carbon atoms C3 and C4, C3-C4 = 1.392(7) Å, C2-C3 = 1.418(7) Å. The allylic ligand is coordinated to Ru4, Ru4-C2 = 2.200(5) Å, Ru4-C3 = 2.186(5) Å, Ru4-C4 = 2.218(5) Å and has an η^3-*anti*,*syn*-$Me_2NC{=}O$-C_3H_3-CH_2-η^1-$O{=}CNMe_2$ conformation. One of the amido groups is coordinated to Ru4, Ru4-O1 = 2,215(3) Å.

The formation of hetero-substituted tail-to-tail olefin coupled products was obtained by the reaction of **8.3** with methyl acrylate. A benzene solution containing **8.3** and an excess of methyl acrylate was refluxed for 46 h at 80 °C to yield two new hetero-substituted olefin products: $Ru_5(\mu_5\text{-}C)(CO)_{12}[\mu\text{-}\eta^3\text{-}O{=}C(NMe_2)CH{=}CH][\eta^2\text{-}CH{=}CHCO_2Me](\mu\text{-}H)$, **8.13** in 3% yield, and $Ru_5(\mu_5\text{-}C)(CO)_{13}[\eta^3$-*anti*,*syn*-$MeO_2CCH_2C_3H_3$-$\eta^1$-$O{=}C(NMe_2)](\mu\text{-}H)$, **8.14** in 30% yield. Compounds **8.13** and **8.14** were both fully characterized by a combination of IR, ^{1}H NMR, mass spectrometry and single-crystal X-ray diffraction. An ORTEP diagram of the molecular structure of **8.13** is shown in Figure 8.8. Compound **8.13** is similar to **8.9** in that it contains two substituted olefins that are not coupled to each other. The dimethylacrylamide fragment is coordinated in a μ-η^2-bridging fashion across metal atoms Ru4 and Ru5, Ru4-C1 = 2.016(6) Å, Ru5-C1 = 2.169(6) Å, Ru5-C2 = 2.275(6) Å. Ru4 is also coordinated to the amido carbonyl oxygen atom O1, Ru4-O1 = 2.153(4) Å. The second olefinic ligand is a coordinated in the conventional η^2-π-olefinic manner, Ru4-C4 = 2.185(6) Å, Ru4-C5 = 2.190(6) Å, of the open Ru_5C cluster. Compound **8.13** also contains a bridging hydrido ligand across the hinge metal atoms Ru1 and Ru2 of the cluster, Ru1-H10 = 1.71(6) Å, Ru2-H10 = 1.79(6) Å, δ = -20.94. With twelve terminal carbonyl ligands, a five-electron μ-η^3-acrylamido ligand, a π-bonded

acrylate ligand, and a bridging hydride the total cluster valence electron count for **8.13** is 76 electrons.

An ORTEP diagram of the molecular structure of **8.14** is shown in Figure 8.9. Compound **8.14** is similar in structure compounds **8.8** and **8.12** that contains a η^3-*anti*,*syn*-$MeO_2CCH_2C_3H_3$-η^1-O=C(NMe_2)](μ-H) ligand, C2-C3 = 1.422(8) Å, C3-C4 = 1.393(7) Å, Ru4-C2 = 2.235(5) Å, Ru4-C3 = 2.191(5) Å, Ru4-C4 = 2.255(5) Å, formed by a tail-to-tail coupling of dimethylacrylamide and methyl acrylate in an open Ru_5C cluster. The dimethylamido carbonyl oxygen atom O1 is coordinated to Ru4, Ru4-O1 = 2.153(4) Å, while the MeO_2CCH_2 group on the η^3-allyl is not coordinated.

To further explore the nature of the effects of the substituents on olefinic C-H activation and functionalization, reactions of **8.1** with vinyl acetate were also investigated. At this time, no examples of coupling between the C-H activated olefin of vinyl acetate and another substituted olefin has been isolated. When compound **8.5** was treated with vinyl acetate at room temperature in the presence of Me_3NO as a activator, the new compound $Ru_5(\mu_5\text{-}C)(CO)_{12}[\mu\text{-}\eta^2\text{-}(MeO_2C)CH{=}CH][\eta^3\text{-}CH_2{=}CHOC(=O)Me](\mu\text{-}H)$, **8.15** was obtained in a very low yield, 3%. Compound **8.15** was fully characterized by a combination of IR, ^{1}H NMR, mass spectrometry and single-crystal X-ray diffraction. An ORTEP diagram of the molecular structure of **8.15** is shown in Figure 8.10. Compound **8.15** contains two uncoupled vinyl acetate ligands that are coordinated similarly to the olefins in compounds **8.9** and **8.13**. One of ligands is a β-CH activated μ-η^2-(MeO_2C)CH=CH bridging vinyl ligand coordinated in a σ-π-fashion to the metal atoms Ru3 and Ru4, Ru3-C3 = 2.1792(19) Å, Ru3-C4 = 2.2724(19) Å, Ru4-C3 = 2.0633(19) Å. The H atoms on C3 and C4 are trans-oriented to each other, $^3J_{H\text{-}H}$ = 9.0 Hz. Evidently, there

has been a shift has been a shift of one of the hydrogen atoms from the exo-CH_2 group in the parent **8.5** to the α-carbon C4. The mechanism for this rearrangement is not known at this time. The other vinyl acetate ligand exhibits the conventional π-olefin coordination to the ruthenium atom Ru4, Ru4-C1 = 2.176(2) Å, Ru4-C2 = 2.1208(19) Å, to metal atom Ru4. The π-vinyl acetate ligand is also coordinated by the acetate oxygen atom O1 to Ru4, Ru4-O1 = 2.1725(14). A similarly coordinated chelating vinyl acetate ligand has been reported for the complex $Os_3(CO)_{10}[CH_2{=}CH(O_2CMe)]$.[26] With twelve terminal carbonyl ligands, a five-electron μ-η^2-vinyl acetate ligand, a four-electron η^3-π-vinyl-acetate substituted ligand, and a bridging hydride the total valence electron count for **8.15** is 76 electrons.

The interconversions between the three η^3-coupled methyl acrylate complexes, **8.7**, **8.8**, and **8.10** has been investigated by ^{1}H NMR. Compound **8.7** was dissolved in d_8-toluene and added to an NMR tube which was placed in a temperature-controlled silicone oil bath at 80 °C for 25 h. At various random time intervals, a ^{1}H NMR was taken of the upfield metal-hydride region to measure the metal-hydride intensities of the three η^3-allyl isomers as the reaction progressed. A stacked-plot of the ^{1}H NMR taken throughout the experiment can be found in Figure 8.11. After 2 h at 80 °C, a H NMR spectra was taken that showed major product was **8.7**, δ = -22.38, a peak at δ = -22.08 for **8.10**, and a peak at δ = -22.04 for **8.8**. The peak heights for **8.8** and **8.10** after 2 h were close to the same intensity. At 7 h reaction time, the starting material peak intensity for **8.7** had significantly decreased. The peak height for **8.10** was now the highest while the peak height for **8.8** had grown some but not at the same rate as **8.10**. A final H NMR was taken after 25 h. The hydride resonance

for **8.10** (64% yield) was almost exclusively the only resonance left with only a very small amount of **8.8** remaining and none of the starting material, **8.9**, remained.

Realizing that compound **8.10** was the most thermodynamically favored product of three isomers, a similar experiment starting with compound **8.8** was investigated to see if similar results would be found. **8.8** was dissolved in d_8-toluene and loaded in an NMR tube which was placed in a temperature-controlled silicone oil bath at 80 °C for 34 h. A stacked-plot of the ^{1}H NMR taken throughout the experiment can be found in Figure 8.12.

A ^{1}H NMR was taken after 1 h. At δ = -22.04 the resonance for the starting material remained the major peak. A minor amount of **8.10** at δ = -22.08 was present and an even smaller amount of **8.7** was present. After 6 h reaction time the intensity of the peak height for **8.10** had increased significantly while minor changes were seen for the peak height of **8.9**. The peak height for the starting material **8.8** at 6 h had decreased by about 50% from its starting intensity. After 34 h reaction time at 80 °C, the only peak remaining with any significant intensity was for **8.10**, further emphasizing **8.10** as the most stable product thermodynamically.

The isomerization of η^3 allyl ligands is a well-known process where the *anti* and *syn* substituents are exchanged in an (η^3) σ-π allyl to an (η^1) σ-allyl group followed by rotation around the newly formed carbon-carbon single bond and reformation of the (η^3) σ-π allyl coordination mode. Utilizing this established mechanism, rearrangements for the interconversion between compounds **8.7**, **8.8** and **8.10** are proposed and shown in Scheme 8.2.

Two competing rearrangement mechanisms are proposed starting with the η^3-allyl-*anti,anti* coupled methyl acrylate complex **8.7**. Based on the location of the release of the π-interaction of the allyl and subsequent rotation about the σ-bond, the isomerization of **8.7** to **8.8** or **8.10** can be realized. The isomerization of **8.7** to **8.8** is proposed to proceed through the release of the π-interaction of the allylic carbons C2 and C1 to Ru4 to yield the (η^1) σ-allyl intermediate **1** (**I_1**)**.** Subsequent rotation about the single bond inverts the H atoms of C2 and C1 and brings their position from the back to the front while at the same time the carboxylate ester group inverts from the front to the back generating intermediate **2** (**I_2**). The final step in the isomerization from **8.7** to **8.8** involves multiple steps which include the release of the carbonyl oxygen atom of the carboxylate ester, restoration of the π bond between atoms C2 and C1 to Ru4, and coordination of inverted carboxylate ester carbonyl oxygen atom to Ru4 generating the η^3-*anti,syn* allyl group in **8.8.** Due to the presence of **8.7** in the isomerization of **8.8**, **8.8** is in equilibrium with **8.7**.

The mechanism for the interconversion of **8.7** to **8.10** involves first the release of the π bond of carbon atoms C3 and C2 of the (η^3) π-allyl on Ru4 to generate the (η^1) σ-allyl intermediate 3 (**I_3**). The transformation of **I_3** to intermediate 4 (**I_4**) involves a ring inversion at the carbon atoms C3 and C2 bringing the H atoms coordinated to C3 and C2 from the back to the front while the methylene group moves to the back. Restoration of the π bond between C3 and C2 to Ru4 completes the isomerization yielding the η^3-*syn,anti* allyl of **8.10**.

8.4 Conclusions

In this work it has been shown that two activated olefin ligands can be added to the pentaruthenium carbonyl complex **8.1**. In general, the ligands have been shown to undergo tail-to-tail C-C bond-forming coupling reactions that proceed to the formation of disubstituted η^3-allyl ligands that are coordinated to the bridging ruthenium atom of an open Ru_5 carbonyl cluster complex. These allyl ligands can isomerize via the conventional mechanisms to yield other stable isomers. Some diolefin compounds **8.9**, **8.13**, and **8.15** have been obtained where the olefins have not been coupled. While it might seem that these would be precursors to the complexes, we have not yet been able to induce C-C bond forming coupled products from them.

Table 8.1. Crystal data, data collection parameters for compounds **8.6** and **8.7**.

Compound	**8.6**	**8.7**
Empirical formula	$Ru_5O_{15}C_{18}H_6$	$Ru_5O_{17}C_{22}H_{12}$
Formula weight	967.58	1053.67
Crystal system	Monoclinic	Monoclinic
Lattice parameters		
a (Å)	10.2498(4)	13.6521(6)
b (Å)	15.3347(6)	10.1964(4)
c (Å)	15.6649(6)	20.9394(9)
α (deg)	90.00	90.00
β (deg)	94.312(2)	95.827(2)
γ (deg)	90.00	90.00
V (Å^3)	2455.20(17)	2899.8(2)
Space group	*P*2(1)/n	*P*2(1)/c
Z value	4	4
ρ_{calc} (g / cm^3)	2.618	2.414
μ (Mo Kα) (mm^{-1})	3.079	2.623
Temperature (K)	100(2)	100(2)
$2\Theta_{max}$ (°)	56.72	50.06
No. Obs. (I > 2σ(I))	6132	5126
No. Parameters	358	445
Goodness of fit (GOF)	1.035	1.073
Max. shift in cycle	0.005	0.000
Residuals*: R1; wR2	0.0320; 0.0511	0.0322; 0.0761
Absorption Correction, Max/min	Multi-scan 0.8867 / 0.5780	Multi-scan 0.378 / 0.313
Largest peak in Final Diff. Map (e$^-$ / Å^3)	1.023	3.925

$R1=\Sigma_{hkl}(\,|\,|F_{obs}|-|F_{calc}|\,|)/\Sigma_{hkl}|F_{obs}|$; $wR2 = [\Sigma_{hkl}w(|F_{obs}|-|F_{calc}|)^2/\Sigma_{hkl}wF^2_{obs}]^{1/2}$; $w=1/\sigma^2(F_{obs})$; $GOF = [\Sigma_{hkl}w(|F_{obs}|-|F_{calc}|)^2/(n_{data}-n_{vari})]^{1/2}$.

Table 8.2. Crystal data, data collection parameters for compounds **8.8**, **8.9** and **8.10**.

Compound	**8.8**	**8.9**	**8.10**
Empirical formula	$Ru_5O_{17}C_{22}H_{12}$	$Ru_5O_{16}C_{21}H_{12}$	$Ru_5O_{17}N_1C_{22}H_{12}$
Formula weight	1053.67	1025.66	1053.67
Crystal system	Monoclinic	Orthorhombic	Monoclinic
Lattice parameters			
a (Å)	9.8554(3)	15.3627(6)	15.4300(8)
b (Å)	16.1343(5)	19.1155(7)	25.3055(14)
c (Å)	38.0020(12)	19.5492(8)	15.7011(9)
α (deg)	90.00	90.00	90.00
β (deg)	90.0930(10)	90.00	98.6480(10)
γ (deg)	90.00	90.00	90.00
V ($Å^3$)	6042.7(3)	5740.9(4)	6061.0(6)
Space group	*P*2(1)/n	*P*bca	*P*2(1)/c
Z value	8	8	8
ρ_{calc} (g / cm^3)	2.316	2.373	2.309
μ (Mo Kα) (mm^{-1})	2.517	2.643	2.510
Temperature (K)	100(2)	100(2)	294(2)
$2\Theta_{max}$ (°)	61.20	52.82	50.06
No. Obs. ($I > 2\sigma(I)$)	18505	5899	10717
No. Parameters	846	405	833
Goodness of fit (GOF)	1.047	1.032	1.071
Max. shift in cycle	0.002	0.005	0.005
Residuals*: R1; wR2	0.0258; 0.0413	0.0320; 0.0562	0.0294; 0.0750
Absorption Correction, Max/min	Multi-scan 0.5644/0.4980	Multi-scan 0.7454/0.6395	Multi-scan 1.000 / 0.737
Largest peak in Final Diff. Map (e^- / $Å^3$)	1.226	1.329	0.972

*$R1 = \Sigma_{hkl}(||F_{obs}| - |F_{calc}||)/\Sigma_{hkl}|F_{obs}|$; $wR2 = [\Sigma_{hkl}w(|F_{obs}| - |F_{calc}|)^2/\Sigma_{hkl}wF^2_{obs}]^{1/2}$; $w = 1/\sigma^2(F_{obs})$; $GOF = [\Sigma_{hkl}w(|F_{obs}| - |F_{calc}|)^2/(n_{data} - n_{vari})]^{1/2}$.

Table 8.3. Crystallographic data for compounds **8.11** and **8.12**.

Compound	**8.11**	**8.12**
Empirical formula	$Ru_5N_2O_{15}C_{24}H_{18}$	$Ru_5N_2O_{15}C_{24}H_{18}$
Formula weight	1079.75	1079.75
Crystal system	Monoclinic	Orthorhombic
Lattice parameters		
a (Å)	15.7433(8)	17.6790(6)
b (Å)	26.5461(13)	10.2451(4)
c (Å)	15.1298(7)	36.1146(13)
α (deg)	90.00	90.00
β (deg)	95.960(2)	90.00
γ (deg)	90.00	90.00
V (Å^3)	6288.9(5)	6541.2(4)
Space group	*P*2(1)/c	*P*bcn
Z value	8	8
ρ_{calc} (g / cm^3)	2.281	2.193
μ (Mo Kα) (mm^{-1})	2.419	2.325
Temperature (K)	100(2)	294(2)
$2\Theta_{max}$ (°)	50.06	50.06
No. Obs. (I > 2σ(I))	11089	5787
No. Parameters	886	443
Goodness of fit (GOF)	1.072	1.138
Max. shift in cycle	0.168	0.001
Residuals*: R1; wR2	0.0282; 0.0485	0.0286; 0.0651
Absorption Correction, Max/min	Multi-scan 0.6942 / 0.5392	Multi-scan 1.000 / 0.813
Largest peak in Final Diff. Map (e$^-$ / Å^3)	0.625	0.434

*$R1=\Sigma_{hkl}(\,|\,|F_{obs}|-|F_{calc}|\,|)/\Sigma_{hkl}|F_{obs}|$; $wR2 = [\Sigma_{hkl}w(|F_{obs}|-|F_{calc}|)^2/\Sigma_{hkl}wF^2_{obs}]^{1/2}$; $w = 1/\sigma^2(F_{obs})$; $GOF = [\Sigma_{hkl}w(|F_{obs}|-|F_{calc}|)^2/(n_{data} - n_{vari})]^{1/2}$.

Table 8.4. Crystallographic data for compounds **8.13**, **8.14**, and **8.15**.

Compound	**8.13**	**8.14**	**8.15**
Empirical formula	$Ru_5N_1O_{16}C_{23}H_{15}$	$Ru_5N_1O_{16}C_{23}H_{15}$	$Ru_5O_{16}C_{21}H_{12}$
Formula weight	1038.70	1066.71	1025.66
Crystal system	Monoclinic	Monoclinic	Triclinic
Lattice parameters			
a (Å)	15.6841(5)	11.1773(3)	9.5428(3)
b (Å)	10.0190(3)	15.4584(5)	17.1502(6)
c (Å)	18.6463(6)	18.1267(5)	17.6020(6)
α (deg)	90.00	90.00	86.670(2)
β (deg)	93.541(2)	93.5940(10)	82.064(2)
γ (deg)	90.00	90.00	79.765(2)
V ($Å^3$)	2916.37(16)	3125.83(16)	2806.10(16)
Space group	*P* 2(1)/c	*P* 2(1)/c	*P* -1
Z value	4	4	4
ρ_{calc} (g / cm^3)	2.366	2.267	2.428
μ (Mo Kα) (mm^{-1})	2.602	2.433	2.704
Temperature (K)	100(2)	100(2)	100(2)
$2\Theta_{max}$ (°)	50.04	50.06	66.46
No. Obs. ($I > 2\sigma(I)$)	5146	5521	21531
No. Parameters	413	432	810
Goodness of fit (GOF)	1.030	1.079	1.031
Max. shift in cycle	0.000	0.000	0.002
Residuals*: R1; wR2	0.0319; 0.0729	0.0244; 0.0514	0.0265; 0.0384
Absorption Correction, Max/min	Multi-scan 0.745 / 0.703	Multi-scan 0.621 / 0.569	Multi-scan 0.4954/0.3881
Largest peak in Final Diff. Map (e^- / $Å^3$)	3.272	1.658	0.738

$R1=\Sigma_{hkl}(\,|\,|F_{obs}|-|F_{calc}|\,|)/\Sigma_{hkl}|F_{obs}|$; $wR2 = [\Sigma_{hkl}w(|F_{obs}|-|F_{calc}|)^2/\Sigma_{hkl}wF^2_{obs}]^{1/2}$; $w = 1/\sigma^2(F_{obs})$; $GOF = [\Sigma_{hkl}w(|F_{obs}|-|F_{calc}|)^2/(n_{data} - n_{vari})]^{1/2}$.

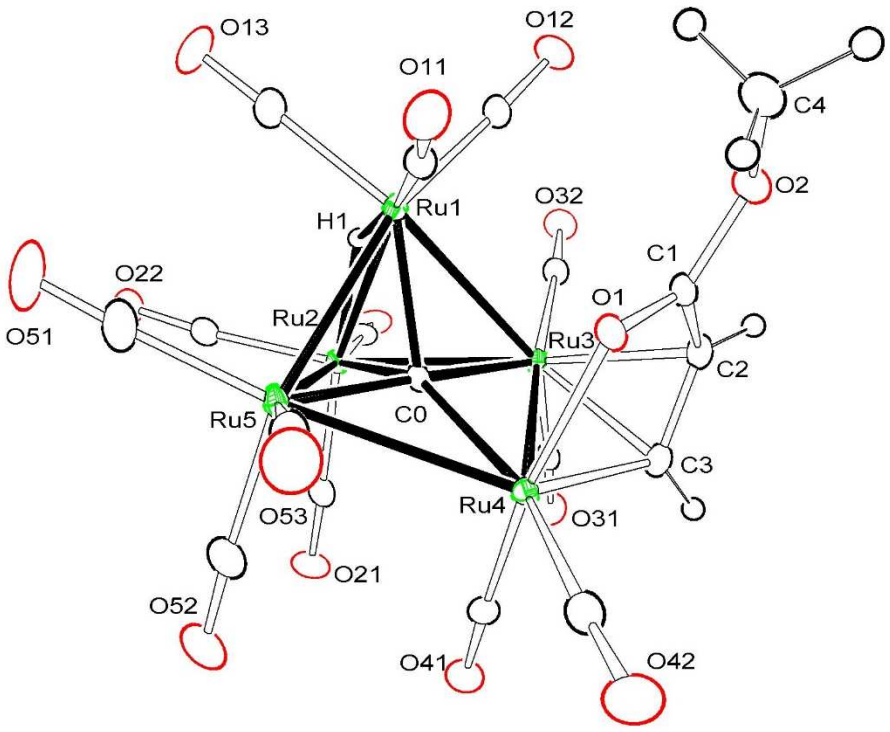

Figure 8.1. ORTEP diagram of the molecular structure of $Ru_5(\mu_5\text{-}C)(CO)_{13}[\mu\text{-}\eta^3\text{-}O{=}CO(Me)CHCH](\mu\text{-}H)$, **8.6**, showing 30% thermal ellipsoid probability. Selected interatomic bond distances (Å) are as follows: Ru1-Ru3 = 2.9515(5), Ru1-Ru5 = 2.8441(5), Ru1-Ru2 = 2.8207(5), Ru2-Ru5 = 2.8836(5) Ru2-Ru3 = 2.8265(5), Ru3-Ru4 = 2.7158(5), Ru4-Ru5 = 3.0003(5), Ru1-H1 = 1.75(4), Ru2-H1 = 1.76(5), Ru4-O1 = 2.182(3), Ru4-C3 = 2.022(4), Ru3-C2 = 2.287(4), Ru3-C3 = 2.205(4), C1-C2 = 1.448(6), C2-C3 = 1.419(6), C1-O1 = 1.255(5), Ru1-C0 = 2.114(4), Ru2-C0 = 2.104(4), Ru3-C0 = 1.959(4), Ru4-C0 = 2.086(4), Ru5-C0 = 1.950(4).

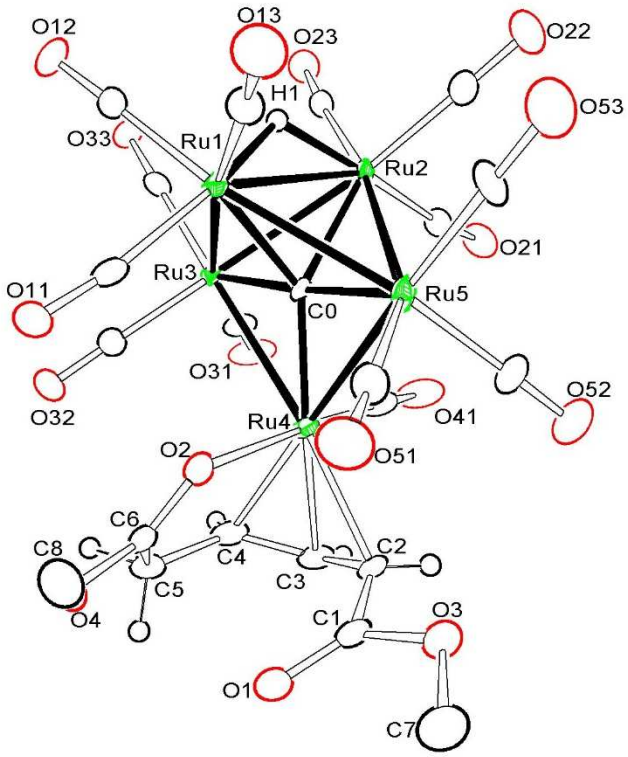

Figure 8.2. ORTEP diagram of the molecular structure of $Ru_5(\mu_5\text{-}C)(CO)_{13}[\eta^3\text{-}anti,anti\text{-}(Me)OC{=}O\text{-}C_3H_3\text{-}\eta^1\text{-}O{=}CO(Me)CH_2](\mu\text{-}H)$, **8.7**, showing 40% thermal ellipsoid probability. Selected interatomic bond distances (Å) are as follows: Ru1-Ru3 = 2.8233(6), Ru1-Ru5 = 2.8483(6), Ru1-Ru2 = 2.8498(6), Ru2-Ru5 = 2.8626(6) Ru2-Ru3 = 2.8793(6), Ru3-Ru4 = 2.9183(6), Ru4-Ru5 = 2.9005(7), Ru1-H1 = 1.59(7), Ru2-H1 = 1.72(7), Ru4-O2 = 2.170(4), Ru4-C2 = 2.225(6), Ru4-C3 = 2.175(6), Ru4-C4 = 2.258(6), C1-C2 = 1.484(9), C2-C3 = 1.419(9), C3-C4 = 1.396(9), C4-C5 = 1.501(9), C6-O2 = 1.247(7), Ru1-C0 = 2.131(5), Ru2-C0 = 2.131(5), Ru3-C0 = 1.971(5), Ru4-C0 = 2.058(5), Ru5-C0 = 1.967(5).

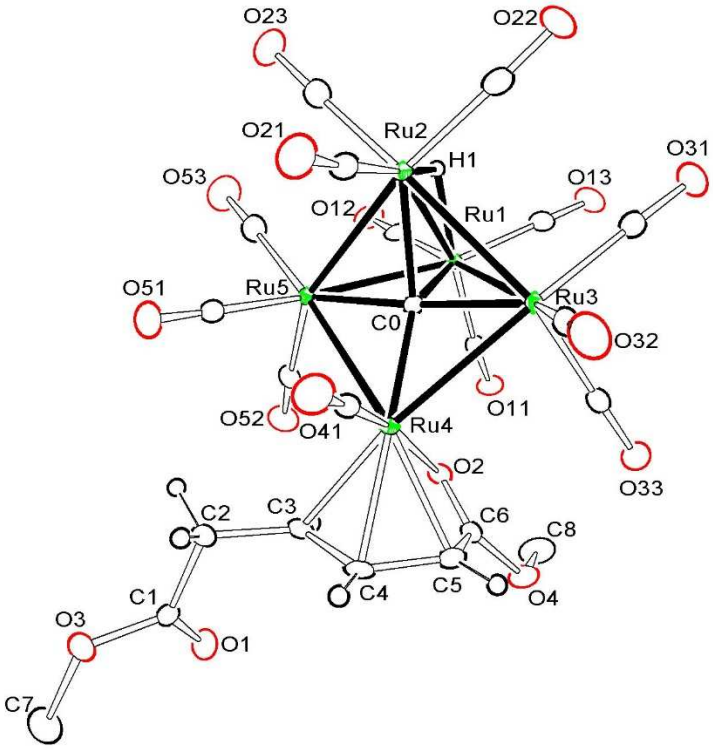

Figure 8.3. ORTEP diagram of the molecular structure of $Ru_5(\mu_5\text{-}C)(CO)_{13}[\eta^3\text{-}anti,syn\text{-}(MeO_2C)CH_2C_3H_3\text{-}CH_2\text{-}\eta^1\text{-}O{=}C(OMe)](\mu\text{-}H)$, **8.8**, showing 45% thermal ellipsoid probability. Selected interatomic bond distances (Å) are as follows: Ru1-Ru3 = 2.8612(3), Ru1-Ru5 = 2.8553(3), Ru1-Ru2 = 2.8391(3), Ru2-Ru5 = 2.8328(3) Ru2-Ru3 = 2.8590(3), Ru3-Ru4 = 2.9222(2), Ru4-Ru5 = 2.8698(3), Ru1-H1 = 1.76(3), Ru2-H1 = 1.72(3), Ru4-O2 = 2.2904(15), Ru4-C3 = 2.228(2), Ru4-C4 = 2.180(2), Ru4-C5 = 2.192(2), C1-C2 = 1.516(3), C2-C3 = 1.503(3), C3-C4 = 1.401(3), C4-C5 = 1.418(3), C5-C6 = 1.464(3), C6-O2 = 1.231(3), Ru1-C0 = 2.116(2), Ru2-C0 = 2.122(2), Ru3-C0 = 1.974(2), Ru4-C0 = 2.037(2), Ru5-C0 = 1.976(2).

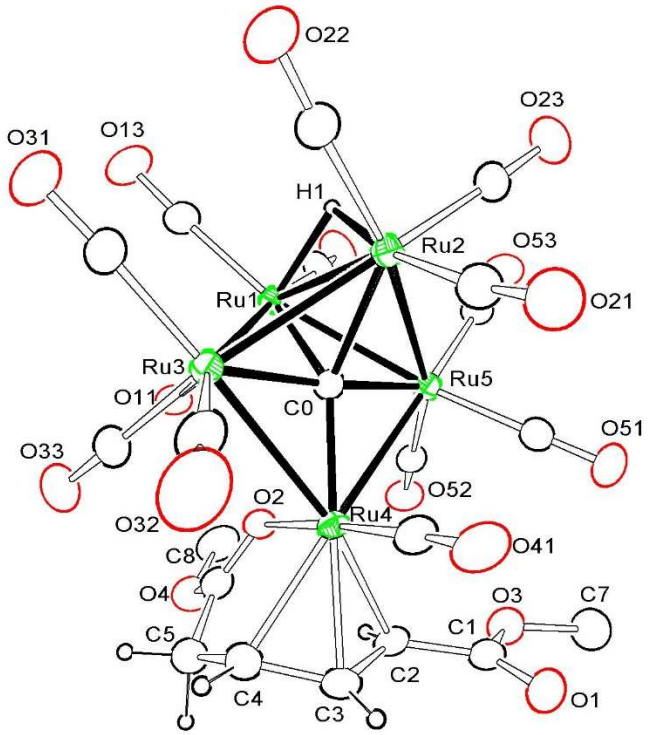

Figure 8.4. ORTEP diagram of the molecular structure of $Ru_5(\mu_5\text{-}C)(CO)_{13}[\eta^3\text{-}syn,anti\text{-}(MeO_2C)C_3H_3\text{-}\eta^1\text{-}O{=}C(OMe)CH_2](\mu\text{-}H)$, **8.10**, showing 20% thermal ellipsoid probability. The methyl hydrogens have been removed for clarity. Selected interatomic bond distances (Å) are as follows: Ru1-Ru3 = 2.8401(5), Ru1-Ru5 = 2.8738(5), Ru1-Ru2 = 2.8322(5), Ru2-Ru5 = 2.8546(5) Ru2-Ru3 = 2.8691(5), Ru3-Ru4 = 2.9239(5), Ru4-Ru5 = 2.8950(6), Ru1-H1 = 1.84(5), Ru2-H1 = 1.76(4), Ru4-O2 = 2.197(3), Ru4-C2 = 2.235(5), Ru4-C3 = 2.191(5), Ru4-C4 = 2.255(5), C1-O1 = 1.203(6), C1-O3 = 1.348(7), C1-C2 = 1.463(7), C2-C3 = 1.422(8), C3-C4 = 1.393(7), C4-C5 = 1.521(9), C5-C6 = 1.481(9), C6-O2 = 1.233(6), Ru1-C0 = 2.121(4), Ru2-C0 = 2.128(4), Ru3-C0 = 1.974(4), Ru4-C0 = 2.033(4), Ru5-C0 = 1.993(4).

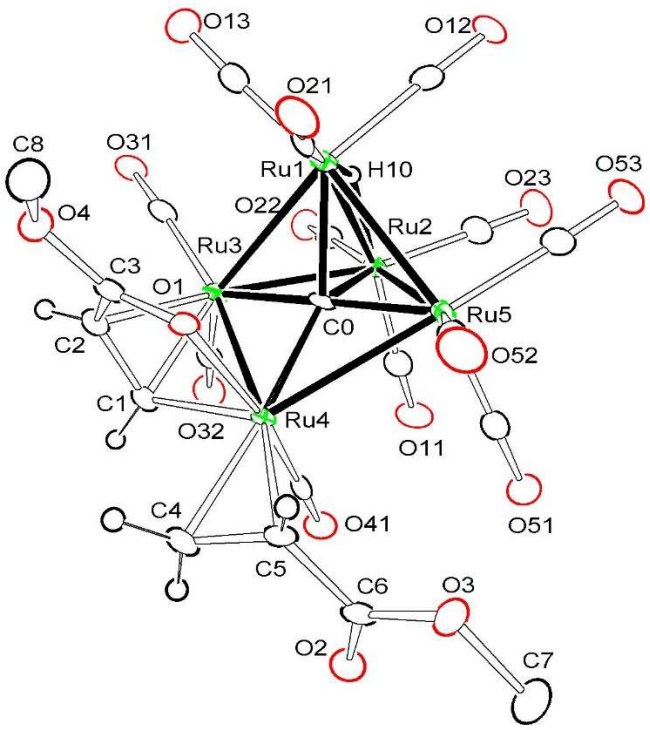

Figure 8.5. ORTEP diagram of the molecular structure of $Ru_5(\mu_5\text{-}C)(CO)_{12}[\mu\text{-}\eta^3\text{-}O{=}C(OMe)CH{=}CH][\eta^2\text{-}CH{=}CHCO_2Me](\mu\text{-}H)$, **8.9**, showing 35% thermal ellipsoid probability. The methyl hydrogens have been removed for clarity. Selected interatomic bond distances (Å) are as follows: Ru1-Ru3 = 2.9441(6), Ru1-Ru5 = 2.8369(6), Ru1-Ru2 = 2.8200(6), Ru2-Ru5 = 2.8884(6) Ru2-Ru3 = 2.8263(6), Ru3-Ru4 = 2.7341(6), Ru4-Ru5 = 3.0065(6), Ru1-H10 = 1.72(6), Ru2-H10 = 1.66(5), Ru4-O1 = 2.196(3), Ru4-C1 = 2.027(5), Ru4-C4 = 2.173(5), Ru4-C5 = 2.176(5), Ru3-C1 = 2.149(5), Ru3-C2 = 2.260(5), C1-C2 = 1.410(7), C2-C3 = 1.451(7), C3-O1 = 1.247(6), C4-C5 = 1.405(7), C5-C6 = 1.485(7), C6-O2 = 1.199(6), C6-O3 = 1.342(6), Ru1-C0 = 2.110(5), Ru2-C0 = 2.111(5), Ru3-C0 = 1.962(45), Ru4-C0 = 2.101(5), Ru5-C0 = 1.947(5).

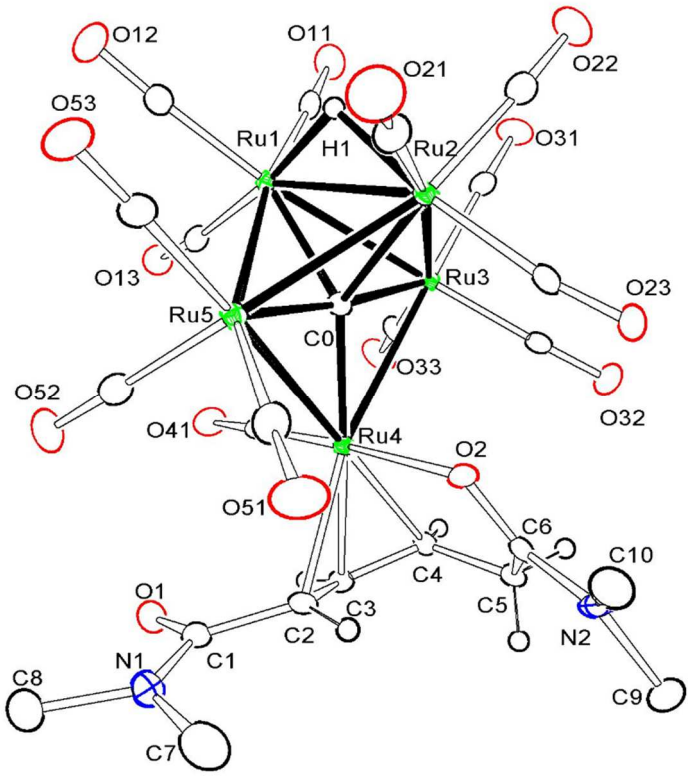

Figure 8.6. ORTEP diagram of the molecular structure of $Ru_5(\mu_5\text{-}C)(CO)_{13}[\eta^3\text{-}syn,anti\text{-}Me_2NC{=}O\text{-}C_3H_3\text{-}\eta^1\text{-}O{=}CNMe_2CH_2](\mu\text{-}H)$, **8.11**, showing 35% thermal ellipsoid probability. The methyl hydrogens have been removed for clarity. Selected interatomic bond distances (Å) are as follows: Ru1-Ru3 = 2.8623(5), Ru1-Ru5 = 2.8540(5), Ru1-Ru2 = 2.8450(5), Ru2-Ru5 = 2.8534(5) Ru2-Ru3 = 2.8258(5), Ru3-Ru4 = 2.9339(5), Ru4-Ru5 = 2.9082(5), Ru1-H1 = 1.77(4), Ru2-H1 = 1.77(4), Ru4-O2 = 2.138(3), Ru4-C2 = 2.260(4), Ru4-C3 = 2.177(4), Ru4-C4 = 2.222(4), C1-C2 = 1.486(6) C2-C3 = 1.406(6), C3-C4 = 1.399(6), C4-C5 = 1.513(6), C5-C6 = 1.502(6), C6-N2 = 1.263(5), Ru1-C0 = 2.128(4), Ru2-C0 = 2.141(4), Ru3-C0 = 1.983(4), Ru4-C0 = 2.036(4), Ru5-C0 = 1.980(4).

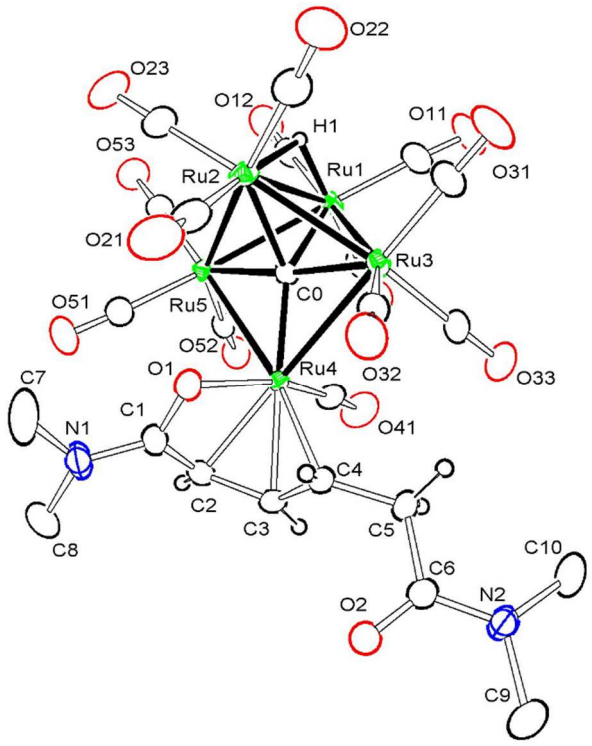

Figure 8.7. ORTEP diagram of the molecular structure of $Ru_5(\mu_5\text{-}C)(CO)_{13}[\eta^3\text{-}anti,syn\text{-}Me_2NC{=}O\text{-}C_3H_3\text{-}CH_2\text{-}\eta^1\text{-}O{=}CNMe_2](\mu\text{-}H)$, **8.12**, showing 20% thermal ellipsoid probability. The methyl hydrogens have been removed for clarity. Selected interatomic bond distances (Å) are as follows: Ru1-Ru3 = 2.8623(5), Ru1-Ru5 = 2.8224(5), Ru1-Ru2 = 2.8407(6), Ru2-Ru5 = 2.8599(5) Ru2-Ru3 = 2.8250(6), Ru3-Ru4 = 2.8912(5), Ru4-Ru5 = 2.9525(5), Ru1-H1 = 1.62(5), Ru2-H1 = 1.83(5), Ru4-O1 = 2.215(3), Ru4-C2 = 2.200(5), Ru4-C3 = 2.186(5), Ru4-C4 = 2.218(5), C1-O1 = 1.272(6), C1-C2 = 1.461(8), C2-C3 = 1.418(7), C3-C4 = 1.392(7), C4-C5 = 1.496(6), C5-C6 = 1.520(7), Ru1-C0 = 2.121(4), Ru2-C0 = 2.128(4), Ru3-C0 = 1.974(4), Ru4-C0 = 2.033(4), Ru5-C0 = 1.993(4).

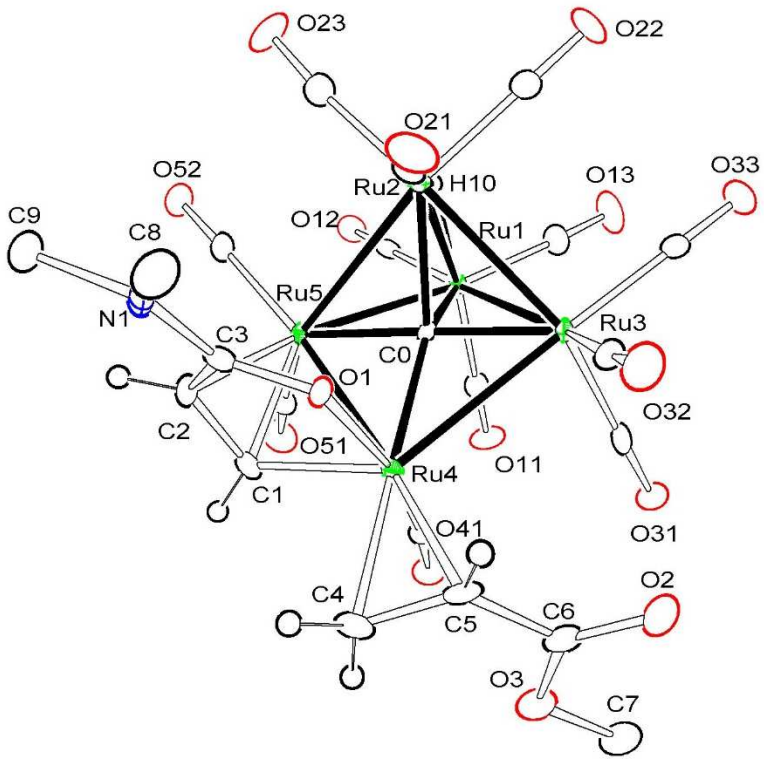

Figure 8.8. ORTEP diagram of the molecular structure of $Ru_5(\mu_5\text{-}C)(CO)_{12}[\mu\text{-}\eta^3\text{-}O{=}C(NMe_2)]CH{=}CH][\eta^2\text{-}CH{=}CHCO_2Me](\mu\text{-}H)$, **8.13**, showing 35% thermal ellipsoid probability. Selected interatomic bond distances (Å) are as follows: Ru1-Ru3 = 2.8643(6), Ru1-Ru5 = 2.8317(6), Ru1-Ru2 = 2.8151(6), Ru2-Ru5 = 2.9536(6) Ru2-Ru3 = 2.8287(6), Ru3-Ru4 = 3.0149(6), Ru4-Ru5 = 2.7359(6), Ru1-H10 = 1.71(6), Ru2-H10 = 1.79(6), Ru4-O1 = 2.153(4), Ru4-C1 = 2.016(6), Ru4-C4 = 2.185(6), Ru4-C5 = 2.190(6), Ru5-C1 = 2.169(6), Ru5-C2 = 2.275(6), C1-C2 = 1.415(9) C2-C3 = 1.467(8), C3-O1 = 1.278(7), C4-C5 = 1.389(9), C5-C6 = 1.482(9), C6-O2 = 1.210(8), C6-O3 = 1.339(7), Ru1-C0 = 2.116(5), Ru2-C0 = 2.096(5), Ru3-C0 = 1.942(5), Ru4-C0 = 2.107(5), Ru5-C0 = 1.968(5).

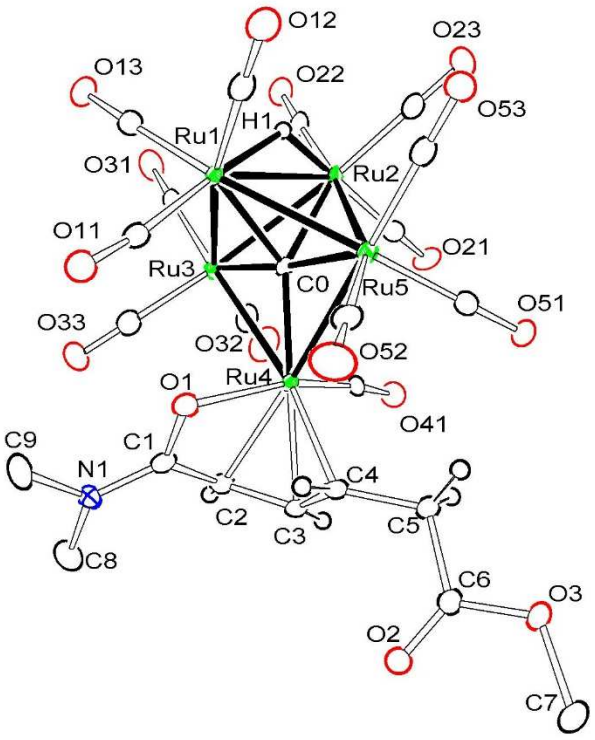

Figure 8.9. ORTEP diagram of the molecular structure of $Ru_5(\mu_5\text{-}C)(CO)_{13}[\eta^3\text{-}anti,syn\text{-}MeO_2CCH_2\ C_3H_3\text{-}\eta^1\text{-}O{=}C(NMe_2)](\mu\text{-}H)$, **8.14**, showing 20% thermal ellipsoid probability. Selected interatomic bond distances (Å) are as follows: Ru1-Ru3 = 2.8401(5), Ru1-Ru5 = 2.8738(5), Ru1-Ru2 = 2.8322(5), Ru2-Ru5 = 2.8546(5) Ru2-Ru3 = 2.8691(5), Ru3-Ru4 = 2.9239(5), Ru4-Ru5 = 2.8950(6), Ru1-H1 = 1.84(4), Ru2-H1 = 1.76(4), Ru4-O2 = 2.197(3), Ru4-C2 = 2.235(5), Ru4-C3 = 2.191(5), Ru4-C4 = 2.255(5), C1-C2 = 1.463(7), C2-C3 = 1.422(8), C3-C4 = 1.393(7), C4-C5 = 1.521(9), C5-C6 = 1.481(9), C6-O2 = 1.233(6), Ru1-C0 = 2.139(4), Ru2-C0 = 2.138(4), Ru3-C0 = 1.980(4), Ru4-C0 = 2.043(4), Ru5-C0 = 1.973(4).

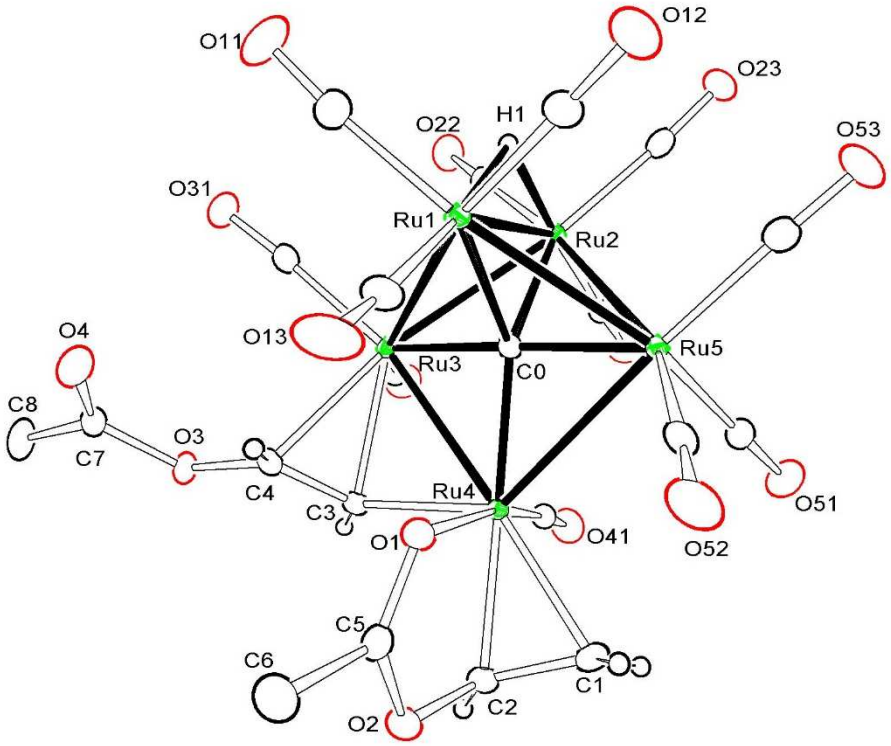

Figure 8.10. ORTEP diagram of the molecular structure of $Ru_5(\mu_5\text{-}C)(CO)_{12}[\mu\text{-}\eta^2\text{-}(MeO_2C)CH{=}CH](\eta^3\text{-}CH_2{=}CHOC(=O)Me)(\mu\text{-}H)$, **8.15**, showing 50% thermal ellipsoid probability. Selected interatomic bond distances (Å) are as follows: Ru1-Ru3 = 2.9414(2), Ru1-Ru5 = 2.8577(2), Ru1-Ru2 = 2.8433(2), Ru2-Ru5 = 2.8524(2) Ru2-Ru3 = 2.8576(2), Ru3-Ru4 = 2.7674(2), Ru4-Ru5 = 2.9575(2), Ru1-H1 = 1.82(2), Ru2-H1 = 1.74(2), Ru4-O1 = 2.1725(14), Ru4-C1 = 2.176(2), Ru4-C2 = 2.1208(19), Ru4-C3 = 2.0633(19), Ru3-C3 = 2.1792(19), Ru3-C4 = 2.2724(19), C1-C2 = 1.394(3), C3-C4 = 1.391(3), Ru1-C0 = 2.0824(19), Ru2-C0 = 2.1113(19), Ru3-C0 = 1.9536(19), Ru4-C0 = 2.1159(18), Ru5-C0 = 1.9512(19).

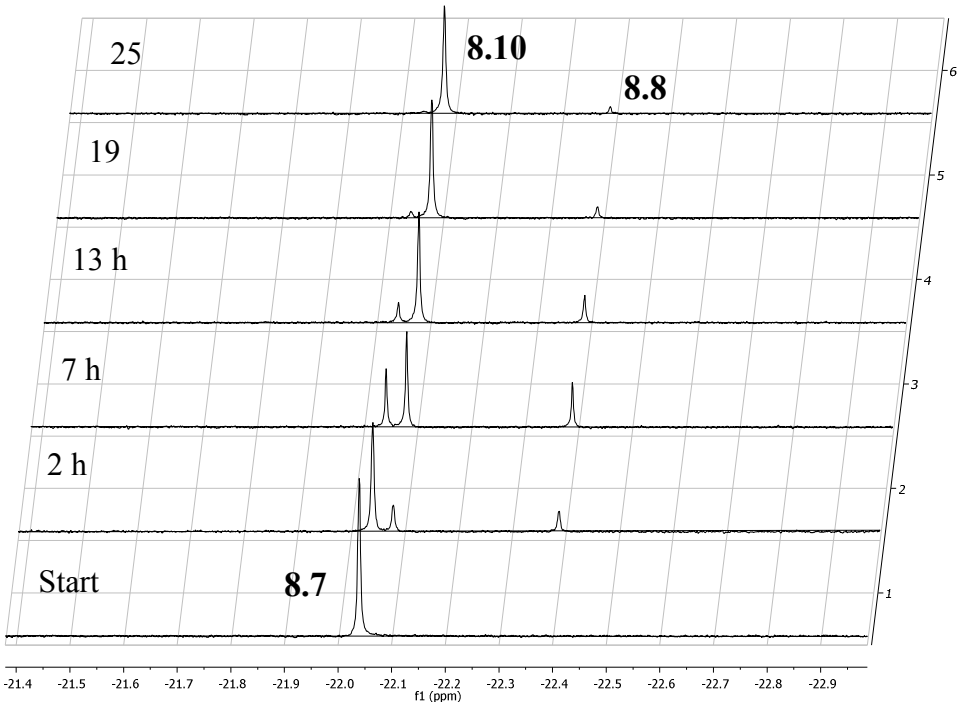

Figure 8.11. Stacked plot for the allyl isomerization of compound **8.7** at 80 °C in d_8-toluene followed by ^{1}H NMR.

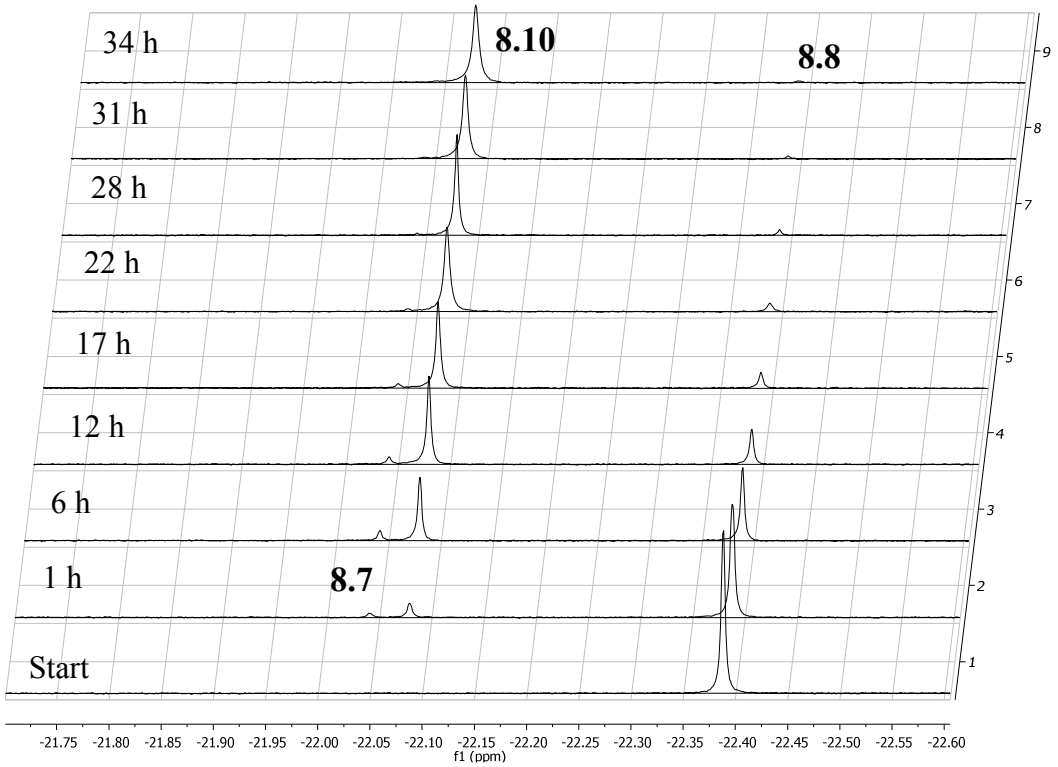

Figure 8.12. Stacked plot for the allyl isomerization of compound **8.8** at 80 °C in d_8-toluene followed by ^{1}H NMR.

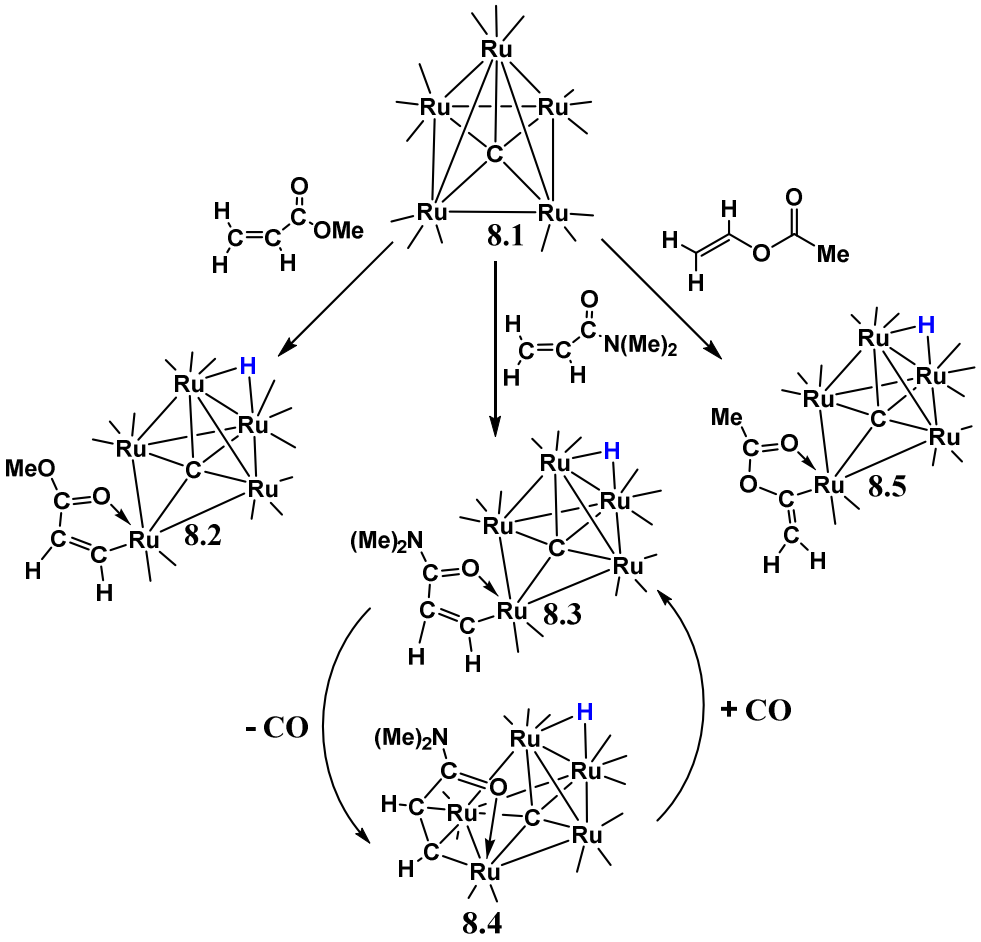

Scheme 8.1. Summary of the C-H activation reactions of **8.1** with substituted olefins.

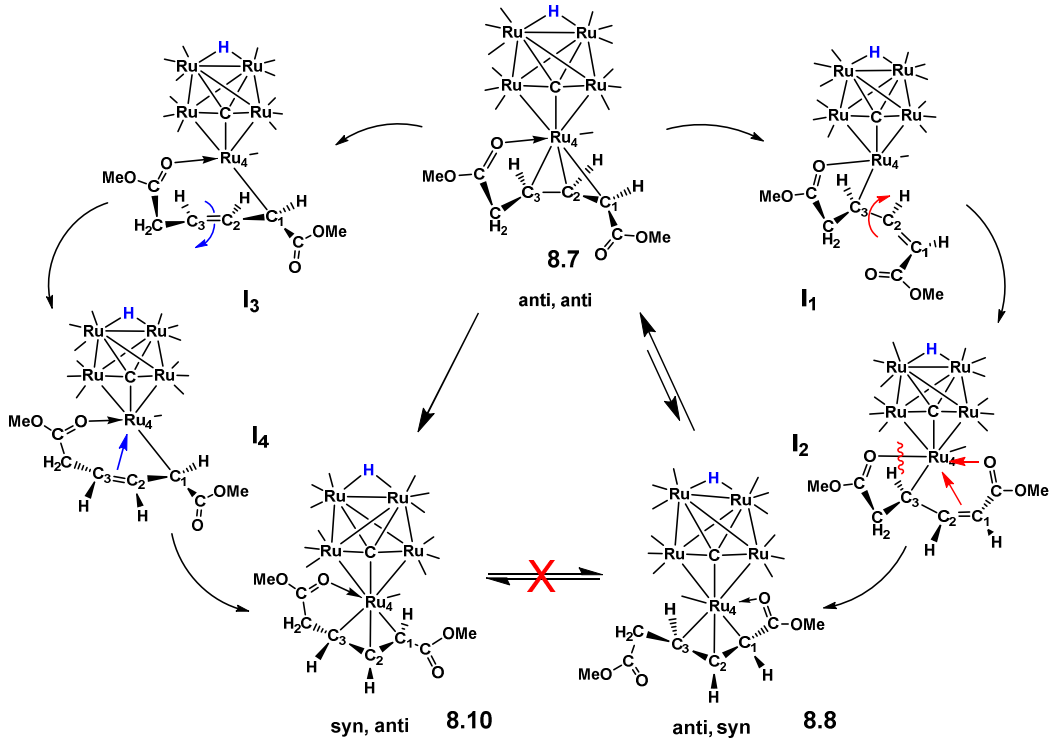

Scheme 8.2. Proposed mechanisms for the interconversion of the isomers **8.7**, **8.8** and **8.10.**

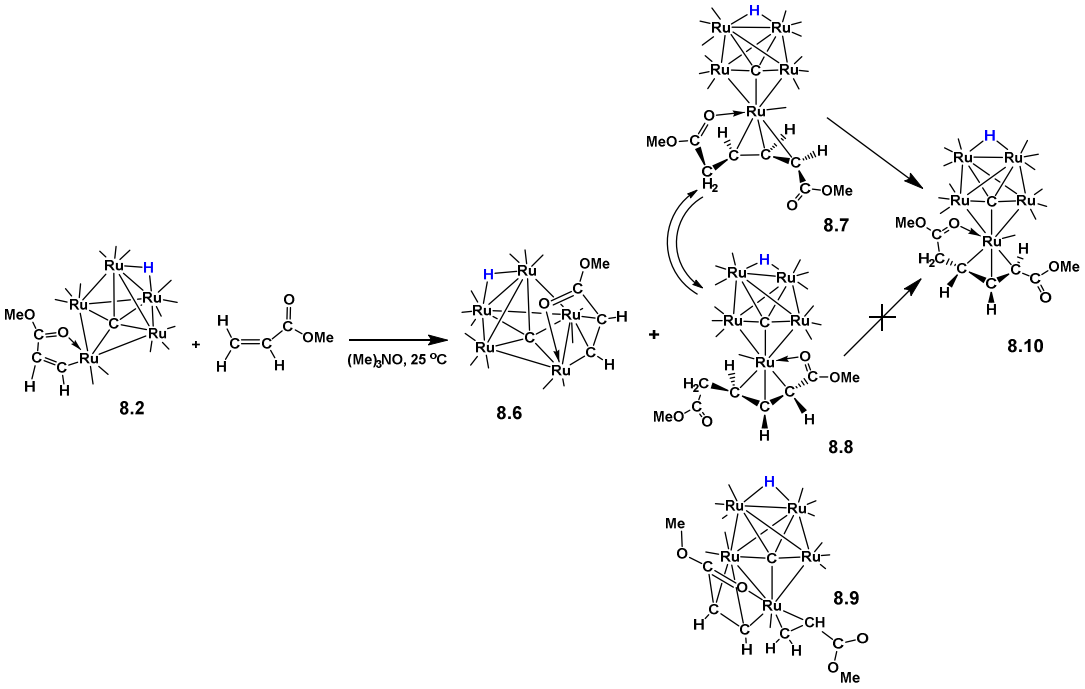

Scheme 8.3. A summary of the reactions of **8.2** with methyl acrylate.

8.5 References

1) Bryliakov, K. P.; Antonov, A. A. *J. Organomet. Chem.* **2018**, 867, 55-61.

2) Brookhart, M.; Hauptman, E.; Lincoln, D. M. *J. Am. Chem. Soc*. **1992**, 114 10394-10401.

3) Al-Sherehy, F. A. *Stud. Surf. Sci. Catal*. **1996**, 100 515-523.

4) Nicholas, C. P. *Appl. Catal. A, Gen*. **2017**, 543, 82–97.

5) Hauptman, E.; Sabo-Etienne, S.; White, P. S.; Brookhart, M.; Gamer, J. M.; Fagan, P. J.; Calabrese, J. C. *J. Am. Chem. Soc.* **1994**, 116 8038-8060.

6) Zimmermann, J.; Tkatchenko, I.; Wasserscheid, P. *Adv. Synth. Catal*. **2003**, 345, 402 – 409.

7) Tembe, G. L.; Bandyopadhyay, A. R.; Ganeshpure; P. A.; Satish, S. *Catal. Rev.-Sci. Eng.* **1996**, 38, 299 – 327.

8) Hirano; M.; Sakate; Y.; Komine; N.; Komiya; S.; Bennett, M. A. *Organometallics* **2009**, 28, 4902 - 4905.

9) Sustmann, R.; Hornung, H. J.; Schupp, T.; Patzke, B. *J. Mol. Catal.* **1993**, 85, 149-152.

10) K. Weissermel, H.-J. Arpe, in *Industrial Organic Chemistry,* 2nd ed., Verlag Chemie: Weinheim, Germany, 1993; Chapters 10.1 and 10.2.

11) McKinney, R. J. *Organometallics* **1986**, 5, 1752 - 1753.

12) Guibert; I.; Neibecker; D.; Tkatchenko, I. *J. Chem. Soc., Chem. Commun*. **1989**, 0, 1850 – 1852.

13) (a) Hirano; M.; Hiroi; Y.; Komine; N.; Komiya, S. *Organometallics* **2010**, 29, 3690–3693. (b) Pertici; P.; Ballantini; V.; Salvadori; P.; Bennett, M. A. *Organometallics* **1995**, 14, 2565 – 2569.

14) (a) Oehme, G.; Pracejus, H. *J. Prakt. Chemie* **1980**, 322, 798-808. (b) McKinney; R. J.; Colto, M. C. *Organometallics* **1986**, 5, 1080-1085.

15) Hatamoto, Y.; Sakaguchi, S.; Ishii, Y. *Org. Lett*. **2004**, 6, 4623 - 4625.

16) Komiya, S.; Ito, T.; Cowie, M.; Yamamoto; A.; Ibers, J. A. *J. Am. Chem. Soc*. **1976**, 98, 3874 – 3884.

17) (a) Ghosh; C. K.; Hoyano; J. K.; Krentz; R.; Graham, W. A. G. *J. Am. Chem. Soc*. **1989**, 111, 5480 – 5481. (b) Werner, H.; Dirnberger, T.; Schulz, M. *Angew. Chem. Int. Ed. Engl*. **1988**, 27, 948 -950. (c) Braunstein, P.; Chetcuti, M. J.; Welter, R. *Chem. Commun.* **2001**, 2508–2509.

18) Adams; R. D.; Smith; M. D.; Tedder, J. D. *Eur. J. Inorg. Chem*. **2018**, 2984-2986.

19) Adams; R. D.; Tedder, J. D. *Inorg. Chem*. **2018**, 57, 5707 – 5710.

20) Adams; R. D.; Akter; H.; Tedder, J. D. *J. Organometal. Chem.* **2018**, submitted.

21) Johnson, B. F. G.; Lewis, J.; Nicholls, J. N.; Puga, J.; Raithby, P. R.; Rosales, M. J.; McPartlin, M.; Clegg, W. J. Chem. Soc. Dalton Trans. **1983**, 277-290.

22) Saint+, Version 6.2a, Bruker Analytical X-ray System, Inc, Madison, WI, **2001**.

23) APEX3 Version 2016.5-0 and SAINT Version 8.34A. Bruker AXS, Inc. Madison, WI, USA.

24) SADABS Version 2016/2. Krause, L., Herbst-IrMer, R., Sheldrick G.M. & Stalke D. *J. Appl. Cryst*. **2015**, 48, 3-10.

25) G.M. Sheldrick, SHELXTL, Version 6.1, Bruker Analytical X-ray Systems, Inc, Madison, WI, **1997**.

26) Boyar, E.; Deeming, A. J.; Rothwell, I. P.; Henrick, K.; McPartlin, M. *J. Chem. Soc. Dalton Trans*. **1986** 1437-1441.

APPENDIX A

Copyright Releases

Permission for reprint from publisher of Chapter 2.

Adams, R. D.; Tedder, J.; Wong, Y. O. *J. Organomet. Chem.* **2015**, 795, 2-10.

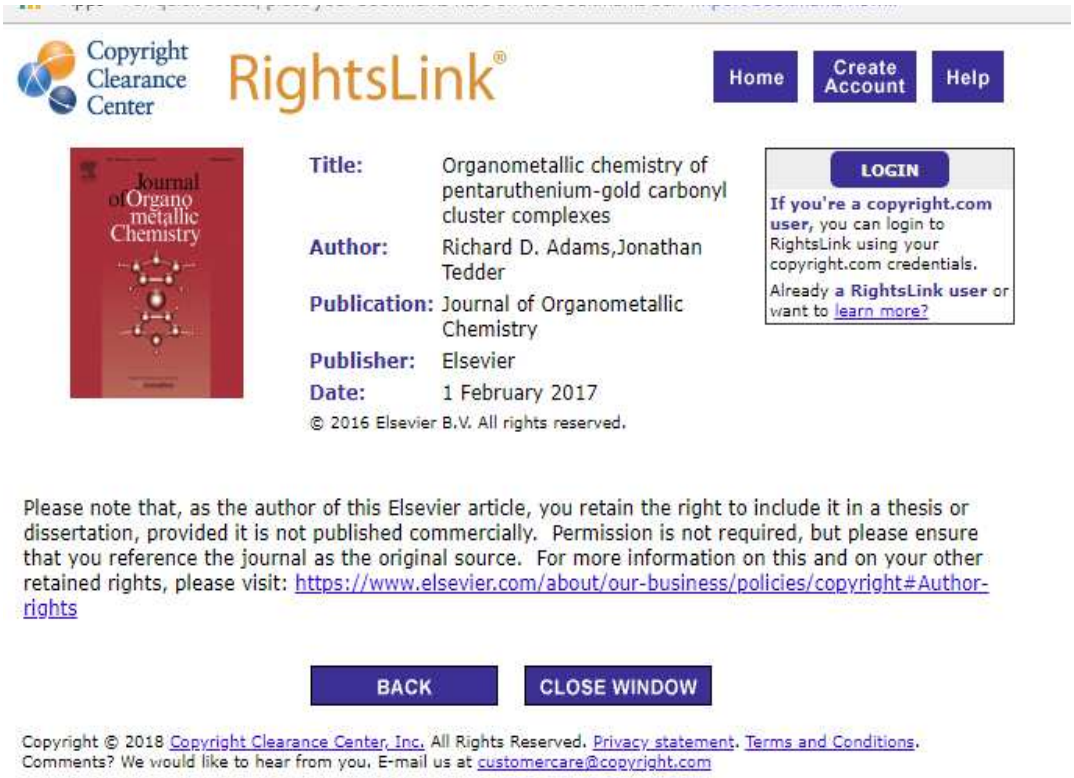

Permission for reprint from publisher of Chapter 3.

Adams, R. D.; Tedder, J. *J. Organomet. Chem.* **2017**, 829, 58-65.

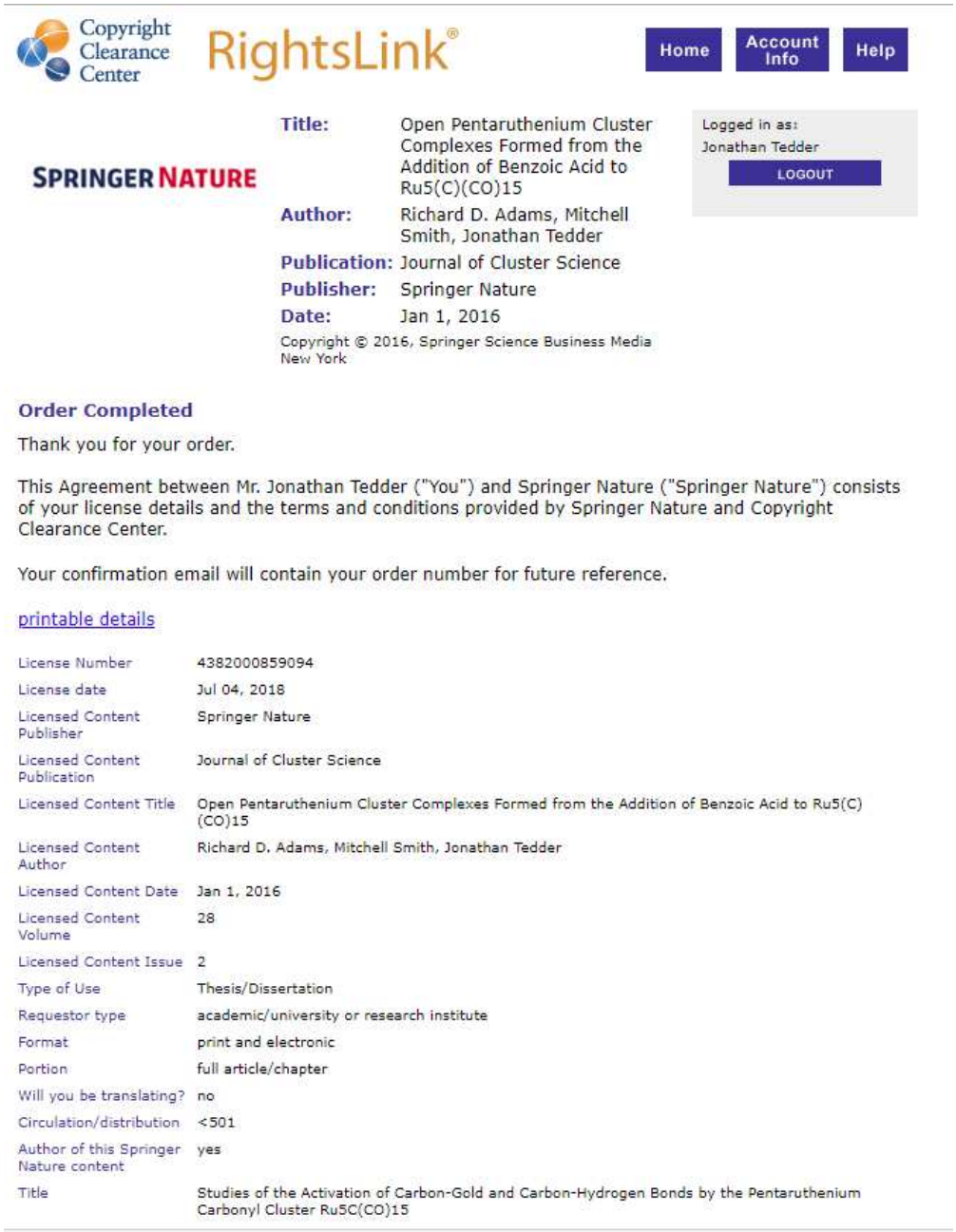

Copyright Clearance Center RightsLink®

Home | Account Info | Help

SPRINGER NATURE

Title: Open Pentaruthenium Cluster Complexes Formed from the Addition of Benzoic Acid to Ru5(C)(CO)15

Author: Richard D. Adams, Mitchell Smith, Jonathan Tedder

Publication: Journal of Cluster Science

Publisher: Springer Nature

Date: Jan 1, 2016

Copyright © 2016, Springer Science Business Media New York

Logged in as: Jonathan Tedder

LOGOUT

Order Completed

Thank you for your order.

This Agreement between Mr. Jonathan Tedder ("You") and Springer Nature ("Springer Nature") consists of your license details and the terms and conditions provided by Springer Nature and Copyright Clearance Center.

Your confirmation email will contain your order number for future reference.

printable details

License Number	4382000859094
License date	Jul 04, 2018
Licensed Content Publisher	Springer Nature
Licensed Content Publication	Journal of Cluster Science
Licensed Content Title	Open Pentaruthenium Cluster Complexes Formed from the Addition of Benzoic Acid to Ru5(C)(CO)15
Licensed Content Author	Richard D. Adams, Mitchell Smith, Jonathan Tedder
Licensed Content Date	Jan 1, 2016
Licensed Content Volume	28
Licensed Content Issue	2
Type of Use	Thesis/Dissertation
Requestor type	academic/university or research institute
Format	print and electronic
Portion	full article/chapter
Will you be translating?	no
Circulation/distribution	<501
Author of this Springer Nature content	yes
Title	Studies of the Activation of Carbon-Gold and Carbon-Hydrogen Bonds by the Pentaruthenium Carbonyl Cluster Ru5C(CO)15

Permission for reprint from publisher of Chapter 4.

Adams, R. D.; Smith, M.; Tedder, J.; *J. Clust. Sci.* **2017**, 28, 695-702.

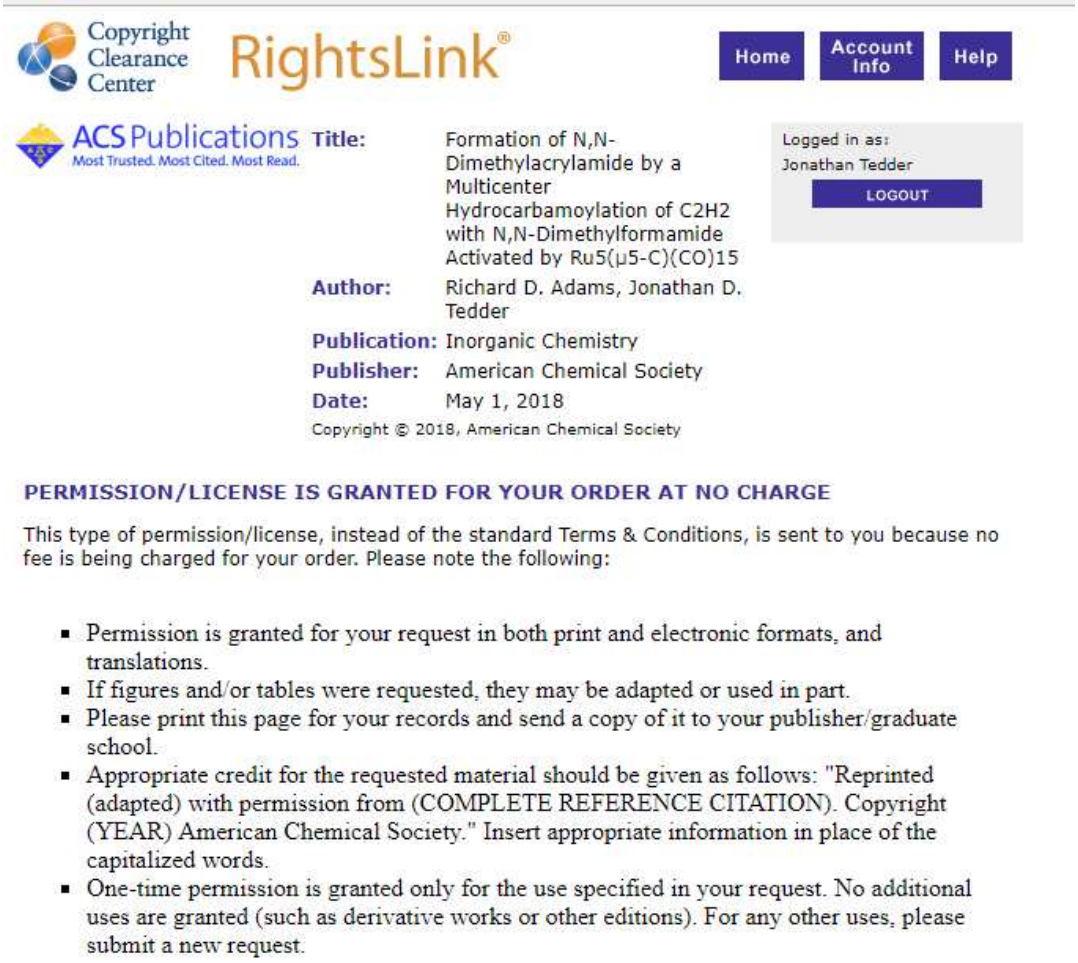

Copyright Clearance Center RightsLink®

Home | Account Info | Help

ACS Publications Most Trusted. Most Cited. Most Read.

Logged in as: Jonathan Tedder

LOGOUT

Title: Formation of N,N-Dimethylacrylamide by a Multicenter Hydrocarbamoylation of C2H2 with N,N-Dimethylformamide Activated by Ru5(μ5-C)(CO)15

Author: Richard D. Adams, Jonathan D. Tedder

Publication: Inorganic Chemistry

Publisher: American Chemical Society

Date: May 1, 2018

Copyright © 2018, American Chemical Society

PERMISSION/LICENSE IS GRANTED FOR YOUR ORDER AT NO CHARGE

This type of permission/license, instead of the standard Terms & Conditions, is sent to you because no fee is being charged for your order. Please note the following:

- Permission is granted for your request in both print and electronic formats, and translations.
- If figures and/or tables were requested, they may be adapted or used in part.
- Please print this page for your records and send a copy of it to your publisher/graduate school.
- Appropriate credit for the requested material should be given as follows: "Reprinted (adapted) with permission from (COMPLETE REFERENCE CITATION). Copyright (YEAR) American Chemical Society." Insert appropriate information in place of the capitalized words.
- One-time permission is granted only for the use specified in your request. No additional uses are granted (such as derivative works or other editions). For any other uses, please submit a new request.

Permission for reprint from publisher of Chapter 6.

Adams, R. D.; Tedder, J. D; *Inorg. Chem.* **2018**, 57, 5707-5710.

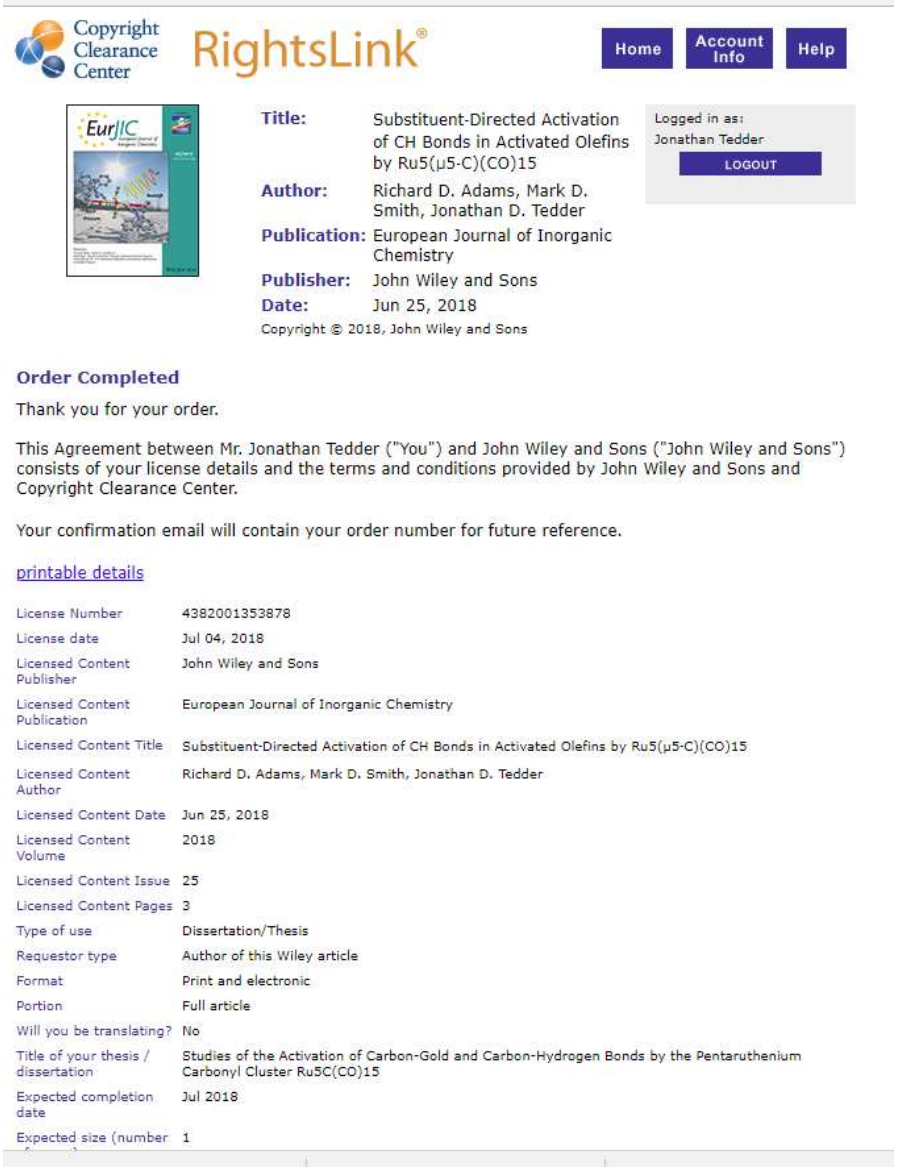

Copyright Clearance Center RightsLink®

Home | Account Info | Help

Logged in as: Jonathan Tedder
LOGOUT

Title: Substituent-Directed Activation of CH Bonds in Activated Olefins by Ru5(μ5-C)(CO)15
Author: Richard D. Adams, Mark D. Smith, Jonathan D. Tedder
Publication: European Journal of Inorganic Chemistry
Publisher: John Wiley and Sons
Date: Jun 25, 2018
Copyright © 2018, John Wiley and Sons

Order Completed

Thank you for your order.

This Agreement between Mr. Jonathan Tedder ("You") and John Wiley and Sons ("John Wiley and Sons") consists of your license details and the terms and conditions provided by John Wiley and Sons and Copyright Clearance Center.

Your confirmation email will contain your order number for future reference.

printable details

License Number	4382001353878
License date	Jul 04, 2018
Licensed Content Publisher	John Wiley and Sons
Licensed Content Publication	European Journal of Inorganic Chemistry
Licensed Content Title	Substituent-Directed Activation of CH Bonds in Activated Olefins by Ru5(μ5-C)(CO)15
Licensed Content Author	Richard D. Adams, Mark D. Smith, Jonathan D. Tedder
Licensed Content Date	Jun 25, 2018
Licensed Content Volume	2018
Licensed Content Issue	25
Licensed Content Pages	3
Type of use	Dissertation/Thesis
Requestor type	Author of this Wiley article
Format	Print and electronic
Portion	Full article
Will you be translating?	No
Title of your thesis / dissertation	Studies of the Activation of Carbon-Gold and Carbon-Hydrogen Bonds by the Pentaruthenium Carbonyl Cluster Ru5C(CO)15
Expected completion date	Jul 2018
Expected size (number	1

Permission for reprint from publisher of Chapter 7.

Adams, R. D.; Smith, M. D.; Tedder, J. D; *Eur. J. Inorg. Chem.* **2018**, 2984-2986.